Clinicians' Guides to Radionuclide Hybrid Imaging · PET/CT
Series Editors: Jamshed B. Bomanji · Gopinath Gnanasegaran
Stefano Fanti · Homer A. Macapinlac

Francesco Fraioli *Editor*

PET/CT in Brain Disorders

BNMS
BRITISH NUCLEAR MEDICINE SOCIETY

Springer

Clinicians' Guides to Radionuclide Hybrid Imaging

PET/CT

Series Editors

Jamshed B. Bomanji
London, UK

Gopinath Gnanasegaran
London, UK

Stefano Fanti
Bologna, Italy

Homer A. Macapinlac
Houston, Texas, USA

More information about this series at http://www.springer.com/series/13803

Francesco Fraioli
Editor

PET/CT in Brain Disorders

Springer

BNMS
BRITISH NUCLEAR MEDICINE SOCIETY

Editor
Francesco Fraioli
Institute of Nuclear Medicine
University College London
London
UK

ISSN 2367-2439 ISSN 2367-2447 (electronic)
Clinicians' Guides to Radionuclide Hybrid Imaging - PET/CT
ISBN 978-3-030-01522-0 ISBN 978-3-030-01523-7 (eBook)
https://doi.org/10.1007/978-3-030-01523-7

Library of Congress Control Number: 2018964423

This Springer imprint is published by the registered company Springer Nature Switzerland AG
The registered company address is: Gewerbestrasse 11, 6330 Cham, Switzerland

PET/CT series is dedicated to Prof Ignac Fogelman, Dr Muriel Buxton-Thomas and Prof Ajit K Padhy

Foreword

Clear and concise clinical indications for PET/CT in the management of the oncology and non-oncology patient are presented in this series of 15 separate booklets.

The impact on better staging, tailored management and specific treatment of the patient with cancer has been achieved with the advent of this multimodality imaging technology. Early and accurate diagnosis will always pay, and clear information can be gathered with PET/CT on treatment responses. Prognostic information is gathered and can forward guide additional therapeutic options.

It is a fortunate coincidence that PET/CT was able to derive great benefit from radionuclide-labelled probes, which deliver good and often excellent target to non-target signals. Whilst labelled glucose remains the cornerstone for the clinical benefit achieved, a number of recent probes are definitely adding benefit. PET/CT is hence an evolving technology, extending its applications and indications. Significant advances in the instrumentation and data processing available have also contributed to this technology, which delivers high throughput and a wealth of data, with good patient tolerance and indeed patient and public acceptance. As an example, the role of PET/CT in the evaluation of cardiac disease is also covered, with emphasis on labelled rubidium and labelled glucose studies.

The novel probes of labelled choline; labelled peptides, such as DOTATATE; and, most recently, labelled PSMA (prostate-specific membrane antigen) have gained rapid clinical utility and acceptance, as significant PET/CT tools for the management of neuroendocrine disease and prostate cancer patients, notwithstanding all the advances achieved with other imaging modalities, such as MRI. Hence a chapter reviewing novel PET tracers forms a part of this series.

The oncological community has recognised the value of PET/CT and has delivered advanced diagnostic criteria for some of the most important indications for PET/CT. This includes the recent Deauville criteria for the classification of PET/CT patients with lymphoma—similar criteria are expected to develop for other malignancies, such as head and neck cancer, melanoma and pelvic malignancies. For completion, a separate section covers the role of PET/CT in radiotherapy planning, discussing the indications for planning biological tumour volumes in relevant cancers.

These booklets offer simple, rapid and concise guidelines on the utility of PET/CT in a range of oncological indications. They also deliver a rapid aide-memoire on the merits and appropriate indications for PET/CT in oncology.

London, UK Peter J. Ell, FMedSci, DR HC, AΩA

Preface

The *Hybrid Imaging* with PET/CT and SPECT/CT combines the best of function and structure to provide accurate localisation, characterisation and diagnosis. There is extensive literature and evidence to support PET/CT, which has made significant impact in oncological imaging and management of patients with cancer. The evidence in favour of SPECT/CT especially in orthopaedic indications is evolving and increasing.

The *Clinicians' Guides to Radionuclide Hybrid Imaging* pocketbook series is specifically aimed at our referring clinicians, nuclear medicine/radiology doctors, radiographers/technologists and nurses who are routinely working in nuclear medicine and participate in multidisciplinary meetings. This series is the joint work of many friends and professionals from different nations who share a common dream and vision towards promoting and supporting nuclear medicine as a useful and important imaging speciality.

We want to thank all those people who have contributed to this work as advisors, authors and reviewers, without whom the book would not have been possible. We want to thank our members from the BNMS (British Nuclear Medicine Society, UK) for their encouragement and support, and we are extremely grateful to Dr. Brian Nielly, Charlotte Weston, the BNMS Education Committee and the BNMS Council Members for their enthusiasm and trust.

Finally, we wish to extend particular gratitude to the industry for their continuous supports towards education and training.

London, UK

Gopinath Gnanasegaran
Jamshed B. Bomanji

Acknowledgements

The series co-ordinators and editors would like to express sincere gratitude to the members of the British Nuclear Medicine Society, patients, teachers, colleagues, students, the industry and the BNMS Education Committee Members, for their continued support and inspiration.

Andy Bradley
Brent Drake
Francis Sundram
James Ballinger
Parthiban Arumugam
Rizwan Syed
Sai Han
Vineet Prakash

Contents

Contributors

Karar Obeed Almansory Institute of Nuclear Medicine, University College London Hospital, London, UK

Khulood Al Riyami Institute of Nuclear Medicine, University College of London Hospital, London, UK

Demetrio Arico' Department of Nuclear Medicine, Humanitas Oncological Centre of Catania, Catania, Italy

Dario Arnaldi Department of Neuroscience, Rehabilitation, Ophthalmology, Genetics, and Mother-Child Health (DINOGMI), Clinical Neurology, Polyclinic San Martino Hospital, University of Genoa, Genoa, Italy

Anna Barnes Institute of Nuclear Medicine, University College London Hospital NHS Foundation Trust, London, UK

Matteo Bauckneht Department of Health Sciences (DiSSAL), University of Genoa and Nuclear Medicine Unit, Polyclinic San Martino Hospital, Genoa, Italy

Jamshed B. Bomanji Institute of Nuclear Medicine, University College London Hospitals NHS Foundation Trust, London, UK

Selene Capitanio Department of Health Sciences (DiSSAL), University of Genoa and Nuclear Medicine Unit, Polyclinic San Martino Hospital, Genoa, Italy

Valentina Ceriani Department of Health Sciences (DiSSAL), University of Genoa and Nuclear Medicine Unit, Polyclinic San Martino Hospital, Genoa, Italy

Patrik Fazio Department of Clinical Neuroscience, Centre for Psychiatry Research, Karolinska University Hospital, Karolinska Institutet, Stockholm, Sweden

Department of Neurology, Karolinska University Hospital, Stockholm, Sweden

Valentina Ferrazzoli Department of Biomedicine and Prevention, Tor Vergata University Hospital, Rome, Italy

Naomi Fersht Department of Oncology, University College Hospital, London, UK

Francesco Fraioli Institute of Nuclear Medicine, University College London, London, UK

Valentina Garibotto Nuclear Medicine and Molecular Imaging Division, Department of Medical Imaging, University Hospitals of Geneva, Geneva, Switzerland

Faculty of Medicine, Geneva University, Geneva, Switzerland

Claudio Giardina Department of Radiology, ASP of Messina–Hospital of Taormina, Taormina, ME, Italy

Ismini C Mainta Nuclear Medicine and Molecular Imaging Division, Department of Medical Imaging, University Hospitals of Geneva, Geneva, Switzerland

Faculty of Medicine of Geneva University, Geneva, Switzerland

Kshitij Mankad Department of Radiology, Great Ormond Street Hospital NHS Foundation Trust, London, UK

Federico Massa Department of Neuroscience, Rehabilitation, Ophthalmology, Genetics, and Mother-Child Health (DINOGMI), Clinical Neurology, Polyclinic San Martino Hospital University of GenoaGenoa, Genoa, Italy

Riccardo Meli Department of Neuroscience, Rehabilitation, Ophthalmology, Genetics, and Mother-Child Health (DINOGMI), Clinical Neurology, Polyclinic San Martino Hospital, University of Genoa, Genoa, Italy

Vincenzo Militano Institute of Nuclear Medicine, University College of London Hospital, London, UK

Silvia Morbelli Department of Health Sciences (DiSSAL), University of Genoa and Nuclear Medicine Unit, Polyclinic San Martino Hospital, Genoa, Italy

Flavio Nobili Department of Neuroscience, Rehabilitation, Ophthalmology, Genetics, and Mother-Child Health (DINOGMI), Clinical Neurology, Polyclinic San Martino Hospital, University of Genoa, Genoa, Italy

Rik Ossenkoppele Alzheimer center, Amsterdam University Medical Center, Amsterdam, The Netherlands

Clinical Memory Research Unit, Lund University, Lund, Sweden

Fabienne Picard Faculty of Medicine of Geneva University, Geneva, Switzerland

EEG and Epilepsy Unit, Neurology Department, University Hospitals of Geneva, Geneva, Switzerland

April-Louise Smith Institute of Nuclear Medicine, University College London Hospital NHS Foundation Trust, London, UK

Francesca Soldá Department of Oncology, University College Hospital, London, UK

Christine Tang Institute of Nuclear Medicine, University College of London Hospital, London, UK

Nelleke Tolboom Nuclear Medicine Physician, Department of Radiology (Imaging Division), University Medical Center Utrecht, Utrecht, The Netherlands

Bart N. van Berckel Department of Radiology and Nuclear Medicine, Amsterdam University Medical Center, Amsterdam, The Netherlands

Andrea Varrone Department of Clinical Neuroscience, Centre for Psychiatry Research, Karolinska University Hospital, Karolinska Institutet, Stockholm, Sweden

Stefan Vöö Institute of Nuclear Medicine, University College of London Hospital, London, UK

Introduction to Brain Disorders

1

Jamshed Bomanji and Francesco Fraioli

Content

The World Health Organization (WHO) data indicate that, together, brain disorders account for one-third of the burden of all diseases in the wealthy part of the world [1], and data show that these disorders are a major public health and economic problem with an estimation of € 800 billion for the healthcare worldwide, comprising direct and indirect assistance. Several definitions have been proposed for brain disorders and the one below recently appeared on the *Bulletin of the World Health Organization* [2].

"Mental and neurological disorders are complex and linked to hundreds of specific diagnoses [3]. The causes of such disorders are heterogeneous, ranging from pathological protein aggregation leading to neurodegeneration or dysregulation of the immune process to developmental and functional abnormalities. These disorders also frequently involve an intricate interplay between genetic and environmental factors."

In this pocket guide for radiologists and nuclear medicine physicians, the authors have reviewed the clinical and research application of PET/CT and PET/MRI in the most common neurological and neuro-oncology disorders.

In the first chapters, the authors will discuss pros and cons of most used radiological imaging techniques, scanners, and main radiopharmaceuticals, with emphasis

J. Bomanji
Institute of Nuclear Medicine, University College London Hospitals NHS Foundation Trust, London, UK

F. Fraioli (✉)
Institute of Nuclear Medicine, University College London, London, UK
e-mail: francesco.faioli@nhs.net

F. Fraioli (ed.), *PET/CT in Brain Disorders*, Clinicians' Guides to Radionuclide Hybrid Imaging, https://doi.org/10.1007/978-3-030-01523-7_1

on the state-of-the-art hybrid modalities and PET/MR and clinical and research tracers used in neurodegeneration, movement disorders, epilepsy, and neuro-oncology.

In the second part of the book, the four killers above will be discussed in detail highlighting the role of PET and molecular imaging in their assessment. All chapters will be correlated with exhaustive images to better explain the diseases.

The final chapter will provide to the readers a large sample of teaching cases and files which can help in the daily clinical practice.

References

1. Olesen J, Leonardi M. The burden of brain diseases in Europe. Eur J Neurol. 2003;10:471–7.
2. Di Luca M, Nutt D, Oertel W, Boyer P, Jaarsma J, Destrebecq F, et al. Towards earlier diagnosis and treatment of disorders of the brain. Bull World Health Organ. 2018;96:298–298A. https://doi.org/10.2471/BLT.17.206599.
3. World Health Organization. International statistical classification of diseases and related health problems. 10th Revision. Geneva: World Health Organization; 2016.

Radiological Imaging in Brain Disorders: An Overview

2

Valentina Ferrazzoli and Kshitij Mankad

Contents

2.1 Neuroimaging Modalities and Techniques

The key role of neuroimaging in brain disorders is to assist clinical management by either making a precise diagnosis or providing clinically relevant differential diagnoses. There is a marked diversity of neuropathologies spanning a constellation of conditions including vascular, infectious-inflammatory, degenerative and neoplastic entities, and the clinical presentations can often be quite nonspecific, hence the key role of neuroimaging is formulating a management plan. Cranial Ultrasonography (US), Computed Tomography (CT) and Magnetic Resonance (MR) are the currently available modalities of neuroimaging, each with its specific strengths and limitations. Overall, MR Imaging (MRI) is the most useful technique to study the brain, given its higher soft tissue contrast, although CT has a central role still in acute imaging and is also the best technique to investigate for associated bony

V. Ferrazzoli (✉)
Department of Biomedicine and Prevention, Tor Vergata University Hospital, Rome, Italy

K. Mankad
Department of Radiology, Great Ormond Street Hospital NHS Foundation Trust, London, UK

F. Fraioli (ed.), *PET/CT in Brain Disorders*, Clinicians' Guides to Radionuclide Hybrid Imaging, https://doi.org/10.1007/978-3-030-01523-7_2

disorders. Cranial US has a vital role in foetal and neonatal imaging given its bedside ease and the presence of a good acoustic window—the skull foramina in this population. This chapter focuses on those clinical applications of neuroimaging that complement the practice of nuclear medicine with special relevance to CT and MRI.

2.1.1 Computed Tomography (CT)

The advent of fast multi-detector CT scanners with superior multi-reformat capabilities and their universally easy availability makes it the primary imaging modality in acute care. The acquisition protocol consists of contiguous thin sections (1 mm or less) or overlapping axial slices (slice thickness no greater than 5 mm). CT is primarily indicated in cases of sudden onset of new symptoms or deterioration, in the assessment of intracranial shunts or in the immediate post-neurosurgical evaluation [1]. It is mainly useful to detect calcifications and to establish the presence of blood within a lesion or in acute head trauma. It can also assist with characterising brain tumours, by showing increased density in hypercellular tumours and presence of calcification and or haemorrhage in tumour matrices. CT scan also provides a much better assessment of the bones of the skull vault and the skull base which can be secondarily affected in some diseases, such as metastases or lymphomas. In some cases, the administration of iodinated contrast medium can provide additional information in the assessment of the blood brain barrier or, through CT angiography (CTA) technique, in the noninvasive investigation of intracranial vessels and vascular malformations.

2.1.2 Magnetic Resonance Imaging (MRI)

MRI is the diagnostic tool of choice in investigating the brain, owing to its superior soft tissue contrast resolution. MRI protocols are tailored on diagnostic indications and all provide multiparametric information. The standard protocol includes T2-weighted (w) sequences, with and without CSF signal suppression (FLAIR), T1-w sequences and diffusion-weighted imaging (DWI). Susceptibility-weighted imaging (SWI) is a helpful adjunct in a large spectrum of diseases in order to identify blood, calcification or iron deposition. The use of different acquisition planes for a three-dimensional evaluation is always useful: in particular the acquisition of sagittal plane to investigate midline structures and coronal acquisition on temporal lobes for the assessment of hippocampal and parahippocampal regions. Three-dimensional T1-w sequences are also commonly employed in neuro-oncology and epilepsy protocols, in guiding neurosurgery (intraoperative neuronavigation) and also for their accuracy in identifying tiny lesions, to facilitate volumetric measurements of tumour burden, and for better alignment of tumour regions on subsequent follow-up examinations [2].

2.1.2.1 Perfusion MRI

MR perfusion imaging is an increasingly common mean for the evaluation of a variety of pathologies mainly tumours and ischaemia. Three techniques are now

available: two of them use T1- or T2-weighted changes after the injection of a gadolinium-based contrast agent, respectively, dynamic contrast-enhanced (DCE) MRI and dynamic susceptibility contrast-enhanced (DSC) MRI, and a third, arterial spin-labelling perfusion (ASL-MRp), in which magnetically labelled arterial blood water is used as an endogenous contrast agent. The main application of perfusion in neuro-oncology is in providing additional information for the differential diagnosis, in particular between lymphomas and glioblastomas or metastases, for the assessment of brain tumour grade and for the evaluation of treatment response. In acute stroke it can be used together with DWI for the identification of potentially salvageable brain tissue or even to assess vasospasm in particular conditions [3].

2.1.2.2 MR Spectroscopy

Spectroscopy provides information about normal and pathological tissue components by an analysis of the chemical environment of the brain. The most commonly studied metabolites are choline (Cho), a marker of cell membrane integrity and cell proliferation; creatine (Cr), a marker of cell metabolism; N-acetyl-aspartate (NAA), a marker of neuronal integrity; lactate (Lac), a marker of anaerobiosis; and lipids (Lip), which correlate with membrane disintegration. The typical indications include detecting the presence of neoplasms, grading of gliomas (low versus high grade), evaluation of temporal lobe epilepsy and certain neurometabolic and neurodegenerative diseases [4].

2.1.2.3 Diffusion Tensor Imaging

Diffusion tensor imaging (DTI) is useful in the preoperative planning for oncology and epilepsy. The technique enables the 3D localisation, orientation and anisotropy of the white matter tracts of the brain and their relationship to the lesion under management [5].

2.1.2.4 Functional MRI (f-MRI)

f-MRI uses blood oxygenation level-dependent imaging (BOLD) technique, which is based on the localisation of hemodynamic changes caused by regionally increased neuronal activity during a cognitive task. This information is useful to determine the hemispheric dominance and the presence of eloquent cortex in relation to a focal lesion to plan surgical treatment [6].

2.2 Radiological Imaging in Neurodegenerative Diseases

Dementia, as a prototypical group of neurodegenerative disorders, can be subclassified based on certain neuroimaging criteria. Alzheimer disease (AD), dementia with Lewy bodies (DBL), frontotemporal dementia (FTD) and vascular dementia are its commonly encountered subtypes. Anatomic neuroimaging with MRI can differentiate normal age-related degenerative processes from early signs of dementia, exclude alternatives causes and identify specific patterns of brain volume loss that can support the clinical diagnosis [7]. Functional and metabolic imaging is suggested for

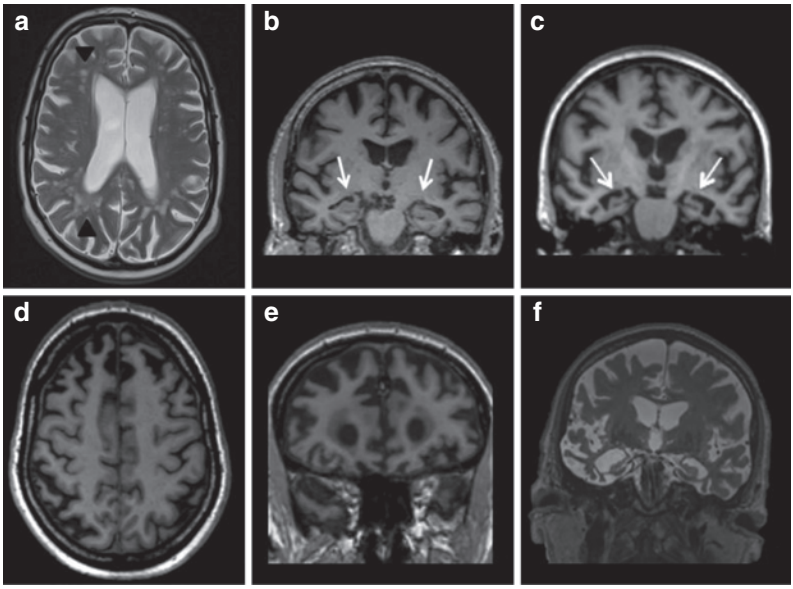

Fig. 2.1 Neurodegenerative diseases. (**a**) Vascular dementia in a 69-year-old patient. (**a**) Axial T2-w image shows moderate diffuse small vessel disease (arrow heads) and generalised brain atrophy. (**b**, **c**) Mild cognitive impairment (MCI) and Alzheimer disease (AD). (**b**) Mild and (**c**) severe atrophy, with reduced volume of the hippocampi (arrows) and enlargement of the liquoral spaces, is seen in patients with MCI and AD. Coronal T1-w images better allow the assessment of medial temporal lobe. (**d**, **e**, **f**) Frontotemporal dementia. (**d**) Axial and (**e**) coronal T1-w images show disproportionate atrophy of the frontal and temporal lobes, with relative sparing of the parietal and occipital lobes in a 67-year-old. (**f**) Coronal T2-w image shows a severe atrophy of frontal and temporal lobes in a 70-year-old (Figures are courtesy of Dr. H. Hyare, University College of London Hospital, NHS Foundation Trust, London)

problem-solving purposes, and a multimodality approach allows an earlier and more confident evaluation [8]. Initially it is important to evaluate if there is a specific pattern of volume loss with a lobar predominance, looking for enlarged temporal and/or frontal ventricular horns, widened sulci and thinned gyri. Disproportionate atrophy of the medial temporal lobes is generally the earliest sign identified in AD, and its progression correlates well with clinical progression of cognitive impairment [9]. The imaging assessment should therefore include the hippocampi, which appear atrophic, the entorhinal cortex and the perirhinal cortex in the coronal plane. AD changes involve parietal and frontal lobes subsequently, whereas the occipital lobes and sensorimotor cortices are relatively spared.

Anatomic imaging findings in FTD on the other hand show symmetric or asymmetric frontal or temporal lobe atrophy, with relative sparing of the parietal and occipital lobes; these signs are subtle at the early stage, but later they can be severe with a 'knife blade' appearance of the atrophied gyri [10]. The pattern of volume loss in DLB is nonspecific, with a relative preservation of the hippocampi [11]. Figure 2.1 shows pattern of volume loss in different types of dementia.

2.3 Radiological Imaging in Movement Disorders

MRI is used to evaluate certain key structures of the brain in parkinsonian disorders, namely, the basal ganglia (caudate, putamen and globus pallidus) and the midbrain, with particular focus on the substantia nigra, the pons and the cerebellum.

The primary step is to exclude structural pathologies involving these areas, for instance, neoplasms, haemorrhagic or ischaemic lesions involving the basal ganglia [12].

Change in the signal pattern at the substantia nigra on susceptibility-weighted MR sequences, relating to an increased iron content, is the most typical feature described in Parkinson's disease (idiopathic parkinsonism). This is eloquently described as the absent swallow tail sign (the swallow tail sign is present in normal individuals as a comma-shaped focus of high signal on susceptibility-weighted sequences in the posterior 1/3 of the substantia nigra). A relative reduction in putaminal volume is also described as an early feature, though it is not specific [13].

In other parkinsonian conditions such as multisystem atrophy (MSA), the putamen is particularly involved, initially with reduced T2 signal along its lateral edge due to iron deposition, with atrophy and even frank gliosis in later stages. This condition is typically accompanied by degeneration of the pons and cerebellum, with associated prominence of the longitudinal and transverse pontine fibres, giving the typical 'hot cross bun' sign of the hind brain in MSA (Fig. 2.2a).

Conversely, in progressive supranuclear palsy (PSP), there is selective atrophy of the midbrain giving rise to the 'hummingbird' sign on a midline sagittal section (Fig. 2.2b). This is accompanied by a widening of the interpeduncular fossa as well as signal abnormality in the superior cerebellar peduncles [14]; this appearances result in the "Mickey Mouse sign" in axial plan (Fig. 2.2c).

Another condition in this respect is corticobasal degeneration (CBD), that presents with movement disorders and cognitive decline and shows selective brain volume loss in the posterior parietal regions (Fig. 2.2d, e).

In paediatric practice, there is a wide differential to movement disorders, and once again MRI has a primary role in the evaluation of relevant structures such as the basal ganglia, in conditions such as neuronal brain iron accumulation (NBIA) (Fig. 2.2f).

2.4 Radiological Imaging in Epilepsy

The role of neuroimaging in epilepsy is multifold: to detect a causative structural lesion, to guide management and to monitor disease. There is a vast and diverse constellation of conditions that can cause seizures and radiology helps in their identification. These entities include malformations of cortical development, tumours, stroke, infections, traumatic brain injuries, vascular malformations, primary or secondary mesial temporal sclerosis (MTS), phakomatoses, hypoxic ischemic encephalopathy and inborn error of metabolism [15]. Twenty to 30% of patients with temporal lobe epilepsy and 20–40% of patients with extra-temporal

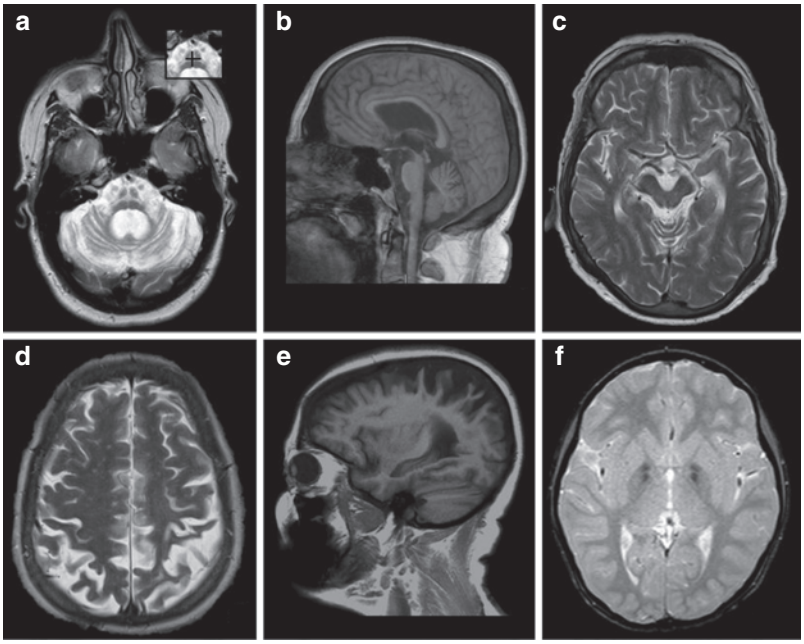

Fig. 2.2 Movement disorders. (**a**) Multisystem atrophy (MSA). T2-w axial image demonstrates the presence of pontine and cerebellar atrophy with degeneration of pontocerebellar tracts passing through the middle cerebellar peduncles that results in the 'hot cross bun sign' at the level of the pons (black lines in magnification). (**b**, **c**) Progressive supranuclear palsy (PSP). (**b**) Sagittal plan shows marked midbrain and tegmental atrophy compared with the pons which results in the appearance referred as "hummingbird sign. (**c**) Axial T2-w image demonstrate atrophy of the midbrain, involving the cerebral peduncles and resulting in the "Mickey Mouse sign". (**d**, **e**) Corticobasal degeneration (CBD). (**d**) Axial T2-w image and (**e**) parasagittal T1-w image show cortical atrophy involving predominantly the pre- and postcentral gyri and the superior parietal lobule. (**f**) Susceptibility-weighted imaging (SWI) demonstrates iron accumulation within the globi pallidi in a 5-year-old patient with movement disorder (ataxia), in keeping with neurodegeneration with brain iron accumulation (NBIA)

epilepsy have no clear lesion visible on a standard conventional MRI [16]; therefore, a dedicated epilepsy protocol and a meticulous review of the scan is essential as structural lesions can be completely resected with long-term seizure freedom. Lesion detection and characterisation are improved with 3T-MRI, especially for cortical lesions. Moreover T2-w and FLAIR coronal oblique images with thin slices (commonly 2–3 mm slice thickness), acquired perpendicular to the hippocampal long axis, in combination with a coronal 3D inversion recovery sequence are crucial for the identification of subtle cortical abnormalities, disturbances in cortical migration and MTS [17]. The latter comprises of gliosis, atrophy and loss of the internal architecture of the hippocampus; atrophy may be present in the other structures of limbic system along with increased T2-w signal in the mesial temporal region. Many times a retrospective review of the MR images after nuclear imaging may reveal a subtle cortical abnormality overlooked at the initial MRI interpretation. Focal epileptogenic lesions, as haemorrhage and vascular

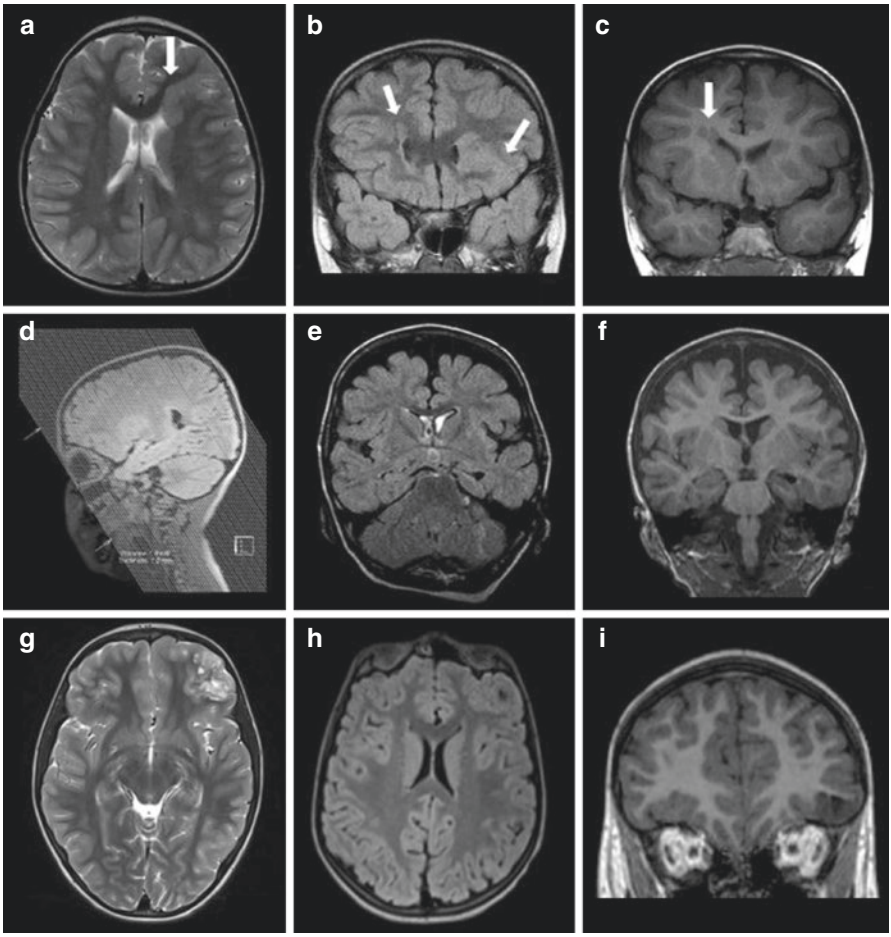

Fig. 2.3 Epilepsy in paediatric patients. (**a**–**c**) A 6-year-old boy with seizures. Axial T2-wi (**a**), coronal FLAIR (**b**) and T1-wi (**c**) show frontal bilateral heterotopic grey matter (white arrows) extending from the ventricular surface to the cortex in keeping with FCD. (**d**–**f**) A 2-year-old boy with temporal epilepsy. Coronal FLAIR (**e**) and T1-w (**f**) images oriented on the temporal pole (**d**) show a smaller left hippocampus which has altered signal and poor detail of the internal architecture: the temporal horn of the left ventricle is consequently enlarged. Symptoms resolved after right pole resection. (**g**–**i**) A 7-year-old girl. Axial T1 and T2-wi and coronal T1-wi show a cortical/subcortical non-enhancing lesion in the left inferior frontal gyrus in keeping with DNET undergoing surgery

malformations, can be better detected on susceptibility-weighted sequences [18]. Contrast injection is useful for the evaluation of known or suspected focal brain lesions or in neurocutaneous syndromes; therefore its use depends on clinical history, especially in the paediatric population. MRI can also show transient seizure-related signal changes, which can mimic other pathologic conditions but normalise over time, and permanent brain injury, including cortical volume loss, laminar necrosis and hippocampal sclerosis [17]. Figure 2.3 shows different causes of epilepsy in paediatric patients.

2.5 Radiological Imaging in Neuro-Oncology

In neuro-oncology diagnostic imaging has to provide, in the first instance, the differential diagnosis between primary or secondary neoplasms and then additional clues for the further management. CT maintains a role in detecting calcifications, typically present in different types of tumours as meningioma, oligodendrogliomas, germinomas, haemorrhages and tumour-related bone changes. However MRI is the modality of choice in the comprehensive characterisation of tumours. Conventional imaging provides essential information about the structure of the tumour, the presence of necrosis, the presence and the type of the enhancement, multifocality, leptomeningeal and/or subependymal seeding; nevertheless these features cannot be specific. DWI, being sensitive to random motion of water molecules, can give information about cellularity, allowing the identification of hypercellular lesions with restricted diffusion and low apparent diffusion coefficient (ADC), as typical lymphomas and embryonal tumours and sometimes germ cells tumour and pineoblastomas (Fig. 2.4a, b). The hypercellularity in these cases is also demonstrated as hyperdensity on CT scanning (Fig. 2.4c). Perfusion-weighted sequences and MR spectroscopy can provide further information of the tumour environment assisting with its grading, characterisation and response to therapy.

As an example, the differentiation between lymphomas and high-grade gliomas (HGG) is crucial considering their different managements. This differentiation is difficult based on conventional sequences, as lymphomas may not have their typical appearances of homogeneous enhancement with involvement of the corpus callosum, lack of calcifications or haemorrhages. Herein, diffusion-weighted imaging helps by showing lower ADC in lymphomas and lower perfusion on PWI that reflects the leakage of contrast in the interstitial space [19, 20] (Fig. 2.4d–f). HGG can be differentiated using these techniques as they usually demonstrate necrotic-ring enhancement, a peritumoral area of signal abnormality with low ADC, increased CHO-NAA ratio on MRS and higher vascularity on PWI [21, 22] (Fig. 2.4g–i).

Another practical application of MRI is the noninvasive grading of gliomas. HGGs demonstrate lower ADC, higher CHO-NAA ratio and relative cerebral blood volume on PWI compared with LGG [21]. These features can even be used to recognise areas with greater anaplasia within a lesion to target biopsy.

The other challenge for diagnostic imaging is response assessment of tumours to various and emerging forms of therapy. In this context it is useful to advocate multimodal imaging, using a combination of conventional imaging, along with perfusion MRI and PET imaging. Comparing true tumour progression to therapy-related necrosis or pseudo progression, for instance, lower relative blood volume on PWI is noted in the latter. Another important role of MRI is the identification of tumour pseudo response after anti-angiogenic treatment. These differentiations are not always obvious, and then repeat imaging is recommended to evaluate for persisting or progressing changes in 3 months' time to confirm true progression [23].

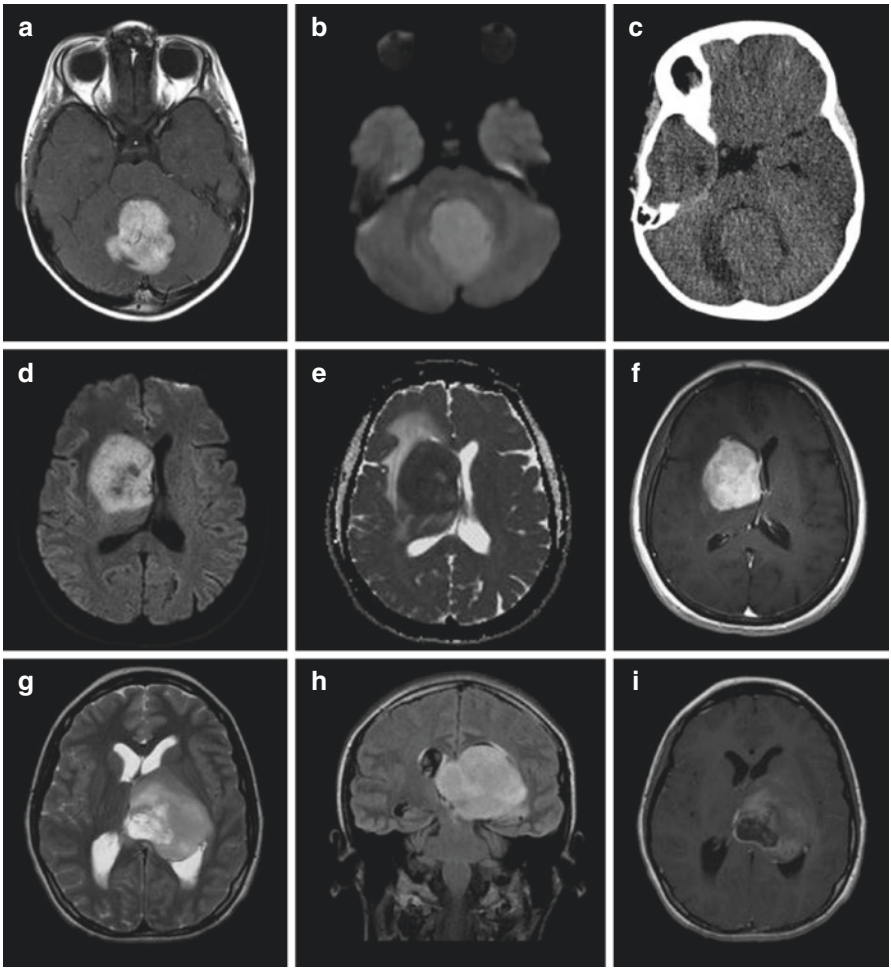

Fig. 2.4 Imaging of brain tumours. (**a**–**c**) Posterior fossa lesion in a 3.5-year-old child. (**a**) Axial post-contrast T1-wi shows a large midline enhancing mass centred in the cerebellum causing effacement of the fourth ventricle. The lesion has restricted diffusion in keeping with hypercellularity (**b**) confirmed by ADC maps (not shown); this finding is congruous with the hyperdensity of the lesion in CT scan (**c**). These appearances are in keeping with the histological diagnosis of medulloblastoma. (**d**–**f**) A large mass in a 39 years old man. (**d**, **e**) DWI and corresponding ADC map show a restricting lesion with very low ADC values centered in the right basal ganglia; (**f**) axial post-contrast T1w image shows intense enhancement of the lesion in keeping with lymphoma. (**g**–**i**) A large mass in a 65-year-old man. (**g**) Axial T2, (**h**) coronal FLAIR and (**i**) axial post-contrast T1-w images show a heterogeneous enhancing mass centred in the left deep grey matter, with a large area of necrosis, confirmed on histology to be a glioblastoma multiforme (Figures **d**–**i** are courtesy of Dr. H. Hyare, University College of London Hospital, NHS Foundation Trust, London)

Key Points

- Key role of neuroimaging is to assist clinical management by either making a precise diagnosis or providing clinically relevant differential diagnosis.
- Computed tomography (CT) is mainly used in cases of sudden onset of new symptoms or deterioration, immediately after neurosurgery, to rule out the presence of calcifications, hemorrhages, or bone alterations.
- Magnetic resonance imaging (MRI) is the most useful technique to investigate the brain, through morphologic and advanced imaging.
- Advanced MR imaging comprises perfusion imaging, mainly used in tumours and ischemia; spectroscopy, which evaluates brain tissue metabolites; and diffusion tensor imaging, employed in pre-surgical planning to study white matter tracts.
- In neurodegenerative diseases, MRI can differentiate normal age-related degenerative processes from early signs of dementia, exclude alternatives causes, and identify specific patterns of brain volume loss that can support the clinical diagnosis.
- In motor disorders MRI is helpful in evaluating key structures, as the basal ganglia (caudate, putamen, and globus pallidus), midbrain, pons, and cerebellum, that can demonstrate signal changes and atrophy.
- The role of neuroimaging in epilepsy is multifold: to detect a causative structural lesion, to guide management, and to monitor disease.
- The combined use of MRI and nuclear imaging in epilepsy management is crucial, as the retrospective review of the MR images after nuclear imaging may reveal a subtle cortical abnormality initially overlooked.
- In neuro-oncology diagnostic imaging has to provide, in the first instance, the differential diagnosis between primary or secondary neoplasms and then additional clues for the further management.
- Multimodal imaging, using PET imaging in combination with conventional MRI and advanced MR techniques, helps in assessing tumour response to therapies.

References

1. ACR-ASNR. ACR-ASNR practice guideline for the performance of computed tomography (CT) of the brain. Oak Brook, IL: ACR-ASNR; 2010.
2. Ellingson BM, Bendszus M, et al. Consensus recommendations for a standardized brain tumor imaging protocol in clinical trial. Neuro Oncol. 2015;17:1188–98.

3. Welker K, Boxerman J, et al. ASFNR recommendations for clinical performance of MR dynamic susceptibility contrast perfusion imaging of the brain. Am J Neurorad. 2015;36:E41–51.
4. ACR-ASNR. ACR/ASNR practice guideline for the performance and interpretation of magnetic resonance spectroscopy of the central nervous system. Oak Brook, IL: ACR-ASNR; 2010.
5. Potgieser AR, Wagemakers M. The role of diffusion tensor imaging in brain tumor surgery: a review of the literature. Clin Neurol Neurosurg. 2014;124:51–8.
6. ACR-ASNR-SPR. ACR-ASNR-SPR practice guideline for the performance of functional magnetic resonance imaging (fMRI) of the brain. Oak Brook, IL: ACR-ASNR; 2012.
7. (NICE/SCIE) National Institute for Health and Care Excellence/Social Care Institute of Excellence. Dementia: supporting people with dementia and their careers in health and social care. Clinical guideline CG42. London: NICE/SCIE; 2016.
8. Martin-Macintosh EL, Broski SM, et al. Multimodality Imaging of neurodegenerative processes: part I, the basics and common dementias. AJR. 2016;207:871–82.
9. Duara R, Loewenstein DA, et al. Medial temporal lobe atrophy on MRI scans and the diagnosis of Alzheimer disease. Neurology. 2008;71:1986–92.
10. Josephs KA. Frontotemporal lobar degeneration. Neurol Clin. 2007;25:683–96.
11. Shams S, Fallmar D, et al. MRI of the swallow tail sign: a useful marker in the diagnosis of Lewy body dementia? AJNR. 2017;38:1737–41.
12. (NICE/SCIE) National Institute for Health and Care Excellence/Social Care Institute of Excellence. Parkinson's disease in adults. Clinical guideline NG71. London: NICE/SCIE; 2017.
13. Seppi K, Poewe W. Brain magnetic resonance imaging techniques in the diagnosis of parkinsonian syndromes. Neuroimaging Clin N Am. 2010;20:29–55.
14. Broski SM, Hunt C, et al. Structural and functional imaging in Parkinsonian syndromes. Radiographics. 2014;34:1273–92.
15. (NICE/SCIE) National Institute for Health and Care Excellence/Social Care Institute of Excellence. Epilepsy: diagnosis and management. Clinical guideline CG137. London: NICE/SCIE; 2016.
16. Téllez-Zenteno JF, Hernandez Ronquillo A, et al. Surgical outcomes in lesional and nonlesional epilepsy: a systematic review and meta-analysis. Epilepsy Res. 2010;89:310–8.
17. Friedman E. Epilepsy imaging in adults: getting it right. AJNR. 2014;203:1093–103.
18. Saini J, Kesavadas C, et al. Susceptibility weighted imaging in the diagnostic evaluation of patients with intractable epilepsy. Epilepsia. 2009;50:1462–73.
19. Haque S, Law M, et al. Imaging of lymphoma of the central nervous system, spine and orbit. Radiol Clin N Am. 2008;46:339–61.
20. Akter M, Hirai T, et al. Diffusion-weighted imaging of primary brain lymphomas: effect of ADC value and signal intensity of T2-weighted imaging. Comput Med Imag Graph. 2008;32:539–43.
21. Nandu H, Wen PY, et al. Imaging in neuro-oncology. Ther Adv Neurol Dis. 2018;11:1–19.
22. Lee EJ, terBrugge K, et al. Diagnostic value of peritumoral minimum apparent diffusion coefficient for differentiation of glioblastoma multiforme from solitary metastatic lesions. AJR. 2011;196:71–6.
23. Okada H, Weller M, et al. Immunotherapy response assessment in neurooncology: a report of the RANO working group. Lancet Oncol. 2015;16:e534–42.

PET Tracers for Brain Imaging

3

Christine Tang and Vincenzo Militano

Contents

3.1 Introduction

Positron emission tomography (PET) is an imaging technology developed to use compounds radiolabelled with positron emitting radioisotopes to image biochemical and molecular properties in vivo. The use of molecular imaging include diagnosing the biological nature of disease and assessment of therapies [1]. 2-[^{18}F] Fluoro-2-deoxyglucose (FDG) is the most widely available tracer used in PET neuroimaging to image cerebral metabolism of glucose.

FDG-PET has been used since the 1970s to examine glucose transport across the cell and phosphorylation. Neuronal glucose metabolism can be increased with synaptic activity or reduced from neural degeneration or dysfunction at the level of the pre or post synapse [2]. There are limitations posed with FDG-PET, for instance, in neuro-oncology imaging, the high baseline glucose metabolic rate of normal brain tissue can lead to underdetection of low-grade tumours or recurrent high-grade tumour post-treatment. Since the development of FDG, several novel PET

C. Tang (✉) · V. Militano
Institute of Nuclear Medicine, University College of London Hospital, London, UK
e-mail: christinetang@nhs.net

F. Fraioli (ed.), *PET/CT in Brain Disorders*, Clinicians' Guides to Radionuclide Hybrid Imaging, https://doi.org/10.1007/978-3-030-01523-7_3

radiotracers over the last decade have been approved by the US Food and Drug Administration (FDA). The findings in PET research are promising in providing information on the neurological processes in normal-functioning brain and pathological diseases which can be overlapping clinically. A comprehensive discussion of all PET radiotracers is beyond the scope of this chapter; instead a summarised overview of some of the most used and few experimental non-FDG-PET tracers used in neuroimaging will be discussed.

3.2 Neurodegenerative

The two main neurodegenerative disorders of interest are Alzheimer's and Parkinson's disease. They are associated with misaggregated proteins; therefore these are targeted by radiotracers to detect and quantify these proteins including amyloid beta, tau and α-synuclein.

Deposition of beta-amyloid is the neuropathological hallmark of Alzheimer's disease (AD) which results in formation of neurofibrillary tangles and the loss of neurons and synapses. Amyloid imaging with ^{11}C-labelled Pittsburgh compound B (PIB) was first reported in 2004 [3]. PIB is a radioligand which crosses the blood-brain barrier and binds to amyloid plaques [3]. The limiting factor with this radioligand is the relatively short half-life of ^{11}C which requires a cyclotron on-site for isotope production. As a result of this limited clinical use, fluorine-18 amyloid beta (Aβ)-specific radiolabelled tracers have been developed for clinical use: florbetapir, flutemetamol and florbetaben which are FDA approved. These amyloid radiotracers have variable kinetic behaviours, Aβ binding and different interpretation criteria for positive studies. The binding to white matter is more variable amongst the ^{18}F-labelled tracers when compared with PIB; however the quantification of cortical Aβ deposition has been found to be comparable with PIB [4, 5]. Currently first-generation ^{18}F Aβ radiotracers have been studied, and further clinical trials will be required to standardise imaging protocol and interpretation criteria. A further ^{18}F radiotracer, NAV4694, is undergoing clinical trials. The regional uptake and distribution in the brain of this radioligand to Aβ deposition are similar in profile to the aforementioned ^{18}F Aβ radiotracers. It has been reported to have high affinity with amyloid fibrils in vitro. Further comparative studies are still being investigated [6].

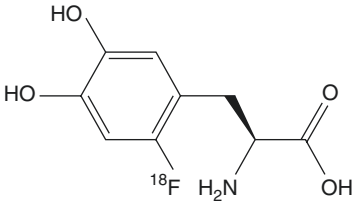

6-[^{18}F]-fluoro-DOPA

Fig. 3.1 The radiopharmaceutical structure of L-FDOPA, an aromatic amino acid

The neuropathological hallmark of Parkinson's disease (PD) is characterised by a combination of abnormal protein aggregation and loss of selective neurons with involvement of serotonergic, cholinergic and noradrenergic pathways.

The loss of dopaminergic neurons in the substantia nigra is the pathological hallmark of Parkinson's disease. PET with radioligands can target these pre-dopaminergic markers and is used to measure dopaminergic function. These include dopa decarboxylases (^{18}F-DOPA) (Fig. 3.1) and vesicular monoamine transporter type 2 [7]. ^{18}F-DOPA uptake in the striatum is determined by the number of functioning dopaminergic cells. There is a reduced striatal uptake typically in the rostrocaudal axis. ^{18}F-DOPA uptake in the striatal and extrastriatal regions can provide information on the clinical behaviour of this neurodegenerative disease and the types of compensatory mechanisms which occurs with disease progression [8].

3.3 Neuroinflammation

Neuroinflammation is the central nervous system's (CNS) immune response to cell injury with activation of microglial cells. This inflammatory process has been implicated also in many neurodegenerative disorders such as AD, PD and frontotemporal dementia which can lead to chronic cerebral damage. In addition to microglial cell activation, there is upregulation of the peripheral benzodiazepine receptor, 18 kDa-translocator protein (TSPO) in neuroinflammation [9]. Increase in TSPO density acts a biomarker of microglial activation and neuroinflammation and thought to be an ideal imaging target to monitor disease progression and therapeutic efficacy of novel treatments in neurodegenerative disorders [9, 10]. Radioligands targeting TSPO expression have been the most studied in the past two decades. The most widely used TSPO radiotracer is a [^{11}C] PK11195 (Fig. 3.2), a lipid soluble 3-isoquinoline carboxamide which was first developed in the 1980s [11]. However there are technical limitations with this radiotracer including poor signal-to-noise ratio due to non-specific binding, low penetration in the brain, high plasma binding and the short half-life of carbon-11 (20 min) [11, 12]. This has resulted in the

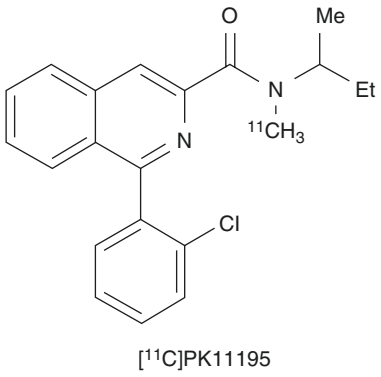

Fig. 3.2 The radiopharmaceutical structure of the TSPO radiotracer, [^{11}C] PK11195

development of second-generation TSPO PET tracers which are currently evaluated. These PET tracers include phenoxyarylacetamides derivatives labelled with carbon-11 (^{11}C-PBR28, ^{11}C-DAA1106) or fluorine-18 (^{18}F-FEPPA (Fig. 3.2), ^{18}F-PBR06), pyrazolopyrimidines derivatives (^{18}F-DPA-714) and imidazopyridines derivatives (^{11}C-CLINME).

These second-generation radioligands demonstrate different binding affinity depending on genetic polymorphism divided into low-affinity, mixed-affinity and high-affinity binders [12]. A recent study by Kreisl et al. [13] demonstrated increased binding of the TSPO radioligand ^{11}C-PBR28 to different regions of the brain including the inferior parietal lobe, precuneus, middle and inferior temporal cortex, hippocampus and occipital cortex in AD patients when compared with control. This radioligand may have a potential role as a biomarker in evaluating AD progression [13]. These findings have yet to be replicated and confirmed in larger studies. These second-generation TSPO radioligands are still undergoing clinical trials with currently few comparative studies (between first- and second-generation tracers) performed. In the published studies in literature, there remains heterogeneity in methodology and results. Currently there is insufficient evidence of reliable microglial activation detection with novel TSPO radioligands [10, 11].

3.4 Neuro-oncology

The fundamental qualities of tracers used in brain tumour imaging would be the ability to transport across the blood-brain barrier (BBB) and imaging the metabolic reaction within cells [14]. Over the past decade, there has been growing interest in seeking novel radiotracers in brain tumour imaging to overcome limitations posed by FDG-PET [15]. The most relevant non-FDG-PET tracers used in neuro-oncology imaging include amino acid and nucleoside radiotracers.

Common amino acid radiotracers utilised in brain tumour imaging include the following radiotracers: ^{18}F labelled amino acid O-(2-[^{18}F]-fluoroethyl)-L-tyrosine (^{18}F-FET) (Fig. 3.3), L-[methyl-^{11}C]methionine [MET] and ^{18}F-fluoro-L-dihydroxyphenylalanine (FDOPA). One of the PET imaging qualities is detecting amino acid metabolism. Protein synthesis is upregulated in tumour tissue with elevated proliferative activity which makes amino acids labelled analogues ideal imaging markers of tumour growth [15, 16]. The common transporter mechanism utilised by the aforementioned radiotracers is the L amino acid transporters, with LAT1 being

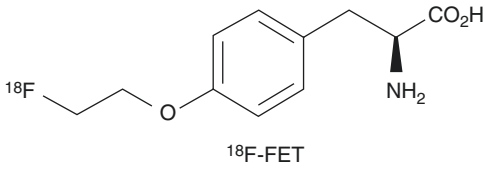

Fig. 3.3 The radiopharmaceutical structure of ^{18}F-FET

widely expressed in cancer cell lines and LAT2 in non-cancer cells. After transportation across the BBB and into the tumour, a number of metabolic reactions can occur which can be utilised in imaging and are fundamental features in brain tumour radiotracers [17].

The use of the nucleoside PET radiotracers [F-18]FLT (3′-deoxy-3′-fluorothymidine) was first developed by Grierson and Shields in the 1990s [18]. FLT is used in glioma tumour detection and treatment response assessment. This radiotracer measures the level of cellular thymidine kinase activity which is proportional to tumour cell proliferative activity. The limitations of this tracer occur at the level of the BBB in low-grade gliomas. Penetration is poor in intact BBB in low-grade gliomas.

3.5 Conclusion

Nuclear imaging is growing in all areas of neuroimaging providing cellular and molecular information. Over the past four decades since the introduction of FDG-PET, there have been a growing number of radiotracers developed and undergoing clinical research, used to target neural receptors and transporters underlying normal and pathological neural processes. In vivo PET imaging provides a noninvasive method in advancing our knowledge of the neuropathological processes, disease evolution and treatment response in many neurodegenerative, neuroinflammatory and neurooncological disorders. Further validation in large clinical trials in order to assess the diagnostic and prognostic value of novel second line radiotracers is required prior to translation into clinical practice. A ‘gold standard’ in diagnosing or evaluating some of the aforementioned neuropathological diseases does not exist. In the future this maybe a combination of multimodality and multi-tracer imaging in order to identify early disease, differentiate from overlapping disease processes and provide prognostic information [16, 19, 20].

Key Points

- ^{18}F-FDG is the most widely available tracer used in PET neuroimaging to image cerebral metabolism of glucose.
- Neuronal glucose metabolism can be increased with synaptic activity or reduced from neural degeneration or dysfunction at the level of the pre- or post-synapse.
- The limitations of FDG-PET in neuro-oncology imaging are related to the high baseline glucose metabolic rate of normal brain tissue which can lead to underdetection of low-grade tumours or recurrent high-grade tumour posttreatment.

- Deposition of beta-amyloid is the neuropathological hallmark of Alzheimer's disease (AD) which results in formation of neurofibrillary tangles and the loss of neurons and synapses
- Fluorine-18 amyloid beta (Aβ)-specific radiolabeled tracers, which cross the blood-brain barrier and bind to amyloid plaques, have been developed for clinical use.
- The loss of dopaminergic neurons in the substantia nigra is the pathological hallmark of Parkinson's disease.
- ^{18}F-DOPA uptake in the striatum is determined by the number of functioning dopaminergic cells.
- Neuroinflammation process has been implicated in many neurodegenerative disorders.
- Increase in TSPO density acts a biomarker of microglial activation and neuroinflammation.
- The most widely used TSPO radiotracer is a [^{11}C] PK11195; however there are technical limitations with this radiotracer including poor signal-to-noise ratio due to non-specific binding, low penetration in the brain, high plasma binding, and the short half-life of carbon-11 (20 min).
- The second-generation TSPO radioligands are still undergoing clinical trials with currently few comparative studies (between first- and second-generation tracers) performed.
- The non-FDG-PET tracers used in neuro-oncology imaging include amino acid and nucleoside radiotracers.
- Common amino acid radiotracers utilized in brain tumour imaging are ^{18}F-FET, ^{11}C-MET, and ^{18}F-DOPA.
- The transporter mechanism utilized by the amino acid radiotracers is the L amino acid transporters, with LAT1 being widely expressed in cancer cell lines and LAT2 in non-cancer cells.
- The nucleoside PET radiotracer ^{18}F-FLT was first developed by Grierson and Shields in the 1990s.
- ^{18}F-FLT measures the level of cellular thymidine kinase activity which is proportional to tumour cell proliferative activity.

References

1. Phelps ME. Positron emission tomography provides molecular imaging of biological processes. Proc Natl Acad Sci U S A. 2000;97:9226–33.
2. Kato T, Inui Y, Nakamura A, Ito K. Brain fluorodeoxyglucose (FDG) PET in dementia. Ageing Res Rev. 2016;30:73–84.
3. Klunk WE, Engler H, Nordberg A, Wang Y, Blomqvist G, Holt DP, et al. Imaging brain amyloid in Alzheimer's disease with Pittsburgh Compound-B. Ann Neurol. 2004;55:306–19.
4. Landau SM, Breault C, Joshi AD, Pontecorvo M, Mathis CA, Jagust WJ, et al. Amyloid-β imaging with Pittsburgh compound B and florbetapir: comparing radiotracers and quantification methods. J Nucl Med. 2013;54:70–7.
5. George N, Gean E, Nandi A, Brašić JR, Wong DF. Radiotracers used to image the brains of patients with Alzheimer's disease. In: Imaging of the human brain in health and disease. Amsterdam: Elsevier; 2014. p. 407–16.
6. Cselényi Z, Jönhagen ME, Forsberg A, Halldin C, Julin P, Schou M, et al. Clinical validation of 18F-AZD4694, an amyloid-β-specific PET radioligand. J Nucl Med. 2012;53:415–24.
7. Politis M, Pagano G, Niccolini F. Imaging in Parkinson's disease. Int Rev Neurobiol. 2017;132:233–74.
8. Pavese N, Brooks DJ. Imaging neurodegeneration in Parkinson's disease. Biochim Biophys Acta Mol basis Dis. 2009;1792:722–9.
9. Dupont AC, Guilloteau D, Kassiou M, Ribeiro MJ, Vercouillie J, Katsifis A, et al. Radiopharmaceuticals for PET imaging of neuroinflammation. Med Nucl. 2016;40:72–81.
10. Cerami C, Iaccarino L, Perani D. Molecular imaging of neuroinflammation in neurodegenerative dementias: the role of in vivo PET imaging. Int J Mol Sci. 2017;18:993.
11. Dupont A-C, Largeau B, Santiago Ribeiro M, Guilloteau D, Tronel C, Arlicot N. Translocator protein-18 kDa (TSPO) positron emission tomography (PET) imaging and its clinical impact in neurodegenerative diseases. Int J Mol Sci. 2017;18:785.
12. Ghadery C, Koshimori Y, Coakeley S, Harris M, Rusjan P, Kim J, et al. Microglial activation in Parkinson's disease using [18F]-FEPPA. J Neuroinflammation. 2017;14:8.
13. Kreisl WC, Lyoo CH, Liow J-S, Wei M, Snow J, Page E, et al. (11)C-PBR28 binding to translocator protein increases with progression of Alzheimer's disease. Neurobiol Aging. 2016;44:53–61.
14. Herholz K. Brain tumors: an update on clinical PET research in gliomas. Semin Nucl Med. 2017;47:5–17.
15. Basu S, Alavi A. Molecular imaging (PET) of brain tumors. Neuroimaging Clin N Am. 2009;19:625–46.
16. Gulyás B, Halldin C. New PET radiopharmaceuticals beyond FDG for brain tumor imaging. Q J Nucl Med Mol Imaging. 2012;56:173–90.
17. Juhász C, Dwivedi S, Kamson DO, Michelhaugh SK, Mittal S. Comparison of amino acid positron emission tomographic radiotracers for molecular imaging of primary and metastatic brain tumors. Mol Imaging. 2014;13 https://doi.org/10.2310/7290.2014.00015.
18. Shields AF, Grierson JR, Dohmen BM, Machulla H-J, Stayanoff JC, Lawhorn-Crews JM, et al. Imaging proliferation in vivo with [F-18]FLT and positron emission tomography. Nat Med. 1998;4:1334–6.
19. Borbely K, Wintermark M, Martos J, Fedorcsak I, Bognar L, Kasler M. The pre-requisite of a second-generation glioma PET biomarker. J Neurol Sci. 2010;298:11–6.
20. Zimmer L, Luxen A. PET radiotracers for molecular imaging in the brain: past, present and future. Neuroimage. 2012;61:363–70.

^{18}F-FDG PET/CT: Brain Imaging

4

April-Louise Smith and Anna Barnes

Contents

4.1 Introduction

^{18}F-2-Fluoro-2-deoxyglucose (^{18}F-FDG) can be used to image regional cerebral glucose consumption which allows diagnostic imaging for a number of neurological indications such as dementia, epilepsy and movement disorders. Although not often used in neuro-oncology, it remains the method of choice in the diagnosis and staging of CNS lymphoma. Adhering to guidelines for patient preparation, using the correct imaging acquisition and reconstruction parameters, as well as defining the optimal image display for reporting are all crucial in order to obtain images of diagnostic quality. Furthermore, reporting images in the presence of neurological degenerative diseases can benefit hugely using additional

A.-L. Smith (✉) · A. Barnes
Institute of Nuclear Medicine, University College London Hospital NHS Foundation Trust, London, UK
e-mail: april-louise.smith@nhs.net

F. Fraioli (ed.), *PET/CT in Brain Disorders*, Clinicians' Guides to Radionuclide Hybrid Imaging, https://doi.org/10.1007/978-3-030-01523-7_4

post-processing and quantification of the images [1, 2]. This chapter summarises published guidelines, at the time of writing, on optimal imaging procedures for brain ^{18}F-FDG PET/CT and introduces the reader to some of the more widely available quantification tools and references for optional further reading of developments in the field.

4.2 Patient Preparation

Patient preparation is broadly similar for all ^{18}F-FDG imaging studies; patients should fast prior to injection. European and American guidance advise 4–6 h [3, 4] to prevent competition between elevated plasma glucose and FDG, especially since the injected volume is at trace concentrations. For this reason it is also recommended that blood glucose levels are checked before administration; European and American guidelines state that patients should be rescheduled if glucose levels are >160 mg/dL [1] or >150–200 mg/dL [2], respectively, and also give recommendations for diabetic patients. Caffeine, alcohol or drugs that may affect cerebral glucose metabolism must also be avoided [5] during the fasting period. Patients are required to stay in a quiet and dimly lit room for several minutes prior to injection and during the uptake phase to avoid enhanced uptake due to brain activity [6] typically in the visual and/or auditory cortex. So for interictal epilepsy imaging, it is important to ensure the patient has not had a recent seizure and the activity is not administered unless the patient has been seizure-free for at least 20 min [3, 4] since for this test the associated affected cortex is detected as a region of hypo-glucose metabolism during the interictal state. There have been some studies that suggest the patient should be seizure-free for at least 24 h prior to imaging since glucose hypermetabolism after a partial seizure may not return to baseline immediately [5, 7]. In the clinical setting, this may not be feasible, but it remains essential that the reporting radiologist is aware of seizure activity that may have occurred prior to imaging. In fact both European and American guidelines suggest EEG monitoring for 2 h prior to injection could help in this regard.

4.3 Imaging Protocol

Table 4.1 outlines the recommended administered activity in the UK for ^{18}F-FDG brain imaging, and associated doses taken from the Administration of Radioactive Substances Advisory Committee (ARSAC) note for guidance [8]. Paediatric administered activity should be kept to a minimum but while still allowing for acceptable image quality. To ensure a robust signal, the reduced activity can be calculated using scaling factors for appropriate patient weights. ARSAC guidance supports advice on scaling provided by the European Association of Nuclear Medicine (EANM) [9] but are of the view that more research is required and further optimisation should be conducted locally. As with all PET/CT, imaging pregnancy is contraindicated.

Table 4.1 ARSAC guidance for administered activity and associated patient dose [8]

Investigation	Radionuclide	Chemical form	Diagnostic reference level (MBq)	Effective dose (mSv)	Dose to the uterus (mGy)
Brain tumour imaging	^{18}F	FDG	250	4.8	4.5
Differential diagnosis of dementia					
Focal epilepsy					

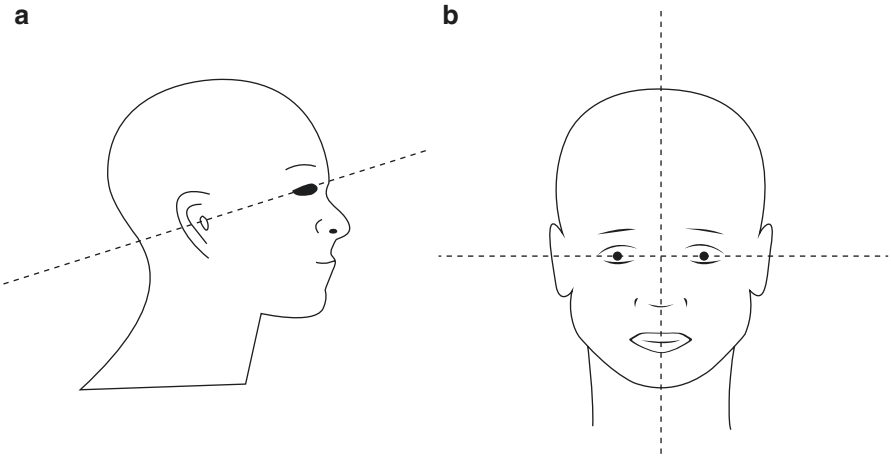

Fig. 4.1 Patient positioning for brain imaging. (**a**) Orbital-meatal plane (**b**) Median sagittal plane

After the injection the patient should remain in a quiet darkened room for a minimum of 30 min [3], although a longer uptake time is useful for neuro-oncological applications since it can give better differentiation between tumour and normal brain tissue. In fact, a longer time of 60 min is usually used in clinical practice since this allows better contrast between white and grey matter in the cortex and still provides sufficient counts for acceptable image quality. It would be advisable, however, for the uptake time to be decided locally and standardised for repeatability; for example, in a busy nuclear medicine department, it is also easier to schedule alongside other FDG PET/CT imaging of the body which requires a minimum 60 min uptake for optimal imaging in oncology, and the ability to schedule PET/CT imaging efficiently should not be taken lightly.

Once sufficient uptake time has passed, the patient should be carefully positioned, aligning the orbital-meatal plane in the *x*-axis and median sagittal plane in the *y*-axis as demonstrated by the diagram in Fig. 4.1.

Modern PET scanners operate in 3D image acquisition mode (as opposed to 2D with collimation) which allows acceptable image quality with 50–200 million detected events [3]; this can equate to scanning times of 10–30 min depending on the scanner sensitivity. Reconstruction of PET images uses an iterative technique which combines information about the scatter properties of the radionuclide as well as the geometry of the scanner to improve image contrast and signal to noise ratio [10]. The last step to providing images for reporting by the radiologist is to apply attenuation correction to account for the attenuating properties of the tissue through which the photon passes. In order to apply this correction, an attenuation map is created using either a transmission scan (a photon source that rotates around the patients head before the scan) or for hybrid scanners, a low-resolution CT or MR image for PET/CT and PET/MRI, respectively. Figure 4.2a shows a uniform region of a phantom with no attenuation correction, giving the appearance of

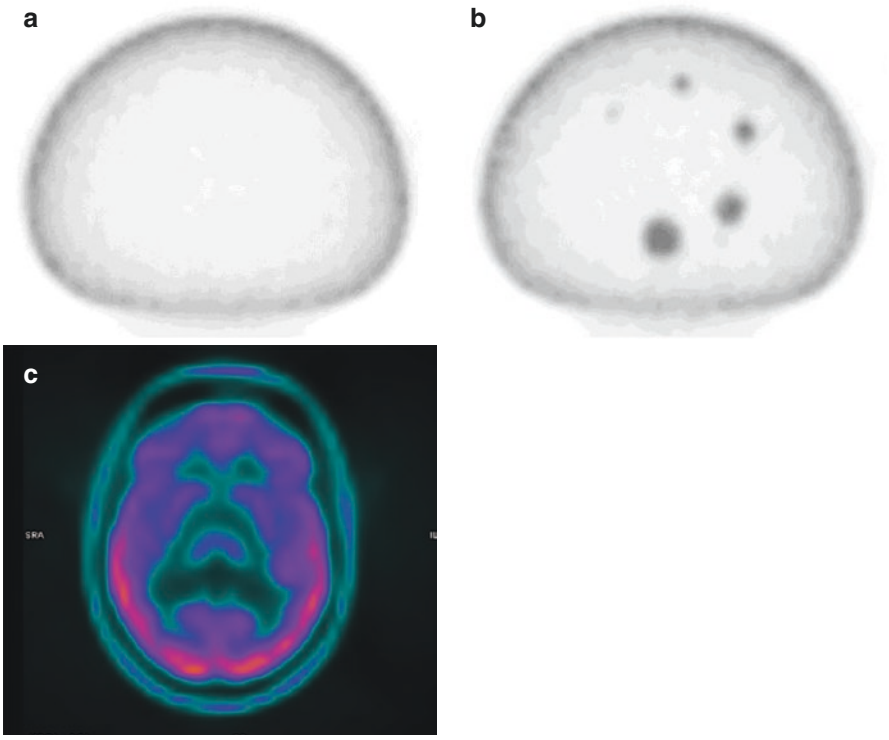

Fig. 4.2 Images with no attenuation correction. (**a**) Uniform area of phantom. (**b**) Active spheres in image quality phantom. (**c**) Example patient ^{18}F-FDG brain image

higher activity at the edge of the phantom. In Fig. 4.3a, the CT attenuation correction has corrected for the counts lost from the centre of the phantom, giving a more uniform appearance. The importance of this correction is further highlighted by Figs. 4.2b and 4.3b where you can see the spheres are clearer in the corrected image (Fig. 4.2b) with better image contrast. Figure 4.2c illustrates this effect on a brain image showing the reduction of detail seen compared to the attenuation corrected image (Fig. 4.3c). One of the recent developments in PET scanner technology is that of PET/MRI a hybrid scanner that is able to image using PET and MR simultaneously. Unlike x-ray CT, the intensity values within a MR image are not directly related to the attenuating properties of the tissue and so a pseudo-CT must be created by assigning a fixed CT value to certain categories of tissue, cortical bone, brain and air (see Fig. 4.4). However, imperfections in the complete

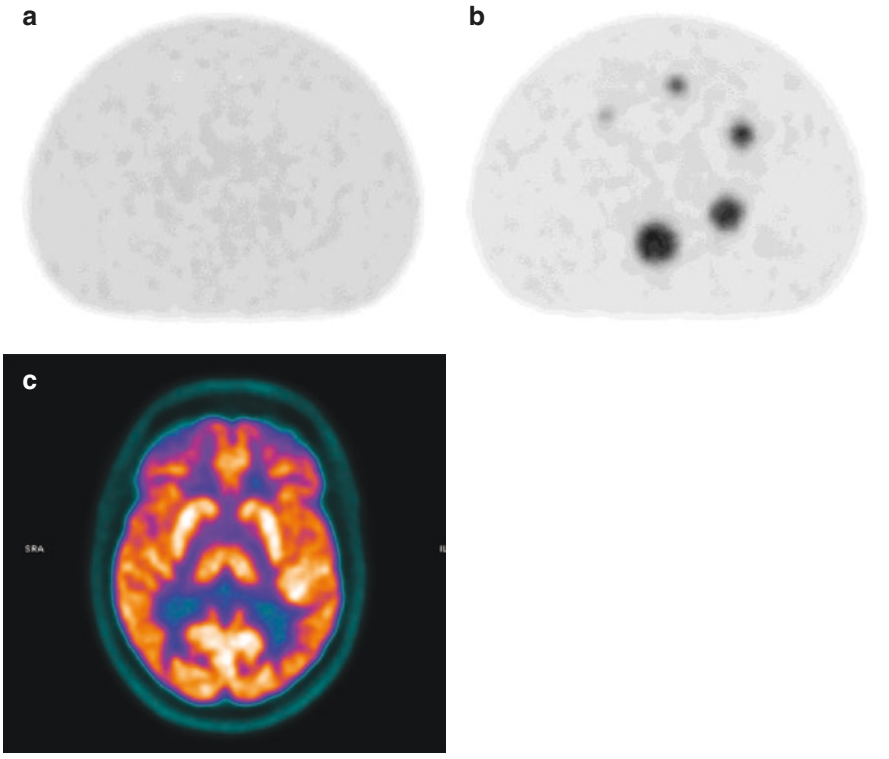

Fig. 4.3 Images with attenuation correction. (**a**) Uniform area of phantom. (**b**) Active spheres in image quality phantom. (**c**) Example patient ^{18}F-FDG brain image

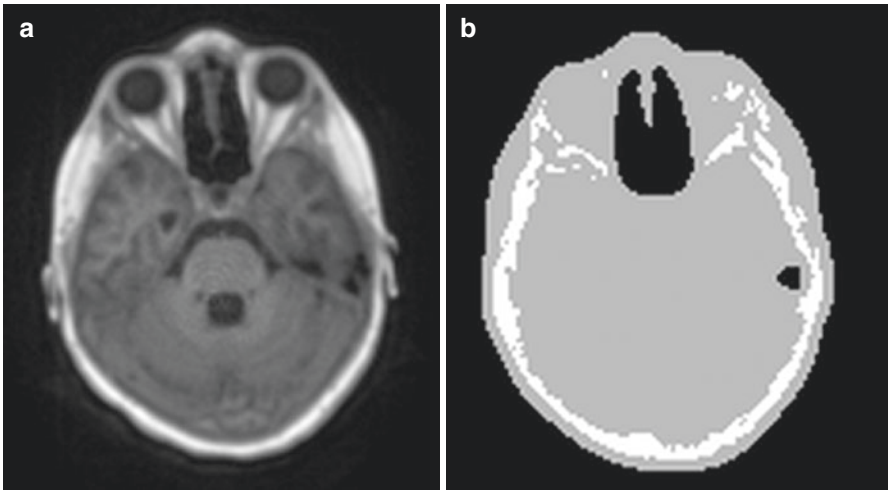

Fig. 4.4 PET/MR attenuation correction map. (**a**) MR UTE image used to create the μ-map. (**b**) MR μ-map showing the different categories (brain, bone and air) tissues has been assigned to

representation of cortical bone in the image can lead to discrepancies in tracer uptake values [11].

Image acquisition can take anywhere between 10 and 30 min, and therefore it is essential to ensure that steps are taken to prevent patient movement both during the acquisition and between the CTAC or MRAC and the PET. A radiographer/nuclear medicine technologist will clearly explain the procedure to the patient and the requirement to remain still. Once the patient has been placed in the preferred orientation (this may be harder in elderly patients due to limited flexibility), they should be restrained but made to feel comfortable by using padding or bandages to hold the head in place. Another measure that can be taken is to acquire the data dynamically (using list mode) and to allow the data to be checked for movement after acquisition (e.g. by reconstructing images at short frame durations), and then the final image is compiled from the frames unaffected by motion. Guidance on image reconstruction is provided by EANM [3].

4.4 Image Processing and Display

Once reconstructed, it is important to ensure that the images are correctly displayed in a standard anatomical position in order to ensure consistent reporting and avoid potential artefacts in the image (Fig. 4.5). This is particularly important in reporting of interictal epilepsy images where asymmetries in the uptake pattern in the temporal lobes are indicative of seizure focus. Although software can be used to align the images in post-processing, correct patient positioning helps this process. The images can also be co-registered with high-resolution x-ray CT or MR for structural

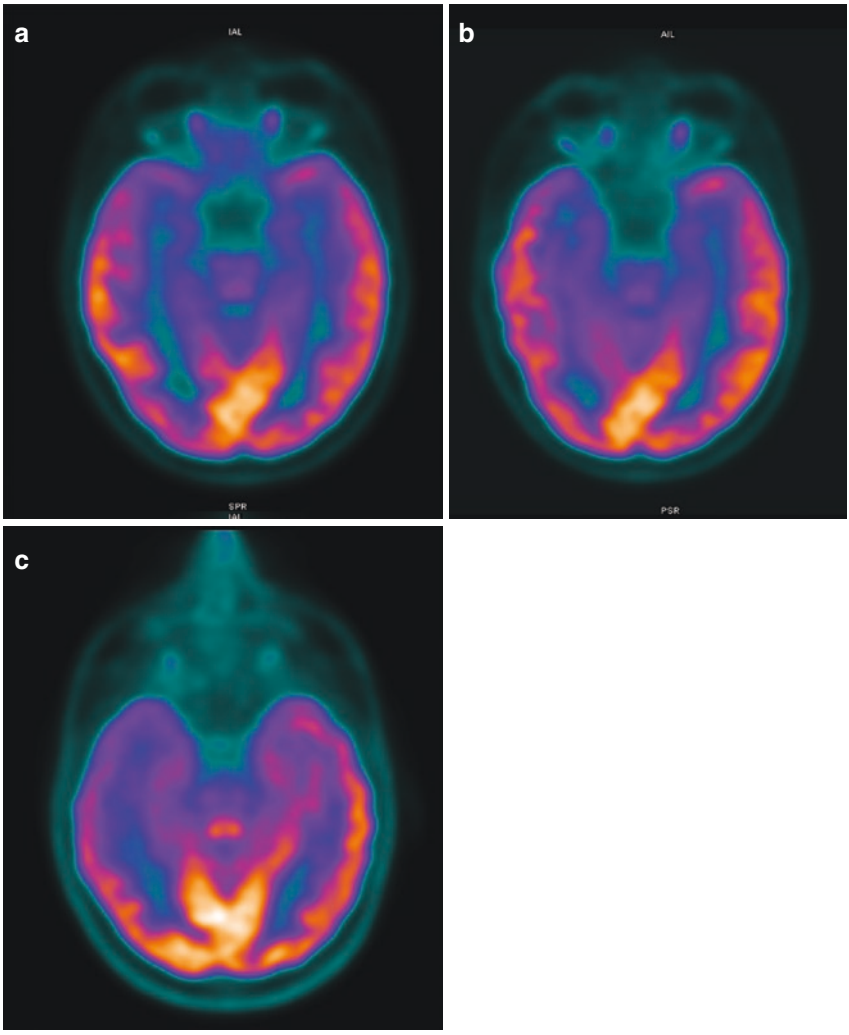

Fig. 4.5 An example of two[18]F-FDG brain PET/CT patient images with indication of epilepsy. The images show how misalignment can contribute to image artefacts. (**a**) Patient 1: A [18]F-FDG brain PET/CT epilepsy scan with normal uptake that has been correctly aligned. (**b**) Patient 1: The same patient with the images rotated in the coronal plane giving an impression of asymmetry in uptake and the potential to be incorrectly reported as the right temporal lobe epilepsy. (**c**) Patient 2: A correctly aligned patient with right temporal lobe epilepsy for comparison

comparisons and anatomical localisation. Images can be displayed in the transaxial, coronal and sagittal planes for reporting, as shown in Figs. 4.6 and 4.7. Further orientations can be used such as the long axis of the temporal lobes (Fig. 4.7c) to provide a more informative representation of the medial temporal lobe in the reporting of interictal images.

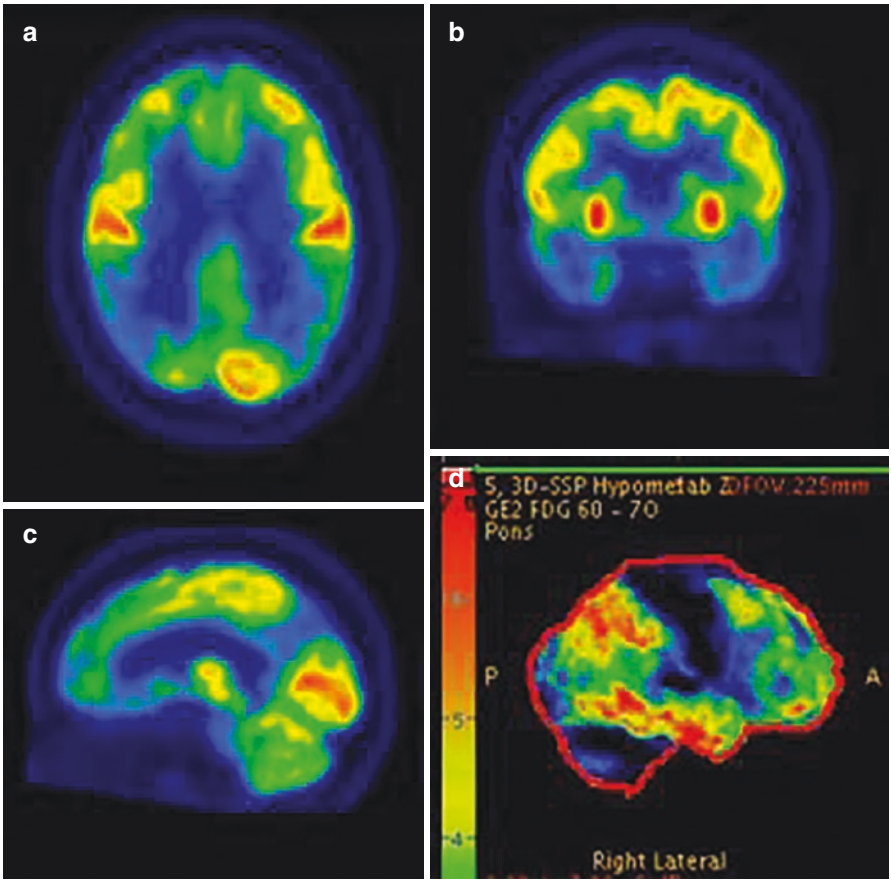

Fig. 4.6 ^{18}F-FDG brain PET/CT for dementia showing optimal display as well as 3D-SSP (stereotactic surface projections) with typical patterns of reduced uptake indicative of Alzheimer's disease. (**a**) Transaxial slice. (**b**) Coronal slice. (**c**) Sagittal slice. (**d**) 3D-SSP showing significant areas of reduced uptake (normalised to pons). Panel **d** demonstrates surface-rendered images of the statistical analysis. Showing a *z*-score map normalised using the pons with a threshold of $z > 2$

4.5 Quantification

There are a variety of PET analysis methods to quantify functional information related to neurodegenerative disease. There are several commercial software packages available (CortexID, GE; Scenium, Siemens; BRASS, Hermes; Vista, MIM and more); none are approved to be used without the supervision of a radiologist that provides this quantitative information to assist with the visual reporting of images. What all these software packages have in common is an image realignment

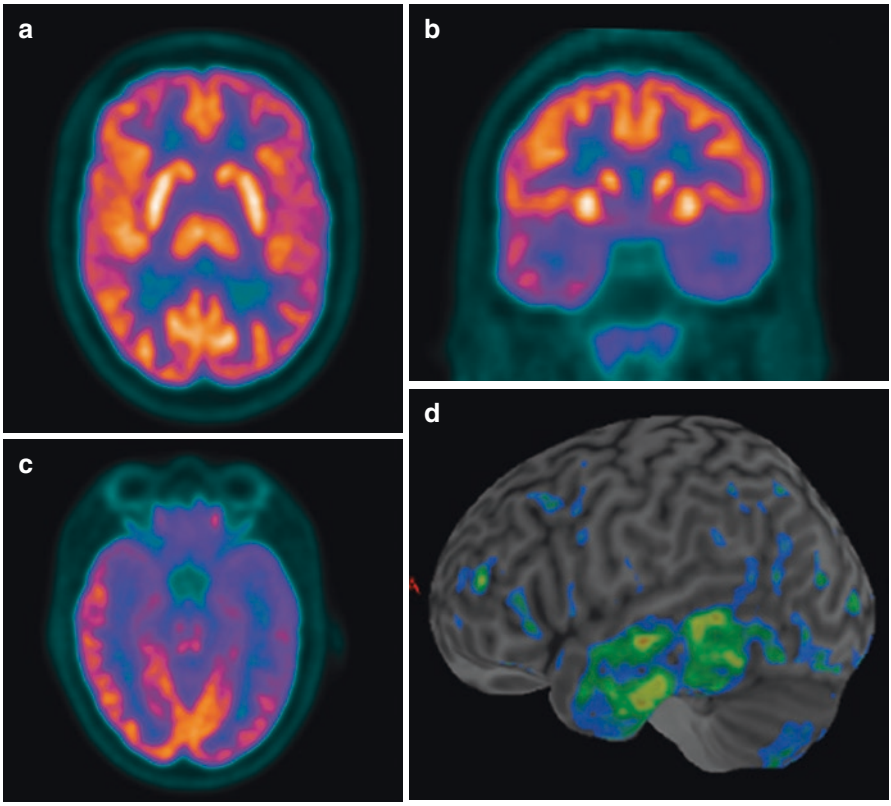

Fig. 4.7 ^{18}F-FDG brain PET/CT for epilepsy image showing hypometabolism in left temporal lobe. (**a**) Transaxial slice. (**b**) Coronal slice. (**c**) Temporal slice. (**d**) Surface-rendered images of the statistical analysis (3D-SSP), showing significant areas of reduced uptake. This is a *z*-score map normalised using the global mean with a threshold of $z > 2$ and overlaid on the patient MRI. This clearly identifies reduced metabolic activity in the left temporal lobe (Cortex ID, GE Healthcare)

step to previous images for longitudinal evaluation or to other modalities for visualisation and display, a co-registration step to standard anatomical templates for statistical comparisons against normal patient databases and univariate or multivariate statistical analysis tools for this purpose, including some kind of intensity normalisation step to account for differences in global measured activity between patients. Statistical comparisons can be done using regions of interest (ROI) or on a voxel-by-voxel basis. Most use simple t-tests or a number of standard deviations to map abnormal regions (Scenium and Cortex ID); other more sophisticated methods use multivariate-type statistics to look at how well each individual patient's pattern fits to an expected pathological pattern [12], e.g., the pattern of regional cerebral glucose metabolism associated with Parkinson's disease.

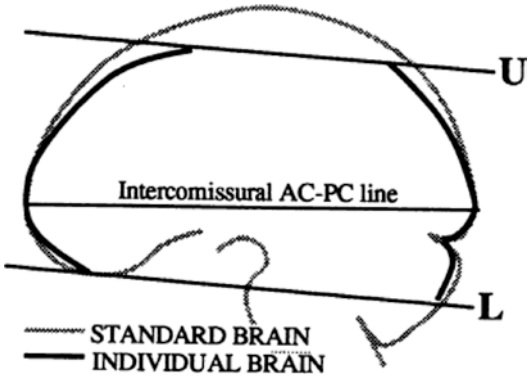

Fig. 4.8 Diagram of AC-PC line for the standard and individual brain for anatomical localisation [16]

4.5.1 Anatomical Standardisation

In order to statistically compare patient images to a control database, the patient image is anatomically standardised, often referred to as spatial normalisation. There are a number of different image templates or brain atlases available [13] that are created from an average of a number of normal datasets such as the Montreal Neurological Institute (MNI) templates [14, 15]. Images are re-orientated, transformed and warped to map the patient image to the template image in standard space [13, 16]. Spatial co-ordinates *x*, *y* and *z*, with reference to the *x*-axis through the Anterior Commissure-Posterior Commissure (ac-pc) line (Fig. 4.8), can then be used to anatomically localise abnormalities in the PET images [13, 17].

4.5.2 Intensity Normalisation

Once the patient study has been mapped to standard space, in order to perform a comparison with metabolic FDG uptake, the dataset must also be normalised for the relative intensity. This is to account for non-pathological differences in uptake for intra-subject comparison and between the patient study and the control database due to differences in imaging protocol, such as differences in administered activity. There are a number of options for intensity normalisation. One option is to simply take the total global counts and normalise to the cerebral global mean. However this can introduce bias if there are large outliers that skew the mean value. To avoid this sort of phenomenon, a reference region can be chosen that is known to be less affected by the disease process; cerebellum, thalamus or pons are popular choices depending on the indication. For example, it is common to use the cerebellum for both differential diagnosis of Alzheimer's disease or for seizure focus localisation in epilepsy. For others, it can be difficult to find an unaffected region. Data-driven intensity normalisation techniques for PET images have also been used to overcome these issues [18].

Figure 4.9 shows an example of statistical analysis for a ^{18}F-FDG scan for a pre-surgical epilepsy patient using Cortex ID. All four images show the same patient

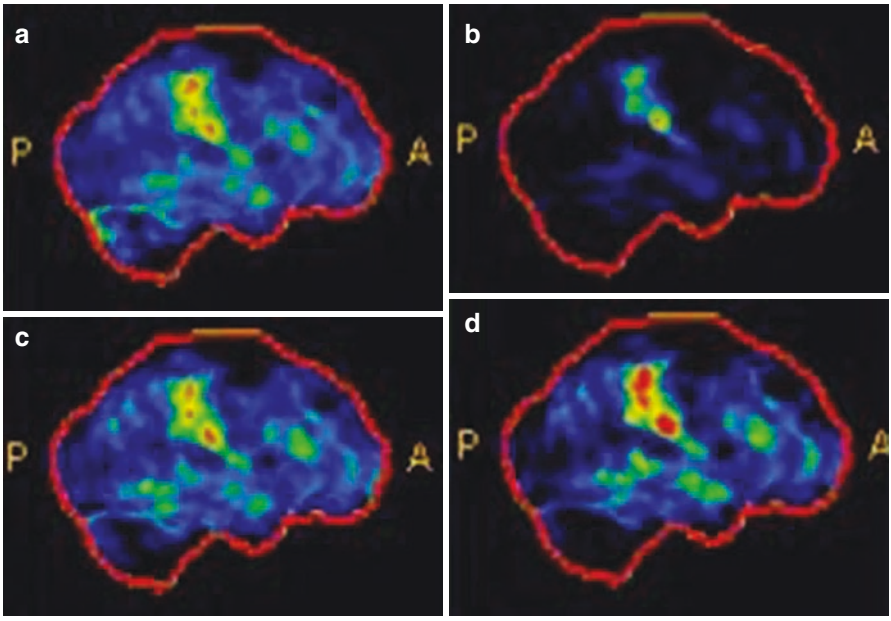

Fig. 4.9 Example patient statistical surface projections, showing effects of intensity normalisation method, processed on commercial software (Cortex ID, GE Healthcare). (**a**) Cerebellum. (**b**) Thalamus. (**c**) Pons. (**d**) Global mean

with different normalisations, (a) cerebellum, (b) thalamus, (c) pons and (d) global cortical mean), illustrating how the chosen normalisation method can affect the results.

4.5.3 Statistical Analysis

The same statistical analysis methods can be used to statistically evaluate ROI-based data as well as voxel-wise data. In this chapter we will use voxel-by-voxel data to describe the method, but ROI could be substituted. Now that the individual patient data has been spatially normalised and intensity normalised a statistical analysis that compares this patient's image to the normal database, image can be performed at each voxel. For example, a z-score can be calculated where z is the number of standard deviations of the patient's voxel value away from the mean voxel value in the normal database. It is important that the age range of individuals that make up the normal database should not be significantly different from that of the patient, as there are known to be systematic differences in cortical glucose metabolism with respect to age [19]. A z-score map can then be displayed onto a corresponding anatomical image or onto a cortical surface rendering where $z < 0$ shows hypermetabolism and $z > 0$ shows hypometabolism (Figs. 4.5d and 4.7d). This allows a threshold to be set to show only the voxels above this threshold (typically z~2 corresponding to a p value of 0.05) on a surface rendered image.

4.5.4 Limitations

There are limitations to voxel-based statistical analysis which users should be aware of when reporting. Transformation errors can occur when mapping an individual's unique anatomical variations on to the template used to create the standard space. This may lead to incorrect deformations and incorrect mapping of brain structures. Spatial smoothing can ameliorate this effect to some extent, but if the anatomical deviation is, for example, unusual brain anatomy, atrophy, surgical resection or of a different age to the template used, then gross mismatches can occur. For paediatric populations cortical gyral folding is age dependent and has been shown not to map to adult MNI standard space terribly well [20] and the normal cortical glucose metabolic rate in children under the age of 10 can be distinctly different to that of adults [21, 22]. In this case it is more appropriate to use an age-matched paediatric population [23], and some commercial applications allow the employment of a locally developed database to be used in their pipelines [24]. In conclusion while these automated image analysis pipelines can be useful, the user must be well informed in normal neuroanatomy and physiology as well as the statistical theory used to calculate these visualisation aids.

Key Points

- Caffeine, alcohol or drugs that may affect cerebral glucose metabolism must be avoided for patient preparation and during the fasting period for the scan. Patients are required to stay in a quiet and dimly lit room for several minutes prior to injection and during the uptake phase to avoid enhanced uptake due to brain activity typically in the visual and/or auditory cortex.
- Once sufficient uptake time has passed (30–60 min), the patient should be carefully positioned, aligning the orbital-meatal plane in the x-axis and median sagittal plane in the y-axis. Scan time is dependent on scanner sensitivity and local protocol. To improve image quality attenuation maps can be created to provide attenuation correction and dynamic imaging can provide benefits to account for patient movement. Once reconstructed, it is important to ensure that the images are correctly displayed in a standard and symmetrical anatomical position in order to ensure consistent reporting and avoid potential artefacts in the image (for example in reporting interictal epilepsy an incorrect reconstruction may cause asymmetries in the uptake pattern in the temporal lobes wrongly indicative of seizure focus).
- There are a variety of PET analysis methods to quantify functional information related to neurodegenerative disease. These software packages can realign images to previous images for longitudinal evaluation or to other modalities for visualisation and display and can perform co-registration to standard anatomical templates for statistical comparisons against normal patient databases.

References

1. Purandare NC, Puranik A, Shah S. Common malignant brain tumors: can 18F-FDG PET/CT aid in differentiation? Nucl Med Commun. 2017;38(12):1109–16.
2. Demetriades AK, Almeida AC, Bhangoo RS, Barrington SF. Applications of positron emission tomography in neuro-oncology: a clinical approach. Surgeon. 2014;12(3):148–57. https://doi.org/10.1016/j.surge.2013.12.001. Epub 2014 Mar 11
3. Varrone A, Asenbaum S, Borght TV, Booij J, Nobili F, Nagren K, et al. EANM procedure guidelines for PET brain imaging using [18F]FDG, version 2. Eur J Nucl Med Mol Imaging. 2009;36(12):2103–10.
4. Waxman AD, Herholz K, Lewis DH, Herscovitch P, Minoshima S, Ichise M, et al. Society of nuclear medicine procedure guideline for FDG PET brain imaging. v1. Society of nuclear medicine molecular imaging. 2009.
5. Sarikaya I. PET studies in epilepsy. Am J Nucl Med Mol Imaging. 2015;5(5):416–30.
6. Boellaard R, O'Doherty MJ, Weber WA, Mottaghy FM, Lonsdale MN, Stroobants SG, et al. FDG PET and PET/CT: EANM procedure guidlines for tumour PET imaging. v1. Eur J Nucl Med Mol Imaging. 2010;37(1):181–200.
7. Leiderman DB, Albert P. The dynamics of metabolic change followingseizures as measured by positron emission tomography with fludeoxyglucose F 18. Arch Neurol. 1994;51(9):932–6.
8. Administration of Radioactive Substances Advisory Committee. Notes for guidance on the clinical administration of radiopharmaceuticals and use of sealed radioactive sources. UK: Public Health England; March 2018.
9. Lassmann M, Biassoni L, Monsieurs M, Franzius C, EANM Dosimetry and Paediatrics Committees. The new EANM paediatric dosage card: additional notes with respect to F-18. Eur J Nucl Med Mol Imaging. 2008;35(9):1666–8.
10. Tong S, Alessio AM, Kinahan PE. Image reconstruction for PET/CT scanners: past achievements and future challenges. Imaging Med. 2010;2(5):529–45.
11. Dickson JC, O'Meara C, Barnes A. A comparison of CT- and MR-based attenuation correction in neurological PET. Eur J Nucl Med Mol Imaging. 2014;41(6):1176–89.
12. Spetsieris PG, Ma Y, Dhawan V, Eidelberg D. Differential diagnosis of parkinsonian syndromes using PCA-based functional imaging features. NeuroImage. 2009;45(4):1241–52.
13. Manda PK, Mahajan R, Dinovc ID. Structural brain atlases: design, rationale, and applications in normal and pathological cohorts. J Alzheimers Dis. 2012;31:169–88.
14. Brett M, Johnsrude IS, Owen AM. The problem of functional localization in the human brain. Nat Rev Neurosci. 2002;3:243–9.
15. Mazziotta JC, Toga AW. A probabilistic atlas of the human brain: theory and rationale for its development: the international consortium for brain mapping (ICBM). NeuroImage. 1995;2:89–101.
16. Minoshima S, Koeppe RA, Frey KA, Kuhl DE. Anatomic standardization: linear scaling and nonlinear warping of functional brain images. J Nucl Med. 1994;35(9):1528–37.
17. Minoshima S, Kuhl DE, Foster NL, Koeppe RA, Frey KA. A diagnostic approach in alzheimer's disease using three-dimensional stereotactic surface projections of fluorine-18-FDG PET. J Nucl Med. 1995;36(7):1238–48.
18. Borghammer P, Aanerud J, Gjedde A. Data-driven intensity normalization of PET group comparison studies is superior to global mean normalization. NeuroImage. 2009;46(4):981–8.
19. Shen X, Liu H, Hu H, Shi P. The relationship between cerebral glucose metabolism and age: report of a large brain PET data set. PLoS One. 2012;7(12):e51517.
20. Groeschel S, Vollmer B, King M, Connelly A. Developmental changes in cerebral grey and white matter volume from infancy to adulthood. Int J Dev Neurosci. 2010;28(6):481–9.
21. Van Bogaert P, Wikler D, Damhaut P, Szliwowski H, Goldman S. Regional changes in glucose metabolism during brain development from the age of 6 years. NeuroImage. 1998;8(1):62–8.

22. Kinnala A, Suhonen-Polvi H, Aärimaa T, Kero P, Korvenranta H, Ruotsalainen U, et al. Cerebral metabolic rate for glucose during the first six months of life: an FDG positron emission tomography study. Arch Dis Child Fetal Neonatal Ed. 1996;74(3):153–7.
23. De Blasi B, Barnes A, Galazzo IB, Hua C, Shulkin B, Koepp M, et al. Age-specific ^{18}F-FDG image processing pipelines and analysis are essential for individual mapping of seizure foci in paediatric patients with intractable epilepsy. J Nucl Med. 2018; https://doi.org/10.2967/jnumed.117.203950.
24. Schenk V. Scenium v.1 and PET, white paper paper. USA: Siemens, Medical Solutions; 2006.

5 ^{18}F-FDG-PET/CT (FDG-PET) in Neurodegenerative Disease

Selene Capitanio, Matteo Bauckneht, Dario Arnaldi, Federico Massa, Riccardo Meli, Valentina Ceriani, Flavio Nobili, and Silvia Morbelli

Contents

5.1 Indications

Neurodegenerative diseases are characterized by the progressive degeneration and death of neurons. They represent a heterogeneous group of conditions characterized by different etiologies and different neuropathological and neurochemical alterations leading to different clinical pictures and courses [1]. As neurodegenerative diseases are associated with deposition of pathological proteins both in the brain and in peripheral organs, their classification is protein-based [2]. However, as the progressive dysfunction and loss of neurons lead to distinct involvement of functional

S. Capitanio · M. Bauckneht · V. Ceriani · S. Morbelli (✉)
Department of Health Sciences (DiSSAL), University of Genoa and Nuclear Medicine Unit, Polyclinic San Martino Hospital, Genoa, Italy
e-mail: silviadaniela.morbelli@hsanmartino.it

D. Arnaldi · F. Massa · R. Meli · F. Nobili
Department of Neuroscience, Rehabilitation, Ophthalmology, Genetics, and Mother-Child Health (DINOGMI), Clinical Neurology, Polyclinic San Martino Hospital, University of Genoa, Genoa, Italy

F. Fraioli (ed.), *PET/CT in Brain Disorders*, Clinicians' Guides to Radionuclide Hybrid Imaging, https://doi.org/10.1007/978-3-030-01523-7_5

systems, major clinical symptoms are mainly determined by the anatomical regions showing neuronal and synaptic dysfunction (which in turn do not necessarily reflect the molecular changes in the background) [2]. Neuropathological studies have demonstrated that in AD and in other neurodegenerative diseases, synaptic degeneration precedes neuronal death for a substantial period of time [3]. This phenomenon can be reflected by the in vivo FDG uptake that is strongly correlated to cerebral synaptic density and activity [4]. For this reason, the hypometabolic pattern highlighted by FDG-PET provides information on the extent and localization of neuronal dysfunction and thus on the endophenotype of neuronal injury. In 2007, the International Working Group (IWG) research criteria [5] included FDG-PET among biomarkers for prodromal AD. In 2011, the National Institute of Aging and the Alzheimer Association defined the so-called NIA-AA criteria which regarded FDG-PET as a biomarker of neuronal injury able to support the diagnosis of mild cognitive impairment (MCI) due to AD [6]. Even before in 2004, based on a large body of literature on its diagnostic value for the identification of AD, FDG-PET imaging was approved by the Centers for Medicare and Medicaid Services (CMS, USA) as a routine examination tool for early and differential diagnosis of AD. FDG-PET has in particular demonstrated impact in patients with MCI or dementia in case of atypical presentation or course [7]. With respect to the differential diagnosis between AD and frontotemporal dementia, several studies demonstrated an accuracy ranging between 87% and 89.2% (similar to what is highlighted for amyloid PET) [8].

The clinical role of FDG-PET is quoted in clinical, neuroimaging-oriented, and procedural guidelines, but specific evidence-based recommendations on the use of FDG-PET in neurodegenerative are still lacking [9–11]. FDG-PET plays its major role in the early diagnosis of MCI due to AD and in the differential diagnosis of AD and other dementing disorders such as dementia with Lewy bodies (DLB) and diseases belonging to the spectrum of frontotemporal degeneration [12–14]. This tool has a well-established role in the evaluation of pre-dementia stage by showing or not specific disease patterns. In fact, given its high sensitivity and negative predictive value, a normal FDG-PET in MCI indicates a low chance of progression to AD dementia, even if there is a clinically evident memory deficit on neuropsychological testing (which in presence of a negative ^{18}F-FDG-PET may be due to non-dementing conditions, such as a depressive trait) [5].

FDG-PET was also found to be superior to postsynaptic dopaminergic imaging with [123I]IBZM SPECT for the differential diagnosis within neurodegenerative parkinsonisms [15]. Pattern of hypometabolism characterizing neurodegenerative Parkinsonian syndromes will be described in a dedicated chapter of this book.

5.2 Classical Patterns

5.2.1 Alzheimer's Disease (AD)

Hypometabolism in the medial temporal lobes (MTL), parietotemporal association area, posterior cingulate cortices, and precuneus is a typical feature of AD dementia [16]. On the contrary, glucose uptake is usually preserved in the primary visual

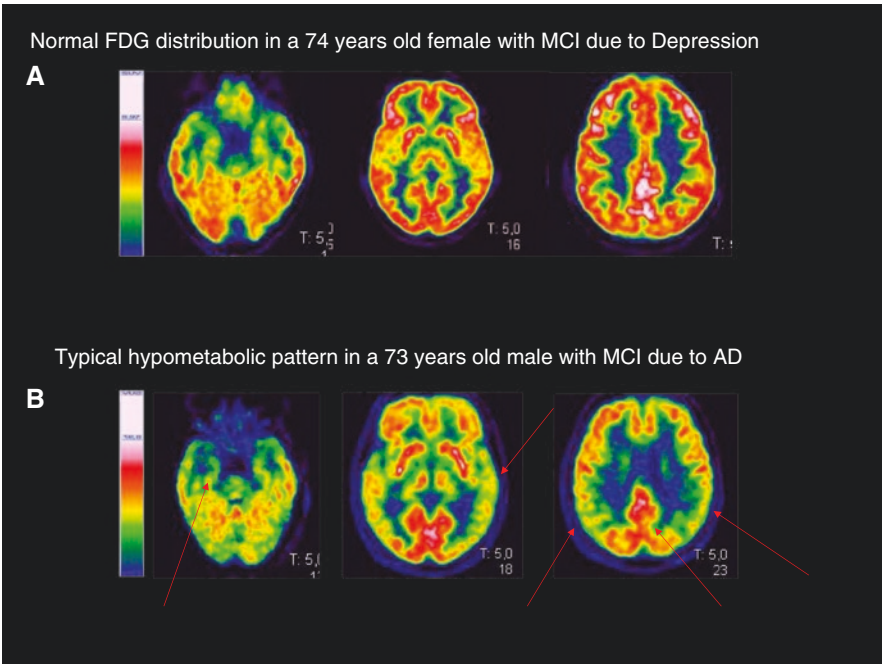

Fig. 5.1 FDG-PET normal distribution and AD-typical pattern in two patients with mild cognitive impairment (MCI). Patient A, showing a normal scan, was confirmed as an MCI due to depression at clinical follow-up, while patient B is an MCI due to AD. Red arrows highlight the AD-typical pattern in patient B (hypometabolism in temporo-medial, temporo-lateral, and posterior parietal cortex as well as in the left precuneus)

cortices, striatum, thalamus, cerebellar hemispheres, and especially primary motor-sensory cortices that usually stand out compared to the adjacent hypometabolic areas (Fig. 5.1). In more advanced stages, frontal associative cortex hypometabolism could also occur [13, 17] with a relative preservation of anterior cingulate gyrus. It should be noted that, while the entorhinal cortex and hippocampus are among the first regions targeted by AD pathology, hypometabolism in MTL is not always clearly evident partially due to the relatively poor resolution of PET equipment (in comparison to hippocampal thickness) [18]. However, the decreased posterior cingulate activity, one of the most sensitive and early FDG-PET indicators for AD, is considered to reflect the decreased connectivity of this region with the entorhinal cortex and hippocampus [19, 20]. To improve MTL evaluation, a different reorientation of PET images (Ohnishi reorientation with 30–40° with the nose upward with respect to the bicommissural plane) has been proposed in order to improve the evaluation of asymmetry in FDG uptake in MTL [21] (see Fig. 5.2). Regardless to the affected cortical regions, a very frequent feature of FDG-PET scans is the asymmetric involvement, especially in the early stages. As a consequence, visual analysis of scans strongly relies on asymmetric evaluation of FDG uptake.

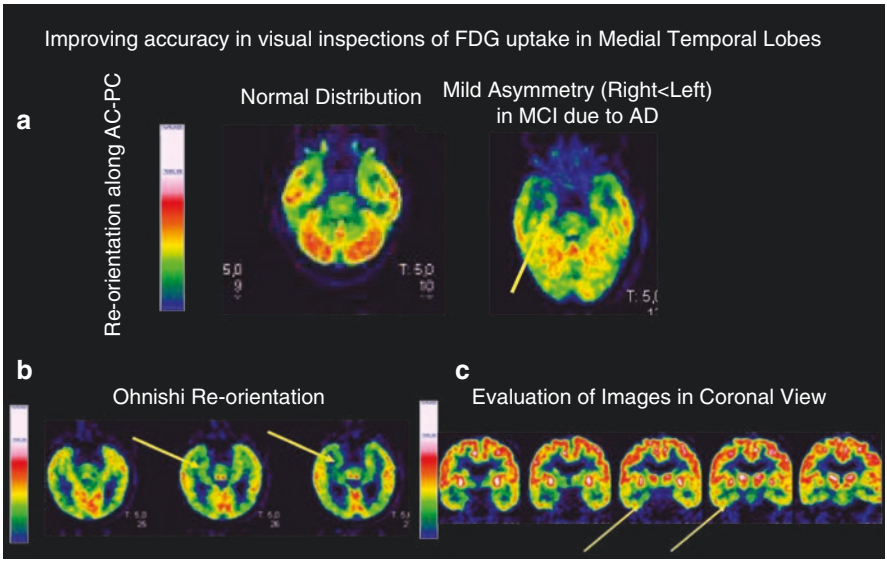

Fig. 5.2 Evaluation of medial temporal lobe (MTL) on FDG-PET. Panel **a**: FDG-PET images of a healthy control (normal scan, left side) and of an AD patient (right side: mild asymmetry in MTL with right < left). Both scans are reoriented along the anterior-commissural/posterior-commissural line (AC-PC). Panels **b** and **c** show the FDG-PET images of the same AD patient visualized according to Ohnishi reorientation and in coronal view, respectively. The asymmetry between right and left MTL (yellow arrows) is more evident both in Panels **b** and **c** than in Panel **a**. See the main text for further details

There are several sources of heterogeneity within the AD-typical pattern. Patients with early-onset AD tend to show a more extended and "neocortical" (parietal and frontal) pattern of hypometabolism than late-onset AD expressing the same level of cognitive impairment. By contrast, late-onset AD patients are characterized by a less extended hypometabolism more typically restricted to the MTL. Indeed, these features are considered to be due to both the disease heterogeneity and the higher cognitive reserve characterizing younger patients [22, 23] (see Fig. 5.3).

Specific features are also evident in AD atypical variants (see Fig. 5.4). In the logopenic variant, a more prominent metabolic reduction tends to be present in the left parietal and posterolateral temporal lobes [24].

A predominant impairment in parieto-occipital visual association cortices is associated to posterior cortical atrophy which is characterized by visuospatial deficits consistent with damage to the dorsal stream of visual processing [25, 26].

Finally, compared to typical AD, frontal metabolism (in particular medial and orbital frontal) is more compromised in patients with atypical behavioral, language, and dysexecutive presentation of AD [27]. All these atypical subtypes are characterized by the presence of brain amyloidosis which further allows an accurate differential diagnosis with respect to frontotemporal dementia [28]. Finally, while the clinical presentation and MRI (rather than FDG-PET) findings are required to support the diagnosis of vascular dementia, FDG-PET might be performed in

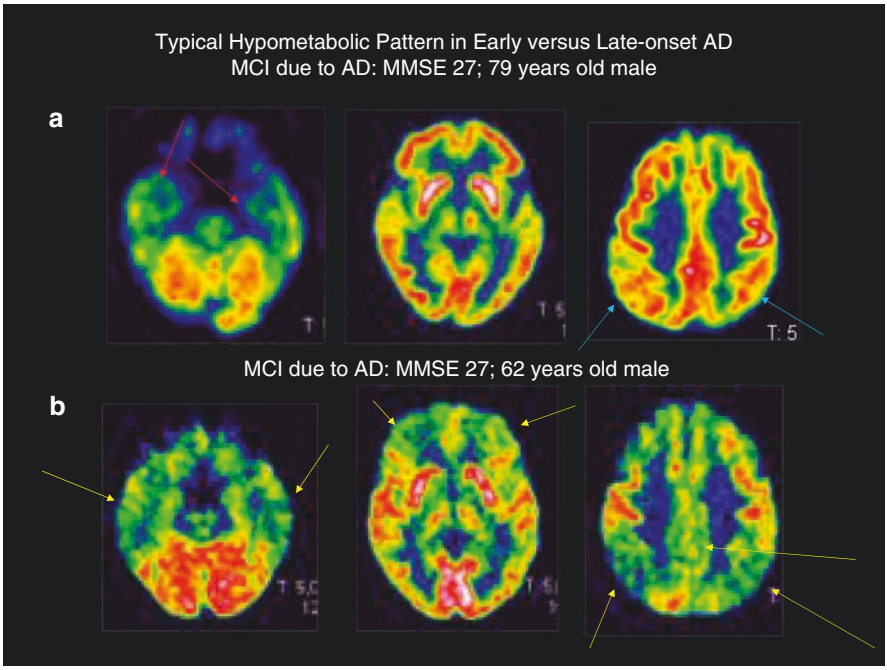

Fig. 5.3 AD-typical hypometabolic pattern in late- (LOAD) versus early-onset AD (EOAD) at the same level of cognitive impairment. In LOAD hypometabolism is less extended and mainly restricted to the medial temporal lobes (red arrows) with only mildly reduced uptake in posterior parietal cortex (light blue arrows). In EOAD the hypometabolic pattern is significantly more extended and involves several neocortical regions including bilateral frontal cortex (yellow arrows). (**a**) AD-typical hypometabolic pattern in late-onset (LOAD) patient. (**b**) AD-typical hypometabolic pattern in early-onset (EOAD) patient

particularly challenging cases to identify an AD-typical pattern in patients with vascular pathology by showing that this hypometabolic pattern is not co-localized with vascular damage on structural MRI [29].

5.3 Frontotemporal Degeneration (FTD)

Frontotemporal degeneration (FTD) refers to a highly heterogeneous group of disorders from the neuropathological, genetic, clinical, and radiological point of view [30]. The most frequent subtype is the behavioral variant of frontotemporal dementia (bvFTD) that is characterized by progressive deterioration in personality, social behavior, and cognition [31]. bvFTD may be hard to recognize, especially in the prodromal stage where behavioral changes may mimic psychiatric disorders and cognitive impairment might be milder. Neuroimaging studies showing typical pattern of atrophy and/or hypometabolism are required by current diagnostic criteria for probable bvFTD at the dementia stage [31]. Moreover the presence of a specific pattern of hypometabolism together with the clinical picture helps not only in the

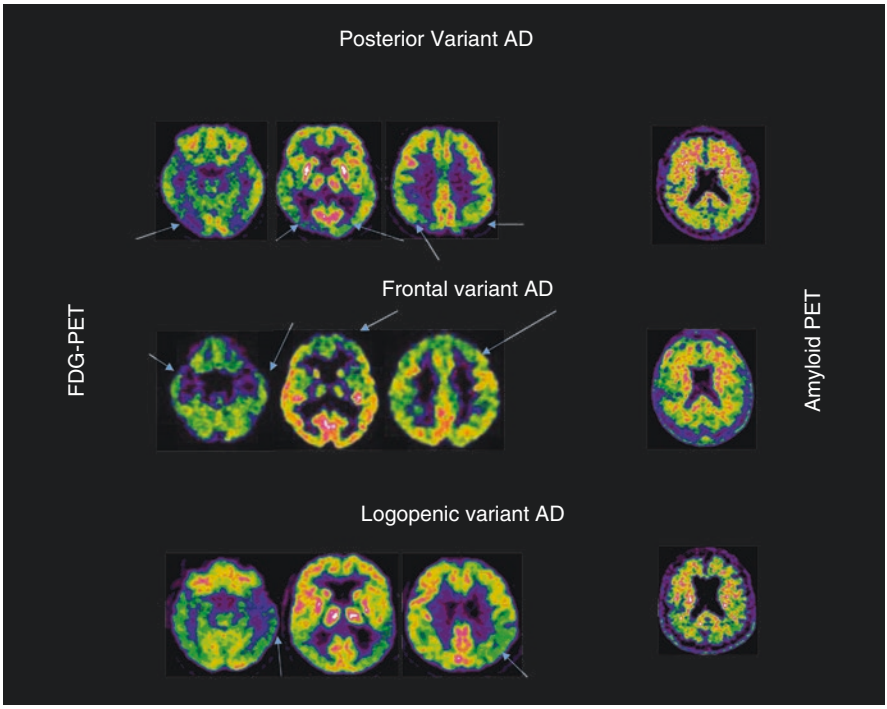

Fig. 5.4 FDG-PET and amyloid PET findings in AD atypical variants. Each AD atypical variant is characterized by a specific pattern of hypometabolism (light blue arrows; see the main text for further details). All these variants are characterized by high amyloid deposition and are thus amyloid PET positive (right panel showing lack of contrast between gray and white matter uptake in the amyloid PET scans of all patients)

differential diagnosis between AD and bvFTD but also within the FTD variants (frontal-behavioral variant, temporal-variant/semantic dementia (SD), and progressive nonfluent aphasia (PNFA) [32, 33]. (See Fig. 5.5.)

Correctly recognizing FTD is particularly important because, despite no specific drugs have been approved yet, the use of cholinesterase inhibitors should be avoided because they can further worsen clinical status [34, 35].

bvFTD is characterized by extensive cortical hypometabolism in the frontal and anterior temporal areas, cingulate gyri, uncus, insula, and subcortical areas, possibly including basal ganglia and thalamic regions [36]. In this framework, anterior cingulate and anterior temporal cortices have showed the higher specificity for the differential diagnosis with AD [37]. FDG-PET might also play a role in the differential diagnosis of progressive primary aphasia (PPA) including the two language-related variants of FTD and the already mentioned logopenic variant of AD [38]. Indeed specific patterns of atrophy and/or hypometabolism are necessary for the diagnosis of PPA according to the available diagnostic criteria [38].

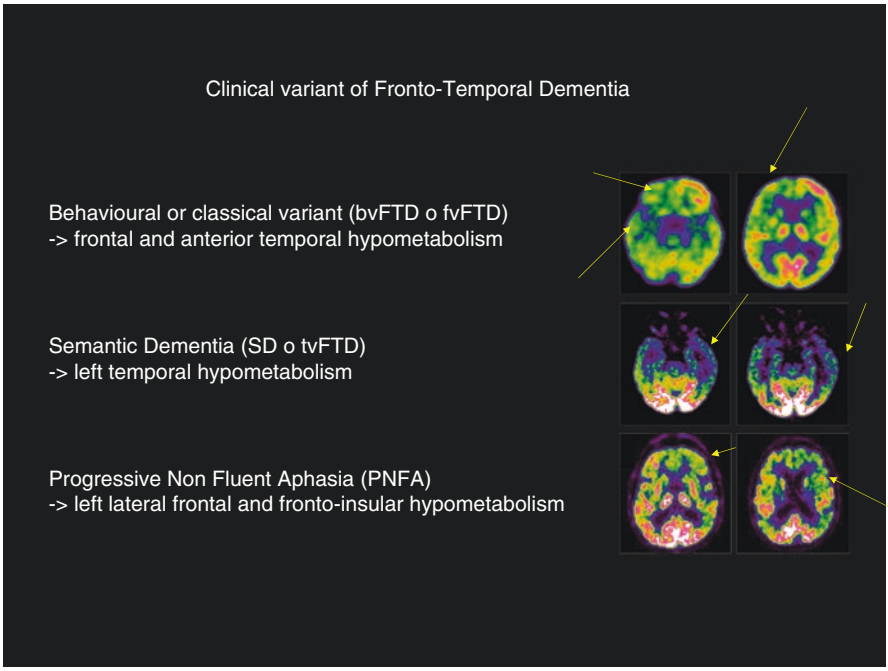

Fig. 5.5 FDG-PET patterns of hypometabolism in clinical variant of frontotemporal dementia

In particular, SD is characterized by an asymmetric predominately anterior temporal lobe pattern of hypometabolism with left dominant asymmetry [39, 40]. Conversely, in PNFA the asymmetric hypometabolism is more evident in the left anterior perisylvian cortical area as well as in the fronto-insular cortex. Finally, two atypical Parkinsonian syndromes, cortico-basal degeneration and progressive supranuclear palsy, belong to the spectrum of FTD and are characterized by specific patterns of hypometabolism which will be commented in the chapter on FDG in Movement Disorders [15].

5.4 Dementia of Lewy Body (DLB)

DLB is the most frequent cause of degenerative dementia after AD. It is characterized by Parkinson's disease-like symptoms such as rigidity and slow movement, with cognitive decline usually being the first symptom, and by the frequent occurrence of hallucinations (usually independent of dopaminergic drugs) and fluctuations in attention and alertness [41]. The diagnosis of DLB is based on the McKeith criteria first published in 2005 and revised in 2017 [41]. During the past decades, FDG-PET has been increasingly used in DLB and is listed among the supportive biomarkers for its identification. The metabolic pattern of DLB is characterized by hypometabolism in posterior associative cortex and by a more prominent

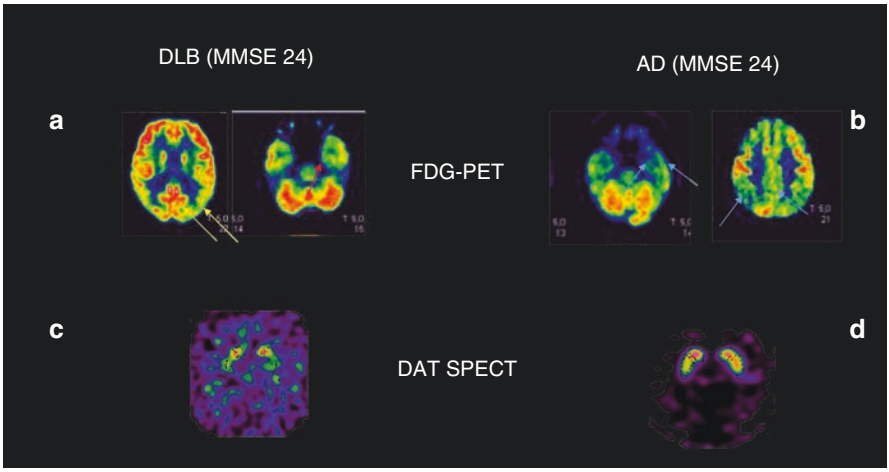

Fig. 5.6 Molecular imaging findings in dementia with Lewy bodies (DLB) versus Alzheimer's disease (AD). Panel **a**: with respect to AD, DLB patients are characterized by hypometabolism in lateral occipital cortex as well as in precuneus with relatively spared metabolism in posterior cingulate (yellow arrows) and in medial temporal lobe (red arrow). Panel **b** shows the temporoparietal hypometabolic pattern (with marked posterior cingulate hypometabolism) in an AD patient expressing the same level of cognitive impairment. It has to be noted that DAT SPECT is to date the most appropriate tool to support the clinical differential diagnosis between DLB (Panel **c**: markedly reduced uptake) and AD (Panel **d**: normal scan)

hypometabolism affecting the primary visual cortex and occipital cortex with relative sparing of subcortical structures and primary somatomotor cortex [42]. In particular, the presence of hypometabolism in the precuneus with a relative preservation of metabolism in posterior cingulate gyrus (the so-called cingulate island sign) has been demonstrated to provide a high specificity for the differential diagnosis with respect to AD (although the specificity of DAT SPECT was demonstrated to be superior in this context [43]) (see Fig. 5.6).

5.5 Other Neurodegenerative Diseases

In recent years research evidence has been provided about specific patterns of hypometabolism in other neurodegenerative diseases including Huntington disease (see Chap. 1 Movement Disorders) and amyotrophic lateral sclerosis (ALS). ALS is a neurodegenerative disease involving upper and lower motor neurons, extra-motor neurons, microglia, and astrocytes.

While FDG-PET is not clinically indicated, several studies have highlighted hypometabolic clusters in frontal, motor, and parietal cortex associate to relative hypermetabolism in the brain stem [44]. Finally, a continuum of frontal lobe metabolic impairment reflecting the clinical and anatomic continuum from pure ALS, through ALS with intermediate cognitive deficits, to ALS-FTD has been highlighted [45].

5.6 Advantages and Limitations

FDG-PET represents a valuable and widely available tool, helping the clinicians in challenging cases since the earliest stages of neurodegenerative dementia. FDG has the unique ability to estimate the local cerebral metabolic rate of glucose consumption, thus providing information on the distribution of neuronal death and synapse dysfunction in vivo [46]. As synaptic failure precedes neuronal death, the presence of patterns of hypometabolism typical of neurodegenerative diseases precedes the appearance of typical pattern of atrophy at structural MRI.

However, FDG-PET is listed among AD neurodegeneration biomarkers which according to some authors should be considered less relevant for the diagnosis and more useful to follow disease progression and to predict time to disease milestones [47, 48]. Considering the current clinical availability of amyloidosis biomarkers (CSF abeta and amyloid PET), the added value of FDG-PET over other AD biomarkers will also need to be addressed as complete definition of a cost-effective diagnostic algorithm in AD has not been established yet [49].

In the last decades, the introduction of statistical mapping approaches in the research field, able to semiquantitatively analyze subtle metabolic changes, has improved the differential diagnostic accuracy of FDG-PET even in the earliest stages of the disease [50].

However, despite a huge amount of literature, available studies show very large range of values for sensitivity and specificity due to heterogeneity of the included patients (converter/nonconverter, inclusion of amnestic or non-amnestic MCI, etc.), and the different methods used to read the images (visual versus semiquantitative reading with different software; lack of cutoff values) [51, 52].

In conclusion, a huge body of literature has suggested that the availability of FDG-PET (and of other biomarkers) can provide advances in the clinical evaluation and understanding of the endophenotype of neurodegenerative diseases. The translations of its use in the clinical setting should be further addressed to balance costs, thus meeting the needs of both patients and health-care systems.

Key Points

- The hypometabolic pattern highlighted by FDG-PET provides information on the extent and localization of neuronal dysfunction and thus on the endo-phenotype of neuronal injury.
- FDG-PET plays its major role in the early diagnosis of MCI due to AD and in the differential diagnosis of AD and other dementing disorders such as dementia with Lewy bodies (DLB) and diseases belonging to the spectrum of frontotemporal degeneration.
- Hypometabolism in the medial temporal lobes (MTL), parietotemporal association area, posterior cingulate cortices, and precuneus is a typical feature of AD dementia. On the contrary, glucose uptake is usually

preserved in the primary visual cortices, striatum, thalamus, cerebellar hemispheres, and especially primary motor-sensory cortices that usually stand out compared to the adjacent hypometabolic areas.

- The most frequent subtype is the behavioral variant of frontotemporal dementia (bvFTD) that is characterized by progressive deterioration in personality, social behavior, and cognition. bvFTD is characterized by extensive cortical hypometabolism in the frontal and anterior temporal areas, cingulate gyri, uncus, insula, and subcortical areas, possibly including basal ganglia and thalamic regions.

References

1. Nasrallah IM, Wolk DA. Multimodality imaging of Alzheimer disease and other neurodegenerative dementias. J Nucl Med. 2014;55:2003–11.
2. Kovacs GG. Molecular pathological classification of neurodegenerative diseases: turning towards precision medicine. Int J Mol Sci. 2016;17:189.
3. Price JL, Morris JC. Tangles and plaques in nondemented aging and "preclinical" Alzheimer's disease. Ann Neurol. 1999;45:358–68.
4. Rocher AB, Chapon F, Blaizot X, Baron JC, Chavoix C. Resting-state brain glucose utilization as measured by PET is directly related to regional synaptophysin levels: a study in baboons. NeuroImage. 2003;20:1894–8.
5. Dubois B, Feldman HH, Jacova C, Dekosky ST, Barberger-Gateau P, Cummings J, et al. Research criteria for the diagnosis of Alzheimer's disease: revising the NINCDS-ADRDA criteria. Lancet Neurol. 2007;6:734–46.
6. Albert MS, DeKosky ST, Dickson D, Dubois B, Feldman HH, Fox NC, et al. The diagnosis of mild cognitive impairment due to Alzheimer's disease: recommendations from the National Institute on Aging-Alzheimer's Association workgroups on diagnostic guidelines for Alzheimer's disease. Alzheimers Dement. 2011;7:270–9.
7. Ossenkoppele R, Prins ND, Pijnenburg YA, Lemstra AW, van der Flier WM, Adriaanse SF, et al. Impact of molecular imaging on the diagnostic process in a memory clinic. Alzheimers Dement. 2013;9:414–21.
8. Rabinovici GD, Rosen HJ, Alkalay A, Kornak J, Furst AJ, Agarwal N, et al. Amyloid vs FDG-PET in the differential diagnosis of AD and FTLD. Neurology. 2011;77:2034–42.
9. Sorbi S, Hort J, Erkinjuntti T, Fladby T, Gainotti G, Gurvit H, et al. EFNS-ENS guidelines on the diagnosis and management of disorders associated with dementia. Eur J Neurol. 2012;19:1159–79.
10. Filippi M, Agosta F, Barkhof F, Dubois B, Fox NC, Frisoni GB, et al. EFNS task force: the use of neuroimaging in the diagnosis of dementia. Eur J Neurol. 2012;19:1487–501.
11. Varrone A, Asenbaum S, Vander Borght T, Booij J, Nobili F, Någren K, et al. EANM procedure guidelines for PET brain imaging using [18F]FDG, version 2. Eur J Nucl Med Mol Imaging. 2009;36:2103–10.
12. Herholz K, Salmon E, Perani D, Baron JC, Holthoff V, Frölich L, et al. Discrimination between Alzheimer dementia and controls by automated analysis of multicenter FDG PET. NeuroImage. 2002;17:302–16.
13. Herholz K, Carter SF, Jones M. Positron emission tomography imaging in dementia. Br J Radiol. 2007;80:S160–7.

14. Mosconi L, Tsui WH, Herholz K, Pupi A, Drzezga A, Lucignani G, et al. Multicenter standardized 18F-FDG PET diagnosis of mild cognitive impairment, Alzheimer's disease, and other dementias. J Nucl Med. 2008;49:390–8.
15. Hellwig S, Amtage F, Kreft A, Buchert R, Winz OH, Vach W, et al. [18F]FDG-PET is superior to [123I]IBZM-SPECT for the differential diagnosis of parkinsonism. Neurology. 2012;79:1314–22.
16. Minoshima S, Frey KA, Koeppe RA, Foster NL, Kuhl DE. A diagnostic approach in Alzheimer's disease using three-dimensional stereotactic surface projections of fluorine-18-FDG PET. J Nucl Med. 1995;36:1238–48.
17. Gallucci M, Limbucci N, Catalucci A, Caulo M. Neurodegenerative diseases. Radiol Clin N Am. 2008;46:799–817.
18. Mosconi L. Brain glucose metabolism in the early and specific diagnosis of Alzheimer's disease. FDG-PET studies in MCI and AD. Eur J Nucl Med Mol Imaging. 2005;32:486–510.
19. Minoshima S, Giordani B, Berent S, Frey KA, Foster NL, Kuhl DE. Metabolic reduction in the posterior cingulate cortex in very early Alzheimer's disease. Ann Neurol. 1997;42:85–94.
20. Morbelli S, Piccardo A, Villavecchia G, Dessi B, Brugnolo A, Piccini A, et al. Mapping brain morphological and functional conversion patterns in amnestic MCI: a voxel-based MRI and FDG-PET study. Eur J Nucl Med Mol Imaging. 2010;37:36–45.
21. Ohnishi T, Hoshi H, Nagamachi S, Jinnouchi S, Flores LG II, Futami S, et al. High-resolution SPECT to assess hippocampal perfusion in neuropsychiatric diseases. J Nucl Med. 1995;36:1163–9.
22. Kim EJ, Cho SS, Jeong Y, Park KC, Kang SJ, Kang E, et al. Glucose metabolism in early onset versus late onset Alzheimer's disease: an SPM analysis of 120 patients. Brain. 2005;128:1790–801.
23. Morbelli S, Perneczky R, Drzezga A, Frisoni GB, Caroli A, van Berckel BN, et al. Metabolic networks underlying cognitive reserve in prodromal Alzheimer disease: a European Alzheimer disease consortium project. J Nucl Med. 2013;54:894–902.
24. Madhavan A, Whitwell JL, Weigand SD, Duffy JR, Strand EA, Machulda MM, et al. FDG PET and MRI in logopenic primary progressive aphasia versus dementia of the Alzheimer's type. PLoS One. 2013;8:e62471.
25. Laforce R Jr, Tosun D, Ghosh P, Lehmann M, Madison CM, Weiner MW, et al. Parallel ICA of FDG-PET and PiB-PET in three conditions with underlying Alzheimer's pathology. Neuroimage Clin. 2014;4:508–16.
26. Rosenbloom MH, Alkalay A, Agarwal N, Baker SL, O'Neil JP, Janabi M, et al. Distinct clinical and metabolic deficits in PCA and AD are not related to amyloid distribution. Neurology. 2011;76:1789–96.
27. Woodward MC, Rowe CC, Jones G, Villemagne VL, Varos TA. Differentiating the frontal presentation of Alzheimer's disease with FDG-PET. J Alzheimers Dis. 2015;44:233–42.
28. Ossenkoppele R, Schonhaut DR, Schöll M, Lockhart SN, Ayakta N, Baker SL, et al. Tau PET patterns mirror clinical and neuroanatomical variability in Alzheimer's disease. Brain. 2016;139:1551–67.
29. Kerrouche N, Herholz K, Mielke R, Holthoff V, Baron JC. 18FDG PET in vascular dementia: differentiation from Alzheimer's disease using voxel-based multivariate analysis. J Cereb Blood Flow Metab. 2006;26:1213–21.
30. Seltman RE, Matthews BR. Frontotemporal lobar degeneration: epidemiology, pathology, diagnosis and management. CNS Drugs. 2012;26:841–70.
31. Rascovsky K, Hodges JR, Knopman D, Mendez MF, Kramer JH, Neuhaus J, et al. Sensitivity of revised diagnostic criteria for the behavioural variant of frontotemporal dementia. Brain. 2011;134:2456–77.
32. Whitwell JL, Josephs KA. Neuroimaging in frontotemporal lobar degeneration—predicting molecular pathology. Nat Rev Neurol. 2012;8:131–42.
33. Morbelli S, Ferrara M, Fiz F, Dessi B, Arnaldi D, Picco A, et al. Mapping brain morphological and functional conversion patterns in predementia late-onset bvFTD. Eur J Nucl Med Mol Imaging. 2016;43:1337–47.

34. Mendez MF, Shapira JS, McMurtray A, Licht E, Miller BL. Accuracy of the clinical evaluation for frontotemporal dementia. Arch Neurol. 2007;64:830–5.
35. Chow TW, Miller BL, Boone K, Mishkin F, Cummings JL. Frontotemporal dementia classification and neuropsychiatry. Neurologist. 2002;8:263–9.
36. Jeong Y, Cho SS, Park JM, Kang SJ, Lee JS, Kang E, et al. 18F-FDG PET findings in frontotemporal dementia: an SPM analysis of 29 patients. J Nucl Med. 2005;46:233–9.
37. Womack KB, Diaz-Arrastia R, Aizenstein HJ, Arnold SE, Barbas NR, Boeve BF, et al. Temporoparietal hypometabolism in frontotemporal lobar degeneration and associated imaging diagnostic errors. Arch Neurol. 2011;68:329–37.
38. Gorno-Tempini ML, Hillis AE, Weintraub S, Kertesz A, Mendez M, Cappa SF, et al. Classification of primary progressive aphasia and its variants. Neurology. 2011;76:1006–14.
39. Matías-Guiu JA, Cabrera-Martín MN, Moreno-Ramos T, Valles-Salgado M, Fernandez-Matarrubia M, Carreras JL, et al. Amyloid and FDG-PET study of logopenic primary progressive aphasia: evidence for the existence of two subtypes. J Neurol. 2015;262:1463–72.
40. Rabinovici GD, Jagust WJ, Furst AJ, Ogar JM, Racine CA, Mormino EC, et al. Abeta amyloid and glucose metabolism in three variants of primary progressive aphasia. Ann Neurol. 2008;64:388–401.
41. McKeith IG, Boeve BF, Dickson DW, Halliday G, Taylor JP, Weintraub D, et al. Diagnosis and management of dementia with Lewy bodies: fourth consensus report of the DLB Consortium. Neurology. 2017;89:88–100.
42. Bauckneht M, Arnaldi D, Nobili F, Aarsland D, Morbelli S. New tracers and new perspectives for molecular imaging in Lewy body diseases. Curr Med Chem. 2018;25(26):3105–30.
43. Graff-Radford J, Murray ME, Lowe VJ, Boeve BF, Ferman TJ, Przybelski SA, et al. Dementia with Lewy bodies: basis of cingulate island sign. Neurology. 2014;83:801–9.
44. Pagani M, Chiò A, Valentini MC, Öberg J, Nobili F, Calvo A, et al. Functional pattern of brain FDG-PET in amyotrophic lateral sclerosis. Neurology. 2014;83:1067–74.
45. Prado LGR, Bicalho ICS, Magalhães D, Caramelli P, Teixeira AL, de Souza LC. C9ORF72 and the FTD-ALS spectrum: A systematic review of neuroimaging studies. Dement Neuropsychol. 2015;9:413–21.
46. Magistretti PJ. Cellular bases of functional brain imaging: insights from neuron-glia metabolic coupling. Brain Res. 2000;886:108–12.
47. Dubois B, Feldman HH, Jacova C, Hampel H, Molinuevo JL, Blennow K, et al. Advancing research diagnostic criteria for Alzheimer's disease: the IWG-2 criteria. Lancet Neurol. 2014;13:614–29.
48. Morbelli S, Bauckneht M, Arnaldi D, Picco A, Pardini M, Brugnolo A, et al. 18F-FDG PET diagnostic and prognostic patterns do not overlap in Alzheimer's disease (AD) patients at the mild cognitive impairment (MCI) stage. Eur J Nucl Med Mol Imaging. 2017;44:2073–83.
49. Morbelli S, Bauckneht M, Scheltens P. Imaging biomarkers in Alzheimer's disease: added value in the clinical setting. Q J Nucl Med Mol Imaging. 2017;61:360–71.
50. Perani D, Della Rosa PA, Cerami C, Gallivanone F, Fallanca F, Vanoli EG, et al. Validation of an optimized SPM procedure for FDG-PET in dementia diagnosis in a clinical setting. Neuroimage Clin. 2014;6:445–54.
51. Smailagic N, Vacante M, Hyde C, Martin S, Ukoumunne O, Sachpekidis C. ^{18}F-FDG PET for the early diagnosis of Alzheimer's disease dementia and other dementias in people with mild cognitive impairment (MCI). Cochrane Database Syst Rev. 2015;1:CD010632.
52. Morbelli S, Garibotto V, Van De Giessen E, Arbizu J, Chételat G, Drezgza A, et al. A Cochrane review on brain [^{18}F]FDG PET in dementia: limitations and future perspectives. Eur J Nucl Med Mol Imaging. 2015;42:1487–91.

[^{18}F]FDG-PET/CT in Movement Disorders

6

Patrik Fazio and Andrea Varrone

Contents

P. Fazio (✉)
Department of Clinical Neuroscience, Centre for Psychiatry Research, Karolinska University Hospital, Karolinska Institutet, Stockholm, Sweden

Department of Neurology, Karolinska University Hospital, Stockholm, Sweden
e-mail: patrik.fazio@ki.se

A. Varrone
Department of Clinical Neuroscience, Centre for Psychiatry Research, Karolinska University Hospital, Karolinska Institutet, Stockholm, Sweden

F. Fraioli (ed.), *PET/CT in Brain Disorders*, Clinicians' Guides to Radionuclide Hybrid Imaging, https://doi.org/10.1007/978-3-030-01523-7_6

6.1 Introduction

Movement disorders are defined as neurologic syndromes in which there is either an excess of movement or a scarcity of voluntary and automatic movements, unrelated to weakness or spasticity [1]. Movement disorders are related to dysfunction of different nervous system structures involved in the modulation and regulation of movement. Among them the basal ganglia, cerebellum, cortex, and different thalamic nuclei represent the dynamic assembly that is differently impaired in movement disorder syndromes. The broad set of functions regulated by those neuronal circuits may explain the variability and richness of clinical signs in different domains expressed by patients with movement disorders. Different neurodegenerative or acquired central nervous system diseases that affect any part of this circuitry may cause movement disorders, which in many of the cases are of neurodegenerative nature. From a classification perspective, movement disorders are classified by the clinical phenomenology of the movement disorders (parkinsonian syndromes, tremor, chorea, myoclonia, dystonia, and ataxias) and are grossly subdivided in hypokinetic and hyperkinetic movement disorders.

The focus of this chapter will be to define the capabilities of [^{18}F]FDG-PET as a supportive diagnostic tool in the aforementioned disease entities. The most known and accepted application of [^{18}F]FDG-PET in movement disorders is the use of it as a supportive instrumental biomarker for the differential diagnosis of parkinsonian syndromes [2]. Indeed the accuracy of the clinical diagnosis of parkinsonism at early stages is low [3] because of a wide overlapping between the described clinical syndromes and by the intrinsic heterogeneity of the underlying pathological processes [4].

The readout of images obtained with [^{18}F]FDG-PET studies is highly correlated with neuropathological findings, and an introduction of different pathological process in those disorders is helpful to explain classical [^{18}F]FDG-PET patterns detected in the different conditions such in parkinsonian syndromes [5].

Other potentially useful applications are in the subfield of choreas with the detection of disease-specific patterns. More recently, efforts have been made to apply molecular imaging techniques on earlier or prodromal phases of different neurodegenerative diseases, and a clear example is given by the experience gained with imaging of premanifest Huntington's disease patients.

6.2 Parkinson's Disease

6.2.1 Clinical Phenotypes

From a neurobiological perspective, the so-called idiopathic Parkinson's disease (PD) has been recently considered more as a group of disorders with a characteristic dopamine deficit due to degeneration of the dopaminergic nigrostriatal system and with a broad set of non-motor symptoms. From a "movement disorder" perspective, PD is characterized itself by a progressive reduction of motor capacities with

rigidity, hypo-/bradykinesia, resting tremor, postural instability, and an overall reduction of automatic movements. These typical motor signs are associated with a variegate set of non-motor signs such as cognitive decline, autonomic dysfunctions, sleep-related disorders, and affective disorders. Non-motor signs and symptoms are becoming progressively more relevant to distinguish all different phenotypes [6] and to characterize the so-called prodromal phase (i.e., rapid eye movement [REM], sleep behavior disorders, constipation, and olfactory dysfunctions).

6.2.2 Neuropathology Findings

The neuropathology of PD is characterized by a multisystemic progressive accumulation of misfolded oligomers and larger aggregates of α-synuclein (α-syn). The extensive distribution of aggregates called Lewy bodies (LB) leads to a widespread neuronal and synaptic deficit responsible for the subsequent global and progressive derangement of the brain signaling in different portions of the nervous systems (central, peripheral, and autonomic) [7]. The variability of biochemical changes and the consequences of the described multisystem LB pathology might very well explain the clinical heterogeneity.

6.2.3 [18F]FDG-PET Typical Patterns

In established PD patients, the defining features of glucose metabolism are characterized by a relative preservation of the metabolism in the dorsolateral putamen accompanied by other supportive features such as an increased metabolism observed in the ventral thalamus, cerebellum, and cortical motor areas and a decrease metabolism in parietal and occipital cortex [8, 9]. In early PD patients, the metabolic reduction seems to be confined in posterior cortical regions [10, 11].

Analysis of [18F]FDG-PET data using spatial covariance image analysis approaches has become a well-recognized approach to analyze [18F]FDG-PET data in cross-sectional and longitudinal clinical studies (Fig. 6.1). This method led to a definition of a disease-specific pattern of glucose metabolism defined as PD-related pattern (PDRP) [5, 12]. The PDRP is characterized by a relative decrease in metabolism in the posterior parietal association cortex, occipital primary visual areas, and lateral premotor and prefrontal cortices and by a relative increase of metabolic activity in different regions involved in motor control such as the putamen and globus pallidus, thalamus, pons, and primary motor cortex [13, 14]. This pattern has been found to be consistent and replicable [14–16] and did correlate with clinical motor scores and with other imaging biomarker such as dopaminergic imaging biomarkers [17, 18]. A clear and established advantage of this approach is that it is automated and thus unbiased. Another value is that the PDRP was able to provide a solid foundation for a differentiation from other parkinsonian syndromes [19].

The PDRP analysis has been recently used to test whether patients in prodromal stages of PD such individuals with a diagnosed RBD retain or show similar

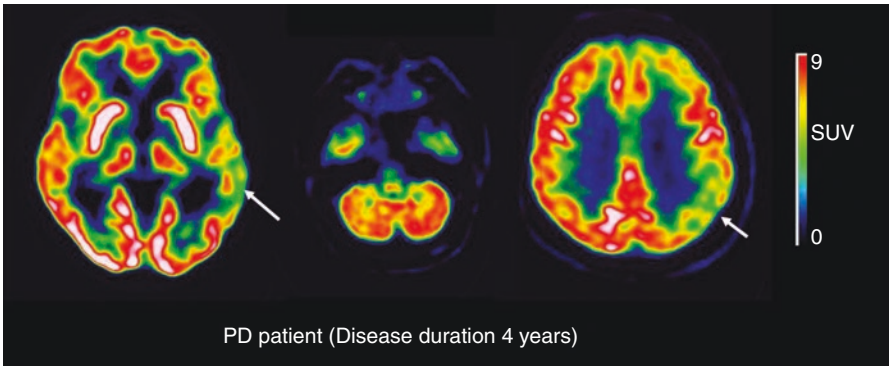

Fig. 6.1 FDG-PET images from a representative Parkinson's disease patients, showing decreased metabolism in the parietal and occipital cortex (arrows). Courtesy of Dr. Stelvio Sestini Nuclear Medicine Unit, Azienda Unità Sanitaria Locale 4, Prato, Italy

metabolic pattern compared to de novo PD patients. Recent data suggested that the RBD-related metabolic pattern is similar but less severe if compared to the PDRP observed in de novo PD patients [20].

[^{18}F]FDG-PET with the spatial covariance analysis has been used to detect metabolic changes after advanced therapeutical approaches such as deep brain stimulation (DBS) [21]. After 1 year of bilateral nucleus subthalamicus (STN) DBS, a significant increase in glucose metabolism was observed in the occipital and parietal cortices associated with a hypometabolism in the frontal cortex and cerebellar cortex [22].

Another useful application of [^{18}F]FDG-PET is represented by the evaluation of cognitive impairment in PD-associated syndromes (e.g., Parkinson's disease dementia (PDD) or PD-mild cognitive impairment (PD-MCI)). The development of a cognitive decline is associated with clear metabolic changes within visual associative and posterior cingulate cortices and in the caudate nucleus [23]. Recently a predictive value for the development of cognitive deficits in early PD has been attributed to the reduction of the FDG metabolism in the inferior parietal lobule [10].

The utility in the clinical practice of [^{18}F]FDG-PET is related to the capability of differentiating the sporadic form PD from atypical parkinsonism such as MSA or PSP/CBD syndromes.

6.3 Multiple System Atrophy

6.3.1 Clinical Phenotypes

MSA is a degenerative disorder characterized by parkinsonism, cerebellar, and autonomic dysfunctions. Depending on the predominant phenomenology, different phenotypes of MSA are possible. The MSA-parkinsonism (MSA-P) is characterized by parkinsonism associated with clinical signs of autonomic failure such as erectile dysfunction, orthostatic hypotension, and urinary symptoms. In MSA cerebellum (MSA-C) cerebellar signs occur together with autonomic failure. Patients with MSA

do present different additional features (e.g., pyramidal signs, myoclonus, dystonia), and usually patients do not show significant cognitive decline [24].

6.3.2 Neuropathology Findings

The pathological hallmark of MSA is the presence in postmortem brain of α-syn inclusions in oligodendroglia and neurons associated with progressive neuronal loss and axonal damages involving mainly different brain structures in the central autonomic, striatonigral, and olivopontocerebellar systems (basal ganglia, cerebellum, and brainstem). Those pathological features are complemented by astrogliosis and microglial activation. The distribution is inherently variable, but the two neuropathological subtypes mirror the two clinical entities so that a predominant olivopontocerebellar degeneration is observed in MSA-C and a predominant striatonigral degeneration is recognized in MSA-P [25].

6.3.3 [18F]FDG-PET Typical Patterns

The classical [18F]FDG-PET pattern detected in MSA is a decrease of glucose metabolism in the striatum (relevant in the posterior part of the putamen) associated or not to a decrease metabolism in the cerebellum (hemispheres) according to the phenotypical subdivision between MSA-P and MSA-C (Figs. 6.2 and 6.3). Reduced regional metabolism is also observed in the brainstem.

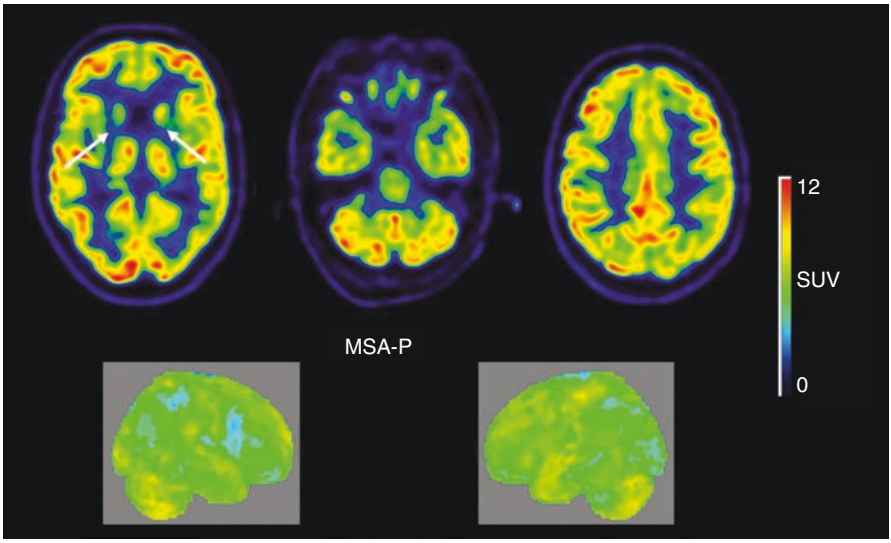

Fig. 6.2 FDG-PET images from a representative case of MSA-P, showing decreased metabolism in the putamen bilaterally (arrows). Courtesy of Dr. Irina Savitcheva, Department of Nuclear Medicine, Karolinska Huddinge University Hospital

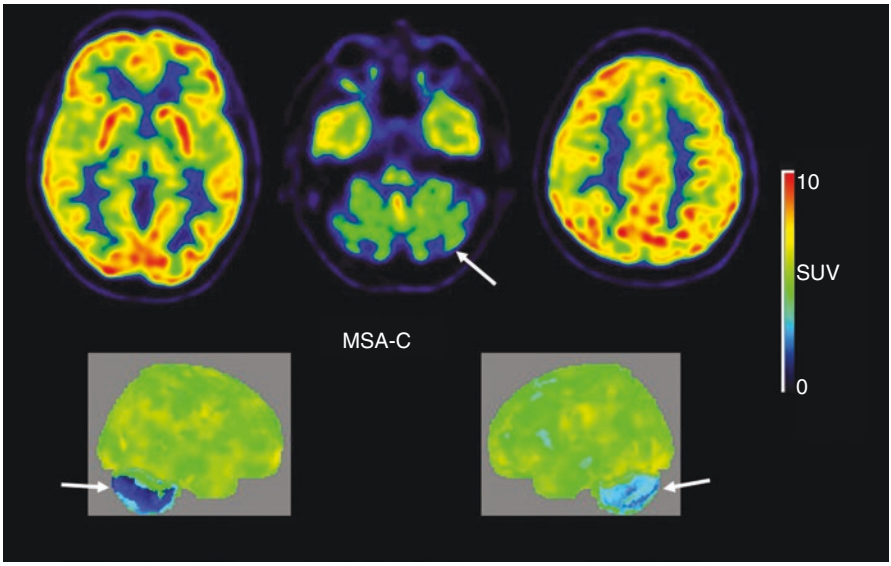

Fig. 6.3 FDG-PET images from a representative case of MSA-C. Decrease metabolism can be observed in the cerebellum (arrows). Courtesy of Dr. Irina Savitcheva, Department of Nuclear Medicine, Karolinska Huddinge University Hospital

Analysis of MSA [^{18}F]FDG-PET data using spatial covariance image approaches led to the description of a MSA-related pattern characterized by a relative hypometabolic pattern in the putamen and caudate nucleus associated with variable reduction in frontal and posterior cortical areas. Relative increases are described in the thalamus and cortical region temporal cortex [13, 14].

The utility in the clinical practice of [^{18}F]FDG-PET is related to the capability of detecting specific patterns of MSA (MSA-P and MSA-C). The diagnostic accuracy for MSA is high and can be easily used as supportive diagnostic tools [2, 5].

6.4 The Spectrum of Progressive Supranuclear Palsy and Corticobasal Degeneration

6.4.1 Clinical Phenotypes

Progressive supranuclear palsy disorders are nowadays considered as a heterogeneous group of clinical syndromes aggregated because of a common neuropathological substrate [26, 27]. The spectrum includes progressive supranuclear palsy-Richardson's syndrome (PSP-RS), corticobasal syndromes (PSP-CBS), progressive supranuclear palsy with parkinsonism (PSP-P), progressive supranuclear palsy with gait freezing (PSP-PGF), and more rare entities such as PSP with

predominant speech or frontal or cerebellar disorder (PSP-SL, PSP-F, PSP-C). The classical PSP-RS form is mainly characterized by a symmetric parkinsonism, axial rigidity, early falls, personality changes, supranuclear vertical gaze palsy, dysphagia, and dysarthria and a lack of response to levodopa. PSP-CBS refers to a rare presentation of PSP that resembles corticobasal degeneration (CBD) but with defined PSP neuropathology. The clinical overlap between the two entities is such that is impossible to distinguish the two phenotypes separately without the neuropathological examination post-mortem [28]. A detailed description of other alternative rare phenotypes described by the new MDS PSP criteria is beyond the scope of this chapter since there are not yet described disease-specific [18F]FDG-PET-related pattern. Clinical CBD phenotypes are characterized by a set of asymmetric motor symptoms such as rigidity, bradykinesia, stimulus-sensitive myoclonus, and focal dystonia and by a broad range of cortical dysfunction that includes dementia, limb apraxia, and alien limb phenomena. There are also specific variants such as progressive fluent aphasia characterized by a language disorder or frontobehavioral spatial syndrome where behavioral dysfunctions dominate the clinical picture [29].

6.4.2 Neuropathology Findings

Neuropathology findings of PSP-related disorders are characterized by a progressive accumulation of a misfolded protein called tau (four repeats) with neuronal and glial tau-immunoreactive lesions located at the postmortem analysis in the basal ganglia, diencephalon, and brainstem (substantia nigra) with an additional involvement of the neocortex (medial frontal and frontoparietal cortex) [30]. Most of the clinical syndromes can present also mixed pathology with other misfolded proteins such as α-syn and β-amyloid that contribute to the neurodegenerative process [31]. The different distribution of pathological findings reflects and partly explains the differences between the clinical variants of PSP-related disorders with a greater cortical pathology in PSP-CBS, PSP-SL, and PSP-F and a more subcortical pathology in PSP-RS, PSP-P, or PSP-PGF [32].

The neuropathology findings in clinically diagnosed CBD are characterized by highly heterogeneous tau pathology associated with asymmetrical and focal cortical atrophy (frontotemporal cortical areas), with frequent ballooned neurons (not so often found in PSP), by the involvement of the substantia nigra and striatal areas, and by a relative preservation in the brainstem [30, 33].

6.4.3 [18F]FDG-PET Typical Patterns

In pathologically confirmed PSP case, a reduction in the glucose metabolism has been described bilaterally in the caudate and in supplementary motor areas in association with a milder hypometabolism in the midbrain and thalamus [34] (Fig. 6.4).

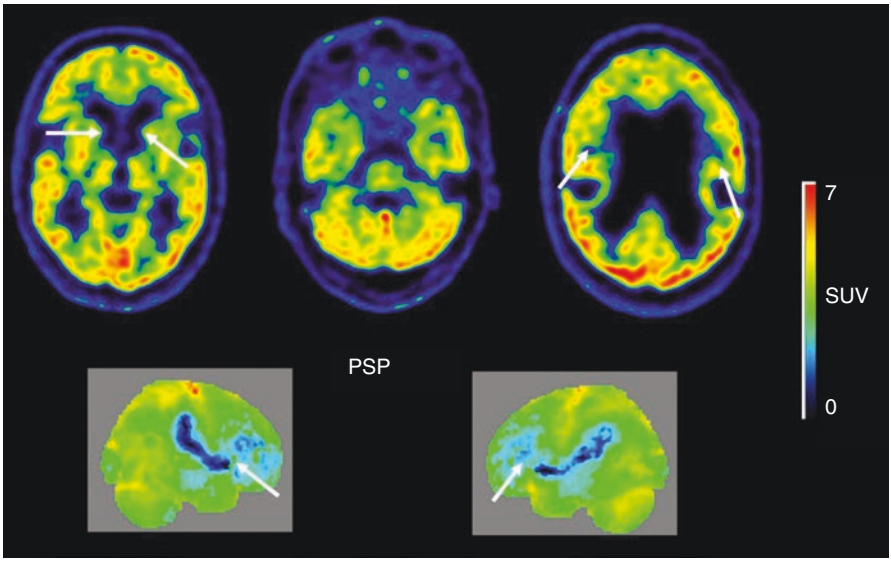

Fig. 6.4 FDG-PET images from a representative case of PSP. Decreased metabolism can be found in the medial frontal cortex and the caudate bilaterally (arrows). Courtesy of Dr. Irina Savitcheva, Department of Nuclear Medicine, Karolinska Huddinge University Hospital

Analysis of PSP [^{18}F]FDG-PET data using spatial covariance image analysis led to the description of a PSP-related pattern characterized by a bilateral relative hypometabolism in prefrontal and frontal cortical regions (mainly motor regions), in the caudate nucleus and in the brainstem associated with a relative hypermetabolism in posterior cortical areas [5, 9, 13]. Despite this clear description, the clinical variety of PSP syndromes described in the new classification is such that the diagnostic utility and phenocopies/subtypes specificity of [^{18}F]FDG-PET in PSP cannot be established [14, 26].

In CBD a characteristic pattern of glucose metabolism has been described in different studies. The most consistent metabolic pattern is characterized by a distinctive asymmetrical hypometabolism in fronto-temporo-parietal cortical areas and basal ganglia structures (contralateral to the most affected side) (Fig. 6.5), associated with a relative hypermetabolism in the same regions but on the opposite side [9, 13].

The utility in the clinical practice of [^{18}F]FDG-PET in the spectrum of progressive supranuclear palsy and corticobasal degeneration is mainly related to the differentiation from the PD and MSA. A distinctive and specific pattern for those two heterogeneous nosological entities is not yet available. One recent suggestion is to use a combined pattern for the PSP/CBD for [^{18}F]FDG-PET readouts [2].

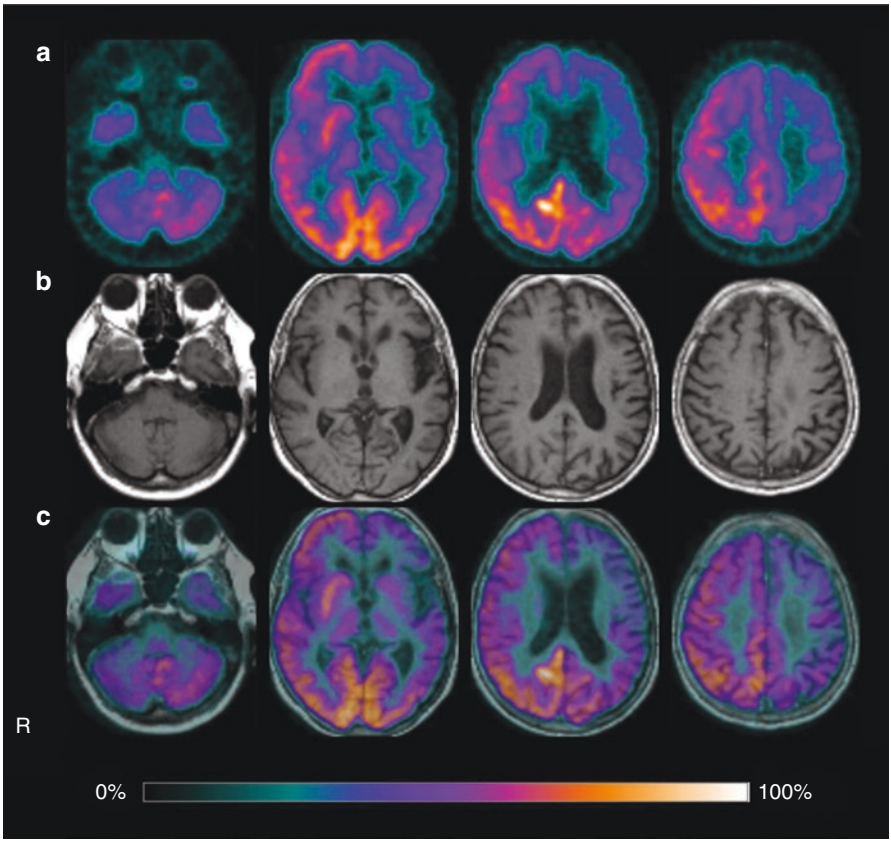

Fig. 6.5 (**a**) FDG-PET, (**b**) MRI, and (**c**) fused PET/MR images from a representative case of CBD. Decreased metabolism can be observed in the cortical regions (frontal, temporal, and parietal cortex, including precuneus) and basal ganglia of the left hemisphere. The degree of hypometabolism seemed to be more severe than the atrophy observed at the MRI. In this case hypometabolism of the cerebellar cortex of the contralateral hemisphere, indicating cerebellar diaschisis, can be observed. The PET examination was performed at the Biostructure and Bioimaging Institute, National Research Council and University Federico II, Naples, Italy

6.5 Huntington's Disease

6.5.1 Clinical Phenotypes

Huntington's disease is a neurodegenerative disorder caused by a single gene mutation characterized by a highly variable and complex clinical phenotype consisting of movement disorders, neuropsychiatric impairments, and cognitive deficits. Motor deficits are characterized by choreic movements, dystonia, parkinsonism,

oculomotor dysfunctions, gait and balance disturbances, dysarthria, and dysphagia. Cognitive symptoms encompass deficits in the executive dysfunction (concentration, attention, multitasking), lack of motivation and insight, reduction of problem-solving, and social cognition. Psychiatric problems include depression, anxiety, obsessive-compulsive disorders, irritability, disinhibition, delusions, apathy, and suicidality [35]. The disease has a well-characterized natural history generally divided in a premanifest stage and in a manifest stage that is conventionally associated with the onset of motor symptoms and reduction of functional measures.

6.5.2 Neuropathology Findings

HD belongs to the family of expanded CAG repeat disorders and is characterized by a progressive accumulation of a misfolded protein called mutant huntingtin (mHTT). The variability and richness of clinical signs in different domains are the consequence of a broad deranged signaling mainly linked to the loss of functions and degeneration of the cortico-striatal connections, to the toxic gain of function of mHTT, and to a toxic accumulation of protein aggregates. The traditional neuropathological grading system was developed according to the neurodegenerative pathological (gross and microscopic level) temporal patterns found in the striatum [36]. It is becoming more evident that the disease has a more multisystem character [37] with evidences of structural and functional abnormalities in the cerebral neo- and allocortex, selected thalamus nuclei, pallidum, and different nuclei of the brainstem such as the substantia nigra, pontine nuclei, reticulotegmental nucleus of the pons, and superior and inferior olives [38].

6.5.3 [^{18}F]FDG-PET Typical Patterns

Different PET imaging studies investigating the glucose metabolism in Huntington's disease gene expression carriers (HDGECs) were able to describe definite subcortical and cortical metabolic patterns across the entire disease spectrum of the neurodegenerative process with a progressive reduction of subcortical and cortical glucose metabolism [39–41]. The reduction in striatal metabolism was an early feature that can be observed in the premanifest phase of the disease (before the motor onset of the disease) (Fig. 6.6).

Noteworthy the striatal reduction of glucose uptake in premanifest HDGECs preceded the beginning of neuronal loss [40, 42]. Longitudinal analysis of premanifest HDGCs using spatial covariance image approaches led to the description of a HD-metabolic progression pattern that consisted in a progressive subcortical and cortical hypometabolism in the striatum, thalamus, insula, posterior cingulate gyrus, and prefrontal and occipital cortex associated to a relative hypermetabolism in the cerebellum and pons [43]. The progressive cortical hypometabolism was correlated with the progression of the cognitive deficits [44]. Unfortunately no specific patterns were detected for the progression of the psychiatric features of the disease.

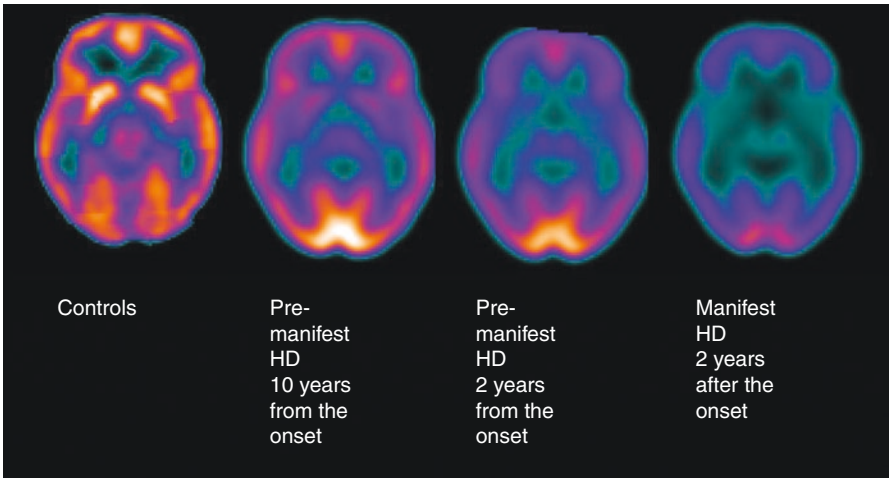

Fig. 6.6 Representative [18F]FDG-PET/CT images at different stages of Huntington's disease. Courtesy of Prof. Andrea Ciarmiello, Nuclear Medicine, S. Andrea Hospital, La Spezia, Italy

The utility in the clinical practice of [18F]FDG-PET is limited to rare occasions in which a suspected or confirmed HDGECs present an unclear motor onset. There are also studies that suggested a possible application of [18F]FDG-PET imaging as a tool to predict the time of symptomatic conversion [45].

HD is the most common form of heredo-degenerative condition that causes choreatic syndromes in adulthood. There are other rare heredo-degenerative conditions, defined as HD phenocopies, that become relevant as alternative diagnosis when the causative HD mutation is excluded [46]. The [18F]FDG-PET metabolic pattern for many of those condition has been described in different small or case studies [47]. Metabolic patterns that essentially mimic those observed in HD (a predominant striatal hypometabolism) have been described for different heredo-degenerative conditions such as in neurochoreacanthocitosis syndromes [48, 49], spinocerebellar ataxia17 (SCA17) [50], or Wilson's disease [51]. According to the literature, the pattern basically reflects the neurodegenerative nature of those conditions. In contrast [18F]FDG-PET imaging studies performed in acquired/non-degenerative forms of chorea such in the antiphospholipid syndrome [51], polycythemia vera [51], and Sydenham's chorea [51] showed an increased striatal metabolism.

6.6 Advantages and Limitations

6.6.1 General Advantages

[18F]FDG-PET is currently the most accurate method to study in vivo the human brain metabolism, and it is increasingly being used to study the brain for diagnostic purposes [52]. This technology is widely available in the current clinical setting,

and an impressive amount of data have been collected in the area of movement disorders. A recent meta-analysis showed that [^{18}F]FDG-PET is highly accurate (>90%) in the differential diagnosis of parkinsonian disorders [2].

6.6.2 General Limitations

Despite its acceptance in clinical practice, several known confounders might potentially represent a limitation for the application of [^{18}F]FDG-PET in the investigation of movement disorders.

In neurodegenerative disorders, drastic structural and functional changes of the composition of brain tissue are the rule. Among them of importance for the present consideration are the known gray matter loss, astrogliosis [53], alteration in permeability of the blood brain barrier [54], and accumulation of misfolded proteins (e.g., α-synuclein, tau, or m-Huntingtin) which are major putative neuropathological processes that occur in neurodegenerative disorders. Altogether those dynamic processes/changes might influence the delivery, the metabolism, and the uptake of FDG in brain tissues. It is already known that heterogeneous tissues might influence the metabolism and the kinetic of FDG uptake [55]. In our view those reflections are more relevant for the interpretation and understanding of the observed metabolic patterns rather than the validity of the aforementioned and described patterns. Another caveat is represented by the incomplete knowledge about the effect of the different medications acting on the central nervous system onto regional FDG brain metabolic patterns. Caffeine, alcohol, amphetamines, cocaine, anesthetics, benzodiazepines, neuroleptics, but also corticosteroids and chemotherapy have a known effect on FDG uptake [56]. Specific studies conducted to evaluate the FDG uptake in PD patients in a levodopa "on" state as compared with patient in "off" levodopa found that the brain glucose metabolism is asymmetrically reduced in the putamen, thalamus, and cerebellum with an impact also on the PD-related pattern activity [57]. Unintended cerebral activations due to motor activation or visual stimulation and artifacts due to the presence of unvoluntary movements (i.e., dyskinesia, dystonia, tremor) might represent an additional caveats in the interpretation of glucose metabolism patterns. Another phenomenon that might affect brain PET studies evaluating regional distributions in basal ganglia subregions is the partial volume effect (PVE). Because of PVE, the radioactivity concentration in different regions is under- or overestimated due to "spillover" of measured radioactivity between neighboring regions. This effect is also enhanced by the presence of significant brain atrophy resulting in predictable underestimations of target availability (e.g., striatal atrophy in the striatum in HD). The application of PVE correction (PVEc) methods is thus important, despite the fact that such methods can be associated with possible biases due to noise amplification.

And last but not least, only recently the notion that the brain glucose consumption is primary generated by neuronal and synaptic activity has been challenged by new evidences that suggest a role for the astroglial unit in the generation FDG uptake [58].

Key Points

- [18F]FDG PET in movement disorders can be used as a supportive instrumental biomarker for the differential diagnosis of parkinsonian syndromes with readouts of images that are correlated with neuropathological findings.
- In clinical practice [18F]FDG PET can be used to differentiate with high accuracy the sporadic Parkinson's disease form from atypical parkinsonisms such as multiple system atrophy (MSA-P and MSA-C).
- The classical [18F]FDG PET pattern detected in MSA is a decrease of glucose metabolism in the striatum associated or not to a decrease metabolism in the cerebellum according to the phenotypical subdivision between MSA-P and MSA-C.
- A distinctive and specific [18F]FDG-PET pattern in the spectrum of progressive supranuclear palsy and corticobasal degeneration is less defined.
- In pathologically confirmed PSP case, a reduction in the glucose metabolism has been described in the caudate and supplementary motor areas, whereas an asymmetric FDG uptake in different cortical regions and basal ganglia is characteristic in corticobasal degeneration syndromes.
- In clinical practice [18F]FDG PET can be used to differentiate acquired or genetic forms of Huntingtonism. In Huntington's disease the utility of [18F]FDG PET is limited to the rare occasions in which suspected or confirmed Huntington's disease gene expression carriers present an unclear clinical motor onset.
- The interpretation and understanding of [18F]FDG-PET patterns in neurodegenerative/movement disorders is challenged by the potential interference of concomitant medication and by the dynamic pathological changes of the brain tissues.

References

1. Fahn S. Classification of movement disorders. Mov Disord. 2011;26:947–57.
2. Meyer PT, Frings L, Rücker G, Hellwig S. 18F-FDG PET in parkinsonism: differential diagnosis and cognitive impairment in Parkinson's disease. J Nucl Med. 2017b;58:1888–98.
3. Rizzo G, Copetti M, Arcuti S, Martino D, Fontana A, Logroscino G. Accuracy of clinical diagnosis of Parkinson disease: a systematic review and meta-analysis. Neurology. 2016;86: 566–76.
4. Hughes AJ, Daniel SE, Kilford L, Lees AJ. Accuracy of clinical diagnosis of idiopathic Parkinson's disease: a clinico-pathological study of 100 cases. J Neurol Neurosurg Psychiatry. 1992;55:181–4.
5. Tang CC, Poston KL, Eckert T, Feigin A, Frucht S, Gudesblatt M, et al. Differential diagnosis of parkinsonism: a metabolic imaging study using pattern analysis. Lancet Neurol. 2010;9:149–58.

6. Fereshtehnejad SM, Zeighami Y, Dagher A, Postuma RB. Clinical criteria for subtyping Parkinson's disease: biomarkers and longitudinal progression. Brain. 2017;140:1959–76.
7. Jellinger KA. The pathomechanisms underlying Parkinson's disease. [Internet]. Expert Rev Neurother. 2014b;14:199–215.
8. Eidelberg D, Moeller JR, Dhawan V, Spetsieris P, Takikawa S, Ishikawa T, et al. The metabolic topography of parkinsonism. J Cereb Blood Flow Metab. 1994;14:783–801.
9. Tripathi M, Dhawan V, Peng S. Differential diagnosis of parkinsonian syndromes using F-18 fluorodeoxyglucose positron emission tomography. Neuroradiology. 2013;55:483–92.
10. Firbank MJ, Yarnall AJ, Lawson RA, Duncan GW, Khoo TK, Petrides GS, et al. Cerebral glucose metabolism and cognition in newly diagnosed Parkinson's disease: ICICLE-PD study. J Neurol Neurosurg Psychiatry. 2017;88:310–6.
11. Teune LK, Bartels AL, De Jong BM, Willemsen ATM, Eshuis SA, De Vries JJ, et al. Typical cerebral metabolic patterns in neurodegenerative brain diseases. Mov Disord. 2010;25:2395–404.
12. Eckert T, Tang C, Eidelberg D. Assessment of the progression of Parkinson's disease: a metabolic network approach. [Internet]. Lancet Neurol. 2007;6:926–32.
13. Eckert T, Barnes A, Dhawan V, Frucht S, Gordon MF, Feigin AS, et al. FDG PET in the differential diagnosis of parkinsonian disorders. Neuroimage. 2005;26:912–21.
14. Teune LK, Renken RJ, Mudali D, De Jong BM, Dierckx RA, Roerdink JBTM, et al. Validation of parkinsonian disease-related metabolic brain patterns. Mov Disord. 2013;28:547–51.
15. Ma Y, Tang C, Spetsieris PG, Dhawan V, Eidelberg D. Abnormal metabolic network activity in Parkinson's disease: test-retest reproducibility. J Cereb Blood Flow Metab. 2007;27:597–605.
16. Tomše P, Jensterle L, Grmek M, Zaletel K, Pirtošek Z, Dhawan V, et al. Abnormal metabolic brain network associated with Parkinson's disease: replication on a new European sample. Neuroradiology. 2017;59:507–15.
17. Huang C, Tang C, Feigin A, Lesser M, Ma Y, Pourfar M, et al. Changes in network activity with the progression of Parkinson's disease. Brain. 2007;130:1834–46.
18. Ko JH, Lee CS, Eidelberg D. Metabolic network expression in parkinsonism: clinical and dopaminergic correlations. J Cereb Blood Flow Metab. 2017;37:683–93.
19. Meyer PT, Frings L, Gerta R, Hellwig S. PET in parkinsonism: differential diagnosis and evaluation of cognitive impairment. J Nucl Med. 2017a;58:1888–99.
20. Meles SK, Renken RJ, Janzen AHO, Vadasz D, Pagani M, Arnaldi D, et al. The metabolic pattern of idiopathic REM sleep behavior disorder reflects early-stage Parkinson's disease. J Nucl Med. 2018;59:1437–44.
21. Kalbe E, Voges J, Weber T, Haarer M, Baudrexel S, Klein JC, et al. Frontal FDG-PET activity correlates with cognitive outcome after STN-DBS in Parkinson disease. Neurology. 2009;72:42–9.
22. Cao C, Zhang H, Li D, Zhan S, Zhang J, Zhang X, et al. Modified fluorodeoxyglucose metabolism in motor circuitry by subthalamic deep brain stimulation. Stereotact Funct Neurosurg. 2017;95:93–101.
23. Bohnen NI, Koeppe RA, Minoshima S, Giordani B, Albin RL, Frey KA, et al. Cerebral glucose metabolic features of Parkinson disease and incident dementia: longitudinal study. J Nucl Med. 2011;52:848–55.
24. Gilman S, Wenning GK, Low PA, Brooks DJ, Mathias CJ, Trojanowski JQ, et al. Second consensus statement on the diagnosis of multiple system atrophy. [Internet]. Neurology. 2008;71:670–6.
25. Jellinger KA. Neuropathology of multiple system atrophy: new thoughts about pathogenesis. Mov Disord. 2014a;29:1720–41.
26. Boxer AL, Yu JT, Golbe LI, Litvan I, Lang AE, Höglinger GU. Advances in progressive supranuclear palsy: new diagnostic criteria, biomarkers, and therapeutic approaches. Lancet Neurol. 2017;16:552–63.
27. Höglinger GU, Respondek G, Stamelou M, Kurz C, Josephs KA, Lang AE, et al. Clinical diagnosis of progressive supranuclear palsy: the movement disorder society criteria. Mov Disord. 2017;32:853–64.

28. Ling H, O'Sullivan SS, Holton JL, Revesz T, Massey LA, Williams DR, et al. Does corticobasal degeneration exist? A clinicopathological re-evaluation. Brain. 2010;133:2045–57.
29. Armstrong MJ, Litvan I, Lang AE, Bak TH, Bhatia KP, Borroni B, et al. Criteria for the diagnosis of corticobasal degeneration. Neurology. 2013;80:496–503.
30. Wakabayashi K, Takahashi H. Symposium: Neuropathological diagnostic criteria and problems of neurodegenerative disorders. Pathological heterogeneity in progressive supranuclear palsy and corticobasal degeneration. Ann Neurol. 2004;24:79–86.
31. Dugger BN, Adler CH, Shill HA, Caviness J, Jacobson S, Driver-Dunckley E, et al. Concomitant pathologies among a spectrum of parkinsonian disorders. Parkinsonism Relat Disord. 2014;20:525–9.
32. Dickson DW, Ahmed Z, Algom AA, Tsuboi Y, Josephs KA. Neuropathology of variants of progressive supranuclear palsy. Curr Opin Neurol. 2010;23:394–400.
33. Boeve BF, Maraganore DM, Parisi JE, Ahlskog JE, Graff-Radford N, Caselli RJ, et al. Pathologic heterogeneity in clinically diagnosed corticobasal degeneration. Neurology. 1999;53:795–800.
34. Zalewski N, Botha H, Whitwell JL, Lowe V, Dickson DW, Josephs KA. FDG-PET in pathologically confirmed spontaneous 4R-tauopathy variants. J Neurol. 2014;261:710–6.
35. Ross CA, Aylward EH, Wild EJ, Langbehn DR, Long JD, Warner JH, et al. Huntington disease: natural history, biomarkers and prospects for therapeutics. Nat Rev Neurol. 2014;10:204–16.
36. Vonsattel JPG, Keller C, Cortes Ramirez EP. Huntington's disease - neuropathology. 1st ed. Amsterdam: Elsevier B.V.; 2011.
37. Rüb U, Hentschel M, Stratmann K, Brunt E, Heinsen H, Seidel K, et al. Huntington's disease (HD): degeneration of select nuclei, widespread occurrence of neuronal nuclear and axonal inclusions in the brainstem. Brain Pathol. 2014;24:247–60.
38. Rüb U, Seidel K, Heinsen H, Vonsattel JP, den Dunnen WF, Korf HW. Huntington's disease (HD): the neuropathology of a multisystem neurodegenerative disorder of the human brain. Brain Pathol. 2016;26:726–40.
39. Antonini A, Leenders KL, Spiegel R, Meier D, Vontobel P, Weigell-Weber M, et al. Striatal glucose metabolism and dopamine D2 receptor binding in asymptomatic gene carriers and patients with Huntington's disease. Brain. 1996;119(Pt 6):2085–95.
40. López-Mora DA, Camacho V, Pérez-Pérez J, Martínez-Horta S, Fernández A, Sampedro F, et al. Striatal hypometabolism in premanifest and manifest Huntington's disease patients [Internet]. Eur J Nucl Med Mol Imaging. 2016;43:2183–9.
41. Young AB, Penney JB, Starosta-rubinstein S, Markel DS, Berent S, Giordani B, et al. PET scan investigations of Huntington's disease: cerebral metabolic correlates of neurological features and functional decline. Ann Neurol. 1986;20:296–303.
42. Ciarmiello A, Cannella M, Lastoria S, Simonelli M, Frati L, Rubinsztein DC, et al. Brain white-matter volume loss and glucose hypometabolism precede the clinical symptoms of Huntington's disease. J Nucl Med. 2006;47:215–22.
43. Tang CC, Feigin A, Ma Y, Habeck C, Paulsen JS, Leenders KL, et al. Metabolic network as a progression biomarker of premanifest Huntington's disease. J Clin Invest. 2013;123:4076–88.
44. Berent S, Giordani B, Lehtinen S, Markel D, Penney JB, Buchtel HA, et al. Positron emission tomographic scan investigations of Huntington's disease: cerebral metabolic correlates of cognitive function. Ann Neurol. 1988;23:541–6.
45. Ciarmiello A, Giovacchini G, Orobello S, Bruselli L, Elifani F, Squitieri F. 18F-FDG PET uptake in the pre-Huntington disease caudate affects the time-to-onset independently of CAG expansion size. Eur J Nucl Med Mol Imaging. 2012;39:1030–6.
46. Martino D, Stamelou M, Bhatia KP. The differential diagnosis of Huntington's disease-like syndromes: 'red flags' for the clinician. J Neurol Neurosurg Psychiatry. 2013;84:650–6.
47. Ehrlich DJ, Walker RH. Functional neuroimaging and chorea: a systematic review. J Clin Mov Disord. 2017;4:8.

48. Cui R, You H, Niu N, Li F. FDG PET brain scan demonstrated glucose hypometabolism of bilateral caudate nuclei and putamina in a patient with chorea-acanthocytosis. Clin Nucl Med. 2015;40:979–80.
49. Tanaka M, Hirai S, Kondo S, Sun X, Nakagawa T, Tanaka S, et al. Cerebral hypoperfusion and hypometabolism with altered striatal signal intensity in chorea-acanthocytosis: a combined PET and MRI study. Mov Disord. 1998;13:100–7.
50. Brockmann K, Reimold M, Globas C, Hauser TK, Walter U, Rolfs A, et al. PET and MRI reveal early evidence of neurodegeneration in spinocerebellar ataxia type 17. J Nucl Med. 2018;53:1074–81.
51. Weindl A, Kuwert T, Leenders KL, Poremba M, GräFin von Einsiedel H, Antonini A, et al. Increased striatal glucose consumption in sydenham's chorea. Mov Disord. 1993;8:437–44.
52. Varrone A, Asenbaum S, Vander BT, Booij J, Nobili F, Någren K, et al. EANM procedure guidelines for PET brain imaging using [18F] FDG, Version 2. Eur J Nucl Med Mol Imaging. 2009;36(12):2103–10.
53. Booth HDE, Hirst WD, Wade-Martins R. The role of astrocyte dysfunction in Parkinson's disease pathogenesis. Trends Neurosci. 2017;40:358–70.
54. Liebner S, Dijkhuizen RM, Reiss Y, Plate KH, Agalliu D, Constantin G. Functional morphology of the blood–brain barrier in health and disease. Acta Neuropathol. 2018;135:1–26.
55. Schmidt K, Lucignani G, Moresco RM, Rizzo G, Gilardi MC, Messa C, et al. Errors introduced by tissue heterogeneity in estimation of local cerebral glucose utilization with current kinetic models of the [18F]fluorodeoxyglucose method. J Cereb Blood Flow Metab. 1992;12:823–34.
56. Berti V, Mosconi L, Pupi A. Brain: normal variations and benign findings in fluorodeoxyglucose-PET/computed tomography imaging. PET Clin. 2014;9:129–40.
57. Feigin A, Fukuda M, Dhawan V, Przedborski S, Jackson-Lewis V, Mentis MJ, et al. Metabolic correlates of levodopa response in Parkinson's disease. Neurology. 2001;57:2083–8.
58. Zimmer ER, Parent MJ, Souza DG, Leuzy A, Lecrux C, Kim H, et al. [18 F]FDG PET signal is driven by astroglial glutamate transport. Nat Neurosci. 2017;20(3):393–5.

^{18}F-FDG PET in Epilepsy

7

Ismini C. Mainta, Fabienne Picard, and Valentina Garibotto

Contents

This chapter will summarize the evidence supporting the clinical use of FDG-PET brain imaging in the evaluation of patients with pharmaco-resistant epilepsy considered for surgical treatment. We will discuss the clinical indications, the main patterns of hypometabolism observed, and the main advantages and limitations associated with its use.

I. C. Mainta
Nuclear Medicine and Molecular Imaging Division, Department of Medical Imaging, University Hospitals of Geneva, Geneva, Switzerland

Faculty of Medicine, Geneva University, Geneva, Switzerland

F. Picard
Faculty of Medicine, Geneva University, Geneva, Switzerland

EEG and Epilepsy Unit, Neurology Department, University Hospitals of Geneva, Geneva, Switzerland

V. Garibotto (✉)
Nuclear Medicine and Molecular Imaging Division, Department of Medical Imaging, University Hospitals of Geneva, Geneva, Switzerland

Faculty of Medicine, Geneva University, Geneva, Switzerland

F. Fraioli (ed.), *PET/CT in Brain Disorders*, Clinicians' Guides to Radionuclide Hybrid Imaging, https://doi.org/10.1007/978-3-030-01523-7_7

7.1 Introduction

Epilepsy is a common chronic neurological condition, affecting 0.7% (0.5–1%) of the population. Patients with epilepsy might suffer from social and professional consequences and might be at risk for accidents and increased mortality. Seizures consist in an abnormal neuroelectrical activity, occurring either in one region of the brain (focal seizures) with or without propagation (with or without secondary generalization) or in both hemispheres already at onset (generalized seizures) [1]. In about 30% of the patients, seizures persist despite antiepileptic drug treatment [2, 3] and surgery, i.e., the resection of the epileptic focus is then the only curative option. The outcome of epilepsy surgery is very good in well-selected patients, with over 50% seizure freedom at long follow-up [4]. The abnormalities most often observed in adult pharmaco-resistant patients are hippocampal sclerosis, low-grade tumors, brain malformations, and vascular abnormalities, while in children tumors and malformations are the most frequent causes [5].

A presurgical evaluation in a specialized center is thus recommended as soon as pharmaco-resistance is documented and a focal origin is possible. The aim of the presurgical work-up is diagnostic and prognostic at once, localizing the abnormality and evaluating the feasibility of surgery. Patients undergo long-term video-EEG recording, MRI, clinical and neuropsychological evaluations, and nuclear medicine investigations, namely, interictal FDG-PET and/or ictal/interictal SPECT [6]. On the basis of the analysis of the multimodal imaging results, patients are selected for invasive EEG recording with intracranial electrodes, in case of discordant results or proximity to eloquent cortex, or for surgical resection [7–9].

7.2 Clinical Indications

^{18}F-FDG is the most explored tracer for PET imaging of epilepsy and provides key additional information, particularly in cases of non-lesional (or "nonstructural") epilepsy or multifocal lesions [1].

In non-lesional focal epilepsy, an undetected focal cortical dysplasia might be suspected. For example in children less than 2 years old, immature myelination and poor gray to white matter differentiation render lesion detection on morphological imaging more difficult [10, 11]. The review of MRI after an FDG PET examination showing a focal abnormality might reveal subtle structural lesions that were previously undetected [12]. The presence of a focal hypometabolism might also, in specific cases, avoid the need for invasive recordings, e.g., in MRI-negative temporal lobe epilepsy. Indeed, patients with a clear unilateral anterior temporal PET abnormality, even without lesions visible at MRI, have an excellent prognostic outcome, comparable to lesional cases [13].

PET can also contribute to the evaluation of patients with multifocal abnormalities. In dual pathology, characterized by the presence of hippocampal sclerosis together with extrahippocampal lesions (i.e., focal cortical dysplasia, tumor, vascular malformation, contusion, infarct) with a frequency ranging from 5 to 30% in patients with refractory partial epilepsy, resection of both pathologies, when possible, has the most favorable outcome [14]. In multifocal disorders, such as tuberous sclerosis (discussed below) PET imaging might help selecting, in a multimodal approach, the "most epileptogenic" lesion.

Finally, FDG-PET can be useful for the evaluation of the functional status of the rest of the cortex, which could serve as a predictor of the cognitive outcome after resection. In children in particular, neural plasticity, expected to a certain degree postsurgically, requires a certain degree of functional integrity of the remaining cortex [10, 11].

7.3 Classical Patterns

7.3.1 Temporal

The hypometabolic region seen on interictal PET-FDG often extends beyond the epileptogenic foci, covering a broader area, rendering the exact localization of the lesion difficult [15]. This hypometabolism may represent areas of neuronal loss, reduction of synaptic activity, or inhibitory phenomena [10, 15].

In mesio-temporal lobe epilepsy, there is anterior and mesial temporal hypometabolism ipsilateral to hippocampal sclerosis (Fig. 7.1) or bilateral, asymmetric with ipsilateral predominance [16].

FDG-PET could help differentiate presurgically mesial from lateral temporal lobe epilepsy, given that in lateral temporal lobe epilepsy there is relative sparing of the mesiotemporal metabolism [17].

Alteration of thalamic metabolic activity, especially the dorsomedial nucleus is a common extratemporal manifestation of temporal lobe epilepsy [18, 19]. Typically we expect a hypometabolism ipsilateral to the temporal anomaly, that can also serve as a supplementary argument for lateralization of the epileptogenic focus [20]. Thalamic hypometabolism can be bilateral but asymmetric with ipsilateral predominance. Other extratemporal alterations that can be observed include ipsilateral hypometabolism of the basal ganglia, insula, inferior frontal lobe, and lateral parietal cortex [16]. Particularly interesting is the presence of hypometabolism in the ipsilateral frontal lobe, as it is the most common route of seizures' spread, arising from the mesio-temporal lobe. Interpretation of frontal lobe hypometabolism in temporal lobe epilepsy is advised to be interpreted in conjunction with the results of ictal SPECT, as hypometabolism could be a consequence of seizures' spread or eventually decreased synaptic activity in the context of surrounding inhibition [15], but further studies need to confirm this hypothesis.

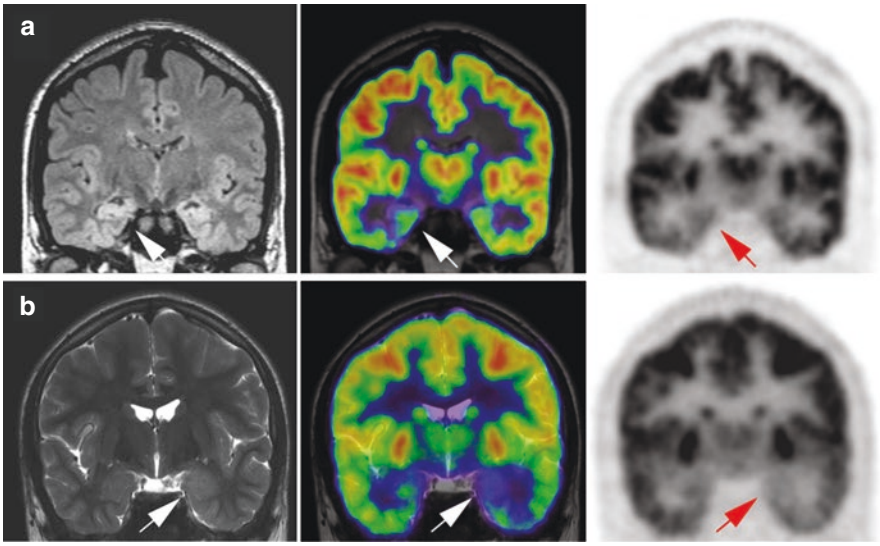

Fig. 7.1 Temporal lobe epilepsy. In patient **a** (coronal plane of MRI T2-weighted fluid-attenuated inversion recovery (FLAIR), PET/MR fusion, and FDG-PET), MRI showed a discrete atrophy of the right hippocampus (white arrow), without clear hippocampal sclerosis. Fusion PET/MR and PET demonstrated a clear mesio-temporal hypometabolism on the right (white and red arrows, respectively). In patient **b** (coronal plane of MRI T2-weighted turbo spin echo (TSE), PET/MR fusion, FDG-PET), MRI showed a hippocampal sclerosis at the left (white arrow), with increased T1 and T2 signal, without evidence of atrophy yet. Fusion PET/MR and PET confirmed the results by revealing a left mesio-temporal hypometabolism (white and red arrows, respectively)

Controlateral cerebellar hypometabolism (crossed cerebellar diaschisis) might occur in patients with temporal lobe epilepsy when prominent frontal lobe hypometabolism is present, possibly suggesting that cerebellar dysfunction in patients with temporal lobe epilepsy is associated with seizures' spread via the frontal lobe [24].

7.3.2 Extratemporal

In extratemporal epilepsy, FDG-PET does not perform as well as for temporal lobe epilepsy, with sensitivities varying from 45% to 92% for frontal lobe epilepsy [10].

FDG-PET may aid in the localization of the epileptogenic region in such difficult cases, with a reported sensitivity for frontal lobe epilepsy of 36% in patients with normal MRI and 73% in patients with MRI abnormalities [21] (Fig. 7.2). The addition of analytical and quantitative approaches can improve the detection rate of epileptogenic foci [22], particularly in frontal lobe epilepsy [23].

Hypometabolism can appear larger than the structural lesion, encompassing the lesion, the peri-lesional epileptic cortex, and a wider area of normal cortex, which becomes functionally hypometabolic (Fig. 7.3).

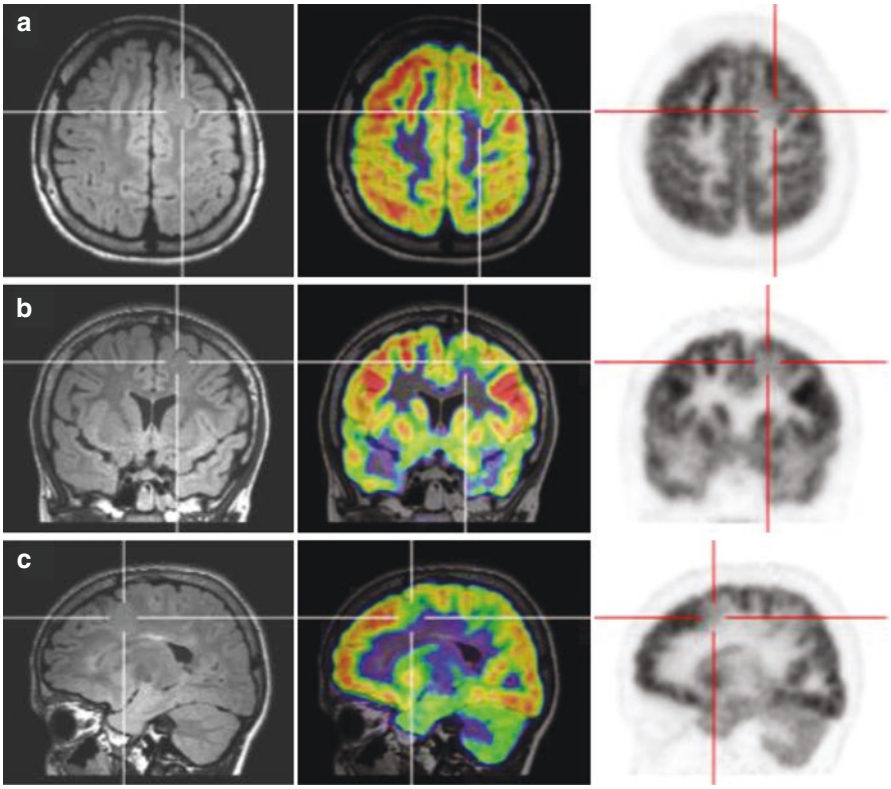

Fig. 7.2 Extratemporal lobe epilepsy. (**a**) axial view; (**b**) coronal view; (**c**) sagittal view of MRI T2-weighted fluid-attenuated inversion recovery (FLAIR), PET/MR fusion, and FDG-PET). Left frontal superior focal cortical dysplasia discretely hyperintense in the FLAIR sequence (white axes in the first column) and isointense in T2 and T1. PET/MR fusion and FDG-PET demonstrated a hypometabolism of the lesion (white and red axes in the second and third columns, respectively)

In addition, remote hypometabolism can be noticed, related to seizure propagation pathways, which could help indirectly to narrow the potential regions of seizure onset. Crossed cerebellar diaschisis is mainly seen in frontal lobe epilepsy, due to the fronto-ponto-cerebellar connections [24], as well as in parietal lobe epilepsy [10, 11]. Ipsilateral thalamic and striatal hypometabolism has also been described in frontal lobe epilepsy [19].

Extratemporal epileptogenic foci are typically hypometabolic, with the exception of heterotopia, malformations of cortical development due to abnormal neuronal migration usually in subcortical and subependymal positions (Fig. 7.4). It can either be a true hypermetabolic lesion, higher than the normal cortex, or relatively hypermetabolic, meaning lower than or similar to the normal cortex, but higher than the surrounding white matter [25, 26].

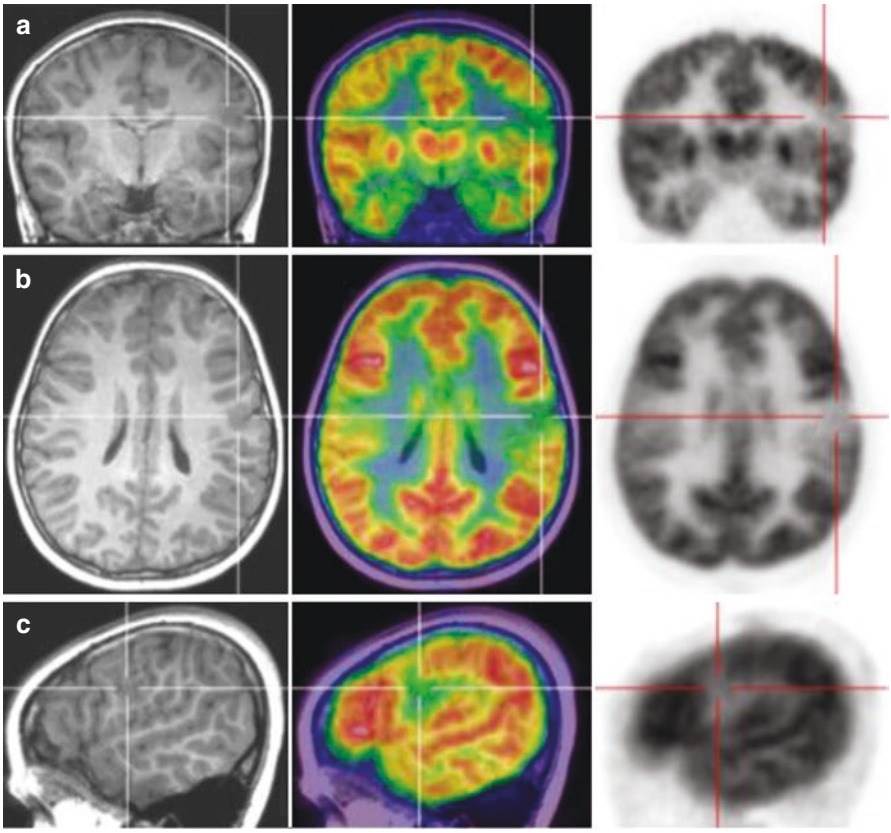

Fig. 7.3 Extratemporal lobe epilepsy. (**a**, coronal view; **b**, axial view; **c**, sagittal view of MRI T1-weighted, PET/MR fusion, and FDG-PET). Left frontal posterolateral cortical dysplasia seen as a focal thickening of the cortex (white axes in the first column). PET/MR fusion and FDG-PET showed a left frontal posterolateral hypometabolic area, larger than the morphological abnormality (white and red axes, in the second and third columns, respectively)

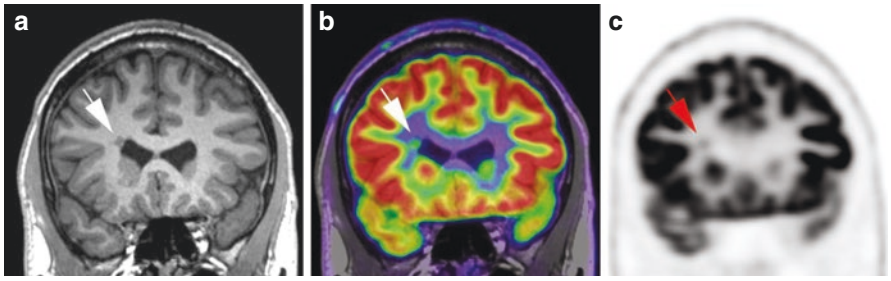

Fig. 7.4 Subependymal cortical heterotopia. Subependymal nodule at the frontal corn of the left ventricule, with intensity similar to the normal cortex ((**a**) T1-weighted magnetization-prepared rapid gradient echo (MP RAGE)) (white arrow), appearing hypermetabolic as compared to the adjacent white matter in PET/MR fusion (**b**), and FDG-PET (**c**) (white and red arrows, respectively)

7.3.3 Syndromes

The main syndromes associated with seizures as well as their metabolic patterns are outlined in Table 7.1 [11, 27–30].

Table 7.1 Syndromes associated with seizures and corresponding metabolic pattern

Metabolic pattern	Impact on surgical management
Epileptic spasms, also known as infantile spasms [11, 27]	
Four metabolic patterns in FDG-PET	
1. Unifocal hypometabolism, probably due to cortical dysplasia	Cessation of spasms and improved cognitive outcome after resection
2. Multifocal hypometabolism	Occasionally palliative surgery, if the majority of the seizures originate from one region, with improvement of the quality of life but restricted cognitive development
3. Diffuse hypometabolism, which is likely associated with an underlying neurodegenerative disorder	Not candidates for surgical treatment and other therapies have to be considered
4. Bilateral temporal hypometabolism, with distinct clinical characteristics, such as severe developmental delay	Not candidates for surgical treatment and other therapies have to be considered
Tuberous sclerosis	
Cortical tubers appear as multiple hypometabolic foci. Both epileptogenic and non-epileptogenic tubers present a decrease of metabolism [11]. The larger hypometabolic volume in FDG-PET relative to the MRI tuber size could help identifying the epileptogenic foci [28]	Cessation of seizures, with improved quality of life and cognitive outcome after resection of the epileptogenic tuber
Lennox-Gastaut syndrome	
Four main metabolic patterns [29]	Surgical outcome in Lennox-Gastaut syndrome usually remains unfavorable [11]
1. Unilateral focal hypometabolism, extending in an area of one hemisphere	In patients with poorly controlled seizures and unilateral focal hypometabolism, if EEG results are consistent with the localization of hypometabolism, cortical resection for seizure control could be considered [29, 30])
2. Unilateral diffuse, with decreased metabolism of practically the whole hemisphere	As most seizures originate from one hemisphere, seizure control could be attempted with corpus callosotomy [29]
3. Bilateral diffuse hypometabolism, with hypometabolism of the whole cortex but sparing of the primary sensory areas (visual and auditory cortex)	Not candidates for surgical treatment
4. Normal cortical metabolism	Not candidates for surgical treatment
Sturge-Weber syndrome [11]	
Hypometabolism of the cortex underlying the leptomeningeal angiomatosis Usually hypometabolism extends beyond the abnormality seen on CT or MRI. The opposite can also occur	
Rapidly evolving hypometabolism	A kind of auto-resection of the affected cortex, with improvement of seizures and cognitive function without surgical intervention

(continued)

Table 7.1 (continued)

Metabolic pattern	Impact on surgical management
Slowly evolving hypometabolism	Surgical intervention required in order to control seizures and improve cognitive function
Paradox hypermetabolism: Hypermetabolism of the affected cortex, possibly due to active cellular damage. Eventually metabolism will decrease in these patients too	Possibly an imaging sign of subsequent severe seizure, requiring early intervention
Hemimegalencephaly [11]	
The affected hemisphere can show hypo- or hypermetabolism depending of the seizure status	FDG-PET has a predictive value on postsurgical seizure control and cognitive outcome
FDG-PET is useful for the evaluation of the contralateral normal hemisphere before surgical intervention	
Rasmussen encephalitis [11]	
Early stage (<1 year from seizure onset): Unilateral hypometabolism in the frontal and temporal cortex, the parietal cortex can also be affected, but the occipital cortex is usually spared	FDG-PET is useful in lateralization of the affected cortex, before biopsy confirmation of the diagnosis, in morphologically equivocal cases and in evaluating the extent of the disease, before surgical intervention
Late stage (>1 year from seizure onset): Hypometabolism of the whole hemisphere, including the occipital cortex	

7.4 Advantages and Limitations

FDG-PET is a noninvasive technique that apart from the localization of the epileptogenic focus provides additional information on the functional status of the rest of the brain [31] with a predictive value on the postoperative seizure control and neurocognitive function. FDG-PET imaging carries important prognostic information in the presurgical evaluation of patients with epilepsy. This is well established for mesial temporal lobe epilepsy, showing that extratemporal changes have a negative prognostic value, while data in extratemporal epilepsies are more limited but suggest a similar association between multifocal FDG-PET abnormalities and worse outcome [32–34].

Although it is an expensive exam, its use has been proven not only diagnostically relevant but also cost-effective when used in cases of discordance between EEG and MRI, with invasive EEG electrodes implantation limited to patients with inconclusive PET results [35].

With routine visual assessment, which is subjective and experience-dependent, subtle hypometabolic lesions may be missed; complementary quantitative approaches add objectivity and could increase the detection rate independently of the reader's experience [22, 23].

FDG-PET image analysis should always include the evaluation of coregistered and fused PET and MRI sequences, to identify focal cortical abnormalities [36, 37].

Due to the relatively slow uptake of FDG (about 20 min), ictal FDG-PET scans are not recommended, as they represent a mixed ictal-postictal-interictal metabolism, rendering conclusions more complex [38], except maybe in cases of continuous or very frequent seizures [39]. In addition, the relatively short half-life of 18-Fluorine (110 min) limits the bedside availability of the radiotracer and scheduling of the PET scan.

Another factor that should be kept in mind during interpretation of the scan is that patients addressed for FDG-PET are under antiepileptic treatment, such as barbiturates, valproate, phenytoin, or carbamazepine, known to globally decrease cerebral metabolism [10, 11].

A novel development in the field is represented by integrated PET/MRI tomographs, offering the possibility to assess in one single session the panel of MRI-based markers and FDG-PET. The feasibility of this approach has been reported with the different tomographs available on the marker, and the main limitation for a wider use is the availability of the technology [40–43].

7.5 Conclusion

Overall, FDG-PET imaging represents a relevant diagnostic and prognostic tool in focal epilepsy and could be offered to all patients undergoing a presurgical evaluation, when available.

Key Points

- About 30–40% of patients with epilepsy suffer from seizures refractory to anti-epileptic drug treatment.
- In well-selected patients with refractory epilepsy and focal origin of seizures, surgical resection is the only curative option.
- The pre-surgical workup involves video-EEG recording, MRI, clinical and neuropsychological evaluations, interictal FDG-PET, and/or ictal/interictal SPECT.
- ^{18}F-FDG PET is a noninvasive technique that provides key additional information particularly in cases of non-lesional epilepsy or multifocal lesions, as well as information on the functional status of the rest of the brain with predictive value on the postsurgical outcome.
- The identification of ^{18}F-FDG PET abnormalities relies on visual analyses of PET images fused with MRI and supported by appropriate semiquantitative analyses comparing the individual scan with a normal reference database.

- In temporal lobe epilepsy, mesio-temporal lesions demonstrate anterior and mesial temporal hypometabolism ipsilateral or bilateral with ipsilateral predominance, while in lateral temporal lesions, there is relative sparing of the mesial basal metabolism.
- Extratemporal manifestations of temporal lobe epilepsy include ipsilateral hypometabolism of the thalamus (the most common), the basal ganglia, insula, inferior frontal and lateral parietal lobe, and contralateral cerebellar hypometabolism.
- Sensitivity is lower for extratemporal epileptogenic foci.
- In extratemporal lobe epilepsy, there is typically hypometabolism of the epileptogenic foci extending to the peri-lesional cortex and a wider area of normal cortex; an exception is heterotopia in subcortical and subependymal positions, where the lesion appears hypermetabolic.
- In syndromes associated with seizures, PET FDG presents typical metabolic patterns, useful in selecting candidates for surgical resection with predictive value on postsurgical seizure control and cognitive outcome.

References

1. Scheffer IE, Berkovic S, et al. ILAE classification of the epilepsies: position paper of the ILAE Commission for Classification and Terminology. Epilepsia. 2017;58(4):512–21.
2. Gschwind M, Seeck M. Modern management of seizures and epilepsy. Swiss Med Wkly. 2016;146:w14310.
3. Kwan P, Arzimanoglou A, et al. Definition of drug resistant epilepsy: consensus proposal by the ad hoc Task Force of the ILAE Commission on Therapeutic Strategies. Epilepsia. 2010;51(6):1069–77.
4. de Tisi J, Bell GS, et al. The long-term outcome of adult epilepsy surgery, patterns of seizure remission, and relapse: a cohort study. Lancet. 2011;378(9800):1388–95.
5. Duncan JS. Imaging in the surgical treatment of epilepsy. Nat Rev Neurol. 2010;6(10):537–50.
6. Mouthaan BE, Rados M, et al. Current use of imaging and electromagnetic source localization procedures in epilepsy surgery centers across Europe. Epilepsia. 2016;57(5):770–6.
7. ILAE. ILAE Neuroimaging Commission recommendations for neuroimaging of patients with epilepsy. Epilepsia. 2005;38(s10):1–2.
8. Lascano AM, Perneger T, et al. Yield of MRI, high-density electric source imaging (HD-ESI), SPECT and PET in epilepsy surgery candidates. Clin Neurophysiol. 2016;127(1):150–5.
9. Von Oertzen J, Urbach H, et al. Standard magnetic resonance imaging is inadequate for patients with refractory focal epilepsy. J Neurol Neurosurg Psychiatry. 2002;73(6):643–7.
10. Kumar A, Chugani HT. The role of radionuclide imaging in epilepsy, Part 1: Sporadic temporal and extratemporal lobe epilepsy. J Nucl Med. 2013a;54(10):1775–81.
11. Kumar A, Chugani HT. The role of radionuclide imaging in epilepsy, Part 2: Epilepsy syndromes. J Nucl Med. 2013b;54(11):1924–30.
12. Chassoux F, Rodrigo S, et al. FDG-PET improves surgical outcome in negative MRI Taylor-type focal cortical dysplasias. Neurology. 2010;75(24):2168–75.

13. Carne RP, O'Brien TJ, et al. MRI-negative PET-positive temporal lobe epilepsy: a distinct surgically remediable syndrome. Brain. 2004;127.(Pt 10:2276–85.
14. Li LM, Cendes F, et al. Surgical outcome in patients with epilepsy and dual pathology. Brain. 1999;122. (Pt 5:799–805.
15. la Fougere C, Rominger A, et al. PET and SPECT in epilepsy: a critical review. Epilepsy Behav. 2009;15(1):50–5.
16. Wieser HG. The role of PET in the diagnosis of epilepsies. Epileptologie. 2004;21:109–16.
17. Guedj E, Bonini F, et al. 18FDG-PET in different subtypes of temporal lobe epilepsy: SEEG validation and predictive value. Epilepsia. 2015;56(3):414–21.
18. Juhasz C, Nagy F, et al. Glucose and [11C]flumazenil positron emission tomography abnormalities of thalamic nuclei in temporal lobe epilepsy. Neurology. 1999;53(9):2037–45.
19. Semah F. PET imaging in epilepsy: basal ganglia and thalamic involvement. Epileptic Disord. 2002;4(Suppl 3):S55–60.
20. Chang CP, Yen DJ, et al. Unilateral thalamic hypometabolism in patients with temporal lobe epilepsy. J Formos Med Assoc. 2008;107(7):567–71.
21. Kim YK, Lee DS, et al. (18)F-FDG PET in localization of frontal lobe epilepsy: comparison of visual and SPM analysis. J Nucl Med. 2002;43(9):1167–74.
22. Wang K, Liu T, et al. Comparative study of voxel-based epileptic foci localization accuracy between statistical parametric mapping and three-dimensional stereotactic surface projection. Front Neurol. 2016;7:164.
23. Mendes Coelho VC, Morita ME, et al. Automated online quantification method for (18)F-FDG positron emission tomography/CT improves detection of the epileptogenic zone in patients with pharmacoresistant epilepsy. Front Neurol. 2017;8:453.
24. Savic I, Altshuler L, et al. Localized cerebellar hypometabolism in patients with complex partial seizures. Epilepsia. 1996;37(8):781–7.
25. Conrad GR, Sinha P. FDG PET imaging of subependymal gray matter heterotopia. Clin Nucl Med. 2005;30(1):35–6.
26. Morioka T, Nishio S, et al. Functional imaging in periventricular nodular heterotopia with the use of FDG-PET and HMPAO-SPECT. Neurosurg Rev. 1999;22(1):41–4.
27. Chugani HT, Conti JR. Etiologic classification of infantile spasms in 140 cases: role of positron emission tomography. J Child Neurol. 1996;11(1):44–8.
28. Chandra PS, Salamon N, et al. FDG-PET/MRI coregistration and diffusion-tensor imaging distinguish epileptogenic tubers and cortex in patients with tuberous sclerosis complex: a preliminary report. Epilepsia. 2006;47(9):1543–9.
29. Chugani HT, Mazziotta JC, et al. The Lennox-Gastaut syndrome: metabolic subtypes determined by 2-deoxy-2[18F]fluoro-D-glucose positron emission tomography. Ann Neurol. 1987;21(1):4–13.
30. You SJ, Lee JK, et al. Epilepsy surgery in a patient with Lennox-Gastaut syndrome and cortical dysplasia. Brain and Development. 2007;29(3):167–70.
31. Sarikaya I. PET studies in epilepsy. Am J Nucl Med Mol Imaging. 2015;5(5):416–30.
32. Chassoux F, Artiges E, et al. (18)F-FDG-PET patterns of surgical success and failure in mesial temporal lobe epilepsy. Neurology. 2017;88(11):1045–53.
33. Wong CH, Bleasel A, et al. The topography and significance of extratemporal hypometabolism in refractory mesial temporal lobe epilepsy examined by FDG-PET. Epilepsia. 2010;51(8):1365–73.
34. Wong CH, Bleasel A, et al. Relationship between preoperative hypometabolism and surgical outcome in neocortical epilepsy surgery. Epilepsia. 2012;53(8):1333–40.
35. Hinde S, Soares M, et al. The added clinical and economic value of diagnostic testing for epilepsy surgery. Epilepsy Res. 2014;108(4):775–81.
36. Desarnaud S, Mellerio C, et al. (18)F-FDG PET in drug-resistant epilepsy due to focal cortical dysplasia type 2: additional value of electroclinical data and coregistration with MRI. Eur J Nucl Med Mol Imaging. 2018;45(8):1449–60.
37. Salamon N, Kung J, et al. FDG-PET/MRI coregistration improves detection of cortical dysplasia in patients with epilepsy. Neurology. 2008;71(20):1594–601.

38. Hodolic M, Topakian R, et al. (18)F-fluorodeoxyglucose and (18)F-flumazenil positron emission tomography in patients with refractory epilepsy. Radiol Oncol. 2016;50(3):247–53.
39. Meltzer CC, Adelson PD, et al. Planned ictal FDG PET imaging for localization of extratemporal epileptic foci. Epilepsia. 2000;41(2):193–200.
40. Garibotto V, Heinzer S, et al. Clinical applications of hybrid PET/MRI in neuroimaging. Clin Nucl Med. 2013;38(1):e13–8.
41. Grouiller F, Delattre BM, et al. All-in-one interictal presurgical imaging in patients with epilepsy: single-session EEG/PET/(f)MRI. Eur J Nucl Med Mol Imaging. 2015;42(7):1133–43.
42. Paldino MJ, Yang E, et al. Comparison of the diagnostic accuracy of PET/MRI to PET/CT-acquired FDG brain exams for seizure focus detection: a prospective study. Pediatr Radiol. 2017;47(11):1500–7.
43. Shin HW, Jewells V, et al. Initial experience in hybrid PET-MRI for evaluation of refractory focal onset epilepsy. Seizure. 2015;31:1–4.

PET in Neuro-Oncology

8

Francesco Fraioli

Contents

8.1 Introduction

Gliomas account for 80% of all intrinsic primary brain tumours, including several subtypes with different prognoses [1]. Histological characterisation following the World Health Organisation (WHO) groups gliomas on cell origin (astrocytoma, oligodendroglioma), with assessment of pathological features of malignancy.

F. Fraioli (✉)
Institute of Nuclear Medicine, University College London, London, UK
e-mail: francesco.faioli@nhs.net

F. Fraioli (ed.), *PET/CT in Brain Disorders*, Clinicians' Guides to Radionuclide Hybrid Imaging, https://doi.org/10.1007/978-3-030-01523-7_8

Low-grade gliomas (LGG, WHO grades I–II) show a better prognosis than high-grade gliomas (HGG, WHO grade III–IV) [2].

Mutations in the isocitrate dehydrogenase (IDH) gene is an early event in gliomagenesis [3] and enables distinction between primary (IDH wild type) and secondary (IDH mutated) glioblastomas. Previous investigations have demonstrated a prognostic role of this mutation. IDH wild-type LGG often presents a clinical course similar to glioblastomas regardless treatment. The new WHO brain tumour classification includes molecular assessment as part of an integrated diagnosis [4].

Anatomical MRI offers excellent visual detail [5] but lacks sensitivity and specificity in prediction of glioma grade, malignant transformation and molecular status. Advanced MRI techniques (diffusion, perfusion and spectroscopy) can add information but do not completely predict tumour grade, possible transformation or molecular status [6]. Molecular imaging has been proposed as emerging imaging technique assisting glioma characterisation noninvasively. In this chapter, the main applications of PET in neuro-oncology will be discussed.

8.2 PET in Primary Glioma Diagnosis and Differential Diagnosis

8.2.1 ^{18}F-FDG

^{18}F-FDG PET is the most used tracer in oncology but effectively not often used in glioma due to the high uptake in cerebral parenchyma which can obscure the visualisation of underlying malignancy. However old studies reported that ^{18}F-FDG PET may distinguish HGG from other malignant brain tumours [7]. Most recent small retrospective studies [8, 9] demonstrated a significantly higher ^{18}F-FDG uptake in CNS lymphomas compared to HGG and metastases. SUV_{max} >12 had sensitivity of 100% (but lower specificity 71.4% for primary central nervous system lymphoma [PCNSL]). These were small studies with no follow-up data, and some patients had pre-PET steroids, known to reduce FDG accumulation, potentially affecting overall results (Fig. 8.1).

8.2.2 ^{11}C-MET

Few data have assessed ^{11}C-MET in brain tumour diagnostics. One paper showed significantly higher ^{11}C-MET uptake in lymphoma compared to glioblastomas [10], which correlated with high FDG uptake. This was done in a small cohort; therefore ^{11}C-MET PET is not recommended at present for the differential diagnosis of brain lesions.

8.2.3 ^{18}F-FET

In five studies with 180 patients included in a meta-analysis, ^{18}F-FET uptake of TBR_{mean} >1.7 (sensitivity 71%, specificity 72%) and TBR_{max} >2.1 (sensitivity 65% and specificity 56%) provided best diagnostic performance for glioma

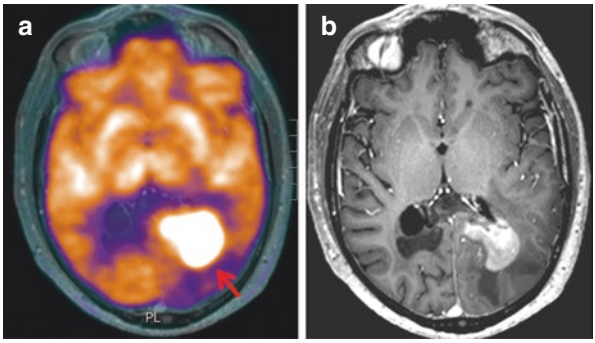

Fig. 8.1 Axial fused 18F FDG PET/MR (**a**) and post contrast T1WI (**b**) demonstrates intense increased FDG uptake in the periventricular region of the posterior horn of the left lateral ventricle (**a**, arrow) which corresponds to an enhancing lesion on the post contrast MR (**b**), in a patient with CNS lymphoma

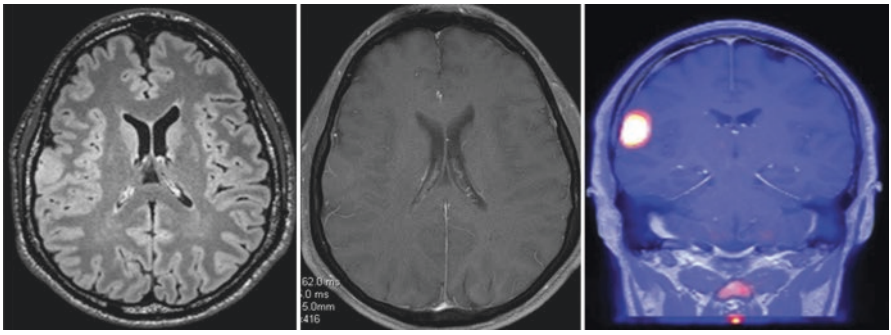

Fig. 8.2 FET-PET/MRI in tumor diagnosis, delineation and grading diagnosis in a 50 y-old patient. MRI: right to left the images show a ill defined, non-enhancing tumor in the right temporal hemisphere. FET PET fused with coronal MRI identifies a focus of uptake at the same level: SUVmax 7.6. Guided biopsy: Pathology: Anaplastic oligoastrocytoma WHO III

characterisation (Fig. 8.2) [11]. In a more recent meta-analysis including patients with brain lesions undergoing both ^{18}F-FET and ^{18}F-FDG PET, it was demonstrated that ^{18}F-FET PET was significantly higher in gliomas than in non-tumoural lesions and superior to ^{18}F-FDG, which could not make this distinction [12].

A study by Rapp et al. showed that neoplastic lesions had significantly higher ^{18}F-FET uptake than nonneoplastic lesions (NNLs). TBRmax >2.5 was the optional cutoff to differentiate between neoplastic lesions and NNLS (sensitivity 57%, specificity 92%). However, the same cutoff value was also optimal for the differentiation between HGG and LGG (sensitivity 79%, specificity 72%). Thus uptake of >2.5 may be useful in excluding HGG only [13].

8.2.4 ^{18}F-FDOPA

Several studies have compared ^{18}F-FDOPA with other tracers. Correlation between ^{18}F-FDOPA and ^{11}C-MET uptake demonstrated almost identical uptake on visual

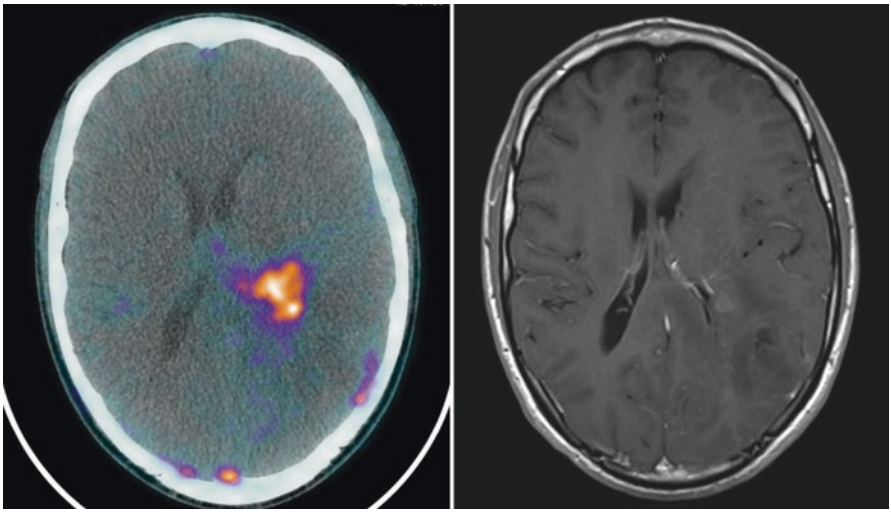

Fig. 8.3 Intense F-Dopa uptake in non-enhancing high grade glioma

inspection [14]. Similar results were shown between ^{18}F-FDOPA and ^{18}F-FET on visual inspection in 27 HGGs (and reported sensitivity 100%) [14]. However, it is worth to remind that even if ^{18}F-FDOPA may be more appropriate for clinical use because of longer half-life and limited scanning time, their cost limits the application in routine clinical setting (Fig. 8.3).

8.2.5 ^{18}F-CHO

In a large retrospective study involving 95 gliomas (grade II–IV), both ^{18}F-CHO and ^{11}C-MET were superior to ^{18}F-FDG in diagnosing gliomas. Only 13.7% of gliomas demonstrated increased uptake (T/N ratio >2) with ^{18}F-FDG, compared to 71.6% with ^{18}F-CHO and 87.4% with ^{11}C-MET. Moreover, ^{18}F-CHO uptake in normal brain parenchyma was lower than that of ^{11}C-MET (SUV_{mean} 0.29 ± 0.007 compared to 1.25 ± 0.39) [15], demonstrating potential adding value of this tracer in tumour burden. Another small sample study comparing ^{18}F-CHO and ^{11}C-MET in imaging brain metastases found that ^{18}F-CHO had significantly higher L/N ratios in tumour tissue (LNR_{median} 6.6) [16] (Fig. 8.4).

8.2.6 ^{18}F-FLT

Different studies have evaluated ^{18}F-FLT in the diagnosis of glioma. In a small cohort of 18 brain tumours (n = 12 HGG, n = 6 LGG) and 8 non-tumoural lesions, ^{18}F-FLT presented sensitivity 79% and specificity of 65% in brain tumour diagnosis [17]. Jacobs et al. investigated with both ^{18}F-FLT and ^{11}C-MET 23 patients and

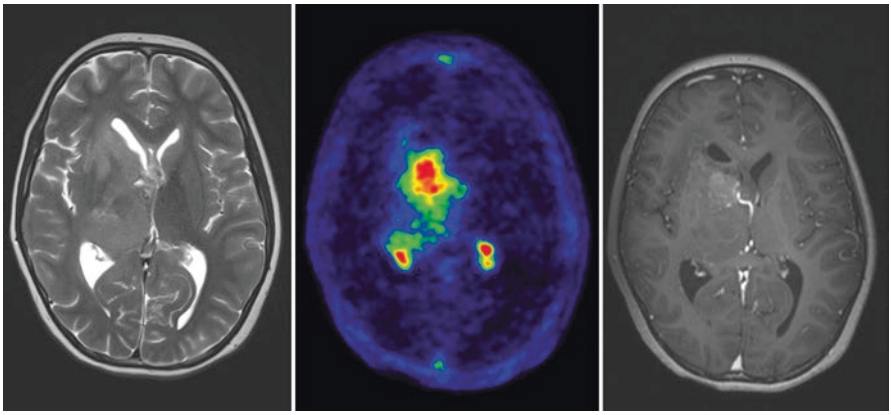

Fig. 8.4 Large WHO 4 glioma with limited enhancement on MRI and intense uptake on F-Choline PET

found that ^{18}F-FLT sensitivity for tumour detection was good (78.3%) but lower than ^{11}C-MET (91.3%) [18]. Similar sensitivity (83.8%) for tumour detection with ^{18}F-FLT was also demonstrated in subsequent comparative study with ^{11}C-MET PET again with ^{11}C-MET superior in sensitivity (87.8%) [19, 20]. ^{18}F-FLT SUV appear lower than with other tracers; TN ratios are higher because of low background uptake, thus providing good image contrast.

In summary, current evidence suggest ^{18}F-FDG is able to distinguish lymphoma from other entities by demonstrating significantly higher SUV values. Amino acid tracers such as ^{11}C-MET have also demonstrated significantly higher uptake in lymphomas compared to gliomas, but due to the limited availability of these tracers, ^{18}F-FDG remains the first choice. ^{18}F-FET appears to have some value in glioma diagnostics where a negative ^{18}F-FET indicates glioma as an unlikely diagnosis. ^{18}F-FDOPA may have similar uptake on visual inspection to ^{11}C-MET and ^{18}F-FET but compared to ^{11}C-MET may be advantageous clinically because of long half-life (but high cost). ^{18}F-CHO appears to have low physiological uptake, with potential benefit in tumour delineation, but has limited evidence for use in gliomas as less sensitive than other tracers. ^{18}F-FLT appears sensitive to malignant glioma, but ^{11}C-MET PET may be more sensitive overall for glioma detection (both HGG and LGG).

8.3 Amino Acid Tracers PET in Glioma Histological Subtyping

^{18}F-FET may be valuable in histological subtyping; low-grade oligodendrogliomas have a higher ^{18}F-FET uptake compared to astrocytomas. Similar observations have been made using ^{11}C-MET and ^{18}F-FDOPA where higher uptake was demonstrated in grade II oligodendrogliomas compared to diffuse astrocytomas [22]. These

observations may be secondary to elevated microvessel density in oligodendrogliomas and higher tumour perfusion allowing for increased amino acid uptake [23]. Oligoastrocytoma tracer uptake is between that of oligodendrogliomas and astrocytomas, perhaps reflecting mixed metabolic features. These studies, however, had no follow-up data, and grading was based on the old WHO classification. Since diffuse astrocytomas are more likely to undergo malignant transformation, one could argue that characterisation of tracer uptake in these tumours would be of greater clinical importance.

8.4 PET in Glioma Grading

Routine methods for tumour grading involve biopsy or surgical resection but as known they are invasive, thus with additional risk to the patient and possible limitations with underestimation and misinterpretation of tumour tissue secondary to tissue sample errors. Discrimination between LGG and HGG remains crucial for treatment-related decisions and prognosis.

8.4.1 ^{18}F-FET

Dunet et al. [25] comparing ^{18}F-FET and ^{18}F-FDG for glioma grading found that both tracers demonstrated higher uptake in HGG compared with LGG. Suggested HGG cutoff values using ^{18}F-FDG were TBR_{mean} >1.4, TBR_{max} >1.8, and ^{18}F-FET TBR_{mean} >2.0, TBR_{max} >3.0 [26]. ^{18}F-FET cutoffs yielded higher sensitivity, specificity and accuracy and have been studied more frequently, but there was statistically no significant difference in using these two tracers for glioma grading ($P > 0.11$).

Rapp et al. also reported significantly higher ^{18}F-FET uptake in HGG compared to LGG. Optimal HGG TBR_{max} cutoff >2.5 (sensitivity 80%, specificity 65%) was lower than that suggested by Dunet et al. Limitations of this latter study was low PPV 66% and NPV 79%, meaning histological confirmation would still be needed.

8.4.2 ^{11}C-MET

In two retrospective studies, ^{11}C-MET uptake was higher in glioblastomas (T/N ratio 5.03 ± 1.65) and anaplastic astrocytomas (3.03 ± 1.02) compared to diffuse astrocytomas (2.24 ± 0.90) ($P < 0.001$) [26]. However none of these studies provided HGG cutoff values. Without standardisation and establishment of reliable cutoff values, interpretation of results is difficult and of limited use clinically [27]. In another small (35 patients) study, Takano et al. used ^{11}C-MET T/N ratio >2 to discriminate HGG from LGG. However results are still controversial, and high uptake does not necessarily indicate HGG [28]. A low uptake could perhaps exclude HGG however but requires careful evaluation.

8.4.3 ^{18}F-FDOPA

^{18}F-FDOPA uptake also appears significantly higher in HGG compared to LGG in newly diagnosed gliomas; SUV_{max} >2.72 discriminated between HGG and LGG (sensitivity 85%, specificity 89%). There was no significant difference in uptakes between recurrent HGG and LGG however [29]. This is in contrast to a more recent study, where a significant difference in uptake was demonstrated regardless of whether tumours were newly diagnosed or recurrent. In this cohort, SUV_{max} >2.5 discriminated between HGG and LGG (sensitivity 76%, specificity of 70%) [13].

Uptake patterns and characterisation of tumour grade may again be difficult due to the inhomogeneous cohort in small retrospective studies.

8.4.4 ^{18}F-FLT

Chen et al. found that ^{18}F-FLT was negative in LGG without MRI contrast enhancement [20]. Studies consistently report negative ^{18}F-FLT PET in LGG, with sensitivity for detecting LGG ranging from 20 to 60% [30]. Also reported is the lack of statistically significant difference in uptakes between grades II and III. This may be due to small sample size. Both these studies demonstrated significant difference between grades III and IV and grades II and IV however. When compared to ^{18F}-FDG, ^{18}F-FLT showed significantly increased uptake in all HGG. In nine gliomas evaluated, ^{18}F-FLT also correlated with tumour grade and cellular proliferation in contrast to ^{8F}-FDG which failed to show any such correlations [31]. T/N ratio varies between studies, due to differences in protocols and study populations some of which include mixed glioma cohort. This makes comparisons difficult, and limited semiquantitative data and cutoff values have been reported.

In a more recent comparison study, both ^{18}F-FLT and ^{18}F-FET were able to differentiate HGG from LGG and differences in SUVmax, and T/N ratio were statistically significant [32]. ^{18}F-FLT detected 100% of the HGG (n = 17) but none of LGG (n = 3). This was in contrast to ^{18}F-FET PET which was positive in all tumours regardless of grade.

8.5 Glioma Treatment Effect and Recurrence

Standard glioma treatment involves maximal resection followed by radiotherapy (RT) with/without adjuvant chemotherapy with PCV (procarbazine, lomustine, vincristine) regimen or temozolonide (TMZ) for glioblastoma. RT planning relies on neuroimaging where targets have to be precise to minimise radiation damage to healthy tissues. The aim of PET and molecular imaging is to improve delineation of metabolically active lesions not necessarily evident on structural MRI [33]. Post treatment, patients undergo MRI surveillance for tumour recurrence (high incidence due to infiltrative nature) [34] and/or treatment-related effects including pseudoprogression (PP) and radiation necrosis (RN). RN occurs in 3–24% post

radio-chemotherapy for glioblastoma [35], and PP occurs in up to 10–30% of glioblastoma following standard treatment.

PP is thought to represent a subacute (within 12 weeks) post-treatment reaction; typically, there is increased enhanced lesion and oedema on MRI, mimicking tumour progression and recurrence. However, it does not require treatment and undergoes spontaneous resolution [2]. RN tends to be a later complication, manifesting within 6 months after standard RT but can occur within months to years [35]. RN is also associated with oedema, contrast enhancement and mass effect on MRI [36], in close vicinity to original tumour [37]. Conventional imaging does not allow for discrimination between PP, RN and recurrence [2], because of similar MRI features; PET may assist in discriminating these entities which is crucial, considering that therapeutic strategies and prognosis are very different; PP and RN are indicators of response to chemo-radiation, associated with prolonged survival in glioma patients. Recurrence, however, is usually more aggressive than the primary tumour, carrying a very poor prognosis.

8.6 PET Tracers in Differentiating Recurrence from Treatment Effects

It is unclear which PET tracer is superior in distinguishing recurrence from RN. One retrospective study comparing ^{11}C-MET, ^{18}F-CHO and ^{18}F-FDG in 50 patients post resection and RT for malignant glioma found that ^{11}C-MET was superior in differentiating glioma recurrence from RN. ^{11}C-MET uptake may be lower in RN than in recurrence; ^{11}C-MET uptake in RN may be through passive diffusion through a disrupted BBB, which is different from tumour recurrence where there is active transport of ^{11}C-MET across cell membranes in proliferating tumour cells. RN may also have increased biological activity, however, in the context of inflammatory reactions and reactive glial cells post treatment. The difficulties with this is when there is mixed pathology, i.e. both RN and residual/recurrent tumour cells. An L/N of >2.51 had sensitivity of 91.3 % and specificity of 87.5% for detection of recurrence [38]. L/N cutoff values were higher in this study compared to previous studies; Terakawa et al., also using ^{11}C-MET in 26 glioma patients, found that a L/N_{mean} cutoff >1.58 provided the best sensitivity and specificity (75% and 75%, respectively) for differentiating recurrence from RN [39]. Takenaka et al. may have found higher values due to multiple injections of PET tracers (three in total in the course of a day) in their population. However, half-lives of ^{11}C-MET and ^{18}F-CHO are short, and PET scans were done after set time intervals to minimise “cross talk” between tracers (Figs. 8.5 and 8.6).

^{18}F-FDOPA has also been used to evaluate recurrence but in much smaller and fewer studies. One prospective study with 21 recurrent gliomas demonstrated ^{18}F-FDOPA T/N ratio of >1.3 (sensitivity of 100% and specificity 85.7%) was superior to ^{18}F-FDG (sensitivity 47.6% and specificity 100%) in evaluating recurrence [40, 41]. Sample size was small and there were few patients in each histological

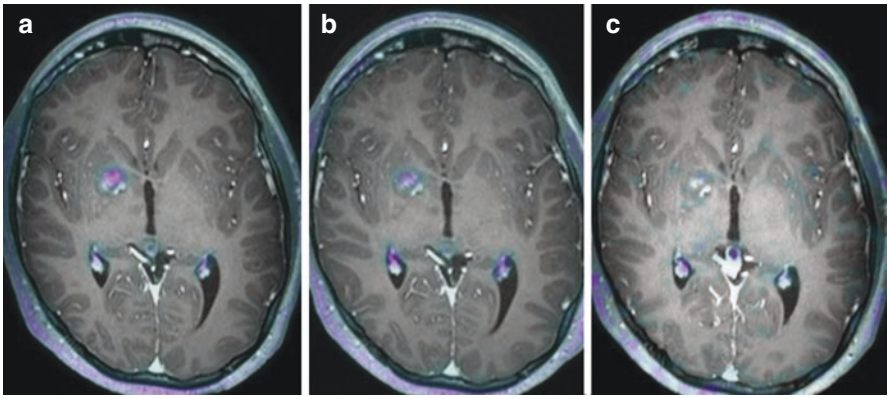

Fig. 8.5 An 18-year-old man with a low-grade glioma. Baseline (a) and postchemotherapy scans (b, 2 months; c, 6 months). Magnetic resonance image shows similar size among the three examinations but with a decrease in SUVmax/mean in 18F-Choline

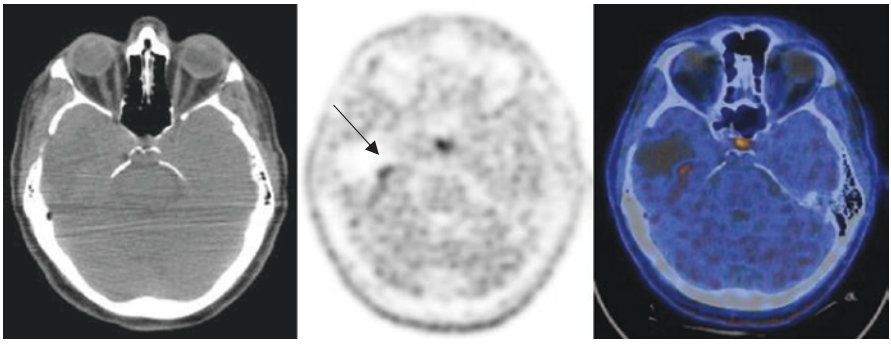

Fig. 8.6 Astrocytoma III after surgery in a 41-year-old female. PET MET shows the presence of a small focus of faint uptake (SUVmax 2 T/B ratio 1.3) in the right temporal lobe. The finding is suspicious for initial local recurrence and deserves strict monitoring (case courtesy of Dr. Castellucci, University St. Orsola Malpighi, Bologna, Italy)

grade. Histopathological conformation of recurrence was only available in four patients, with the remaining diagnosed as such based on clinical deterioration or death in keeping with recurrence. The seven nonrecurrent patients were disease-free at 1 year follow-up. Fifteen patients were evaluated in another prospective study, with nine patients having recurrence and all visualised on ^{18}F-FDOPA PET. Only six of these were visualised on ^{18}F-FDG [42]. Because of a small sample, they did not provide cutoff values for SUV Max for comparison among the two tracers.

Evidence for tracers other than ^{18}F-FDG, ^{18}F-FDOPA and ^{11}C-MET is sparse. Although studies may suggest increased amino acid uptake in recurrence, validation of these results are needed in larger prospective multi-centre studies to provide larger quantitative data sets for comparisons.

8.7 Conclusion

PET in conjunction with structural data appears to be useful in some oncological settings to characterise and quantify metabolically active tumours, differentiating these from normal tissue. In brain imaging, high physiological glucose uptake has made ^{18}F-FDG, a widely available tracer, less reliable. While the interest for amino acid tracers is increasing, major limitations to their use include difficulties in production and short half-lives. Based on the hypothesis that amino acid transport is upregulated in tumour cells, high tracer uptake in gliomas has been demonstrated in several studies; these imaging techniques may differentiate between glioma and non-glial tumours and predict tumour grade and, in some cases, possibly support glioma work up in the clinical setting. However, without standardisation of PET techniques, results remain difficult to compare and interpret. High tracer uptake is also frequently reported in non-tumoural lesions, which reduces its specificity. Reliable diagnostic tracer uptake values and cutoffs are currently lacking in the literature, thus limiting the value of these techniques clinically. There is no strong evidence for clinical use currently, bearing in mind the additional radiation burden associated with PET. More prospective, multi-centred studied are needed, to validate PET as a beneficial noninvasive imaging technique in glioma diagnostics, grading and assessment of molecular status.

Key Points

- Anatomical MRI offers excellent visual detail but lacks sensitivity and specificity in prediction of glioma grade, malignant transformation, and molecular status. Molecular imaging has been proposed as emerging imaging technique assisting glioma characterization noninvasively.
- ^{18}F-FDG uptake is much higher in CNS lymphomas compared to HGG and metastases. ^{18}F-FDG PET is not effectively often used in glioma due to the high uptake in cerebral parenchyma which can obscure the visualization of underlying malignancy.
- Amino acid PET tracers have demonstrated a certain value in discriminating low- and high-grade gliomas.
- Conventional imaging does not allow for discrimination between pseudoprogression, radiation necrosis, and recurrence, because of similar MRI features; PET may assist in discriminating these entities.
- Several reports showed an impact of FET-PET, MET PET, and FDOPA PET to assess treatment response, superior to MRI.

References

1. Parsons DW, Jones S, Zhang X, Lin JC-H, Leary RJ, Angenendt P, et al. An integrated genomic analysis of human glioblastoma multiforme. Science. 2008;321(5897):1807–12.
2. Miyake K, Ogawa D, Okada M, Hatakeyama T, Tamiya T. Usefulness of positron emission tomographic studies for gliomas. Neurol Med Chir (Tokyo). 2016;56(7):396–408.
3. Brandner S, von Deimling A. Diagnostic, prognostic and predictive relevance of molecular markers in gliomas. Neuropathol Appl Neurobiol. 2015;41(6):694–720.
4. Louis DN, Perry A, Reifenberger G, von Deimling A, Figarella-Branger D, Cavenee WK, et al. The 2016 World Health Organization classification of tumors of the central nervous system: a summary. Acta Neuropathol. 2016;131(6):803–20.
5. Hutterer M, Nowosielski M, Putzer D, Jansen NL, Seiz M, Schocke M, et al. [18F]-fluoro-ethyl-L-tyrosine PET: a valuable diagnostic tool in neuro-oncology, but not all that glitters is glioma. Neuro Oncol. 2013;15(3):341–51.
6. Janvier L, Olivier P, Blonski M, Morel O, Vignaud J-M, Karcher G, et al. Correlation of SUV-derived indices with tumoral aggressiveness of gliomas in static 18F-FDOPA PET: use in clinical practice. Clin Nucl Med. 2015;40(9):e429–35.
7. Albert NL, Weller M, Suchorska B, Galldiks N, Soffietti R, Kim MM, et al. Response Assessment in Neuro-Oncology working group and European Association for Neuro-Oncology recommendations for the clinical use of PET imaging in gliomas. Neuro Oncol. 2016;18(9):1199–208.
8. Kosaka N, Tsuchida T, Uematsu H, Kimura H, Okazawa H, Itoh H. 18F-FDG PET of common enhancing malignant brain tumors. AJR Am J Roentgenol. 2008;190(6):W365–9.
9. Makino K, Hirai T, Nakamura H, Murakami R, Kitajima M, Shigematsu Y, et al. Does adding FDG-PET to MRI improve the differentiation between primary cerebral lymphoma and glioblastoma? Observer performance study. Ann Nucl Med. 2011;25(6):432–8.
10. Okada Y, Nihashi T, Fujii M, Kato K, Okochi Y, Ando Y, et al. Differentiation of newly diagnosed glioblastoma multiforme and intracranial diffuse large B-cell Lymphoma using (11) C-methionine and (18)F-FDG PET. Clin Nucl Med. 2012;37(9):843–9.
11. Dunet V, Rossier C, Buck A, Stupp R, Prior JO. Performance of 18F-fluoro-ethyl-tyrosine (18F-FET) PET for the differential diagnosis of primary brain tumor: a systematic review and metaanalysis. J Nucl Med. 2012;53(2):207–14.
12. Dunet V, Pomoni A, Hottinger A, Nicod-Lalonde M, Prior JO. Performance of 18F-FET versus 18F-FDG-PET for the diagnosis and grading of brain tumors: systematic review and meta-analysis. Neuro Oncol. 2016;18(3):426–34.
13. Rapp M, Heinzel A, Galldiks N, Stoffels G, Felsberg J, Ewelt C, et al. Diagnostic performance of 18F-FET PET in newly diagnosed cerebral lesions suggestive of glioma. J Nucl Med. 2013;54(2):229–35.
14. Bell C, Dowson N, Puttick S, Gal Y, Thomas P, Fay M, et al. Increasing feasibility and utility of (18)F-FDOPA PET for the management of glioma. Nucl Med Biol. 2015;42(10):788–95.
15. Kato T, Shinoda J, Nakayama N, Miwa K, Okumura A, Yano H, et al. Metabolic assessment of gliomas using 11C-methionine, [18F] fluorodeoxyglucose, and 11C-choline positron-emission tomography. Am J Neuroradiol. 2008;29(6):1176–82.
16. Rottenburger C, Hentschel M, Kelly T, Trippel M, Brink I, Reithmeier T, et al. Comparison of C-11 methionine and C-11 choline for PET imaging of brain metastases: a prospective pilot study. Clin Nucl Med. 2011;36(8):639–42.
17. Wagner M, Seitz U, Buck A, Neumaier B, Schultheiss S, Bangerter M, et al. 3′-[18F] fluoro-3′-deoxythymidine ([18F]-FLT) as positron emission tomography tracer for imaging proliferation in a murine B-Cell lymphoma model and in the human disease. Cancer Res. 2003;63(10):2681–7.

18. Jacobs AH, Thomas A, Kracht LW. 18-F-3-Fluoro-3-deoxy-thymidine and 11C-methyilmetionine as markers of increased transport and proliferation in brain tumor. J Nucl Med. 2005;46(12):1948–59.
19. Gulyas B, Halldin C. New PET radiopharmaceuticals beyond FDG for brain tumor imaging. Q J Nucl Med Mol Imaging. 2012;56(2):173–90.
20. Shields AF, Grierson JR, Dohmen BM, Machulla HJ, Stayanoff JC, Lawhorn-Crews JM, et al. Imaging proliferation in vivo with [F-18]FLT and positron emission tomography. Nat Med. 1998;4(11):1334–6.
21. Kato T, Shinoda J, Oka N, Miwa K, Nakayama N, Yano H, et al. Analysis of 11C-methionine uptake in low-grade gliomas and correlation with proliferative activity. AJNR Am J Neuroradiol. 2008;29(10):1867–71.
22. Lapa C, Linsenmann T, Monoranu CM, Samnick S, Buck AK, Bluemel C, et al. Comparison of the amino acid tracers 18F-FET and 18F-DOPA in high-grade glioma patients. J Nucl Med. 2014;55(10):1611–6.
23. Pichler R, Dunzinger A, Wurm G, Pichler J, Weis S, Nussbaumer K, et al. Is there a place for FET PET in the initial evaluation of brain lesions with unknown significance? Eur J Nucl Med Mol Imaging. 2010;37(8):1521–8.
24. Chen W, Cloughesy T, Kamdar N, Satyamurthy N, Bergsneider M, Liau L, et al. Imaging proliferation in brain tumors with key words. J Nucl Med. 2005;46:945–52.
25. Glaudemans AWJM, Enting RH, Heesters MAAM, Dierckx RAJO, van Rheenen RWJ, Walenkamp AME, et al. Value of 11C-methionine PET in imaging brain tumours and metastases. Eur J Nucl Med Mol Imaging. 2013;40(4):615–35.
26. Takano K, Kinoshita M, Arita H, Okita Y, Chiba Y, Kagawa N, et al. Diagnostic and prognostic value of 11C-methionine PET for nonenhancing gliomas. AJNR Am J Neuroradiol. 2016;37(1):44–50.
27. Juhász C, Dwivedi S, Kamson DO, Michelhaugh SK, Mittal S. Comparison of amino acid positron emission tomographic radiotracers for molecular imaging of primary and metastatic brain tumors. Energy. 2010;81(13):5218–25.
28. Yamamoto Y, Ono Y, Aga F, Kawai N, Kudomi N, Nishiyama Y. Correlation of 18F-FLT uptake with tumor grade and Ki-67 immunohistochemistry in patients with newly diagnosed and recurrent gliomas. J Nucl Med. 2012;53(12):1911–5.
29. Gempt J, Bette S, Ryang Y-M, Buchmann N, Peschke P, Pyka T, et al. 18F-fluoro-ethyl-tyrosine positron emission tomography for grading and estimation of prognosis in patients with intracranial gliomas. Eur J Radiol. 2015;84(5):955–62.
30. Grierson JR, Shields AF. Radiosynthesis of 3J-Deoxy-3J-[18F] fluorothymidine: [18F] FLT for imaging of cellular proliferation in vivo. Science. 2000;27(99):143–56.
31. Barthel H, Perumal M, Latigo J, He Q, Brady F, Luthra SK, et al. The uptake of 3′-deoxy-3′-[18F]fluorothymidine into L5178Y tumours in vivo is dependent on thymidine kinase 1 protein levels. Eur J Nucl Med Mol Imaging. 2005;32(3):257–63.
32. Jeong SY, Lim SM. Comparison of 3′-deoxy-3′-[18F]fluorothymidine PET and O-(2-[18F] fluoroethyl)-L-tyrosine PET in patients with newly diagnosed glioma. Nucl Med Biol. 2012;39(7):977–81.
33. Buck AK, Schirrmeister H, Hetzel M, Von Der Heide M, Halter G, Glatting G, et al. 3-deoxy-3-[(18)F]fluorothymidine-positron emission tomography for noninvasive assessment of proliferation in pulmonary nodules. Cancer Res. 2002;62(12):3331–4.
34. Galldiks N, Langen K-J, Pope WB. From the clinician's point of view - what is the status quo of positron emission tomography in patients with brain tumors? Neuro Oncol. 2015;17(11):1434–44.
35. Yang I, Aghi MK. New advances that enable identification of glioblastoma recurrence. Nat Rev Clin Oncol. 2009;6(11):648–57.
36. Cobben DCP, Jager PL, Elsinga PH, Maas B, Suurmeijer AJH, Hoekstra HJ. 3'-18F-fluoro-3′-deoxy-L-thymidine: a new tracer for staging metastatic melanoma? J Nucl Med. 2003;44(12):1927–32.

37. Francis DL, Visvikis D, Costa DC, Arulampalam THA, Townsend C, Luthra SK, et al. Potential impact of [18F]3′-deoxy-3′-fluorothymidine versus [18F]fluoro-2-deoxy-D-glucose in positron emission tomography for colorectal cancer. Eur J Nucl Med Mol Imaging. 2003;30(7):988–94.
38. Giovannini E, Lazzeri P, Milano A, Gaeta MC, Ciarmiello A. Clinical applications of choline PET/CT in brain tumors. Curr Pharm Des. 2015;21(1):121–7.
39. Li W, Ma L, Wang X, Sun J, Wang S, Hu X. (11)C-choline PET/CT tumor recurrence detection and survival prediction in post-treatment patients with high-grade gliomas. Tumour Biol. 2014;35(12):12353–60.
40. Seung JC, Jae SK, Jeong HK, Seung JO, Jeong GL, Chang JK, et al. [18F]3′-deoxy-3′-fluorothymidine PET for the diagnosis and grading of brain tumors. Eur J Nucl Med Mol Imaging. 2005;32(6):653–9.

^{18}F-FDG PET/CT Indications, Pitfalls and Limitations in Brain Imaging

9

Stefan Vöö and Jamshed Bomanji

Contents

9.1 Introduction

^{18}F-labeled fluoro-2-deoxyglucose (^{18}F-FDG) positron emission tomography/computed tomography (PET/CT) is currently the most useful and broadly used neuroimaging modality of global brain activity in neurologic patients. The images provide a tridimensional information on both cortical and subcortical structures allowing to consider brain activity in functional networks.

The local glucose consumption, and thus the ^{18}F-FDG cerebral uptake, correlates strictly with local neuronal activity. It proportionally increases with stimulus intensity or frequency [1] or decreases in conditions of sensory deprivation [2]. Such metabolic variations take place at the level of synaptic connections [3]. As such, neurotransmission

S. Vöö (✉) · J. Bomanji
Institute of Nuclear Medicine, University College London Hospitals NHS Foundation Trust, London, UK
e-mail: stefan.voo@nhs.net

F. Fraioli (ed.), *PET/CT in Brain Disorders*, Clinicians' Guides to Radionuclide Hybrid Imaging, https://doi.org/10.1007/978-3-030-01523-7_9

and signal transduction are the processes with the highest energetic requirements. It has been estimated that the energetic demand of neurotransmission and related events exceeds 80% of total cerebral energetic consumption [4].

There is already a large body of literature demonstrating that ^{18}F-FDG PET/CT adds significant value to the diagnostic evaluation of several neurological diseases, including brain tumours.

9.2 Indications

The National Comprehensive Cancer Network and the European Association of Neuro-Oncology have incorporated ^{18}F-FDG PET/CT in the practice guidelines and management algorithm of a variety of malignancies including brain cancer [5, 6]. The use of ^{18}F-FDG PET/CT in neuro-oncology is recommended in the following clinical scenarios: (1) identification of low-grade gliomas undergoing malignant conversion, (2) differentiation of radiation effect from tumour recurrence, (3) guidance of biopsy to site of maximum uptake and (4) planning radiation therapy [5, 6].

On the other hand, ^{18}F-FDG PET/CT is indicated in the evaluation of seizure disorder patients in the interictal. Furthermore, it substantially improves accuracy and differential diagnosis and enables earlier and better treatment planning of neurodegenerative diseases [7, 8].

9.3 Classical Pattern of ^{18}F-FDG Uptake in the Brain

Glucose is the only source of energy of the brain, which is known to account for as much as 20% of total-body glucose metabolism in the fasting state. For this reason, the brain exhibits an intense ^{18}F-FDG uptake compared to other tissues in the body. ^{18}F-FDG uptake is predominant in the grey matter, as in the cerebral cortex, cerebellum, basal ganglia and thalamus, while ^{18}F-FDG uptake in white matter is about one-third to one-fourth that of the grey matter.

Differences in ^{18}F-FDG distribution have been described among different brain regions. ^{18}F-FDG uptake is usually higher in the frontal, parietal and occipital areas than in the temporal cortex, while the basal ganglia have slightly higher activity than the cortex [9]. Moreover, focal areas of increased uptake were observed in frontal eye fields, posterior cingulate cortex and visual cortex of normal subjects. On the contrary, metabolic activity is lower in the medial temporal cortex, including hippocampal areas, than in neocortical regions (Table 9.1 and Fig. 9.1) [9, 10]

Table 9.1 Normal pattern of ^{18}F-FDG uptake [12]

Areas of higher metabolic activity	Basal ganglia
	Frontal eye fields
	Posterior cingulate cortex
	Visual cortex
Areas of lower metabolic activity	Medial temporal cortex

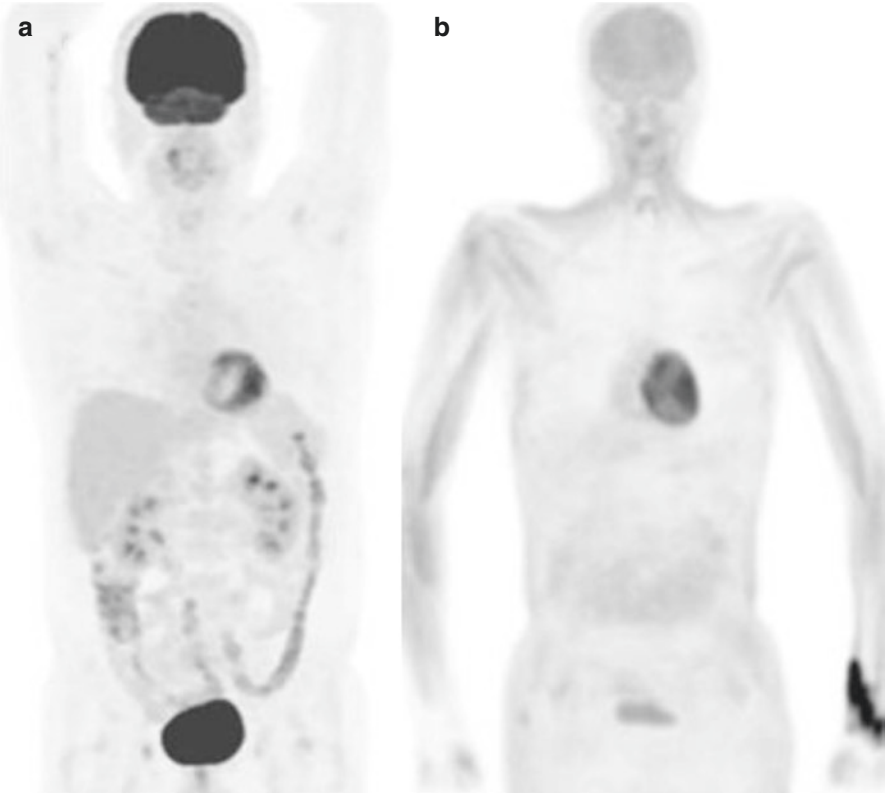

Fig. 9.1 Coronal maximal intensity pixel FDG PET/CT images. (**a**) There is a normal distribution of FDG uptake throughout the body with intense uptake in the brain. (**b**) FDG PET/CT of a patient with increased plasma glucose level during FDG administration shows altered FDG uptake with low FDG accumulation in the brain but high uptake in the heart and skeletal muscles

Brain ^{18}F-FDG uptake is usually homogeneous and symmetrical. Slight asymmetries in ^{18}F-FDG uptake have been described in the Wernicke area, the frontal eye fields and the angular gyrus, with a prevalence of generally less than 10% [11].

Importantly, many factors can influence and alter the cerebral metabolic activity and, thus, change the normal distribution of ^{18}F-FDG in the central nervous system. It is therefore imperative that, for an accurate diagnosis of pathological conditions, these variations in ^{18}F-FDG uptake are recognised.

9.4 Pitfalls and Limitations

The value of ^{18}F-FDG PET/CT in brain tumour imaging is hampered by the poor tumour-to-background contrast due to the physiologically increased glucose uptake of cortical and subcortical structures in the brain. On the other hand, the intense

physiological glucose metabolism in the brain cortex makes ^{18}F-FDG PET/CT a powerful imaging modality in identifying brain hypometabolism occurring in the interictal phase after an epileptogenic onset or hypometabolism in neurodegenerative disorders.

9.4.1 Scanning Time After ^{18}F-FDG Administration

Regional ^{18}F-FDG uptake differences were observed in the normal human brain depending on scanning starting time after intravenous tracer administration. Studies comparing the ^{18}F-FDG uptake in the cortex at different time points after tracer injection have shown relatively higher ^{18}F-FDG uptake in the bilateral posterior cingulate gyrus, parietal and frontal association cortices and subcallosal cortices at 60 min postinjection compared to the earlier images [13]. In contrast, a lower uptake in the cerebellum and orbitofrontal areas is observed at 60 min postinjection [13]. While the cause of such effects remains unclear, this might be due to regional differences in ^{18}F-FDG transportation from plasma to tissue, or in glucose phosphorylation or dephosphorylation kinetics in different regions over time [14].

9.4.2 Patient's Age

While the adult pattern of ^{18}F-FDG uptake in the brain is established by the age of 2, there are subtle differences between the normal adult distribution of ^{18}F-FDG and that in the brain of younger patients.

In the newborn, there is decreased perfusion and metabolism of the frontal and parieto-temporal cortical regions, while the glucose metabolism is the highest in primitive brain areas, such as the basal ganglia, cerebellar vermis, thalamus, visual cortex and senso-motor cortex, and comparable to the level observed in adults [15, 16].

Ageing can also alter the distribution of ^{18}F-FDG in the brain. The most common metabolic reductions with advancing age have been observed in the frontal lobes. In particular, the reduction in ^{18}F-FDG uptake involves anterior cingulate cortex, dorsolateral and medial prefrontal cortices and orbitofrontal cortex bilaterally [17–24]. The metabolic reduction in medial prefrontal cortices is correlated with age-associated cognitive decline in healthy subjects [24].

In contrast, several cortical and subcortical areas have been reported to be relatively unaffected during ageing, including the primary motor cortices, occipital cortices, precuneus, mesial temporal lobes, thalamus, putamen, pallidum and cerebellum (Table 9.2) [18, 19, 21, 25].

Dementia can alter the normal distribution of ^{18}F-FDG in the brain and, by the resulting pattern of distribution, can help characterise the particular type of dementia sometimes years before clinical signs or symptoms occur. For instance, the regional distribution of age-related hypometabolism, which involves primarily the frontal lobes, is substantially different from the patterns of brain metabolic impairment typical of Alzheimer's disease and other dementias. Alzheimer's disease is

Table 9.2 Age-related metabolic changes in healthy individuals

Age-related hypometabolism	Frontal lobes • Anterior cingulate • Dorsolateral and medial prefrontal cortices • Orbitofrontal cortex Insula Temporal lobes • Temporal pole • Lateral temporal cortex Parietal lobes • Supramarginal, superior and inferior parietal cortices
Least altered regions during ageing	Primary motor cortices Occipital cortices • Visual areas • Posterior cingulate cortex • Precuneus Mesial temporal lobes • Hippocampus • Amygdala • Parahippocampal gyrus Thalamus Putamen, pallidum Cerebellum

characterised by hypometabolism in precuneus and posterior cingulate cortex, parieto-temporal regions and, more variably, medial temporal regions, while the frontal cortex becomes affected at late disease stages [7, 26].

9.4.3 Patient's Gender

Several [18]F-FDG PET/CT studies focused on the effect of gender on brain metabolism to highlight possible metabolic differences and corresponding behavioural differences between men and women. Brain volume is reportedly greater in men than in women, with a higher percentage of grey matter in female and a higher percentage of white matter in male subjects [27]. However, [18]F-FDG findings have been controversial. The inconsistencies among studies are likely due to differences in sample size, subjects' age and image analysis procedures. Hormones (i.e. oestrogen) are another potential source of variations in cerebral metabolism of female subjects [28]. The lack of correction for differences in brain size and skull thickness between gender groups is another potential confounding factor which should be taken into account [29].

9.4.4 Brain Stimulation Conditions, Substances and Medications

Cerebral activation during and shortly after [18]F-FDG injection leads to increased uptake in the brain cortex. Cognitive performance leads to an increase of 2–5% in

cerebral ^{18}F-FDG uptake. The visual cortex, in particular, shows elevated glucose metabolism and 30% increase in FDG uptake under subject's exposure to intense or stroboscopic light. For brain scanning, it is therefore advisable to follow standard procedures that include FDG injection in a darkened room.

Insulin stimulates ^{18}F-FDG uptake in the somatic cells, and, therefore, injection of insulin or the presence of postprandial, endogenous insulin often results in relatively diminished ^{18}F-FDG uptake in the brain, with alternatively increased uptake within the skeletal muscles and other soft tissues (Fig. 9.1).

Among the substances capable of altering cerebral metabolism, caffeine is one of the most commonly used. Caffeine is part of the methylxanthine family and plays a vasoconstrictive effect. It has been shown that caffeine consumption prior PET examination decreases global cerebral glucose metabolism as measured with ^{18}F-FDG with a mean change of −18%; the reduction is particularly prominent in the anterior cingulate cortex [30].

Alcohol has a broad range of actions on many neurotransmitter systems. The brain metabolic response to acute administration of ethanol in healthy subjects has been investigated in several studies, and it has been consistently shown a global reduction in brain glucose metabolism after ethanol administration, although with various degrees across different studies [31–33]. The greatest metabolic decrease in absolute metabolism usually occurs in the occipital cortex and in the cerebellum. Moderate hypometabolism has been observed in the limbic system, parietal cortex, frontal cortex, cingulate gyrus, temporal cortex, thalamus and midbrain. The smallest decrease could be observed in the basal ganglia. [31–33]

Abused substances such as amphetamines and cocaine significantly alter glucose brain metabolism. Low doses of amphetamines affect cerebral metabolism by decreasing metabolic rates of glucose of cortical and subcortical areas [34]. On the contrary, high doses of amphetamines increase the whole brain glucose metabolism, particularly in the striatum, thalamus and anterior cingulate cortex [35]. Cocaine consumption before ^{18}F-FDG examination induces a significant increase of brain metabolism in several cortical and subcortical areas, particularly in the medial prefrontal cortex [36].

Medications, such as sedatives, general anaesthetics and corticosteroids, can also result in a decrease in cortical FDG uptake. For instance, patients with brain tumours may present decreased glucose metabolism in the contralateral cortex. This phenomenon might be caused by corticosteroids, but a functional inactivation of the contralateral hemisphere by differentiation of the input from the ipsilateral hemisphere cannot be excluded [37]. Benzodiazepines, sometimes used to reduce the uptake within the brown adipose tissue, can also decrease FDG uptake within the brain [38].

Finally, brain ^{18}F-FDG PET/CT scan in cognitively normal subjects may show a lower brain metabolism after chemotherapy than before the treatment (Fig. 9.2). This condition, known as "chemo-brain", could be observed also years after the chemotherapy, with reduction of cortical metabolism, particularly in the inferior frontal gyrus [39, 40]. Similarly, a long-term consequence after radiotherapy may be a reduction up to −5% of cerebral metabolic activity in the irradiated brain tissue, as compared to nonirradiated brain tissue [41].

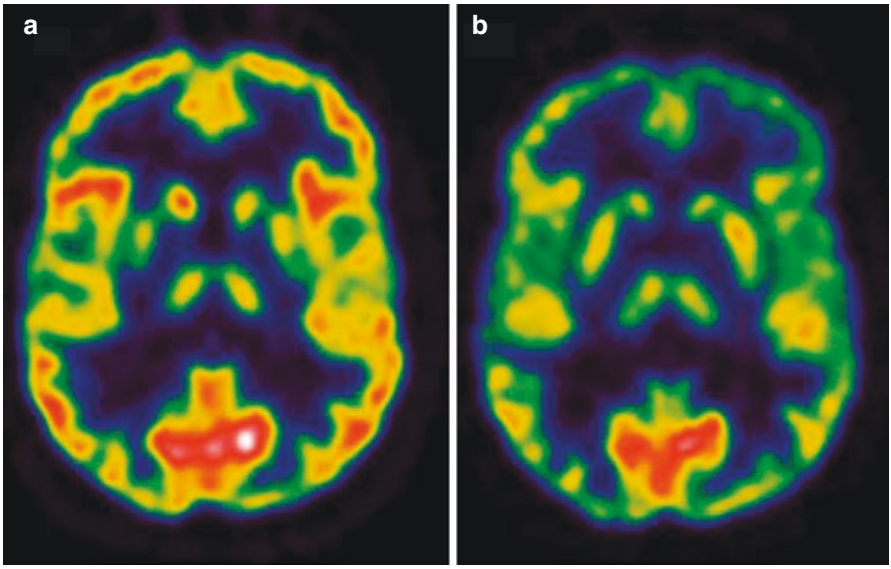

Fig. 9.2 Brain FDG PET/CT of a patient diagnosed with Hodgkin disease. (**a**) FDG PET/CT at diagnosis, 1 week before commencing the therapy, showing normal FDG uptake throughout the cortex and basal ganglia. (**b**) Interval FDG PET/CT at 21 days after the first two cycles of chemotherapy (consisting of adriamycin, bleomycin, vinblastine and dacarbazine) which shows a decreased generalised FDG uptake in the brain

9.4.5 Artefacts Related to Patient Movement

One of the limitations of PET/CT, and most neuroimaging acquisitions even besides ^{18}F-FDG, is the necessity to keep the patient in a constant position. If the patient moves during the acquisition the activity will be blurred over brain structures, resolution will be degraded and the results' interpretation will be difficult or even impossible [42]. The most recent PET devices have increased count rate capabilities, which allow shortening the duration of the acquisition and thus improving patient tolerance and reducing the likelihood of experiencing significant movements. However, an ^{18}F-FDG brain study is typically completed within 10–20 min. Different possibilities to constrain head position can be used, and these depend mostly on the environment, type of patients and the opportunities of the clinical setting [43].

9.4.6 Artefacts Related to Attenuation Correction

In routine clinical practice, the attenuation correction is achieved using the CT data. There are two distinct issues that may significantly degrade the quality of the metabolic study.

Firstly, movements between PET and CT acquisitions will offset the reconstruction μ-map and generate attenuation-corrected images that do not reflect the actual

distribution of the tracer. The image quality is grossly degraded, and this pitfall is easily recognised when the movement between PET and CT is marked, but minor movements may lead to subtle changes in the images and affect the interpretation. Visual inspection of both data sets is mandatory, as manual correction of the registration easily corrects the issue. Automated registration algorithms have also been developed to avoid this problem [44].

Secondly, the presence of metallic artefacts, such as reconstructive skull plates, may lead to overcorrecting the emission data and artefactual areas of increased uptake in the PET images [45]. In this case, calculated attenuation correction using the ellipse method improves the image quality even though the quantitative assessment remains biased. Smaller metallic objects such as electroencephalogram electrodes may generate local foci of increased activity at their location outside of the brain, without altering the diagnosis when it is made visually. It may become an issue, however, when comparing quantitative analyses of ^{18}F-FDG brain studies performed with and without electroencephalogram electrodes [46].

The effect of misregistrated μ-map and emission data becomes even more important when performing dynamic studies or when using high-resolution PET scanners such as the high-resolution research tomograph that displays a 2 mm isotropic spatial resolution. In these cases, motion correction has to be applied [43, 47, 48].

9.4.7 Artefacts Related to Patient's Positioning in the Scanner

Dependent on the patient's morphology, positioning may be a real difficulty for patients with limited neck mobility. Consequently, the image quality may be decreased if the head is not positioned in the centre of the field of view, where the resolution is optimal. Identifying brain regional activity and the visual interpretation of the PET images may be difficult if changes in orientation occur. The superimposition of structural images improves the readability and increases the accuracy of reorientation of the whole brain volume [43].

Key Points

- Glucose is the only source of energy of the brain, which is known to account for as much as 20% of total-body glucose metabolism in the fasting state. For this reason, the brain exhibits an intense ^{18}F-FDG uptake compared to other tissues in the body. ^{18}F-FDG uptake is predominant in the gray matter, as in the cerebral cortex, cerebellum, basal ganglia, and thalamus, while ^{18}F-FDG uptake in white matter is about one-third to one-fourth that of the gray matter.

- Slight asymmetries in ^{18}F-FDG uptake have been described in the Wernicke area, the frontal eye fields, and the angular gyrus, with a prevalence of generally less than 10%.
- Scanning time after FDG administration, age, gender, brain stimulation, conditions, substances, and medications are all physiological conditions or pitfalls that may lead to possible differences in cerebral metabolic uptake. Knowing these conditions is critical for a correct interpretation of brain images.

References

1. Sokoloff L, Reivich M, Kennedy C, Des Rosiers MH, Patlak CS, Pettigrew KD, Sakurada O, Shinohara M. The [14c]deoxyglucose method for the measurement of local cerebral glucose utilization: theory, procedure, and normal values in the conscious and anesthetized albino rat. J Neurochem. 1977;28:897–916.
2. Kennedy C, Des Rosiers MH, Sakurada O, Shinohara M, Reivich M, Jehle JW, Sokoloff L. Metabolic mapping of the primary visual system of the monkey by means of the autoradiographic [14c]deoxyglucose technique. Proc Natl Acad Sci U S A. 1976;73:4230–4.
3. Sokoloff L. Energetics of functional activation in neural tissues. Neurochem Res. 1999;24:321–9.
4. Shulman RG, Rothman DL, Behar KL, Hyder F. Energetic basis of brain activity: implications for neuroimaging. Trends Neurosci. 2004;27:489–95.
5. Podoloff DA, Ball DW, Ben-Josef E, Benson AB III, Cohen SJ, Coleman RE, Delbeke D, Ho M, Ilson DH, Kalemkerian GP, Lee RJ, Loeffler JS, Macapinlac HA, Morgan RJ Jr, Siegel BA, Singhal S, Tyler DS, Wong RJ. NCCN task force: clinical utility of PET in a variety of tumor types. J Natl Compr Cancer Netw. 2009;7(Suppl 2):S1–26.
6. Albert NL, Weller M, Suchorska B, Galldiks N, Soffietti R, Kim MM, la Fougere C, Pope W, Law I, Arbizu J, Chamberlain MC, Vogelbaum M, Ellingson BM, Tonn JC. Response assessment in neuro-oncology working group and European Association for Neuro-Oncology recommendations for the clinical use of PET imaging in gliomas. Neuro-Oncology. 2016;18:1199–208.
7. Mosconi L, Tsui WH, Herholz K, Pupi A, Drzezga A, Lucignani G, Reiman EM, Holthoff V, Kalbe E, Sorbi S, Diehl-Schmid J, Perneczky R, Clerici F, Caselli R, Beuthien-Baumann B, Kurz A, Minoshima S, de Leon MJ. Multicenter standardized 18F-Fdg PET diagnosis of mild cognitive impairment, Alzheimer's disease, and other dementias. J Nucl Med. 2008;49:390–8.
8. Silverman DH, Small GW, Chang CY, Lu CS, Kung De Aburto MA, Chen W, Czernin J, Rapoport SI, Pietrini P, Alexander GE, Schapiro MB, Jagust WJ, Hoffman JM, Welsh-Bohmer KA, Alavi A, Clark CM, Salmon E, de Leon MJ, Mielke R, Cummings JL, Kowell AP, Gambhir SS, Hoh CK, Phelps ME. Positron emission tomography in evaluation of dementia: regional brain metabolism and long-term outcome. JAMA. 2001;286:2120–7.
9. Kochunov P, Ramage AE, Lancaster JL, Robin DA, Narayana S, Coyle T, Royall DR, Fox P. Loss of cerebral white matter structural integrity tracks the gray matter metabolic decline in normal aging. NeuroImage. 2009;45:17–28.
10. Ibanez V, Pietrini P, Furey ML, Alexander GE, Millet P, Bokde AL, Teichberg D, Schapiro MB, Horwitz B, Rapoport SI. Resting state brain glucose metabolism is not reduced in normotensive healthy men during aging, after correction for brain atrophy. Brain Res Bull. 2004;63:147–54.

11. Ivancevic V, Alavi A, Souder E, Mozley PD, Gur RE, Benard F, Munz DL. Regional cerebral glucose metabolism in healthy volunteers determined by fluorodeoxyglucose positron emission tomography: appearance and variance in the transaxial, coronal, and sagittal planes. Clin Nucl Med. 2000;25:596–602.
12. Berti V, Mosconi L, Pupi A. Brain: normal variations and benign findings in fluorodeoxyglucose-PET/computed tomography imaging. PET Clin. 2014;9:129–40.
13. Ishii K, Sakamoto S, Hosaka K, Mori T, Sasaki M. Variation in FDG uptakes in different regions in normal human brain as a function of the time (30 and 60 minutes) after injection of FDG. Ann Nucl Med. 2002;16:299–301.
14. Sasaki H, Kanno I, Murakami M, Shishido F, Uemura K. Tomographic mapping of kinetic rate constants in the fluorodeoxyglucose model using dynamic positron emission tomography. J Cereb Blood Flow Metab. 1986;6:447–54.
15. Chugani HT, Phelps ME, Mazziotta JC. Positron emission tomography study of human brain functional development. Ann Neurol. 1987;22:487–97.
16. Kinnala A, Suhonen-Polvi H, Aarimaa T, Kero P, Korvenranta H, Ruotsalainen U, Bergman J, Haaparanta M, Solin O, Nuutila P, Wegelius U. Cerebral metabolic rate for glucose during the first six months of life: An FDG positron emission tomography study. Arch Dis Child Fetal Neonatal Ed. 1996;74:F153–7.
17. Garraux G, Salmon E, Degueldre C, Lemaire C, Laureys S, Franck G. Comparison of impaired subcortico-frontal metabolic networks in normal aging, subcortico-frontal dementia, and cortical frontal dementia. NeuroImage. 1999;10:149–62.
18. Herholz K, Salmon E, Perani D, Baron JC, Holthoff V, Frolich L, Schonknecht P, Ito K, Mielke R, Kalbe E, Zundorf G, Delbeuck X, Pelati O, Anchisi D, Fazio F, Kerrouche N, Desgranges B, Eustache F, Beuthien-Baumann B, Menzel C, Schroder J, Kato T, Arahata Y, Henze M, Heiss WD. Discrimination between Alzheimer dementia and controls by automated analysis of multicenter FDG PET. NeuroImage. 2002;17:302–16.
19. Willis MW, Ketter TA, Kimbrell TA, George MS, Herscovitch P, Danielson AL, Benson BE, Post RM. Age, sex and laterality effects on cerebral glucose metabolism in healthy adults. Psychiatry Res. 2002;114:23–37.
20. Fujimoto T, Matsumoto T, Fujita S, Takeuchi K, Nakamura K, Mitsuyama Y, Kato N. Changes in glucose metabolism due to aging and gender-related differences in the healthy human brain. Psychiatry Res. 2008;164:58–72.
21. Kalpouzos G, Chetelat G, Baron JC, Landeau B, Mevel K, Godeau C, Barre L, Constans JM, Viader F, Eustache F, Desgranges B. Voxel-based mapping of brain gray matter volume and glucose metabolism profiles in normal aging. Neurobiol Aging. 2009;30:112–24.
22. Kim IJ, Kim SJ, Kim YK. Age- and sex-associated changes in cerebral glucose metabolism in normal healthy subjects: statistical parametric mapping analysis of F-18 fluorodeoxyglucose brain positron emission tomography. Acta Radiol. 2009;50:1169–74.
23. Hsieh YJ, Cho CY. Age-related changes of arm movements in dual task condition when walking on different surfaces. Hum Mov Sci. 2012;31:190–201.
24. Pardo JV, Lee JT, Sheikh SA, Surerus-Johnson C, Shah H, Munch KR, Carlis JV, Lewis SM, Kuskowski MA, Dysken MW. Where the brain grows old: decline in anterior cingulate and medial prefrontal function with normal aging. NeuroImage. 2007;35:1231–7.
25. Brickman AM, Buchsbaum MS, Shihabuddin L, Hazlett EA, Borod JC, Mohs RC. Striatal size, glucose metabolic rate, and verbal learning in normal aging. Brain Res Cogn Brain Res. 2003;17:106–16.
26. Mosconi L, Mistur R, Switalski R, Tsui WH, Glodzik L, Li Y, Pirraglia E, De Santi S, Reisberg B, Wisniewski T, de Leon MJ. FDG-PET changes in brain glucose metabolism from normal cognition to pathologically verified Alzheimer's disease. Eur J Nucl Med Mol Imaging. 2009;36:811–22.
27. Cosgrove KP, Mazure CM, Staley JK. Evolving knowledge of sex differences in brain structure, function, and chemistry. Biol Psychiatry. 2007;62:847–55.
28. Reiman EM, Armstrong SM, Matt KS, Mattox JH. The application of positron emission tomography to the study of the normal menstrual cycle. Hum Reprod. 1996;11:2799–805.

29. Miura SA, Schapiro MB, Grady CL, Kumar A, Salerno JA, Kozachuk WE, Wagner E, Rapoport SI, Horwitz B. Effect of gender on glucose utilization rates in healthy humans: a positron emission tomography study. J Neurosci Res. 1990;27:500–4.
30. Chen Y, Parrish TB. Caffeine's effects on cerebrovascular reactivity and coupling between cerebral blood flow and oxygen metabolism. NeuroImage. 2009;44:647–52.
31. Volkow ND, Hitzemann R, Wolf AP, Logan J, Fowler JS, Christman D, Dewey SL, Schlyer D, Burr G, Vitkun S, et al. Acute effects of ethanol on regional brain glucose metabolism and transport. Psychiatry Res. 1990;35:39–48.
32. Zhu W, Volkow ND, Ma Y, Fowler JS, Wang GJ. Relationship between ethanol-induced changes in brain regional metabolism and its motor, behavioural and cognitive effects. Alcohol Alcohol. 2004;39:53–8.
33. Volkow ND, Wang GJ, Franceschi D, Fowler JS, Thanos PP, Maynard L, Gatley SJ, Wong C, Veech RL, Kunos G, Kai Li T. Low doses of alcohol substantially decrease glucose metabolism in the human brain. NeuroImage. 2006;29:295–301.
34. Wolkin A, Angrist B, Wolf A, Brodie J, Wolkin B, Jaeger J, Cancro R, Rotrosen J. Effects of amphetamine on local cerebral metabolism in normal and schizophrenic subjects as determined by positron emission tomography. Psychopharmacology. 1987;92:241–6.
35. Vollenweider FX, Maguire RP, Leenders KL, Mathys K, Angst J. Effects of high amphetamine dose on mood and cerebral glucose metabolism in normal volunteers using positron emission tomography (PET). Psychiatry Res. 1998;83:149–62.
36. Henry PK, Murnane KS, Votaw JR, Howell LL. Acute brain metabolic effects of cocaine in rhesus monkeys with a history of cocaine use. Brain Imaging Behav. 2010;4:212–9.
37. Roelcke U, Blasberg RG, von Ammon K, Hofer S, Vontobel P, Maguire RP, Radu EW, Herrmann R, Leenders KL. Dexamethasone treatment and plasma glucose levels: relevance for fluorine-18-fluorodeoxyglucose uptake measurements in gliomas. J Nucl Med. 1998;39:879–84.
38. Wang GJ, Volkow ND, Levy AV, Felder CA, Fowler JS, Pappas NR, Hitzemann RJ, Wong CT. Measuring reproducibility of regional brain metabolic responses to lorazepam using statistical parametric maps. J Nucl Med. 1999;40:715–20.
39. Silverman DH, Dy CJ, Castellon SA, Lai J, Pio BS, Abraham L, Waddell K, Petersen L, Phelps ME, Ganz PA. Altered frontocortical, cerebellar, and basal ganglia activity in adjuvant-treated breast cancer survivors 5–10 years after chemotherapy. Breast Cancer Res Treat. 2007;103:303–11.
40. Simo M, Rifa-Ros X, Rodriguez-Fornells A, Bruna J. Chemobrain: a systematic review of structural and functional neuroimaging studies. Neurosci Biobehav Rev. 2013;37:1311–21.
41. Kesner AL, Lau VK, Speiser M, Hsueh WA, Agazaryan N, DeMarco JJ, Czernin J, Silverman DH. Time-course of effects of external beam radiation on [18F]FDG uptake in healthy tissue and bone marrow. J Appl Clin Med Phys. 2008;9:2747.
42. Montgomery AJ, Thielemans K, Mehta MA, Turkheimer F, Mustafovic S, Grasby PM. Correction of head movement on PET studies: comparison of methods. J Nucl Med. 2006;47:1936–44.
43. Salmon E, Bernard Ir C, Hustinx R. Pitfalls and limitations of PET/CT in brain imaging. Semin Nucl Med. 2015;45:541–51.
44. Khurshid K, Berger KL, McGough RJ. Automated PET/CT brain registration for accurate attenuation correction. Conf Proc IEEE Eng Med Biol Soc. 2009;2009:5805–8.
45. Almodovar S, White SL, Modarresifar H, Ojha BC. The usefulness of calculated attenuation correction in the evaluation of metallic artifacts on brain PET/CT imaging. Clin Nucl Med. 2006;31:554–5.
46. Lemmens C, Montandon ML, Nuyts J, Ratib O, Dupont P, Zaidi H. Impact of metal artefacts due to EEG electrodes in brain PET/CT imaging. Phys Med Biol. 2008;53:4417–29.
47. Son YD, Kim HK, Kim ST, Kim NB, Kim YB, Cho ZH. Analysis of biased PET images caused by inaccurate attenuation coefficients. J Nucl Med. 2010;51:753–60.
48. Keller SH, Sibomana M, Olesen OV, Svarer C, Holm S, Andersen FL, Hojgaard L. Methods for motion correction evaluation using 18F-FDG human brain scans on a high-resolution PET scanner. J Nucl Med. 2012;53:495–504.

Clinical Applications of Non-^{18}F-FDG PET/CT Tracers in Brain Imaging

10

Vincenzo Militano, Christine Tang, Demetrio Arico', and Claudio Giardina

Contents

10.1 Introduction

In the last decade, many tracers have been introduced to overcome some limitations of ^{18}F-FDG in brain imaging including large neutral amino acid tracers ^{11}C-methionine [^{11}C-MET], ^{18}F-fluoroethyl-tyrosine [^{18}F-FET], ^{18}F-fluorodopa [^{18}F-DOPA] and ^{18}F-choline [^{18}FCH] and hypoxia tracers as ^{18}F-fluoromisonidazole [^{18}F-MISO] and ^{18}F-Fluoroazomycin arabinofuranoside [^{18}F-FAZA]. Most of these tracers have been specifically developed for brain tumour imaging and will be better described in the

V. Militano (✉) · C. Tang
Institute of Nuclear Medicine, University College of London Hospital, London, UK
e-mail: vincenzo.militano@nhs.net

D. Arico'
Department of Nuclear Medicine, Humanitas Oncological Centre of Catania, Catania, Italy

C. Giardina
Department of Radiology, ASP of Messina – Hospital of Taormina, Taormina, ME, Italy

F. Fraioli (ed.), *PET/CT in Brain Disorders*, Clinicians' Guides to Radionuclide Hybrid Imaging, https://doi.org/10.1007/978-3-030-01523-7_10

dedicated tumour section. In the present review, we will provide a brief introduction of some clinical data on their main advantages and limitations.

10.2 Large Neutral Amino Acid Tracer

10.2.1 ^{11}C-Methionine (^{11}C-MET)

Studies have shown that ^{11}C-MET is taken up avidly by tumours of many types [1]. Due to low ^{11}C-MET uptake in the normal brain, every area of uptake higher than the background is considered potentially pathological [2] (Fig. 10.1). The most

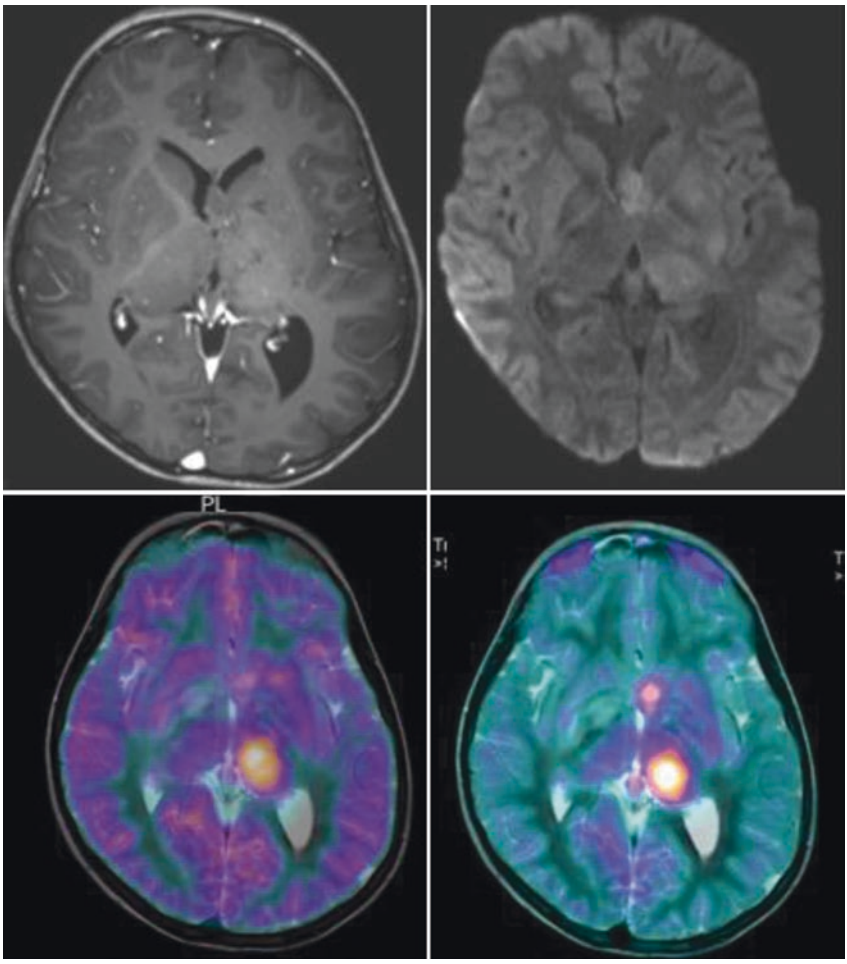

Fig. 10.1 Nonenhancing left thalamic tumour showing mild restricted diffusion (top right). FDG PET (bottom left) shows intense metabolic activity in the left thalamus but ^{11}C-MET PET (bottom right) clearly demonstrates the presence of viable tissue also in the anterior commissure

often used calculation method is the tumour-to-normal background ratio (T/N ratio), comparing the uptake in the tumour to that in the contralateral frontal lobe or the corresponding contralateral hemisphere. There are different proposed thresholds from 1.5 to 1.9 for the diagnosis of brain tumour. The standardized uptake value (SUV) is still debated. Unfortunately, ^{11}C-MET is not the ideal tumour tracer, since inflammatory processes are also known to show increased ^{11}C-MET uptake [3]. This may cause problems in differentiation after radiotherapy, where the uptake is thought to be related to disruption of the blood–brain barrier and vascular proliferation [4, 5]. The sensitivity of ^{11}C-MET PET for the diagnosis and characterization of gliomas from non-malignant lesions have been estimated to be around 75–95% with specificity range between 87% and 100% [6]. The poor relation between ^{11}C-MET uptake and grading does not recommend its routine use in tumour grading [6, 7]. Few reports have investigated the role of this tracer in the pathological proof of infiltration of brain tissue and reported that ^{11}C-MET PET delineates a larger volume in comparison to MR or ^{18}F-FDG PET and, thus, by combining ^{11}C-MET PET with MR images, has additional value for planning surgery or radiotherapy, with ensuing clinical impact in about 80% of the procedures. Following surgical or radiation therapy, ^{11}C-MET PET can be repeated for assessing response to treatment (Fig. 10.2), as well as for planning potential second-look surgeries [8, 9].

10.2.2 18F-fluoroethyl-tyrosine (^{18}F-FET)

The use of fluorinated compounds, such as ^{18}F-FET PET, overcomes most of the limitations related to the short half-life of ^{11}C. ^{18}F-FET is an amino acid tracer, an analogue of tyrosine that is not incorporated into proteins, and the uptake by tumoural cells is mediated by amino acid transporters with a high in vivo stability [10]. The rapid and intensive tumour uptake, the slower accumulation in the normal cortex, the low uptake in inflammatory tissue, the high imaging contrast and its easy synthesis make ^{18}F-FET a good tracer for the study of brain tumours [11]. Also, the kinetic analysis of ^{18}F-FET uptake provides information on tumour grade in cerebral gliomas. High-grade gliomas, III or IV, are characterized by an early peak around 10–15 min after injection followed by a decrease of ^{18}F-FET uptake [12, 13]. In contrast, time–activity curves in low-grade diffuse gliomas, grades I and II, increase slightly and steadily (Fig. 10.3). This is probably due to the higher regional blood volume as a result of hypervascularization, the increased angiogenesis and the higher intra-tumoural microvessel density. Also the facilitated amino acid transport in the tumour vessels might be responsible for the higher initial uptake in high-grade compared with low-grade gliomas [14, 15] (Fig. 10.4). For these reasons, it is mandatory to perform a dynamic acquisition up to 40 min after intravenous injection. Further studies suggested a tumour-to-brain ratio (TBR) cut-off of 1.6. This cut-off was based on a biopsy-controlled study in cerebral gliomas and differentiated best between tumoural and peri-tumoural tissue [13, 16] (Fig. 10.3). Static and dynamic ^{18}F-FET PET parameters are also helpful to discriminate between isocitrate dehydrogenase (IDH)-mutated astrocytomas and IDH wild-type glioblastomas

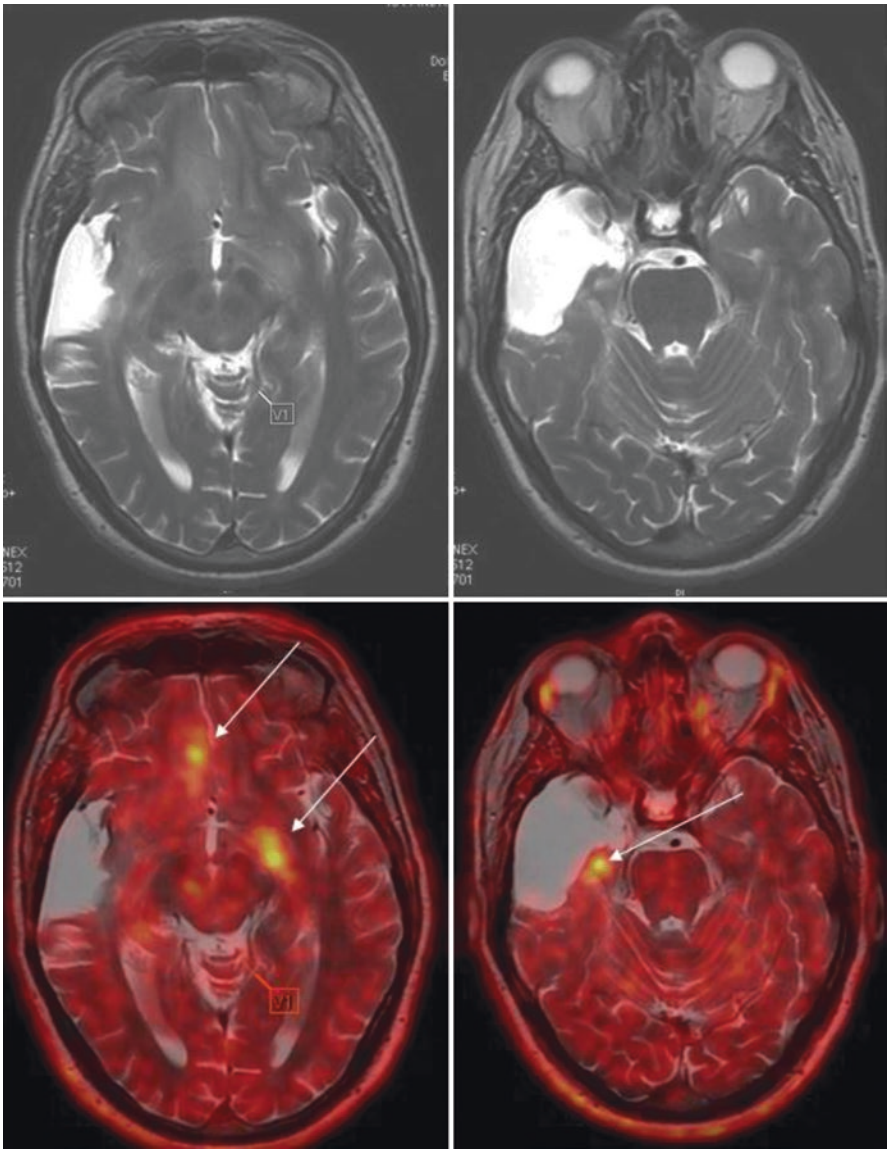

Fig. 10.2 PET with Methionine performed 2 weeks after MR (Post processing fused images with MR). Three small foci of increased uptake in the right temporal lobe and in the left temporal lobe, consistent with the presence of multiple foci of relapse (case courtesy of Dr. Castellucci, University St. Orsola Malpighi, Bologna, Italy)

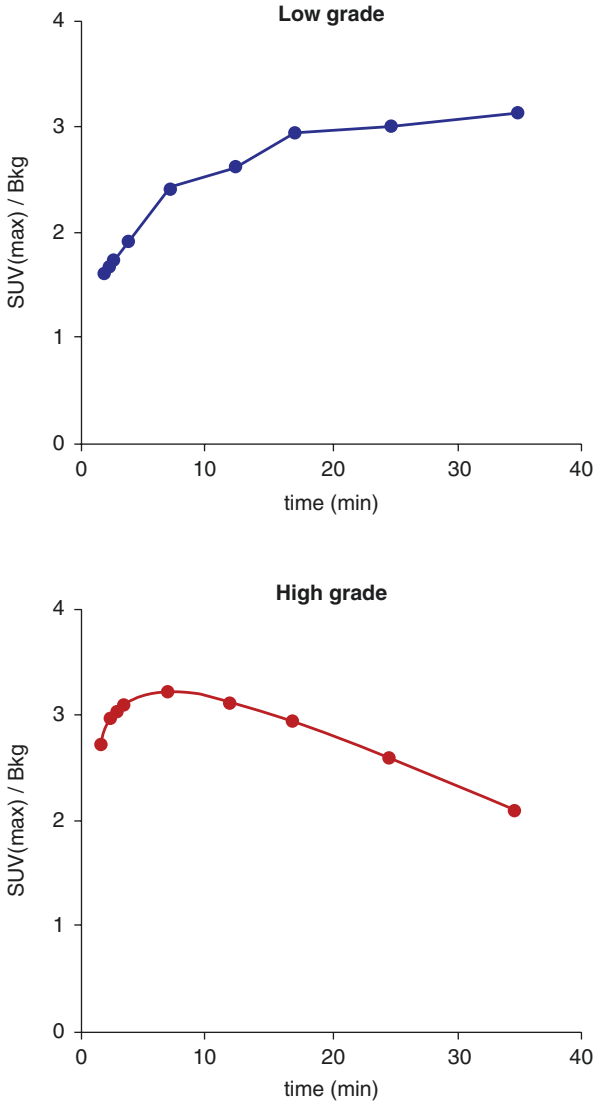

Fig. 10.3 On top the dynamic evaluation shows increasing SUV until end of acquisition typical of the low grade glioma. On bottom an example of decreasing curve with early peak typical of high grade glioma

[17]. In low-grade gliomas, particularly, ^{18}F-FET kinetics may be useful to locate regions of malignant transformation and poor prognosis with a sensitivity of 72–79% to identify hot spots for biopsy guidance [18]. Furthermore, ^{18}F-FET PET is predictive for anti-VEGF treatment and can identify in a subset of patient's tumour progression and treatment failure earlier than standard MRI with a sensitivity of 87.5% and specificity of 100% (Fig. 10.5) [19].

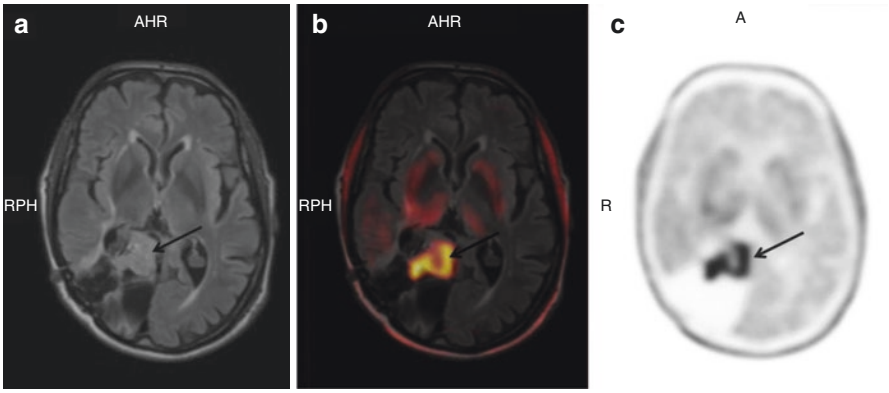

Fig. 10.4 Axial MRI (**a**), fused ^{18}F-FET PET/MRI (**b**) and ^{18}F-FET PET (**c**) images in a 64 years old female patient treated with surgery and radiochemotherapy for a right temporal-occipital high-grade glioma and with a contrast-enhanced area suspicious for disease relapse or radionecrosis at MRI (arrows). ^{18}F-FET PET shows increased radiopharmaceutical uptake corresponding to the MRI abnormality, suggesting a disease relapse as confirmed by histology. *Courtesy of Dr. Giorgio Treglia of the Oncology Institute of Southern Switzerland, Bellinzona, Switzerland*

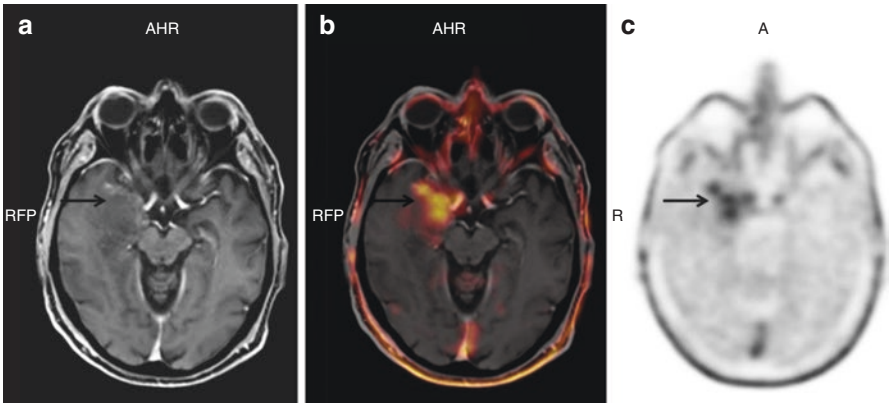

Fig. 10.5 Axial MRI (**a**), fused ^{18}F-FET PET/MRI (**b**) and ^{18}F-FET PET (**c**) images in a 54 years old female patient with a suspicious right temporal glioma (arrows). ^{18}F-FET PET shows an area of increased radiopharmaceutical uptake corresponding to the anterior portion of the cerebral lesion and suggesting a high-grade glioma, as confirmed by ^{18}F-FET PET-guided biopsy. *Courtesy of Dr. Giorgio Treglia of the Oncology Institute of Southern Switzerland, Bellinzona, Switzerland*

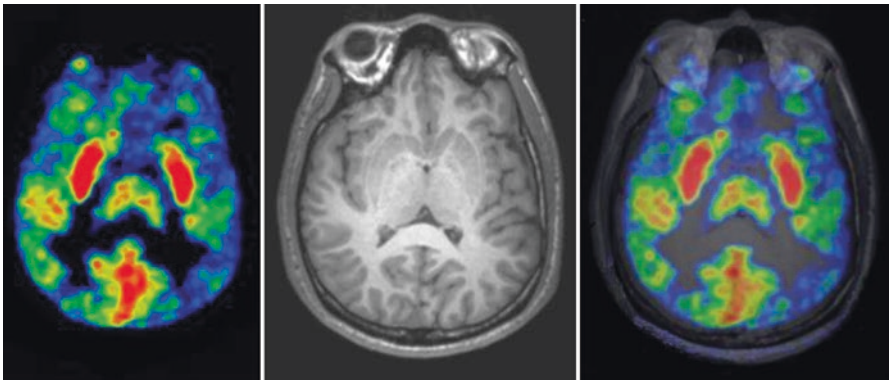

Fig. 10.6 Physiological basal ganglia uptake (^{18}F-DOPA)

10.2.3 ^{18}F-fluorodopa(^{18}F-DOPA)

^{18}F-DOPA is a precursor of dopamine after the same metabolic pathways, including the synthesis of catecholamines. ^{18}F-DOPA PET has been initially proposed in the assessment of patients with movement disorders due to the uptake of ^{18}F-DOPA by the terminals of dopaminergic neurones and its conversion to ^{18}F-dopamine by dopa decarboxylase and subsequently to other dopamine metabolites [20]. The uptake of dopamine precursors reflects the integrity of presynaptic dopaminergic receptors; hence its deficiency has been shown to accurately reproduce the monoaminergic disturbances in Parkinson's disease (Fig. 10.6). ^{18}F-DOPA PET is very accurate (sensitivities 90–100% and specificities 91%) for differentiating Parkinson's disease from other Parkinson-like entities in selected cases, in which a clinical diagnosis is challenging [21, 22]. More recently ^{18}F-DOPA have been most successful in the field of brain tumour imaging due to their favourable mechanism of uptake, which depends on the increased expression of the L-type amino acid transport system on tumour cells [23]. This metabolic pathway is highly specific for cancer cells and largely independent of the blood–brain barrier breakdown, resulting in excellent tumour-to-background contrast (Fig. 10.6). Pathological amino acid uptake usually extends beyond contrast-enhanced T1-weighted (ce-T1-W) abnormalities and is more specific than T2-weighted (or FLAIR) hyperintensities (Fig. 10.7) [24]. The inclusion of amino acid PET tracers in the workup of brain tumours complements and improves the diagnostic performances of conventional MRI in several settings, including biopsy targeting, prediction of anaplastic transformation, response assessment and treatment planning for both high-grade and low-grade gliomas.

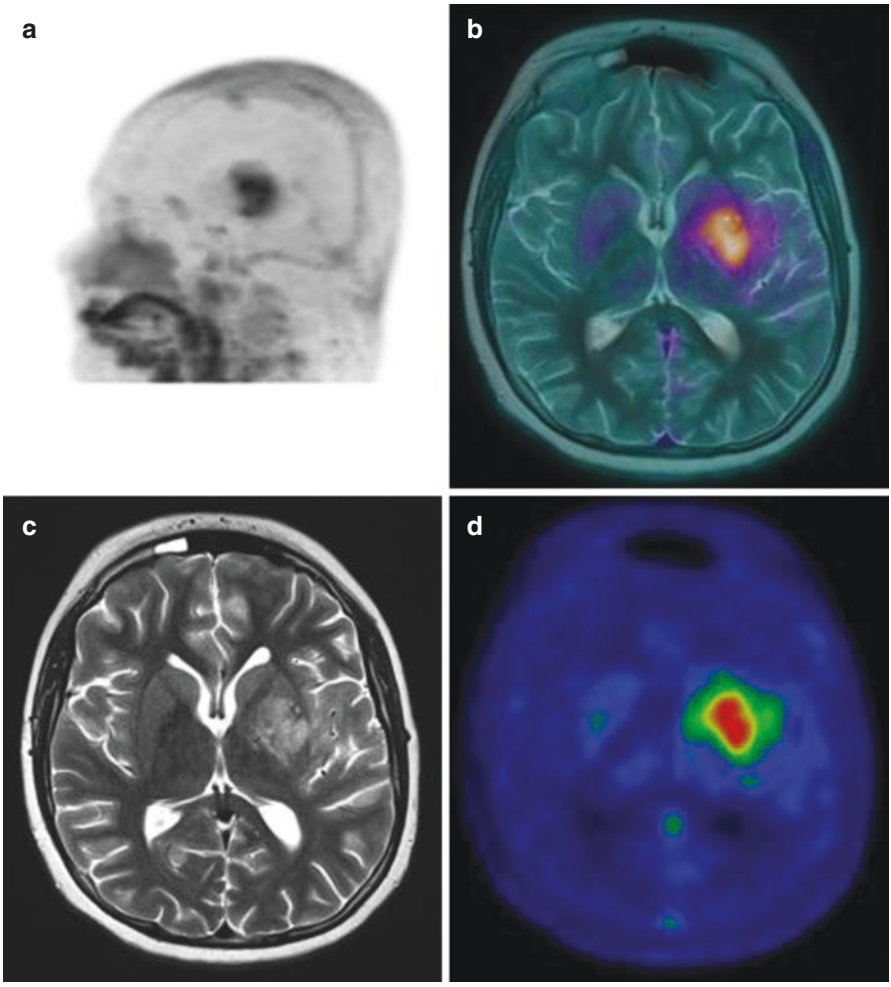

Fig. 10.7 (**a**) MIP, (**b**) Axial fused PET/MR, (**c**) Axial MRI, (**d**) Axial PET in a patient with glioma of the left thalamus (^{18}G-DOPA)

10.3 Proliferation Cell Membrane Tracer

10.3.1 [^{11}C] or 18F-choline (^{11}C/^{18}FCH)

Choline is a component of phosphatidylcholine, an important element of cell membranes; as known, biosynthesis of the cell membrane is very fast in tumour tissues, and the up-regulation of choline kinase activity is a characteristic of many tumours, including brain cancer. Previous studies with MRI have shown elevated levels of choline metabolites on MR spectroscopy, confirming that in brain tumour cells there

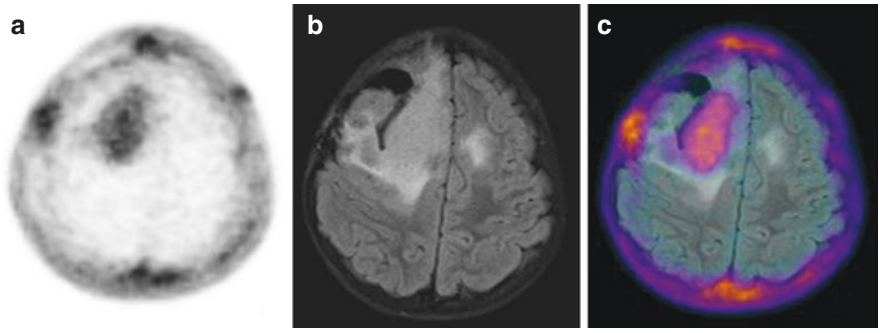

Fig. 10.8 (**a**) PET, (**b**) MRI, (**c**) Fused. High ^{18}FCH uptake in a the large GBM of the left frontal lobe

is higher uptake of ^{11}C/^{18}FCH [25]. Further the low concentration of ^{11}C/^{18}FCH uptake in the normal cerebral cortex allows excellent tumour-to-background ratio and good delineation of tumour contours. Investigations reported a difference in gradient of uptake between high-grade gliomas compared to low-grade gliomas [26], brain metastasis and meningiomas [27] (Fig. 10.8). High-grade gliomas, brain metastases and benign lesions could be distinguished based on their ^{11}C/^{18}FCH uptake, as metastases demonstrated significantly greater uptake than high-grade gliomas. In addition, high-grade gliomas could be visually distinguished from brain metastases based on a characteristic pattern of increased ^{11}C/^{18}FCH uptake beyond the areas of contrast enhancement on MRI. This pattern of 'peritumoural' uptake was hypothesized to be due to infiltration of the white matter by malignant cells [26]. Authors also found that in patients who had previously undergone radiation therapy (ten with high-grade glioma, four with brain metastases), ^{11}C/^{18}FCH PET was able to differentiate between recurrent tumour and radiation-induced changes [28]. This feature has been useful to guide biopsy and for radiotherapy planning [29]. Nevertheless, pitfalls may also occur. False positives are generally a greater concern than false negatives, owing to the accumulation of the tracer in inflammatory lesions [30].

10.4 Hypoxia Tracers

10.4.1 [^{18}F]-fluoromisonidazole (^{18}F-MISO)

Tumour hypoxia influences the outcome of treatment with radiotherapy, chemotherapy and even surgery, not only for the treatment of large tumours with extensive necrosis but also in the treatment of small primary tumours and recurrences, micrometastases and surgical margins with microscopic tumour involvement. Because hypoxic tumour cells are resistant to radiation and to many anticancer drugs [31] tumour hypoxia is a major independent prognostic factor influencing tumour progression, response to therapy and overall survival in many

malignancies [32–34]. At the present time, ^{18}F-MISO is the most widely used PET tracer to quantify tumour hypoxia [35].The main drawbacks of ^{18}F-MISO are the slow uptake in the target tissue and the slow clearance of the unbound tracer from non-hypoxic tissue resulting in high background in PET images [36]. For this reason, some authors have proved that performing acquisition at 4 h, rather than 2 h, provides a superior image contrast [37]. ^{18}F-MISO accumulation in vivo demonstrates that a median oxygen level of <10 mmHg is generally required for hypoxia-specific retention. The ^{18}F-MISO accumulation has been found to reflect hypoxia in glioma, and several clinical studies have shown that a

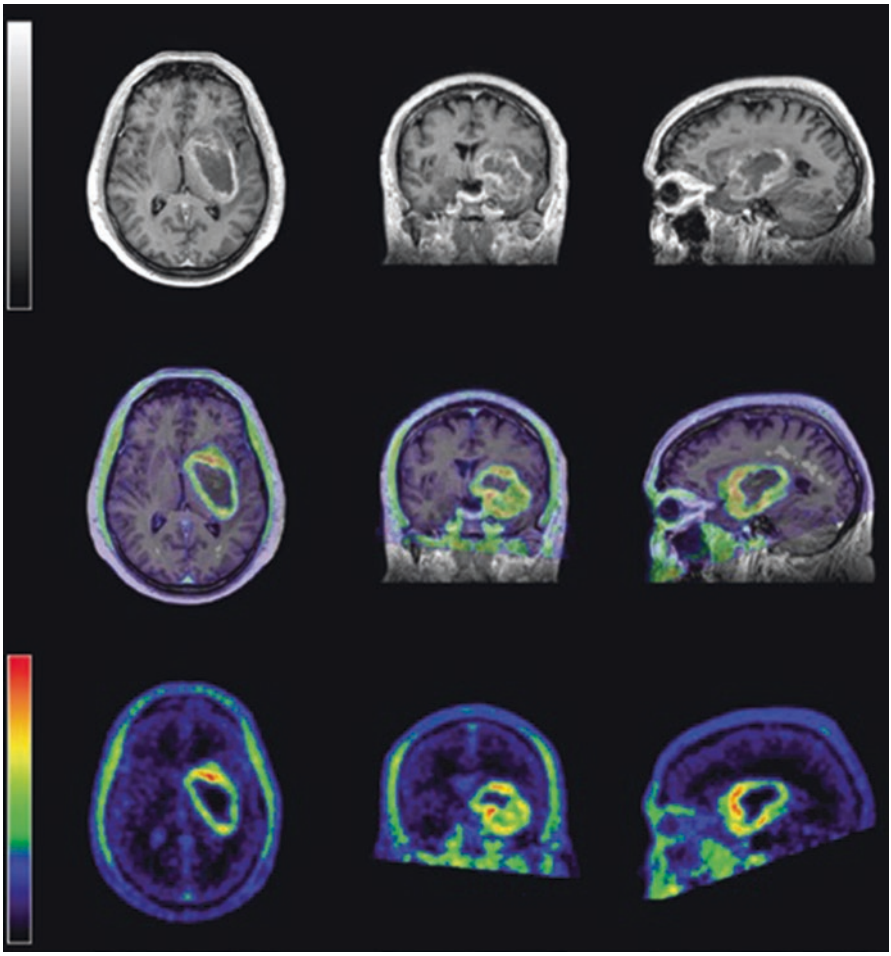

Fig. 10.9 ^{18}F-FAZA PET image (90–150 min smoothed with 4-mm Gaussian filter) overlaid on post-contrast T1-weighted MR image of glioblastoma patient. Note the different patterns of ^{18}F-FAZA brain uptake and gadolinium enhancement in the high grade tumour, particularly in the coronal (middle) and sagittal (right) views. *For courtesy of Dr. Natale Quartuccio and Dr. Marie-Claude Asselin* [43]

tumour-to-blood activity ratio of >1.2 imaged after at least 2 h postinjection can be generally considered as indicative of hypoxia [38]. High ^{18}F-MISO retention has been associated with a higher risk of loco-regional failure and shorter progression-free survival [39] and a predictor of poor treatment response and prognosis [40].

10.4.2 [^{18}F]-Fluoroazomycin arabinofuranoside (^{18}F-FAZA)

To overcome the limitations of ^{18}F-MISO, other tracers have been developed for the detection of tumour hypoxia. The most promising is probably ^{18}F-FAZA, which is less lipophilic than ^{18}F-MISO [35]. ^{18}F-FAZA is, like ^{18}F-MISO, a 2-nitroimidazole compound, but sugar-coupled and demonstrates a higher contrast with non-target tissues; this is probably due to the limited ability to cross the intact blood–brain barrier [41]. Therefore, ^{18}F-FAZA exhibits negligible cell-to-cell variability and no binding in normoxic cells [42] (Fig. 10.9).

Several studies had identified a tumour-to-background cut-off ratio of >1.2–1.5.

The role of tumour hypoxia depicted by ^{18}F-FAZA is a useful predictor of anticancer treatment response and the overall survival [44].

Given the good imaging properties with acceptable tumor to brain ratio (T/B ratios), ^{18}F-FAZA seems to be a very favourable hypoxia imaging agent, especially for gliomas.

Key Points

- To overcome some limitations of ^{18}F-FDG in brain imaging including large neutral amino acid tracers ^{11}C-MET, ^{18}F-FET, and ^{18}F-DOPA, proliferation cell membrane tracer ^{18}FCH, and hypoxia tracers as ^{18}F-MISO and ^{18}F-FAZA.
- ^{11}C-MET have a good tumour/background ratio; further there are different proposed thresholds from 1.5 to 1.9 for the diagnosis of brain tumour.
- Limitation: inflammatory processes are known to show increased ^{11}C-MET uptake and poor relation between ^{11}C-MET uptake and grading.
- ^{11}C-MET PET for the diagnosis and characterization of gliomas sensitivity 75–95% and specificity 87–100%.
- ^{11}C-MET PET can be used for assessing response to treatment.
- ^{18}F-FET is an amino acid tracer, an analogue of tyrosine. Dynamic acquisition up to 40 min after intravenous injection for evaluate the kinetic of the tracer is mandatory.
- The kinetic analysis of ^{18}F-FET uptake provides information on tumour grade in cerebral gliomas. High-grade gliomas, III or IV, are characterized

by an early peak around 10–15 min after injection followed by a decrease of ^{18}F-FET uptake. In contrast, time-activity curves in low-grade diffuse gliomas, grades I and II, increase slightly and steadily.

- ^{18}F-DOPA is a precursor of dopamine after the same metabolic pathways, including the synthesis of catecholamines.
- ^{18}F-DOPA PET is very accurate, sensitivities 90–100% and specificities 91%, for differentiating Parkinson's disease from other Parkinson-like entities.
- ^{18}F-DOPA have been most successfully used in the field of brain tumour imaging due to the increased expression of the 1-type amino acid transport system on tumour cells and an excellent tumour-to-background contrast.
- Choline is a component of phosphatidylcholine, an important element of cell membranes.
- The low concentration of ^{11}C/^{18}FCH uptake in the normal cerebral cortex allows excellent tumour-to-background ratio and good delineation of tumour contours.
- Difference in gradient of uptake between high-grade gliomas compared to low-grade gliomas, brain metastasis, and meningiomas has been reported.
- Tumour hypoxia influences the outcome of treatment with radiotherapy, chemotherapy, and even surgery.
- ^{18}F-MISO is the most widely used PET tracer to quantify tumour hypoxia.
- The main limits of ^{18}F-MISO are the slow uptake in the target tissue and the slow clearance of the unbound tracer from non-hypoxic tissue resulting in high background in PET images.
- The ^{18}F-MISO accumulation has been found to reflect hypoxia in glioma and considered a tumour-to-blood activity ratio of >1.2 imaged after at least 2 h postinjection indicative of hypoxia.
- High ^{18}F-MISO retention has been associated with poor treatment response and prognosis.
- ^{18}F-FAZA is like ^{18}F-MISO but demonstrates a higher contrast with nontarget tissues with a tumour-to-background cutoff ratio of >1.2–1.5.
- The role of tumour hypoxia depicted by ^{18}F-FAZA is a useful predictor of anticancer treatment response and the overall survival.
- The inclusion of these PET tracers in the workup of brain tumours complements and improves the diagnostic performances of conventional MRI in several settings, including biopsy targeting, prediction of anaplastic transformation, response assessment, and treatment planning for both high-grade and low-grade gliomas.

References

1. Jager PL, Vaalburg W, Pruim J, de Vries EG, Langen KJ, Piers DA. Radiolabeled amino acids: basic aspects and clinical applications. J Nucl Med. 2001;42:432–45.
2. Minamimoto R, Saginoya T, Kondo C, Tomura N, Ito K, et al. Differentiation of brain tumor recurrence from post-radiotherapy necrosis with 11C-methionine PET: visual assessment versus quantitative assessment. PLoS One. 2015;10(7):e0132515.
3. Stober B, Tanase U, Herz M, Seidl C, Schwaiger M, Senekowitsch-Schmidtke R. Differentiation of tumour and inflammation: characterisation of [methyl-3H]methionine (MET) and O-(2-[18F]fluoroethyl)-L-tyrosine (FET) uptake in human tumour and inflammatory cells. Eur J Nucl Med Mol Imaging. 2006;33:932–9.
4. Kracht LW, Friese M, Herholz K, Schroeder R, Bauer B, Jacobs A, et al. Methyl-[11C]-l-methionine uptake as measured by positron emission tomography correlates to microvessel density in patients with glioma. Eur J Nucl Med Mol Imaging. 2003;30:868–73.
5. Spaeth N, Wyss MT, Pahnke J, Biollaz G, Lutz A, Goepfert K, et al. Uptake of 18F-fluorocholine18F-fluoro-ethyl-L-tyrosine and18F-fluoro-2-deoxyglucose in F98 gliomas in the rat. Eur J Nucl Med Mol Imaging. 2006;33:673–82.
6. Kubota R, Kubota K, Yamada S, et al. Methionine uptake by tumor tissue: a microautoradiographic comparison with FDG. J Nucl Med\. 1995;36:484–92.
7. Utriainen M, Komu M, Vuorinen V, et al. Evaluation of brain tumor metabolism with [11C] choline PET and 1H-MRS. J Neurooncol. 2003;62:329–38.
8. Pirotte B, Goldman S, Van Bogaert P, et al. Integration of [11C]methionine-positron emission tomographic and magnetic resonance imaging for image-guided surgical resection of infiltrative low-grade brain tumors in children. Neurosurgery. 2005;57(1 Suppl):128–39.
9. Pirotte BJ, Levivier M, Goldman S, et al. Positron emission tomography-guided volumetric resection of supratentorial high-grade gliomas: a survival analysis in 66 consecutive patients. Neurosurgery. 2009;64:471–81.
10. Albert NL, Weller M, Suchorska B, Galldiks N, Soffietti R, Kim MM, et al. Response assessment in Neuro-Oncology working group and European Association for Neuro-Oncology recommendations for the clinical use of PET imaging in gliomas. Neuro Oncol. 2016;18(9):1199–208.
11. Langen KJ, Hamacher K, Weckesser M, Floeth F, Stoffels G, Bauer D, et al. O-(2-[18F] fluoroethyl)-l-tyrosine: uptake mechanisms and clinical applications. Nucl Med Biol. 2006;33(3):287–94.
12. Galldiks N, Stoffels G, Filss C, Rapp M, Blau T, Tscherpel C, Ceccon G, Dunkl V, Weinzierl M, Stoffel M, Sabel M, Fink GR, Shah NJ, Langen K-J. The use of dynamic O-(2-18F-fluoroethyl)-l-tyrosine PET in the diagnosis of patients with progressive and recurrent glioma. Neuro Oncol. 2015;17(9):1293–300.
13. Rapp M, Heinzel A, Galldiks N, Stoffels G, Felsberg J, Ewelt C, Sabel M, Steiger HJ, Reifenberger G, Beez T, Coenen HH, Floeth FW, Langen K-J. Diagnostic performance of 18F-FET PET in newly diagnosed cerebral lesions suggestive of glioma. J Nucl Med. 2013;54(2):229–35.
14. Muoio B, Giovanella L, Treglia G. Recent developments of 18F-FET PET in neuro-oncology. Curr Med Chem. 2018;25(26):3061–73.
15. Pöpperl G, Kreth FW, Mehrkens JH, et al. FET PET for the evaluation of untreated gliomas: correlation of FET uptake and uptake kinetics with tumour grading. Eur J Nucl Med Mol Imaging. 2007;34(12):1933–42.
16. Pauleit D, Floeth F, Hamacher K, et al. O-(2-[18F]fluoroethyl)-L-tyrosine PET combined with MRI improves the diagnostic assessment of cerebral gliomas. Brain. 2005;128(Pt 3):678–87.
17. Verger A, Stoffels G, Bauer EK, Lohmann P, Blau T, Fink GR, Neumaier B, Shah NJ, Langen KJ, Galldiks N. Static and dynamic 18F–FET PET for the characterization of gliomas defined by IDH and 1p/19q status. Eur J Nucl Med Mol Imaging. 2018;45(3):443–51.

18. Floeth FW, Pauleit D, Sabel M, Stoffels G, Reifenberger G, Riemenschneider MJ, et al. Prognostic value of 18F-FET PET and MRI in low-grade glioma. J Nucl Med. 2007;48:519–27.
19. Hutterer M, Nowosielski M, Putzer D, Waitz D, Tinkhauser G, Kostron H, et al. 18F-FET PET predicts failure of antiangiogenic treatment in patients with recurrent high-grade glioma. J Nucl Med. 2011;52(6):856–64.
20. Rufini V, Treglia G, Montravers F, Giordano A. Diagnostic accuracy of [18F]DOPA PET and PET/CT in patients with neuroendocrine tumors: a meta-analysis. Eur J Nucl Med Mol Imaging. 2013;39(7):1144–53.
21. Ibrahim N, Kusmirek J, Struck AF, Floberg JM, Perlman SB, Gallagher C, Hall LT. The sensitivity and specificity of F-DOPA PET in a movement disorder clinic. Am J Nucl Med Mol Imaging. 2016;6(1):102–9.
22. Struck AF, Hall LT, Kusmirek JE, Gallagher CL, Floberg JM, Jaskowiak CJ, Perlman SB. (18) F-DOPA PET with and without MRI fusion, a receiver operator characteristics comparison. Am J Nucl Med Mol Imaging. 2012;2(4):475–82.
23. Calabria FF, Chiaravalloti A, Jaffrain-Rea ML, Zinzi M, Sannino P, Minniti G, Rubello D, Schillaci O. 18F-DOPA PET/CT physiological distribution and pitfalls. Clin Nucl Med. 2016;41(10):753–60.
24. Calabria F, Cascini GL. Current status of 18F-DOPA PET imaging in the detection of brain tumor recurrence. Hell J Nucl Med. 2015;18(2):152–6.
25. Kwee SA, Coel MN, Lim J, Ko JP. Combined use of F-18 fluorocholine positron emission tomography and magnetic resonance spectroscopy for brain tumor evaluation. J Neuroimaging. 2004;14(3):285–9.
26. Hara T, Kondo T, Hara T, Kosaka N. Use of 18F-choline and 11C-choline as contrast agents in positron emission tomography imaging-guided stereotactic biopsy sampling of gliomas. J Neurosurg. 2003;99(3):474–9.
27. Giovacchini G, Fallanca F, Landoni C, et al. C-11 choline versus F-18 fluorodeoxyglucose for imaging meningiomas: an initial experience. Clin Nucl Med. 2009;34(1):7–10.
28. Kwee SA, Ko JP, Jiang CS, Watters MR, Coel MN. Solitary brain lesions enhancing at MR imaging: evaluation with fluorine 18fluorocholine PET. Radiology. 2007;244(2):557–65.
29. Grosu AL, Piert M, Weber WA, et al. Positron emission tomography for radiation treatment planning. Strahlenther Onkol. 2005;181(8):483–99.
30. Huang Z, Zuo C, Guan Y, et al. Misdiagnoses of 11C-choline combined with 18F-FDG PET imaging in brain tumours. Nucl Med Commun. 2008;29(4):354–8.
31. Rockwell S, Dobrucki IT, Kim EY, Tucker Marrison S, Vu VT. Hypoxia and radiation therapy: past history, ongoing research, and future promise. Curr Mol Med. 2009;9(4):442–58.
32. Cherk MH, Foo SS, Poon AM, et al. Lack of correlation of hypoxic cell fraction and angiogenesis with glucose metabolic rate in non-small cell lung cancer assessed by 18F-Fluoromisonidazole and 18F-FDG PET. J Nucl Med. 2006;47(12):1921–6.
33. Lewis JS, Welch MJ. PET imaging of hypoxia. Q J Nucl Med. 2001;45(2):183–8.
34. Souvatzoglou M, Grosu AL, Roper B, et al. Tumour hypoxia imaging with [18F]FAZA PET in head and neck cancer patients: a pilot study. Eur J Nucl Med Mol Imaging. 2007;34(10):1566–75.
35. Rajendran JG, Krohn KA. F-18 fluoromisonidazole for imaging tumor hypoxia: imaging the microenvironment for personalized cancer therapy. Semin Nucl Med. 2015;45(2):151–62.
36. Shetty D, Jeong JM, Shim H. Stroma targeting nuclear imaging and radiopharmaceuticals. Int J Mol Imaging. 2012;2012:817682.
37. Abolmaali N, Haase R, Koch A, Zips D, Steinbach J, Baumann M, et al. Two or four hour [(1) (8)F]FMISO-PET in HNSCC. When is the contrast best? Nuklearmedizin. 2011;50(1):22–7.
38. Valk PE, Mathis CA, Prados MD, Gilbert JC, Budinger TF. Hypoxia in human gliomas: demonstration by PET with fluorine-18-fluoromisonidazole. J Nucl Med. 1992;33(12):2133–7.
39. Rischin D, Hicks RJ, Fisher R, Binns D, Corry J, Porceddu S, Peters LJ. Prognostic significance of [18F]-misonidazole positron emission tomography-detected tumor hypoxia in patients with advanced head and neck cancer randomly assigned to chemoradiation with or

without tirapazamine: a substudy of Trans–Tasman Radiation Oncology Group study. J Clin Oncol. 2006;24(13):2098–104.
40. Lee ST, Scott AM. Hypoxia positron emission tomography imaging with 18F-fluoromisonidazole. Semin Nucl Med. 2007;37(6):451–61.
41. Postema EJ, McEwan AJ, Riauka TA, Kumar P, Richmond DA, Abrams DN, et al. Initial results of hypoxia imaging using 1-alpha-D: -(5-deoxy-5-[18F]-fluoroarabinofuranosyl)-2-nitroimidazole (18F-FAZA). Eur J Nucl Med Mol Imaging. 2009;36(10):1565–73.
42. Busk M, Horsman MR, Jakobsen S, Bussink J, van der Kogel A, Overgaard J. Cellular uptake of PET tracers of glucose metabolism and hypoxia and their linkage. Eur J Nucl Med Mol Imaging. 2008;35(12):2294–303.
43. Quartuccio N, Asselin M-C. The validation path of hypoxia PET imaging: focus on brain tumours. Curr Med Chem. 2018;25(26):3074–95.
44. Lopci E, Grassi I, Chiti A, Nanni C, Cicoria G, Toschi L, Fonti C, Lodi F, Mattioli S, Fanti S. PET radiopharmaceuticals for imaging of tumor hypoxia: a review of the evidence. Am J Nucl Med Mol Imaging. 2014;4(4):365–84.

Amyloid-β PET Imaging in Aging and Dementia

11

Nelleke Tolboom, Rik Ossenkoppele, and Bart N. van Berckel

Contents

11.1 Literature Review

Amyloid-β imaging with positron emission tomography (PET) has been around since the early 2000s. It has transformed neuroimaging in Alzheimer's disease (AD) by facilitating in vivo detection (and quantification) of amyloid-β plaques, one of the core pathological features of AD [1]. Initially, it was primarily used for research purposes and only infrequently in clinical practice. Now, more than a decade after the initial publications, it has become a standard diagnostic aid in specialised memory clinics.

N. Tolboom (✉)
Imaging Division, Department of Radiology, University Medical Center Utrecht, Utrecht, The Netherlands
e-mail: N.Tolboom@umcutrecht.nl

R. Ossenkoppele
Alzheimer Center, Amsterdam University Medical Center, Amsterdam, The Netherlands

Clinical Memory Research Unit, Lund University, Lund, Sweden

B. N. van Berckel
Department of Radiology and Nuclear Medicine, Amsterdam University Medical Center, Amsterdam, The Netherlands

F. Fraioli (ed.), *PET/CT in Brain Disorders*, Clinicians' Guides to Radionuclide Hybrid Imaging, https://doi.org/10.1007/978-3-030-01523-7_11

The first widely used PET ligand for in vivo imaging of amyloid-β is carbon-11 (^{11}C)-labelled Pittsburgh compound B (PiB) [2]. ^{11}C-PiB is a derivative of thioflavin-T, which is often used by neuropathologists to detect amyloid-β in post-mortem brain tissue. PiB binds to fibrillar Aβ deposits [3] and has a very high (90% or greater) sensitivity for the detection of amyloid pathology in the brain and a good correlation between in vivo amyloid load compared to post-mortem assessment of amyloid-β [4]. There are only a few PiB-negative AD patients, and these are neuropathologically proven to be caused by specific types of amyloid pathology, different from the amyloid pathology in sporadic AD [5, 6]. The clinical specificity, meaning having an abnormal PiB scan without having an underlying AD, depends on the age of the subjects and is lower with increasing age [7].

Following the success of PiB, a new generation of amyloid-β tracers labelled with fluorine-18 has been developed. Three F18 amyloid imaging ligands have already been approved for clinical use by the Food and Drug Administration (FDA) and the European Medicines Agency (EMA): Florbetapir (Amyvid®, Eli Lilly and Company) [8], Flutemetamol (Vizamyl®, GE Healthcare) [9], and Florbetaben (Neuraceq®, Piramal Imaging) [10]. Flutemetamol is a structural analogue of PiB, while the other two are based on stilbenes. There are some differences compared to PiB and compared to each other in imaging protocols, methods for analysing the data, as well as the way the scans are read (see Table 11.1). Furthermore, the nonspecific white matter binding is higher with the F18 ligands compared to PiB. This results in different target to nontarget ratios between tracers for visual interpretation. However, after proper reader training, these differences do not seem to affect their diagnostic performance in clinical populations [11–13].

Table 11.1 ^{18}F tracers for amyloid imaging

	Status approval	Administered activity (MBq)	Start and acquisition time static images	Interpretation
^{18}F-Florbetapir (Amyvid®) AVID/Lilly	FDA April 2012, EMA Jan 2013	370	30–50 min p.i. 10 min	Black and white
^{18}F-Flutemetamol (Vizamyl®) GE Healthcare	FDA Oct 2013, EMA Sept 2014	185	60–120 min p.i. 10–20 min	Colour scale (e.g. rainbow or Sokoloff)
^{18}F-Florbetaben (Neuraceq®) Piramal	FDA March 2014, EMA March 2014	300	90 min p.i. 20 min	Grey scale

Slight differences between the three FDA- and EMA-approved F18 amyloid imaging ligands
FDA Food and Drug Administration, *EMA* European Medicines Agency, *p.i.* postinjection

11.2 Indications

After a decade of research, much-needed indications for amyloid imaging in clinical practice have emerged. The Society of Nuclear Medicine and Molecular Imaging (SNMMI) and the Alzheimer's Association (AA) recently published appropriate use criteria [14]. Stating that 'Amyloid imaging is appropriate in certain patients whose clinical management would benefit from the knowledge of the amyloid status in the brain'. Three clinical scenarios have been agreed upon in which amyloid imaging is most beneficial:

1. The first clinical indication described by Johnson et al. [14] is in 'patients with persistent or progressive unexplained mild cognitive impairment (MCI)'. MCI is a heterogeneous group of patients with objectified (mostly memory) deficits, but without clinical dementia [15]. Of these patients, around 50% can show amyloid load with PET [16], of which the majority is thought to be at risk to progress towards AD dementia [17]. The other half is likely to have memory problems due to other causes, some unrelated to neurodegenerative processes. MCI patients without amyloid load on the PET scan are unlikely to have an underlying AD. Amyloid PET therefore aids to exclude AD as a cause of the cognitive impairment.
2. The second clinical indication is in 'patients satisfying core clinical criteria for possible AD because of an unclear clinical presentation, either atypical clinical course or etiologically mixed presentation'. The degree of certainty of the diagnosis of AD dementia varies between patients. Some patients are classified as 'probable' AD, a diagnosis with a relative high degree of certainty, when they meet certain clinical and cognitive criteria. Others are classified as 'possible AD', a diagnosis with a lower degree of certainty, due to atypical presentation or mixed course [18]. Clinical management of patients with 'possible' AD would benefit from knowing their amyloid status, whereas management of patients with probable AD would not likely change a lot.
3. The third clinical indication is in 'patients with progressive dementia and atypically early age of onset (usually defined as 65 years or less in age)'. The two main causes of dementia in this age group are AD and frontotemporal lobar degeneration (FTLD) [19]. FTLD is a group of neurodegenerative disorders affecting the frontal and anterior temporal lobes. There is some overlap in the early clinical presentation, leading to diagnostic difficulties and even misdiagnosis [20, 21]. The histopathology in FTLD is heterogeneous, but amyloid-β plaques are not considered part of the FTLD pathologic spectrum [22]. The relatively young age of the individuals makes for a low a priori chance of secondary (or age-related) comorbid amyloid load [23, 24]. Clinical studies revealed varying percentages of FTLD patients having amyloid load on PET imaging with unclear aetiology, possibly due to misdiagnosis. However, amyloid PET is thought to be helpful in the differentiation between AD and FTLD [25, 26].

Another important indication is the potential use of amyloid imaging in clinical trials. Amyloid imaging can be used to compose a homogeneous study population. It can identify subjects with underlying amyloid-β pathology who might benefit most from a potential new therapy targeted at amyloid and help to exclude dementia patients without amyloid load in the brain. It could also be used to monitor the potential treatment effect of certain therapies.

Other than the aforementioned official indications, there is still relatively limited use in daily clinical practices. Amyloid imaging does show promise in other neurodegenerative diseases, and research efforts are ongoing to clarify more potential indications. Vascular dementia, for instance, particularly in older patients, can be difficult to distinguish from AD clinically. Amyloid PET could have a clinical role in identifying patients with comorbid amyloid load, who therefore may potentially benefit from AD treatments. In dementia with Lewy bodies (DLB), it is unlikely that amyloid PET will be frequently used in clinical practice to differentiate from an underlying AD. In DLB patients, there is a high frequency of positive amyloid PET scans [27] in agreement with a high rate of amyloid-β plaques at post-mortem examination [28]. Therefore, scans demonstrating the absence of amyloid load are most useful in the differential diagnosis.

11.3 Classical Patterns

Amyloid-β deposition in the brain has been estimated to start ~15–20 years before patients develop symptoms [16, 29, 30]. After reaching a certain level, the amyloid-β deposition is believed to plateau [31], although a persistent slight increase through time has been reported [32]. The pattern of amyloid-β deposition seen with amyloid imaging throughout these (subclinical) stages closely resembles the pattern of the amyloid-β deposition described by neuropathologists [33].

In AD patients the classical pattern of amyloid ligand accumulation is diffuse and symmetric, regardless of the clinical presentation of AD. Only few exceptions with asymmetrical binding patterns have been described [34–36].

The classical pattern shows highest binding in the prefrontal cortex, precuneus cortex, and posterior cingulate cortex. The lateral parietal and lateral temporal cortex and striatum also show high tracer accumulation. This distribution is seen in almost all abnormal amyloid scans (see Fig. 11.1). Only in autosomal dominant AD (ADAD) (~1% of AD cases and due to either underlying mutations in *PSEN1* (chromosome 14, the most commonly involved gene), amyloid precursor protein (APP, chromosome 21), or *PSEN2* (presenilin-2, chromosome 1)), the pattern of amyloid deposition differs from the classical pattern seen in sporadic AD: in ADAD, it begins and is high in the striatum [37] (see Fig. 11.2).

In MCI patients with abnormal amyloid PET scans, the pattern of tracer accumulation is similar to that seen in AD. This is not surprising as the amyloid deposition starts many years before patients develop symptoms and often has already reached high levels in the clinical MCI stage [26].

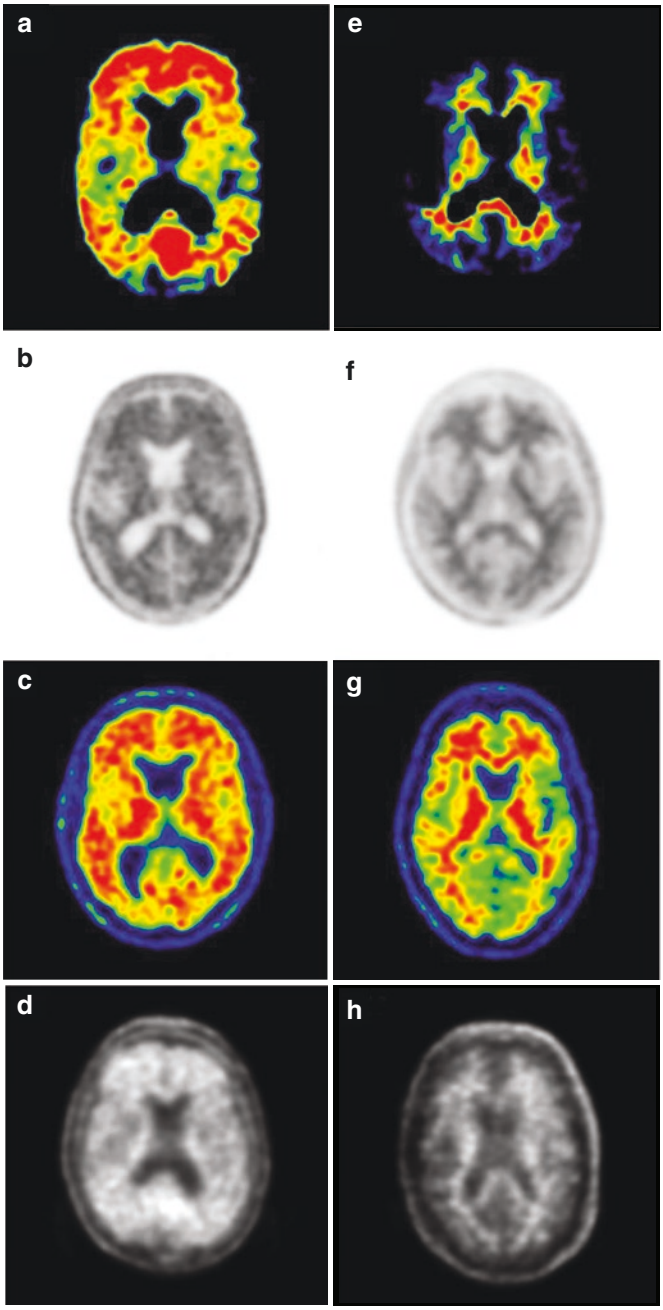

Fig. 11.1 Example of ^{11}C-PiB (panel **a**), ^{18}F-Florbetapir (panel **b**), ^{18}F-Flutemetamol (panel **c**), and ^{18}F-Florbetaben (panel **d**) scans. Left row are abnormal amyloid PET scans: increased tracer accumulation in cortical grey matter. Note the increased contrast with the white matter. Right row are normal amyloid PET scans without amyloid load and only nonspecific binding in white matter

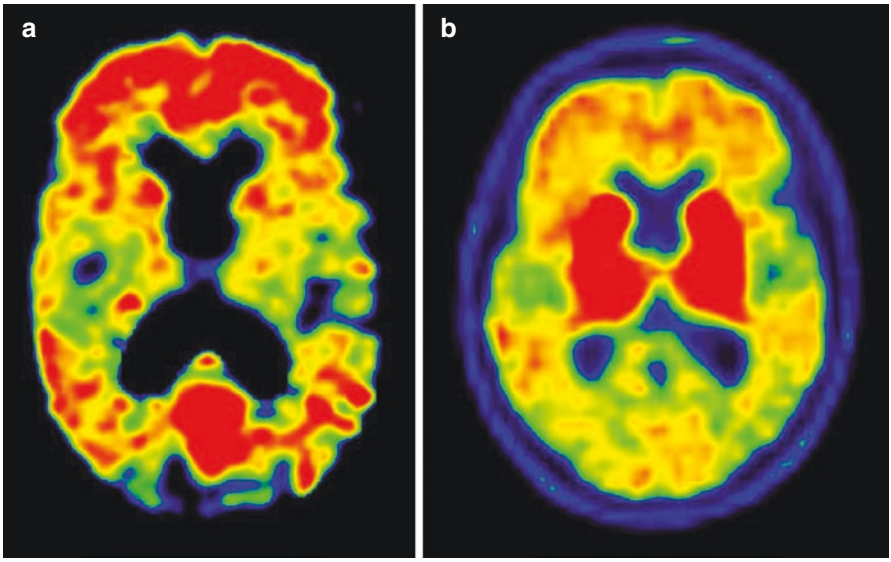

Fig. 11.2 Abnormal amyloid PET scan in a typical AD patient (panel **a**) with the classical pattern showing highest binding in the prefrontal cortex, precuneus cortex, and posterior cingulate cortex. The lateral parietal and lateral temporal cortex and striatum also show high tracer accumulation. Abnormal amyloid PET scan in a patient with autosomal dominant AD (panel **b**) showing marked increased binding in the striatum compared with the other regions

In DLB there is variation between patients, consistent with the findings at autopsy: some patients will display binding similar to AD patients but with a lower overall binding, while others have negligible amyloid load [26, 27].

Healthy controls span across the whole spectrum, with some controls showing no amyloid deposition, while others present with a pattern similar to AD [16, 26].

11.4 Advantages and Limitations

Amyloid imaging with PET has changed neuroimaging in AD by adding the possibility to detect the presence or absence of amyloid in the brain during life. It has tremendously helped in certain differential diagnostic dilemmas in dementia. Although still relatively limited data are available, it has proven its value in memory clinic settings [38–40]. Studies on the clinical use of amyloid imaging revealed changes in diagnosis in ~30% of patients, increases in diagnostic confidence in ~60% patients, and changes in patient management in ~60% of cases [41]. It has complementary value to amyloid-β analysis in cerebrospinal fluid (CSF) in diagnostics [42, 43] besides also giving regional information and being less invasive. Although relative limited data is available on cost-effectiveness [44, 45], initial simulation studies reveal a potential positive effect. More research is needed on this topic, but cost-effectiveness will certainly dramatically increase once disease-modifying treatments are being found and clinically approved.

There are also some caveats. In the elderly population, amyloid PET has a relatively lower sensitivity. Healthy elderly controls can show various levels of amyloid deposition measured using PET [7] in keeping with amyloid deposition in the brain of cognitively normal people at autopsy [46]. However, having amyloid depositions in the brain does seem to put people at risk to develop AD. Abnormal amyloid PET scans in the healthy elderly population is strongly related to the presence of the ApoE-4 allele, the largest known genetic risk factor for late-onset sporadic AD [47].

Another caveat is cut-off points: which amount of amyloid is too much and when. For clinical reporting in patients with dementia, a visual analysis using a binary approach (amyloid 'abnormal' or 'high' versus amyloid 'normal' or 'low') seems to be sufficient. In research and in preclinical AD, a more sophisticated approach is necessary by using semiquantitative values and cut-off points. Several ways to determine them have been described [48]. Since amyloid deposition in preclinical AD and in controls is subtler, a more conservative (lower) cut-off compared to the cut-off for differential diagnosis could be useful. Additionally, to enable more accurate comparison between sites and amyloid tracers, a so-called Centiloid scale has been proposed [49].

A relatively underexposed but important topic is the issue of dynamic imaging. Most centres perform static imaging of amyloid PET and use simplified methods like the standard uptake value ratio (SUVr) to analyse the data [50]. While this may be sufficient for making a clinical diagnosis, it is insufficient in longitudinal studies and in drug-intervention studies. Without correction for changes in blood flow, results could be interpreted as falsely lowering the amyloid burden while in fact it could potentially be the effect of reduced tracer delivery due to reduced blood flow [51]. Therefore, in longitudinal and drug intervention studies, dynamic imaging is warranted to guarantee optimal and reliable results.

Amyloid imaging is still subject to ongoing investigations, and certain topics like cost-effectiveness, validity of the appropriate use criteria, and clinical benefit could use some further clarification. But the whole new research field that has arisen from this new PET technique shows that amyloid imaging has changed nuclear medicine for the better and is here to stay.

Key Points

- The clinical specificity, meaning having an abnormal amyloid scan without having underlying AD, depends on the age of the subjects and becomes lower with increasing age.

  Healthy elderly controls can show various levels of amyloid in keeping with amyloid deposition in the brain of cognitively normal people at autopsy.
- There are only a few amyloid-negative AD patients on PET, and these are neuropathologically proven to be caused by specific types of amyloid pathology, different from the amyloid pathology observed in sporadic AD.

- The Society of Nuclear Medicine and Molecular Imaging (SNMMI) and the Alzheimer's Association (AA) published appropriate use criteria for amyloid imaging. Appropriate use includes certain patients whose clinical management would benefit from the knowledge of the amyloid status. Three clinical scenarios in which amyloid imaging is suggested to be most beneficial are:
  - "Patients with persistent or progressive unexplained mild cognitive impairment (MCI)." Amyloid PET aids to exclude AD as a cause of the cognitive impairment.
  - "Patients satisfying core clinical criteria for possible AD because of an unclear clinical presentation, either atypical clinical course or etiologically mixed presentation."
  - "Patients with progressive dementia and atypically early age of onset (usually defined as 65 years or less in age)." The two main causes of dementia in this age group are AD and frontotemporal lobar degeneration (FTLD). Amyloid PET is thought to be helpful in the differentiation between AD and FTLD.

References

1. Hardy J, Allsop D. Amyloid deposition as the central event in the aetiology of Alzheimer's disease. Trends Pharmacol Sci. 1991;12(10):383–8.
2. Klunk WE, Engler H, Nordberg A, Wang Y, Blomqvist G, Holt DP, et al. Imaging brain amyloid in Alzheimer's disease with Pittsburgh Compound-B. Ann Neurol. 2004;55(3):306–19.
3. Ikonomovic MD, Klunk WE, Abrahamson EE, Mathis CA, Price JC, Tsopelas ND, et al. Post-mortem correlates of in vivo PiB-PET amyloid imaging in a typical case of Alzheimer's disease. Brain. 2008;131(Pt 6):1630–45.
4. Bergeron D, Ossenkoppele R Jr, Laforce R. Evidence-based interpretation of amyloid-beta PET results: a clinician's tool. Alzheimer Dis Assoc Disord. 2018;32(1):28–34.
5. Scholl M, Wall A, Thordardottir S, Ferreira D, Bogdanovic N, Langstrom B, et al. Low PiB PET retention in presence of pathologic CSF biomarkers in Arctic APP mutation carriers. Neurology. 2012;79(3):229–36.
6. Tomiyama T, Nagata T, Shimada H, Teraoka R, Fukushima A, Kanemitsu H, et al. A new amyloid beta variant favoring oligomerization in Alzheimer's-type dementia. Ann Neurol. 2008;63(3):377–87.
7. Rowe CC, Ellis KA, Rimajova M, Bourgeat P, Pike KE, Jones G, et al. Amyloid imaging results from the Australian Imaging, Biomarkers and Lifestyle (AIBL) study of aging. Neurobiol Aging. 2010;31(8):1275–83.
8. Clark CM, Schneider JA, Bedell BJ, Beach TG, Bilker WB, Mintun MA, et al. Use of florbetapir-PET for imaging beta-amyloid pathology. JAMA. 2011;305(3):275–83.
9. Vandenberghe R, Van Laere K, Ivanoiu A, Salmon E, Bastin C, Triau E, et al. 18F-flutemetamol amyloid imaging in Alzheimer disease and mild cognitive impairment: a phase 2 trial. Ann Neurol. 2010;68(3):319–29.
10. Barthel H, Gertz HJ, Dresel S, Peters O, Bartenstein P, Buerger K, et al. Cerebral amyloid-beta PET with florbetaben (18F) in patients with Alzheimer's disease and healthy controls: a multicentre phase 2 diagnostic study. Lancet Neurol. 2011;10(5):424–35.

11. Landau SM, Breault C, Joshi AD, Pontecorvo M, Mathis CA, Jagust WJ, et al. Amyloid-beta imaging with Pittsburgh compound B and florbetapir: comparing radiotracers and quantification methods. J Nucl Med. 2013;54(1):70–7.
12. Wolk DA, Zhang Z, Boudhar S, Clark CM, Pontecorvo MJ, Arnold SE. Amyloid imaging in Alzheimer's disease: comparison of florbetapir and Pittsburgh compound-B positron emission tomography. J Neurol Neurosurg Psychiatry. 2012;83(9):923–6.
13. Villemagne VL, Mulligan RS, Pejoska S, Ong K, Jones G, O'Keefe G, et al. Comparison of 11C-PiB and 18F-florbetaben for Abeta imaging in ageing and Alzheimer's disease. Eur J Nucl Med Mol Imaging. 2012;39(6):983–9.
14. Johnson KA, Minoshima S, Bohnen NI, Donohoe KJ, Foster NL, Herscovitch P, et al. Appropriate use criteria for amyloid PET: a report of the Amyloid Imaging Task Force, the Society of Nuclear Medicine and Molecular Imaging, and the Alzheimer's Association. Alzheimers Dement. 2013;9(1):16.
15. Petersen RC. Mild cognitive impairment as a diagnostic entity. J Intern Med. 2004;256(3):183–94.
16. Jansen WJ, Ossenkoppele R, Knol DL, Tijms BM, Scheltens P, Verhey FR, et al. Prevalence of cerebral amyloid pathology in persons without dementia: a meta-analysis. JAMA. 2015;313(19):1924–38.
17. Villemagne VL, Pike KE, Chetelat G, Ellis KA, Mulligan RS, Bourgeat P, et al. Longitudinal assessment of Abeta and cognition in aging and Alzheimer disease. Ann Neurol. 2011;69(1):181–92.
18. McKhann GM, Knopman DS, Chertkow H, Hyman BT, Jack CR, Kawas CH, et al. The diagnosis of dementia due to Alzheimer's disease: recommendations from the National Institute on Aging-Alzheimer's Association workgroups on diagnostic guidelines for Alzheimer's disease. Alzheimers Dement. 2011;7(3):263–9.
19. Rabinovici GD, Miller BL. Frontotemporal lobar degeneration: epidemiology, pathophysiology, diagnosis and management. CNS Drugs. 2010;24(5):375–98.
20. Alladi S, Xuereb J, Bak T, Nestor P, Knibb J, Patterson K, et al. Focal cortical presentations of Alzheimer's disease. Brain. 2007;130(Pt 10):2636–45.
21. Ossenkoppele R, Jansen WJ, Rabinovici GD, Knol DL, van der Flier WM, van Berckel BN, et al. Prevalence of amyloid PET positivity in dementia syndromes: a meta-analysis. JAMA. 2015;313(19):1939–49.
22. Mackenzie IR, Neumann M, Bigio EH, Cairns NJ, Alafuzoff I, Kril J, et al. Nomenclature and nosology for neuropathologic subtypes of frontotemporal lobar degeneration: an update. Acta Neuropathol. 2010;119(1):1–4.
23. Mintun MA, Larossa GN, Sheline YI, Dence CS, Lee SY, Mach RH, et al. [11C]PIB in a nondemented population: potential antecedent marker of Alzheimer disease. Neurology. 2006;67(3):446–52.
24. Morris JC, Roe CM, Xiong C, Fagan AM, Goate AM, Holtzman DM, et al. APOE predicts amyloid-beta but not tau Alzheimer pathology in cognitively normal aging. Ann Neurol. 2010;67(1):122–31.
25. Rabinovici GD, Furst AJ, O'Neil JP, Racine CA, Mormino EC, Baker SL, et al. 11C-PIB PET imaging in Alzheimer disease and frontotemporal lobar degeneration. Neurology. 2007;68(15):1205–12.
26. Rowe CC, Ng S, Ackermann U, Gong SJ, Pike K, Savage G, et al. Imaging beta-amyloid burden in aging and dementia. Neurology. 2007;68(20):1718–25.
27. Gomperts SN, Rentz DM, Moran E, Becker JA, Locascio JJ, Klunk WE, et al. Imaging amyloid deposition in Lewy body diseases. Neurology. 2008;71(12):903–10.
28. Ballard C, Ziabreva I, Perry R, Larsen JP, O'Brien J, McKeith I, et al. Differences in neuropathologic characteristics across the Lewy body dementia spectrum. Neurology. 2006;67(11):1931–4.
29. Bateman RJ, Xiong C, Benzinger TL, Fagan AM, Goate A, Fox NC, et al. Clinical and biomarker changes in dominantly inherited Alzheimer's disease. N Engl J Med. 2012;367(9):795–804.

30. Price JL, McKeel DW, Buckles VD, Roe CM, Xiong C, Grundman M, et al. Neuropathology of nondemented aging: presumptive evidence for preclinical Alzheimer disease. Neurobiol Aging. 2009;30(7):1026–36.
31. Villemagne VL, Burnham S, Bourgeat P, Brown B, Ellis KA, Salvado O, et al. Amyloid beta deposition, neurodegeneration, and cognitive decline in sporadic Alzheimer's disease: a prospective cohort study. Lancet Neurol. 2013;12(4):357–67.
32. Villain N, Chetelat G, Grassiot B, Bourgeat P, Jones G, Ellis KA, et al. Regional dynamics of amyloid-beta deposition in healthy elderly, mild cognitive impairment and Alzheimer's disease: a voxelwise PiB-PET longitudinal study. Brain. 2012;135.(Pt 7:2126–39.
33. Thal DR, Rub U, Orantes M, Braak H. Phases of A beta-deposition in the human brain and its relevance for the development of AD. Neurology. 2002;58(12):1791–800.
34. Frings L, Hellwig S, Spehl TS, Bormann T, Buchert R, Vach W, et al. Asymmetries of amyloid-beta burden and neuronal dysfunction are positively correlated in Alzheimer's disease. Brain. 2015;138(Pt 10):3089–99.
35. Ossenkoppele R, Zwan MD, Tolboom N, van Assema DM, Adriaanse SF, Kloet RW, et al. Amyloid burden and metabolic function in early-onset Alzheimer's disease: parietal lobe involvement. Brain. 2012;135(Pt 7):2115–25.
36. Martersteck A, Murphy C, Rademaker A, Wieneke C, Weintraub S, Chen K, et al. Is in vivo amyloid distribution asymmetric in primary progressive aphasia? Ann Neurol. 2016;79(3):496–501.
37. Klunk WE, Price JC, Mathis CA, Tsopelas ND, Lopresti BJ, Ziolko SK, et al. Amyloid deposition begins in the striatum of presenilin-1 mutation carriers from two unrelated pedigrees. J Neurosci. 2007;27(23):6174–84.
38. Zwan MD, Bouwman FH, Konijnenberg E, van der Flier WM, Lammertsma AA, Verhey FR, et al. Diagnostic impact of [(18)F]flutemetamol PET in early-onset dementia. Alzheimers Res Ther. 2017;9(1):4.
39. Ossenkoppele R, Prins ND, Pijnenburg YA, Lemstra AW, van der Flier WM, Adriaanse SF, et al. Impact of molecular imaging on the diagnostic process in a memory clinic. Alzheimers Dement. 2013;9(4):414–21.
40. Grundman M, Johnson KA, Lu M, Siderowf A, Dell'Agnello G, Arora AK, et al. Effect of amyloid imaging on the diagnosis and management of patients with cognitive decline: impact of appropriate use criteria. Dement Geriatr Cogn Disord. 2016;41(1–2):80–92.
41. Barthel H, Sabri O. Clinical use and utility of amyloid imaging. J Nucl Med. 2017; 58(11):1711–7.
42. Ben Bouallegue F, Mariano-Goulart D, Payoux P, Alzheimer's Disease Neuroimaging Initiative (ADNI). Comparison of CSF markers and semi-quantitative amyloid PET in Alzheimer's disease diagnosis and in cognitive impairment prognosis using the ADNI-2 database. Alzheimers Res Ther. 2017;9(1):32.
43. Mattsson N, Insel PS, Donohue M, Landau S, Jagust WJ, Shaw LM, et al. Independent information from cerebrospinal fluid amyloid-beta and florbetapir imaging in Alzheimer's disease. Brain. 2015;138(Pt 3):772–83.
44. Hornberger J, Michalopoulos S, Dai M, Andrade P, Dilla T, Happich M. Cost-effectiveness of florbetapir-PET in Alzheimer's disease: a Spanish Societal perspective. J Ment Health Policy Econ. 2015;18(2):63–73.
45. Hornberger J, Bae J, Watson I, Johnston J, Happich M. Clinical and cost implications of amyloid beta detection with amyloid beta positron emission tomography imaging in early Alzheimer's disease - the case of florbetapir. Curr Med Res Opin. 2017;33(4):675–85.
46. Knopman DS, Parisi JE, Salviati A, Floriach-Robert M, Boeve BF, Ivnik RJ, et al. Neuropathology of cognitively normal elderly. J Neuropathol Exp Neurol. 2003; 62(11):1087–95.
47. Reiman EM, Chen K, Liu X, Bandy D, Yu M, Lee W, et al. Fibrillar amyloid-beta burden in cognitively normal people at 3 levels of genetic risk for Alzheimer's disease. Proc Natl Acad Sci U S A. 2009;106(16):6820–5.

48. Jack CR Jr, Wiste HJ, Weigand SD, Therneau TM, Lowe VJ, Knopman DS, et al. Defining imaging biomarker cut points for brain aging and Alzheimer's disease. Alzheimers Dement. 2017;13(3):205–16.
49. Klunk WE, Koeppe RA, Price JC, Benzinger TL, Devous MD Sr, Jagust WJ, et al. The Centiloid Project: standardizing quantitative amyloid plaque estimation by PET. Alzheimers Dement. 2015;11(1):4.
50. McNamee RL, Yee SH, Price JC, Klunk WE, Rosario B, Weissfeld L, et al. Consideration of optimal time window for Pittsburgh compound B PET summed uptake measurements. J Nucl Med. 2009;50(3):348–55.
51. van Berckel BN, Ossenkoppele R, Tolboom N, Yaqub M, Foster-Dingley JC, Windhorst AD, et al. Longitudinal amyloid imaging using 11C-PiB: methodologic considerations. J Nucl Med. 2013;54(9):1570–6.

The Use of PET/CT in Radiotherapy Planning for Brain Tumours

12

Francesca Soldá and Naomi Fersht

Contents

12.1 Introduction

Accurate identification of the treatment target is of crucial importance in modern brain radiotherapy, where the implementation of high-precision techniques of irradiation (intensity-modulated radiotherapy (IMRT), stereotactic radiotherapy (SRT) and stereotactic radiosurgery (SRS)) and the use of image guidance (IGRT) allow maximisation of the dose to the tumour volume identified while simultaneously sparing the surrounding uninvolved healthy brain [1].

In general, CT imaging for radiotherapy planning is performed with the patient lying in the treatment position using a head immobilisation device and co-registered with a planning MRI performed with or without immobilisation. While the extension of the visible tumour (gross tumour volume or GTV) and the adjacent critical structures are better visualised on predefined MRI sequences, the plan dosimetry is calculated using the CT scan data. Depending on the specific brain tumour characteristics (histological grade and invasiveness), a clinical target volume (CTV) is

F. Soldá (✉) · N. Fersht
Department of Oncology, University College Hospital, London, UK
e-mail: francesca.solda@nhs.net

F. Fraioli (ed.), *PET/CT in Brain Disorders*, Clinicians' Guides to Radionuclide Hybrid Imaging, https://doi.org/10.1007/978-3-030-01523-7_12

defined as the GTV plus a margin to account for the microscopic extension of disease needing to be encompassed by the entire treatment target [2].

MRI is the mainstay of imaging in brain radiotherapy, both in identifying tumour extension and treatment response [3]. Nonetheless, conventional T1-weighted (with or without contrast) and T2-weighted/FLAIR sequences, when used for radiotherapy planning, are unable to reflect the molecular and functional properties of brain tumours. These limitations are particularly evident in non-enhancing tumours (WHO grade II and a significant number of WHO grade III gliomas), where the lack of contrast uptake on MRI reduces the ability to precisely identify the tumour extension. Also, conventional MRI is inadequate to clearly distinguish residual or recurrent sellar or skull base lesions (pituitary adenomas and meningiomas) from postoperative changes [4, 5].

PET, and integrated PET/CT, can provide a combination of anatomical and biological information for radiotherapy planning purposes, overcoming some of the intrinsic limitations of conventional MRI. The use of different tracers allows identification of specific metabolic processes such as proliferation, biosynthesis, uptake of amino acid analogues and glucose consumption [6], all widely described in tumour tissues.

^{18}F-FDG is the most extensively used PET tracer in oncology, exploiting the increased metabolic state of most tumour cells. However, the high and regionally variable FDG uptake in normal brain makes the interpretation of imaging challenging [7, 8]. Furthermore, other primary tumours, as meningiomas, show reduced uptake of FDG [9, 10]. Other tracers are currently employed or under investigation in molecular imaging with PET/CT for brain tumours (Table 12.1). Radiolabelled

Table 12.1 PET/CT tracers used in brain tumour radiotherapy planning

Radiotracer	Category and mechanism	Role in brain RT planning
^{11}C-MET (methionine)	Amino acid ^{11}C-labelled MET uptake reflects increased intracellular transport mediated by type L amino acid carrier *Due to short half-life (20 min), its use is limited to facilities with on-site cyclotron*	HGG LGG Meningiomas Brain metastases
^{18}F-FET (fluoroethyl-L-tyrosine)	Artificial amino acid ^{18}F-labelled FET uptake correlates with increased cellular density	HGG LGG
^{18}F-FDOPA (dihydroxyphenylalanine)	^{18}F-labelled DOPA is an analogue of L-DOPA, precursor of dopamine (CNS neurotransmitter). Increased uptake correlates with tumour proliferation and grade and can distinguish radionecrosis from tumour recurrence	HGG
Somatostatin analogues (^{68}Ga-DOTATATE, ^{68}Ga-DOTATOC, ^{68}Ga-DOTANOC)	Increased uptake is detected in tumours highly expressing somatostatin receptors (neuroendocrine tumours and meningiomas)	Meningiomas

HGG high-grade gliomas, *LGG* low-grade gliomas

amino acid (^{11}C-MET, ^{18}F-FET, ^{18}F-DOPA) and somatostatin analogue compounds (^{68}Ga-DOTATATE, ^{68}Ga-DOTATOC) and their value in the context of defining the radiotherapy target volume will be described in this chapter.

12.2 Image Quality for Planning Purposes

While functional imaging plays already an important role in the initial diagnosis and follow-up of brain tumour patients [6], the integration of PET/CT in the radiotherapy planning process requires a superior level of reproducibility and image quality acquisition than the one provided for diagnostic imaging.

A PET/CT for planning purposes needs to be acquired with the patient positioned and immobilised as for during treatment delivery, preferably acquiring a high-quality CT scan for planning purposes together with the PET scan avoiding the need of additional image registration. In this scenario, the system of laser positioning between the PET/CT suit and radiotherapy facility will need to be mirrored (this obviously includes the use of the same flat-top couches). If contrast injection is required with the planning CT scan, an additional low-dose CT scan can be performed and used for attenuation and scatter correction independently from the planning CT, or an attenuation corrected contrast-enhanced CT can be acquired.

The impact of patient motion during imaging is generally well controlled with modern brain immobilisation devices, but other sources of uncertainties (such as scanner calibration and image processing) need careful evaluation when PET imaging is used for radiotherapy planning. The imaging spatial resolution is a limitation of a PET imaging, with lesions smaller than 5–10 mm being poorly discernible from the background noise [11], which makes molecular imaging less useful for target delineation [12].

12.3 PET/CT for Radiotherapy Planning in Brain Gliomas

High-grade gliomas (HGGs) include anaplastic glial tumours (WHO grade III astrocytomas and oligodendrogliomas) and glioblastomas (WHO grade IV). Radiotherapy represents the mainstay of treatment in this group of patients since evidence was shown of its role in improving postoperative survival [13–15] even in cases of recurrence [16]. The information provided by conventional contrast-enhanced MRI is the result of the blood-brain barrier (BBB) disruption and does not necessarily reflect the real tumour extension, often observed in the surrounding oedema or in the adjacent normal appearing brain [17–19]. This might result in underestimating the GTV and, consequently, the CTV extension and final treatment target.

The rationale behind the introduction of PET/CT in treatment target definition for HGGs relies on the ability of specific PET tracers to identify abnormal biological and metabolic activity corresponding to areas at high risk of disease/recurrence (with low uptake in the normal tissue) beyond the contrast-enhanced volume on MRI. Several data suggest that brain tumour imaging with PET using amino acids

is more reliable than MRI in defining the extent of cerebral gliomas [20–23]. Amino acid tracers such as ^{11}C-MET, ^{18}F-FET and ^{18}F-DOPA have been investigated in small prospective and retrospective studies to assess their value in detecting the tumour extension (often referred as BTV, biological tumour volume) in comparison to target volumes outlined with traditional MRI in radiotherapy planning (Table 12.2). BTVs larger than corresponding MRI-based volumes were often outlined [17, 24–26]. The inadequate coverage of BTV by morphological GTV was associated with an increased risk of non-central failures in glioblastomas [25]. In recurrent HGGs, the use of PET/CT for target delineation was suggested to improve the high variability in target definition observed with conventional MRI [27]. The

Table 12.2 Studies on PET/CT for radiotherapy planning in brain gliomas

Tracer	Study	Design	Findings
^{18}F-FET	Weber 2008 [26]	14 GBM 5 AA Concomitant chemoradiotherapy	Size and geometrical location of GTVs and BTVs differed in majority of patients
	Piroth 2009 [34]	16 GBM Integrated boost IMRT or 3DCRT	FET-PET-based automatically contoured PTV leads to complex geometric configurations, limiting achievable mean dose in the boost volume
	Vees 2009 [35]	18 GBM 2 AA 2 ODG	PET-based GTVs were smaller than GTV_{MRI} PET detected tumours not visible on MRI and added tumour extension outside the GTV_{MRI} in 33% of cases
	Niyazi 2011 [24]	17 GBM Concomitant chemoradiotherapy 3DCRT	PET-based GTVs (BTVs) larger than corresponding MRI-based GTVs, with major differences in 11 cases
	Rieken 2013 [29]	37 HGG 4 LGG Combination of photon/carbon ion RT	Integrating FET uptake into the delineation of GTVs yields larger volumes. Combined modality-derived PTVs are enlarged in high-grade glioma patients and in case of primary RT
	Schinkelshoek 2014 [36]	31 Primary/recurrent GBM Conformal RT	In 65% cases BTV resulted in a modification of the CTV. MET-PET/CT only predictor demonstrating significant correlation with PFS and OS
	Munck of Rosenschold 2015 [37]	35 WHO grade IV 19 WHO grade III IMPT/rapid arc IMRT (coplanar and noncoplanar)	5 pts PET negative Incorporating FET-positive volume into a combined MR/PET GTV caused the GTV to increase overall PET-positive volume was strongly associated with WHO grade IV glioma 90% PET-positive volumes were encompassed by T1 MRI with contrast plus a 20-mm margin

(continued)

Table 12.2 (continued)

Tracer	Study	Design	Findings
	Moller 2016 [38]	25 WHO grade IV 6 WHO grade III Reirradiation with stereotactic RT	Baseline BTV and baseline MRI volumes (necrotic/cystic cavities subtracted) were prognostic for OS in multivariate analysis
	Poulsen 2017 [39]	146 GBM Concomitant chemoradiotherapy	Large BTV on FET-PET is independent prognostic factor of poor OS and PFS in GBM
	Jaymanne 2018 [40]	5 GMB 1 AA with contraindications to MRI	FET-PET is useful in aiding CT-based voluming in patients with contraindications to MRI
^{11}C-MET	Grosu 2005 [17]	27 WHO grade IV 12 WHO grade III Stereotactic hypofractionated RT	MET uptake detected up to 45 mm beyond GD enhancement and up to 4 mm beyond T2 hyperintensity-defined area
	Mahasittiwat 2008 [41]	4 AA 12 GBM Carbon ion RT	PET-based target volumes included in CTV/MRI T1- and T2-based volumes in 82.3% and 68.8%, respectively
	Matsuo 2012 [42]	32 GBM Stereotactic RT	BTV with ^{11}C-MET describes GTV with greater accuracy than MRI
	Miwa 2014 [43]	21 recurrent GBM Hypofractionated RT	GTV based on co-registered PET/CT/MRI was used for treatment
^{18}F-FDOPA	Kosztyla 2013 [44]	19 GBM Concomitant chemoradiotherapy (3DCR, IMRT, VMAT)	PET-based volume larger than MRI based. All but 1 recurrence extended outside PET-based volumes

3DCRT three-dimensional conformal radiotherapy, *IMRT* intensity-modulated radiotherapy, *IMPT* intensity-modulated proton therapy

longer half-life of ^{18}F-labelled tracers contributes to a wider use of FET and DOPA in the clinical practice.

The value of PET/CT has been less extensively assessed in radiotherapy planning for low-grade gliomas (LGGs) with only few studies exploring its use in the treatment setting [28, 29], although the effectiveness of amino acid PET in defining tumour extension has been demonstrated in histology-validated series [30–33].

12.4 PET/CT for Radiotherapy Planning in Meningiomas

The exact extension of recurrent or residual meningiomas for radiotherapy treatment can be hard to define due to bone thickening, enhancing dural tails and postoperative changes (Fig. 12.1). Although high local control rates following radiotherapy are observed in meningiomas [45], this does not negate the need for accurate target definition, especially with modern highly conformal treatment approaches. In fact, older radiotherapy techniques may have compensated for undercontouring where extra normal tissue was inevitably covered by the prescribed dose.

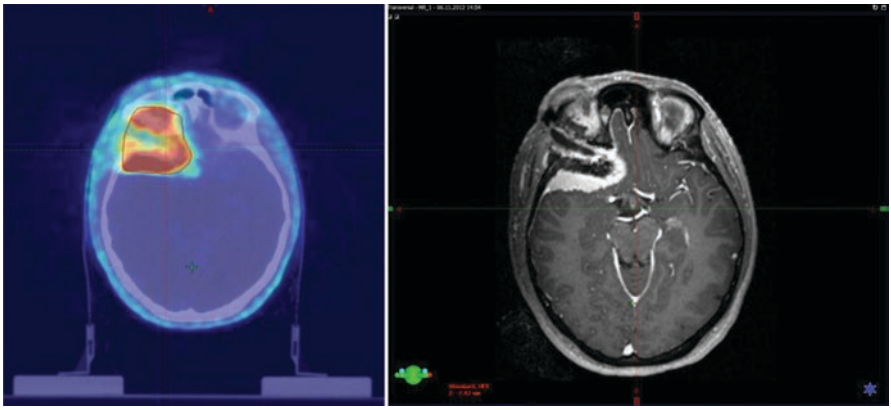

Fig. 12.1 Planning ^{68}Ga-DOTATATE PET/CT (left) used for GTV (blue line) definition in a large right sphenoid wing meningioma. CE-T1 MRI does not define the tumour extension into the right orbit (right)

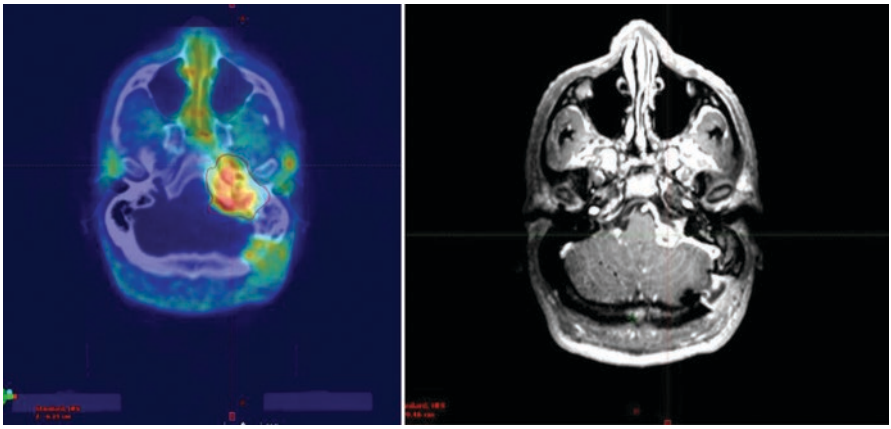

Fig. 12.2 Tumour extension at the level of the skull base on RT planning ^{68}Ga-DOTATATE PET/CT (left) in comparison with CE-T1 MRI (right)

The uptake of ^{18}F-FDG showed to significantly correlate with the WHO grade in meningiomas [9, 46], but its brain uptake is not tumour specific and may increase in the presence of inflammatory tissue [47].

Because of the overexpression of somatostatin receptors (SSTRs) in meningiomas (with subtype 2 receptors found to be the most abundant isoform) [48], radiolabelled SSTR ligands (^{68}Ga-DOTATATE, ^{68}Ga-DOTATOC, ^{68}Ga-DOTANOC) have been widely investigated in view of their high tumour-to-background ratio and valuable information provided on the extent of meningiomas beneath osseous structures, especially in the skull base [49] (Fig. 12.2).

Table 12.3 Studies on PET/CT for radiotherapy planning in meningiomas

Tracer	Study	Design	Findings
^{68}Ga-DOTATOC	Milker-Zabel 2006 [52]	26 meningiomas Fractionated stereotactic RT	Radiation targeting with fused DOTATOC PET, CT and MRI resulted in significant alterations in target definition in 73%
	Gehler 2009 [53]	26 meningiomas IMRT	Radiation targeting with fused DOTATOC PET, CT and MRI resulted in significant alterations in CTV definition in 65%
	Nyuyki 2010 [54]	42 meningiomas (2 negative PET) Stereotactic RT	GTV alteration in 72% of cases
	Combs 2013 [55]	70 meningiomas Protons and carbon ion RT	PET imaging helped defining between meningeal thickening and tumour extension
	Graf 2013 [56]	16 meningiomas Fractionated stereotactic RT	^{68}Ga-DOTATOC PET/CT improved volume delineation. Reduced PET-based GTV compared with MRI and CT
^{68}Ga-DOTATATE	Maclean 2017 [57]	10 meningiomas IMRT (PET/MRI and PET/CT)	IOV in contouring challenging meningioma cases was large and only slightly improved with the addition of ^{68}Ga DOTATATE PET
^{11}C-MET	Grosu 2006 [58]	10 meningiomas Fractionated stereotactic RT	Information of MET-PET useful to delineate GTV in the area of cavernous sinus, orbit and base of the skull
	Astner 2008 [59]	32 meningiomas Fractionated stereotactic RT	MET-PET was beneficial for GTV delineation in all but 3 patients, detecting tumour portions not visible on CT/MRI

IMRT intensity-modulated radiotherapy, *IOV* interobserver variability

PET/CT with SSTR ligands has considerable impact on radiotherapy target definition where both normal dura and tumour tissue show high contrast enhancement on MRI or when tumour margins infiltrating the bone are poorly defined despite bone window on CT scan (Table 12.3).

PET/CT with ^{11}C-MET also demonstrated to significantly influence GTV delineation in patients with meningiomas, by highlighting areas otherwise not visualised on conventional planning CT or MRI (Table 12.3).

PET-based delineation was investigated for other brain lesions (glomus tumours, pituitary adenomas) with the aim to reduce interobserver variability [50, 51], but few data have been published so far.

12.5 PET/CT for Radiotherapy Planning in Brain Metastases

Few published studies have quantified tumour extension in brain metastases from PET/CT and MRI, comparing the two modalities in the context of radiotherapy planning. However, small metastases can only be identified by MRI, and an unspecific uptake in inflammatory processes has been described in FDG PET scans in comparison with imaging obtained with other radiopharmaceuticals [60, 61].

Miwa [62] evaluated 42 metastatic brain tumours at baseline and at specific follow-up intervals after stereotactic radiotherapy (SRT). In the study, MET-PET images were imported in the planning software for the SRT dosimetry as additional information. The final target volume was defined on the stereotactic MR image, taking into account MET-PET and MRI findings. MET-PET was useful in providing additional information for diagnosis and follow-up after radiotherapy.

In a similar study [63], MET-PET was used for GTV delineation in 19 patients with a total of 95 brain metastatic lesions. The authors concluded that MET-PET has the potential for precise delineation of target volumes in lesions with a volume bigger than 0.5 mL.

12.6 Conclusion

The use of PET to plan and monitor treatment is an active area of investigation. With the development of targeted therapies, PET biomarkers might be used to identify patients who are likely to respond to treatment, as well as to monitor treatment response. The major limitations to the integration of PET/CT imaging in radiotherapy planning for brain tumours are represented by the low spatial resolution of PET studies, leading to false-negative findings in the case of small lesions, and in the possibility of unspecific uptake shortly after surgery [64].

Furthermore, a high level of expertise is required for correct image interpretation.

The recently proposed international guidelines for target delineation in glioblastomas do not currently include PET imaging as a standard modality for radiotherapy planning [3]. Instead, the RANO/PET group recommended (evidence level 2) amino acid PET and ^{68}Ga-DOTATOC PET for radiotherapy planning to improve GTV definition and dose sparing of organs at risk [65].

The implementation of PET/CT in everyday RT planning is expected to be defined in prospective randomised trials aimed to clarify its role in comparison with conventional MRI sequences.

Key Points

- Modern brain radiotherapy techniques aim at maximizing the dose within the treatment target while sparing the uninvolved healthy brain.
- Correct target identification is therefore of critical importance in highly precise brain radiotherapy.
- In radiotherapy planning, the treatment target is identified on high-resolution imaging (thin cuts MRI sequences with contrast) accurately fused with CT imaging acquired for planning purposes.

- MRI is the mainstay of imaging in brain radiotherapy, both in identifying tumour extension and treatment response.
- Conventional MRI sequences are unable to reflect the molecular and functional properties of brain tumours.
- PET and PET/CT could provide additional anatomical and biological information for the purpose of radiotherapy planning.
- While ^{18}F-FDG is an extensively used PET tracer in oncology, its use in neuro-oncology is mainly limited by the high rate of glucose metabolism in normal brain.
- Several reports showed an impact of FET-PET, MET PET, and FDOPA PET on target volume delineation primarily in high-grade gliomas, although their role has not been fully validated.
- PET/CT with SSTR ligands has a considerable impact on radiotherapy target identification in brain meningiomas.
- The impact of PET/CT in radiotherapy planning needs to be compared with a variety of promising advanced MRI techniques in well-designed studies.

References

1. Khuntia D, Tomé WA, Mehta MP. Radiation techniques in neuro-oncology. Neurotherapeutics. 2009;6:487–99.
2. Burnet NG, Thomas SJ, Burton KE, Jefferies SJ. Defining the tumour and target volumes for radiotherapy. Cancer Imaging. 2004;4:153–61.
3. Niyazi M, Brada M, Chalmers AJ, Combs SE, Erridge SC, Fiorentino A, et al. ESTRO-ACROP guideline "target delineation of glioblastomas". Radiother Oncol. 2016;118:35–42.
4. Albert NL, Weller M, Suchorska B, Galldiks N, Soffietti R, Kim MM, et al. Response Assessment in Neuro-Oncology working group and European Association for Neuro-Oncology recommendations for the clinical use of PET imaging in gliomas. Neuro Oncol. 2016;18:1199–208.
5. Jaeckle KA. Neuroimaging for central nervous system tumors. Semin Oncol. 1991;18:150–7.
6. la Fougère C, Suchorska B, Bartenstein P, Kreth F-W, Tonn J-C. Molecular imaging of gliomas with PET: opportunities and limitations. Neuro Oncol. 2011;13:806–19.
7. Ricci PE, Karis JP, Heiserman JE, Fram EK, Bice AN, Drayer BP. Differentiating recurrent tumor from radiation necrosis: time for re-evaluation of positron emission tomography? AJNR Am J Neuroradiol. 1998;19:407–13.
8. Wong TZ, van der Westhuizen GJ, Coleman RE. Positron emission tomography imaging of brain tumors. Neuroimaging Clin N Am. 2002;12:615–26.
9. Di Chiro G, Hatazawa J, Katz DA, Rizzoli HV, De Michele DJ. Glucose utilization by intracranial meningiomas as an index of tumor aggressivity and probability of recurrence: a PET study. Radiology. 1987;164:521–6.
10. Valotassiou V, Leondi A, Angelidis G, Psimadas D, Georgoulias P. SPECT and PET imaging of meningiomas. ScientificWorldJournal. 2012;2012:412580.

11. Kumar R, Chauhan A, Zhuang H, Chandra P, Schnall M, Alavi A. Clinicopathologic factors associated with false negative FDG-PET in primary breast cancer. Breast Cancer Res Treat. 2006;98:267–74.
12. Jeraj R, Bradshaw T, Simoncic U. Molecular imaging to plan radiotherapy and evaluate its efficacy. J Nucl Med. 2015;56:1752–65.
13. Kristiansen K, Hagen S, Kollevold T, Torvik A, Holme I, Nesbakken R, et al. Combined modality therapy of operated astrocytomas grade III and IV. Confirmation of the value of postoperative irradiation and lack of potentiation of bleomycin on survival time: a prospective multicenter trial of the Scandinavian Glioblastoma Study Group. Cancer. 1981;47:649–52.
14. Walker MD, Alexander E Jr, Hunt WE, MacCarty CS, Mahaley MS Jr, Mealey J Jr, et al. Evaluation of BCNU and/or radiotherapy in the treatment of anaplastic gliomas. A cooperative clinical trial. J Neurosurg. 1978;49:333–43.
15. Stupp R, Mason WP, van den Bent MJ, Weller M, Fisher B, Taphoorn MJ, et al. Radiotherapy plus concomitant and adjuvant temozolomide for glioblastoma. N Engl J Med. 2005;352:987–96.
16. Niyazi M, Siefert A, Schwarz SB, Ganswindt U, Kreth FW, Tonn JC, et al. Therapeutic options for recurrent malignant glioma. Radiother Oncol. 2011;98:1–14.
17. Grosu AL, Weber WA, Riedel E, Jeremic B, Nieder C, Franz M, et al. L-(methyl-11C) methionine positron emission tomography for target delineation in resected high-grade gliomas before radiotherapy. Int J Radiat Oncol Biol Phys. 2005;63:64–74.
18. Susheela S, Revannasiddaiah S, Madhusudhan N, Bijjawara M. The demonstration of extension of high-grade glioma beyond magnetic resonance imaging defined edema by the use of ^{11}C-methionine positron emission tomography. J Cancer Res Ther. 2013;9:715–7.
19. Zetterling M, Roodakker KR, Berntsson SG, Edqvist PH, Latini F, Landtblom AM, et al. Extension of diffuse low-grade gliomas beyond radiological borders as shown by the coregistration of histopathological and magnetic resonance imaging data. J Neurosurg. 2016;125:1155–66.
20. Lee SW, Fraass BA, Marsh LH, Herbort K, Gebarski SS, Martel MK, et al. Patterns of failure following high-dose 3-D conformal radiotherapy for high-grade astrocytomas: a quantitative dosimetric study. Int J Radiat Oncol Biol Phys. 1999;43:79–88.
21. Macdonald DR, Cascino TL, Schold SC Jr, Cairncross JG. Response criteria for phase II studies of supratentorial malignant glioma. J Clin Oncol. 1990;8:1277–80.
22. Giantsoudi D, Adams J, MacDonald SM, Paganetti H. Proton treatment techniques for posterior fossa tumors: consequences for linear energy transfer and dose-volume parameters for the brainstem and organs at risk. Int J Radiat Oncol Biol Phys. 2017;97:401–10.
23. Oppitz U, Maessen D, Zunterer H, Richter S, Flentje M. 3D-recurrence-patterns of gliobastomas after CT-planned postoperative irradiation. Radiother Oncol. 1999;53:53–7.
24. Niyazi M, Geisler J, Siefert A, Schwarz SB, Ganswindt U, Garny S, et al. FET-PET for malignant glioma treatment planning. Radiother Oncol. 2011;99:44–8.
25. Lee IH, Piert M, Gomez-Hassan D, Junck L, Rogers L, Hayman J, et al. Association of 11C-methionine PET uptake with site of failure after concurrent temozolomide and radiation for primary glioblastoma multiforme. Int J Radiat Oncol Biol Phys. 2009;73:479–85.
26. Weber DC, Zilli T, Buchegger F, Casanova N, Haller G, Rouzaud M, et al. [(18)F] Fluoroethyltyrosine-positron emission tomography-guided radiotherapy for high-grade glioma. Radiat Oncol. 2008;3:44.
27. Grosu AL, Weber WA, Franz M, Stark S, Piert M, Thamm R, et al. Reirradiation of recurrent high-grade gliomas using amino acid PET (SPECT)/CT/MRI image fusion to determine gross tumor volume for stereotactic fractionated radiotherapy. Int J Radiat Oncol Biol Phys. 2005;63:511–9.
28. Nuutinen J, Sonninen P, Lehikoinen P, Sutinen E, Valavaara R, Eronen E, et al. Radiotherapy treatment planning and long-term follow-up with [^{11}C]methionine PET in patients with low-grade astrocytoma. Int J Radiat Oncol Biol Phys. 2000;48:43–52.
29. Rieken S, Habermehl D, Giesel FL, Hoffmann C, Burger U, Rief H, et al. Analysis of FET-PET imaging for target volume definition in patients with gliomas treated with conformal radiotherapy. Radiother Oncol. 2013;109:487–92.

30. Fueger BJ, Czernin J, Cloughesy T, Silverman DH, Geist CL, Walter MA, et al. Correlation of 6-18F-fluoro-L-dopa PET uptake with proliferation and tumor grade in newly diagnosed and recurrent gliomas. J Nucl Med. 2010;51:1532–8.
31. Kracht LW, Miletic H, Busch S, Jacobs AH, Voges J, Hoevels M, et al. Delineation of brain tumor extent with [11C]L-methionine positron emission tomography: local comparison with stereotactic histopathology. Clin Cancer Res. 2004;10:7163–70.
32. Tripathi M, Sharma R, D'Souza M, Jaimini A, Panwar P, Varshney R, et al. Comparative evaluation of F-18 FDOPA, F-18 FDG, and F-18 FLT-PET/CT for metabolic imaging of low grade gliomas. Clin Nucl Med. 2009;34:878–83.
33. Pauleit D, Floeth F, Hamacher K, Riemenschneider MJ, Reifenberger G, Muller HW, et al. O-(2-[18F]fluoroethyl)-L-tyrosine PET combined with MRI improves the diagnostic assessment of cerebral gliomas. Brain. 2005;128:678–87.
34. Piroth MD, Pinkawa M, Holy R, Stoffels G, Demirel C, Attieh C, et al. Integrated-boost IMRT or 3-D-CRT using FET-PET based auto-contoured target volume delineation for glioblastoma multiforme—a dosimetric comparison. Radiat Oncol. 2009;4:57.
35. Vees H, Senthamizhchelvan S, Miralbell R, Weber DC, Ratib O, Zaidi H. Assessment of various strategies for 18F-FET PET-guided delineation of target volumes in high-grade glioma patients. Eur J Nucl Med Mol Imaging. 2009;36:182–93.
36. Schinkelshoek M, Lopci E, Clerici E, Alongi F, Mancosu P, Rodari M, et al. Impact of 11C-methionine positron emission tomography/computed tomography on radiation therapy planning and prognosis in patients with primary brain tumors. Tumori. 2014;100:636–44.
37. Munck af Rosenschold P, Costa J, Engelholm SA, Lundemann MJ, Law I, Ohlhues L, et al. Impact of [(18)F]-fluoro-ethyl-tyrosine PET imaging on target definition for radiation therapy of high-grade glioma. Neuro Oncol. 2015;17:757–63.
38. Moller S, Law I, Munck af Rosenschold P, Costa J, Poulsen HS, Engelholm SA, et al. Prognostic value of ^{18}F-FET PET imaging in re-irradiation of high-grade glioma: results of a phase I clinical trial. Radiother Oncol. 2016;121:132–7.
39. Poulsen SH, Urup T, Grunnet K, Christensen IJ, Larsen VA, Jensen ML, et al. The prognostic value of FET PET at radiotherapy planning in newly diagnosed glioblastoma. Eur J Nucl Med Mol Imaging. 2017;44:373–81.
40. Jaymanne DT, Kaushal S, Chan D, Schembri G, Brazier D, Bailey D, et al. Utilizing 18F-fluoroethyl-l-tyrosine positron emission tomography in high grade glioma for radiation treatment planning in patients with contraindications to MRI. J Med Imaging Radiat Oncol. 2018;62:122–7.
41. Mahasittiwat P, Mizoe JE, Hasegawa A, Ishikawa H, Yoshikawa K, Mizuno H, et al. l-[METHYL-(11)C] methionine positron emission tomography for target delineation in malignant gliomas: impact on results of carbon ion radiotherapy. Int J Radiat Oncol Biol Phys. 2008;70:515–22.
42. Matsuo M, Miwa K, Tanaka O, Shinoda J, Nishibori H, Tsuge Y, et al. Impact of [11C]methionine positron emission tomography for target definition of glioblastoma multiforme in radiation therapy planning. Int J Radiat Oncol Biol Phys. 2012;82:83–9.
43. Miwa K, Matsuo M, Ogawa S-I, Shinoda J, Yokoyama K, Yamada J, et al. Re-irradiation of recurrent glioblastoma multiforme using (11)C-methionine PET/CT/MRI image fusion for hypofractionated stereotactic radiotherapy by intensity modulated radiation therapy. Radiat Oncol. 2014;9:181.
44. Kosztyla R, Chan EK, Hsu F, Wilson D, Ma R, Cheung A, et al. High-grade glioma radiation therapy target volumes and patterns of failure obtained from magnetic resonance imaging and 18F-FDOPA positron emission tomography delineations from multiple observers. Int J Radiat Oncol Biol Phys. 2013;87:1100–6.
45. Combs SE, Ganswindt U, Foote RL, Kondziolka D, Tonn JC. State-of-the-art treatment alternatives for base of skull meningiomas: complementing and controversial indications for neurosurgery, stereotactic and robotic based radiosurgery or modern fractionated radiation techniques. Radiat Oncol. 2012;7:226.

46. Lee JW, Kang KW, Park SH, Lee SM, Paeng JC, Chung JK, et al. 18F-FDG PET in the assessment of tumor grade and prediction of tumor recurrence in intracranial meningioma. Eur J Nucl Med Mol Imaging. 2009;36:1574–82.
47. Liu RS, Chang CP, Guo WY, Pan DH, Ho DM, Chang CW, et al. 1-11C-acetate versus 18F-FDG PET in detection of meningioma and monitoring the effect of gamma-knife radiosurgery. J Nucl Med. 2010;51:883–91.
48. Dutour A, Kumar U, Panetta R, Ouafik L, Fina F, Sasi R, et al. Expression of somatostatin receptor subtypes in human brain tumors. Int J Cancer. 1998;76:620–7.
49. Henze M, Schuhmacher J, Hipp P, Kowalski J, Becker DW, Doll J, et al. PET imaging of somatostatin receptors using [68GA]DOTA-D-Phe1-Tyr3-octreotide: first results in patients with meningiomas. J Nucl Med. 2001;42:1053–6.
50. d'Amico A, Stapor-Fudzinska M, Tarnawski R. CyberKnife radiosurgery planning of a secreting pituitary adenoma performed with (6)(8)Ga DOTATATE PET and MRI. Clin Nucl Med. 2014;39:1043–4.
51. Astner ST, Bundschuh RA, Beer AJ, Ziegler SI, Krause BJ, Schwaiger M, et al. Assessment of tumor volumes in skull base glomus tumors using Gluc-Lys[(18)F]-TOCA positron emission tomography. Int J Radiat Oncol Biol Phys. 2009;73:1135–40.
52. Milker-Zabel S, Zabel-du Bois A, Henze M, Huber P, Schulz-Ertner D, Hoess A, et al. Improved target volume definition for fractionated stereotactic radiotherapy in patients with intracranial meningiomas by correlation of CT, MRI, and [^{68}Ga]-DOTATOC-PET. Int J Radiat Oncol Biol Phys. 2006;65:222–7.
53. Gehler B, Paulsen F, Öksüz MÖ, Hauser T-K, Eschmann SM, Bares R, et al. [(68)Ga]-DOTATOC-PET/CT for meningioma IMRT treatment planning. Radiat Oncol. 2009;4:56.
54. Nyuyki F, Plotkin M, Graf R, Michel R, Steffen I, Denecke T, et al. Potential impact of 68Ga-DOTATOC PET/CT on stereotactic radiotherapy planning of meningiomas. Eur J Nucl Med Mol Imaging. 2010;37:310–8.
55. Combs SE, Welzel T, Habermehl D, Rieken S, Dittmar J-O, Kessel K, et al. Prospective evaluation of early treatment outcome in patients with meningiomas treated with particle therapy based on target volume definition with MRI and 68Ga-DOTATOC-PET. Acta Oncol. 2013;52:514–20.
56. Graf R, Nyuyki F, Steffen IG, Michel R, Fahdt D, Wust P, et al. Contribution of ^{68}Ga-DOTATOC PET/CT to target volume delineation of skull base meningiomas treated with stereotactic radiation therapy. Int J Radiat Oncol Biol Phys. 2013;85:68–73.
57. Maclean J, Fersht N, Sullivan K, Kayani I, Bomanji J, Dickson J, et al. Simultaneous (68)Ga DOTATATE positron emission tomography/magnetic resonance imaging in meningioma target contouring: feasibility and impact upon interobserver variability versus positron emission tomography/computed tomography and computed tomography/magnetic resonance imaging. Clin Oncol. 2017;29:448–58.
58. Grosu A-L, Weber WA, Astner ST, Adam M, Krause BJ, Schwaiger M, et al. ^{11}C-methionine PET improves the target volume delineation of meningiomas treated with stereotactic fractionated radiotherapy. Int J Radiat Oncol Biol Phys. 2006;66:339–44.
59. Astner ST, Dobrei-Ciuchendea M, Essler M, Bundschuh RA, Sai H, Schwaiger M, et al. Effect of 11C-methionine-positron emission tomography on gross tumor volume delineation in stereotactic radiotherapy of skull base meningiomas. Int J Radiat Oncol Biol Phys. 2008;72:1161–7.
60. Glaudemans AW, Enting RH, Heesters MA, Dierckx RA, van Rheenen RW, Walenkamp AM, et al. Value of 11C-methionine PET in imaging brain tumours and metastases. Eur J Nucl Med Mol Imaging. 2013;40:615–35.
61. Stober B, Tanase U, Herz M, Seidl C, Schwaiger M, Senekowitsch-Schmidtke R. Differentiation of tumour and inflammation: characterisation of [methyl-3H]methionine (MET) and O-(2-[18F]fluoroethyl)-L-tyrosine (FET) uptake in human tumour and inflammatory cells. Eur J Nucl Med Mol Imaging. 2006;33:932–9.
62. Miwa K, Matsuo M, Shinoda J, Aki T, Yonezawa S, Ito T, et al. Clinical value of [(1)(1)C] methionine PET for stereotactic radiation therapy with intensity modulated radiation therapy to metastatic brain tumors. Int J Radiat Oncol Biol Phys. 2012;84:1139–44.

63. Matsuo M, Miwa K, Shinoda J, Kako N, Nishibori H, Sakurai K, et al. Target definition by C11-methionine-PET for the radiotherapy of brain metastases. Int J Radiat Oncol Biol Phys. 2009;74:714–22.
64. Götz I, Grosu AL. [(18)F]FET-PET imaging for treatment and response monitoring of radiation therapy in malignant glioma patients – a review. Front Oncol. 2013;3:104.
65. Galldiks N, Albert NL, Sommerauer M, Grosu AL, Ganswindt U, Law I, et al. PET imaging in patients with meningioma-report of the RANO/PET Group. Neuro Oncol. 2017;19:1576–87.

Clinical Applications of PET/MRI in Brain Imaging

13

Francesco Fraioli and Karar Obeed Almansory

Contents

13.1 Introduction

Brain imaging is one of the valuable applications of the hybrid PET/MRI given the anatomical and physiological complexity of the brain and the subtlety of the neurological changes that accompany many of the neurodegenerative, epileptic, and oncological diseases. The limited resolution of CT in imaging brain makes the MRI the ideal modality for neuroimaging. This resulted in growing interest in the medical, physics and pharmaceutical communities to develop novel radiopharmaceuticals and apply new MRI sequences for early diagnosis, predicting the behavior and having a better insight of the neurological disorders [1].

Acquisition of the PET/MRI is either done sequentially or simultaneously. Sequential acquisition acquires the MRI and PET data in separated devices either at the same location or at different ones. Specialized softwares combine the data from the two scans to produce PET/MRI fused images [1, 2]. This method is more prone to motion artifacts and misregistration, but can be corrected to some degree

F. Fraioli · K. O. Almansory, MBChB, MRCP, MD (✉)
Institute of Nuclear Medicine, University College London, London, UK
e-mail: karar.almansory@nhs.net

F. Fraioli (ed.), *PET/CT in Brain Disorders*, Clinicians' Guides to Radionuclide Hybrid Imaging, https://doi.org/10.1007/978-3-030-01523-7_13

with motion correction software. The other more advanced way is to use the integrated PET/MRI machine (hybrid). Since its introduction by Siemens, the commercial hybrid PET/MRI machines (molecular MRI, mMR) allowed simultaneous acquisition of the MRI and PET signals in space and time. This was a challenging task due to the MRI magnetic interference with PET components. Although it is not as simple as it sounds, this technical problem was solved by using a ring of magnetic-field insensitive PET detectors inside a 3T MRI gantry [3]. Brain imaging was the first application of the simultaneous PET/MRI given the fact that the brain is less prone to motion artifact [4].

13.2 Application of PET/MRI

13.2.1 Neurodegenerative Diseases

One advantage of PET/MRI over PET/CT is related to the superior/additional anatomical and molecular information that MRI can provide. Hybrid PET/MRI allows simultaneous aquisition and combination of the MRI anatomical and functional information with metabolic one from the PET during the same examination. Higher spatial resolution of the structural MRI sequences allow better morphological definition of the brain parts. This improves the diagnostic ability of the scan and also helps to rule out other pathologies that could attribute to the patient's symptoms. In Alzheimer's disease (AD) medial temporal lobe atrophy, especially in the entorhinal cortex, amygdala, hippocampus, and parahippocampal gyrus, is a characteristic finding. Combining these information with the metabolic data from the FDG-PET (AD metabolic pattern) supports the diagnosis and increases the accuracy of the test (Fig. 13.1). Another example of the synergistic findings between the PET

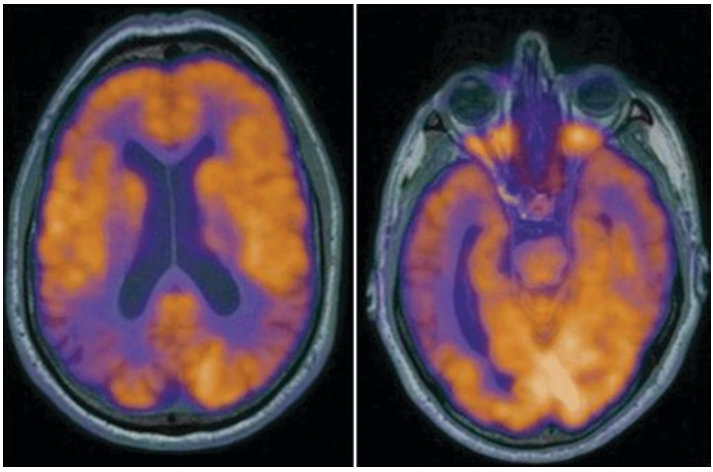

Fig. 13.1 FDG PET/MRI in a patient with early AD demonstrating glucose hypometabolism in the parietal and temporal lobes (right >left)

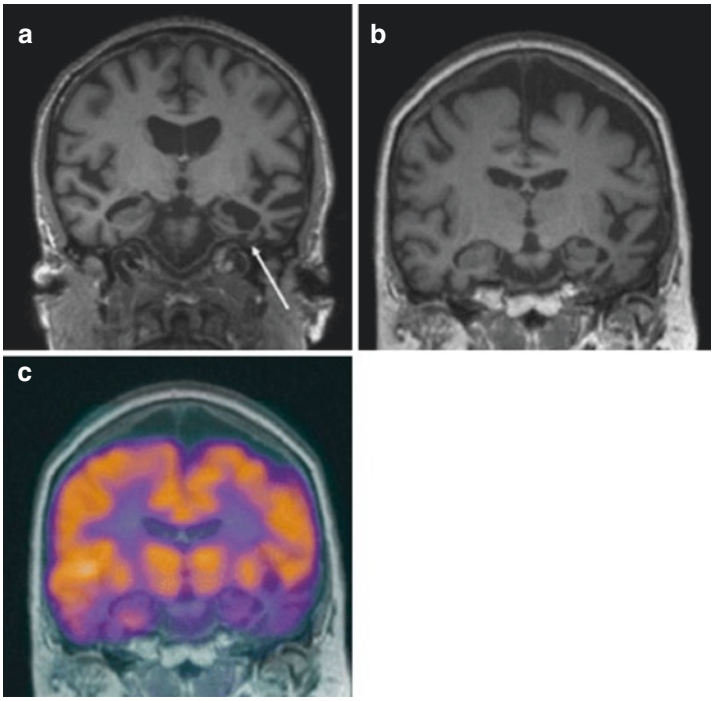

Fig. 13.2 Coronal T1-weighted images (**a** and **b**) and fused FDG-PET/MRI image (**c**) in a patient with sematic variant PPA (semantic dementia). **a** and **b**: marked asymmetrical volume loss is found in the left temporal lobe affecting all temporal gyri and particularly the fusiform gyrus (arrow). **c**: the FDG-PET/MRI demonstrates glucose hypometabolism not only in the left but also in the right temporal lobe, which shows much less atrophy. PPA (primary progressive aphasia)

and the MRI is shown in Fig. 13.2 for a patient with semantic variant primary progressive aphasia (semantic dementia).

Computerized gray and white matter volume assessment in AD is also possible with the MRI by using specialized software such as voxel-based morphometry (VBM) which allows early diagnosis and monitoring of disease progression [5, 6]. Other functional MRI sequences can be utilized to support the finding of the PET scan; Arterial spin labeling (ASL) is one of these sequences. Some studies found a concordance between the reduced regional blood flow in the hippocampus and the hypometabolic pattern on the PET in patient with mild cognitive impairment (MCI) and AD [7]. Other functional imagings are diffusion tensor imaging (DTI) and tractography that can assess white matter integrity and allow better understanding of the disease development and progression [8, 9].

13.2.2 Intracranial Neoplasms

Contrast MRI scan is the gold standard method for diagnosis and assessment of brain tumors [10]. Morphological sequences are essential to achieve the diagnosis

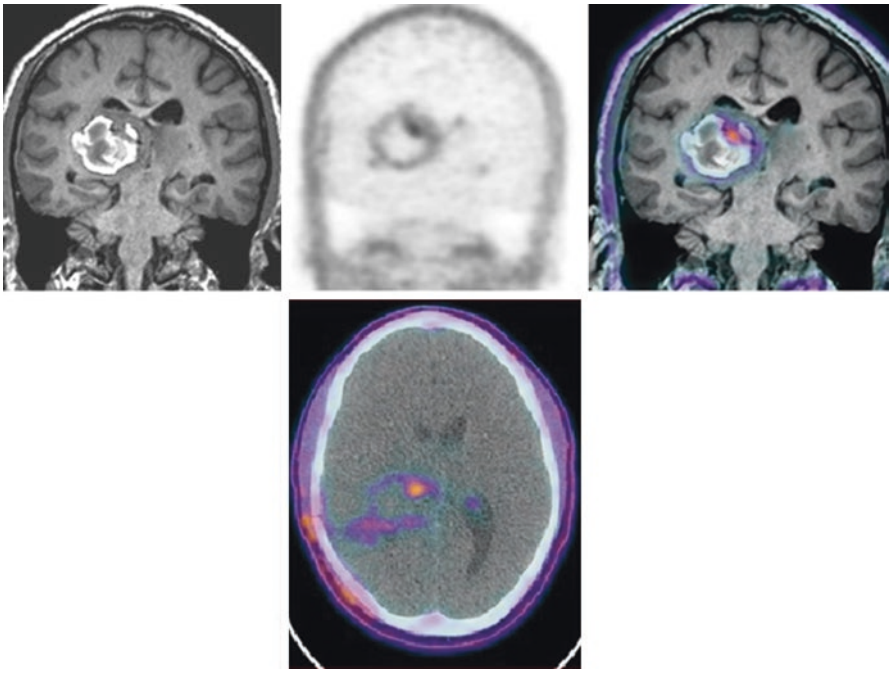

Fig. 13.3 Brain tumor on T1 MRI, ^{18}F choline PET, fused PET/MRI, and PET/CT. Notice the metabolic activity on ^{18}F choline which indicates the most aggressive part of the tumor. The high signal on T1 is because of the hemorrhage after biopsy

(or the differential diagnosis) and assess the extent of the disease and the surrounding cytotoxic edema and to evaluate their pressure effect [10, 11]. Other sequences such as diffusion-weighted images (DWI), perfusion-weighted images (PWI), and gadolinium-enhanced T1-weighted images and MRI spectroscopy (MRS) provide information on the tumor microstructure, blood supply, blood-brain barrier (BBB) disruption and the metabolic microenvironment, respectively [11]. Nevertheless, conventional MRI faces problems especially in differentiating between low and high-grade gliomas and also in post-therapy assessment (differentiating residual/progressive tumour from post-therapy necrosis/pseudo-progression). On gadolinium-enhanced MRI, low-grade gliomas sometimes show enhancement; on the other hand, 10% of glioblastomas and 30% of anaplastic astrocytomas do not show enhancement [1, 12, 13]. Simultaneous PET/MRI using specific tracers, such as ^{18}F-fluorotyrosine, ^{18}F-deoxyphenylalanine, and ^{11}C-Met (which are labeled amino acids (AA) /indicators of AA uptake), or ^{11}C-choline and ^{18}F-choline (which are indicators of cell membrane turnover), allows better spatial distribution of the tracer in the tumor and makes it more feasible to target most aggressive part for sampling (Fig. 13.3) [1]. In one study, ^{11}C-Met PET/MRI identified the most aggressive parts of the tumors which were not always related to the areas of cell membrane proliferation (choline/*N*-acetylaspartate) seen on MRS. This allowed more precise metabolic mapping of the gliomas [14].

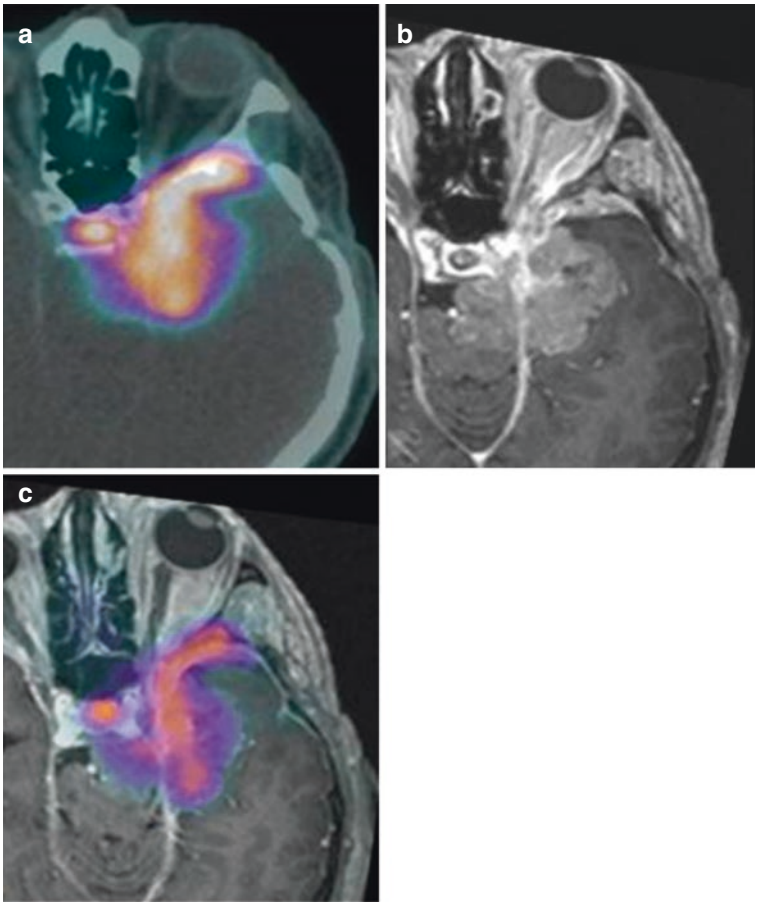

Fig. 13.4 Meningioma with close proximity to the pituitary gland in a patient who is a candidate for radiotherapy. PET/CT (**a**) demonstrates a ^{68}Ga-DODATATE avid lesion in the left middle fossa. The MRI (**b**) shows higher anatomical details. PET/MRI allows visualization the exact extension of the disease. A pituitary sparing field of irradiation was chosen after the precise information provided by PET/MR scan. ^{68}Ga-DODATATE avidity in the pituitary is physiological [1]

Other intracranial benign tumors could impose a serious health problem due to their critical location or proximity to vital parts. Figure 13.4 shows meningioma at the base of the skull with close proximity to the pituitary gland [1].

Simultaneous PET/MRI is more convenient option in oncological patients who are more prone to have multiple functional/anatomical scans, especially in pediatric population, with less ionizing radiation exposure compared to PET/CT. Also, having simultaneous PET/MRI in one set eliminates the need for two separated visits, and in turn improves the workflow, eases patient's stress, and reduces the need for multiple administration of general anesthesia/sedatives in some claustrophobic patients and young children [15].

13.2.3 Epilepsy

In refractory epilepsy, hybrid PET/MRI allows correlation of the superior soft tissue contrast resolution of the MRI with the metabolic information from the FDG-PET, simultaneously in space and time. The discordance between the findings of the two scans is quite common; some of the epileptogenic lesions, such as focal cortical dysplasia (FCD), are visible in the MRI but they may lack the characteristic hypometabolic pattern on the FDG-PET, and vice versa (Fig. 13.5). In one study, around 25% of FCD were not visible on the MRI (especially type I), and also 25% were

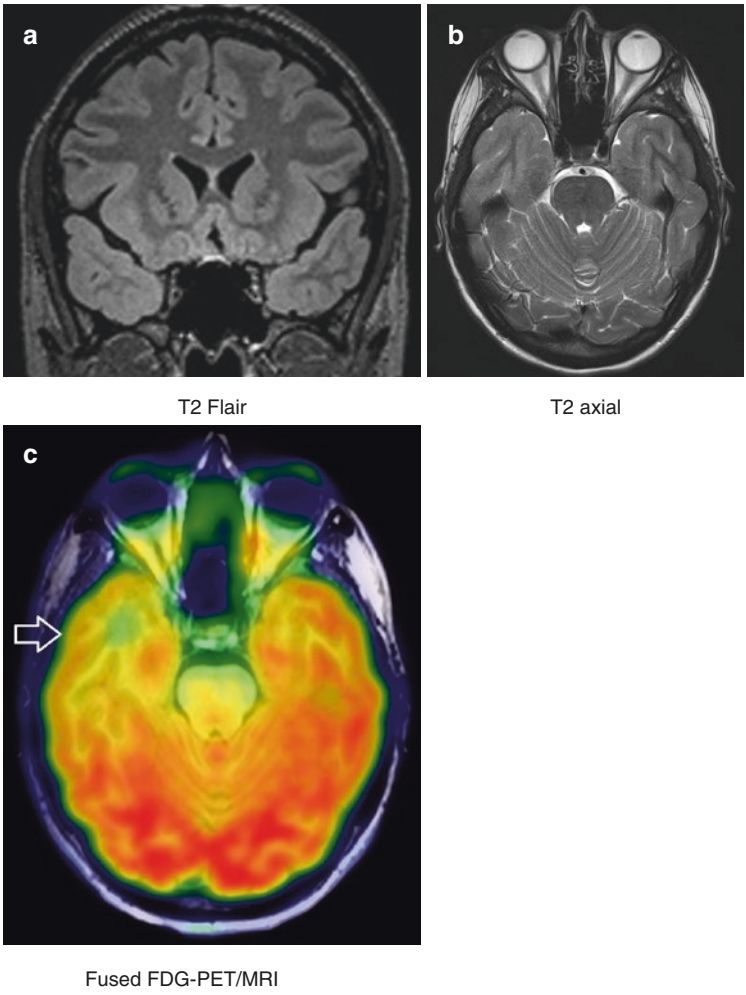

Fig. 13.5 Young patient with complex partial seizure. The T2 flair and T2 axial 3T MRI (**a** and **b**) show normal appearance of both temporal lobes. Fused FDG-PET/MR and coronal and axial FDG-PET (**c**–**e**) identify reduced metabolism in the right temporal lobe (arrows), in keeping with the epileptogenic focus. This is also confirmed by Minoshima maps (**f**) (arrowhead) which identify spreading of the hypometabolism to the inferior surface of the right frontal lobe

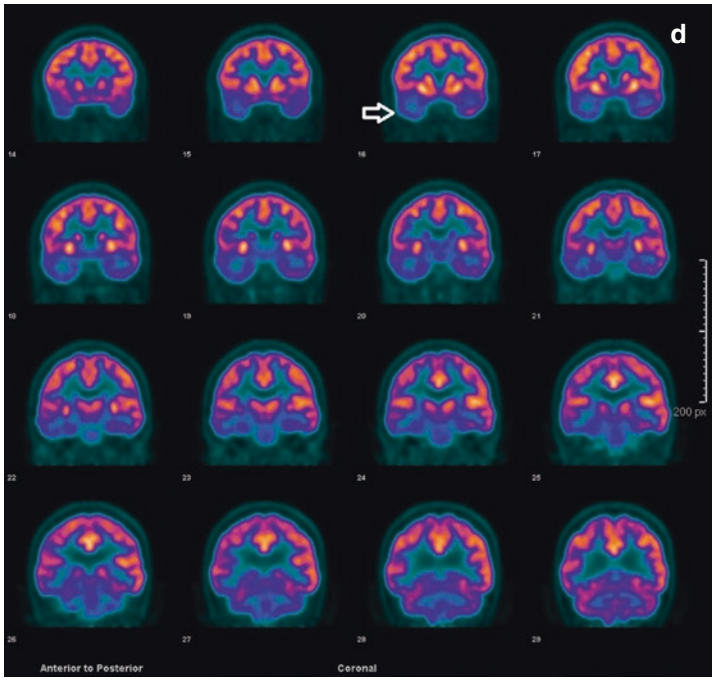

FDG-PET, coronal plane

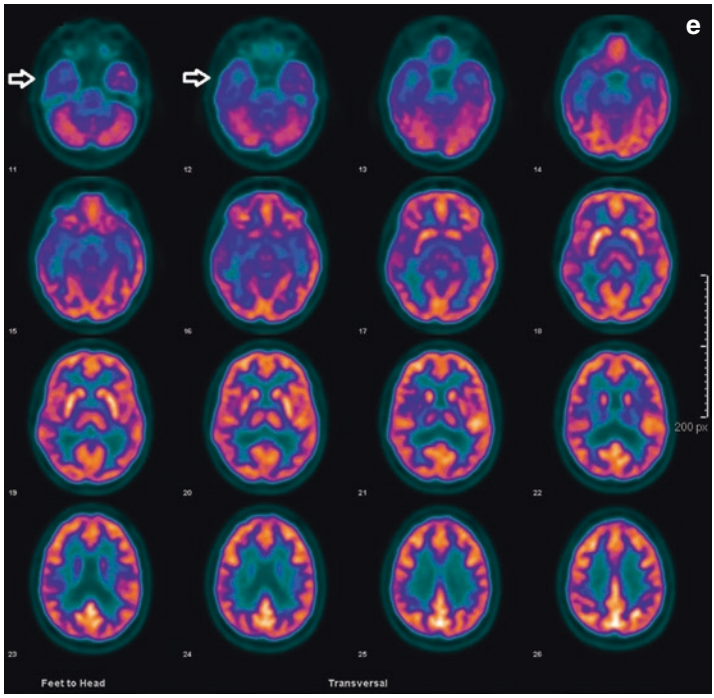

FDG-PET, axial plane

Fig. 13.5 (continued)

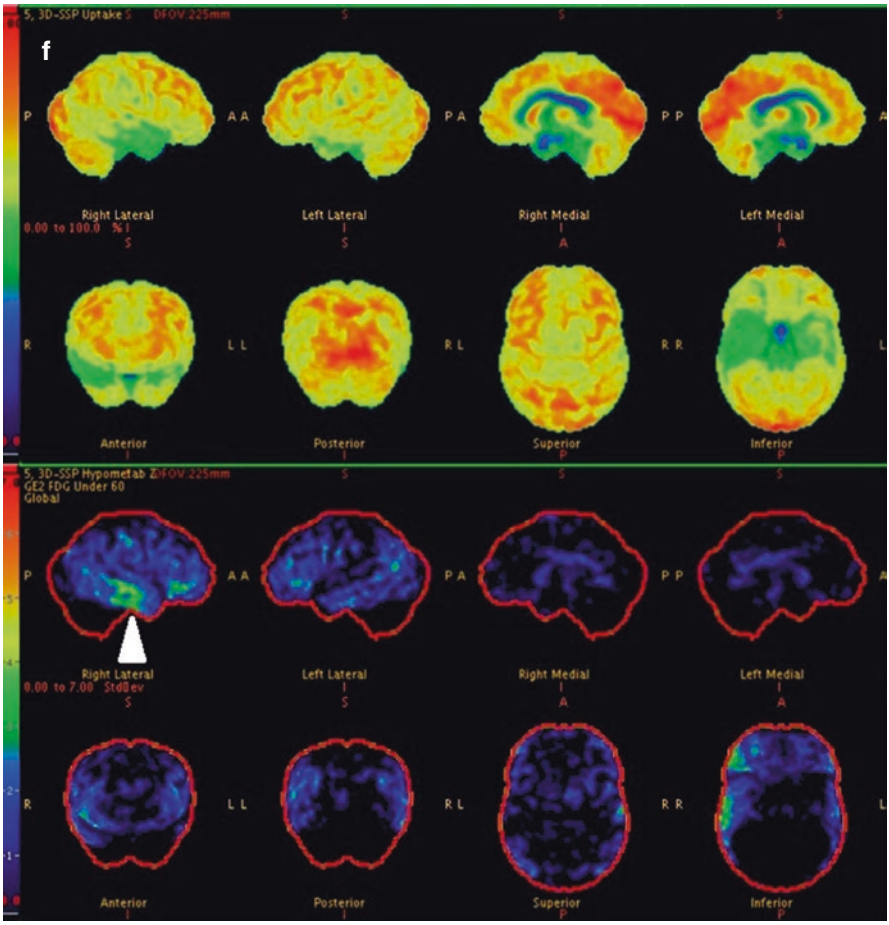

Fig. 13.5 (continued)

negative on the PET scan, and only 11% of the lesions were negative on both scans [16]. This increases the diagnostic yields, as the two scans complement each other, and subsequently improves the presurgical planning of the patients with drug-resistant epilepsy [16, 17].

13.3 Advantages and Disadvantages of the Simultaneous PET/MRI

Simultaneous PET/MRI has many advantages over separated PET and MRI scans or the PET/CT, however, it also comes with some disadvantages. Pros and cons of the simultaneous PET/MRI are summarized in Table 13.1.

Table 13.1 Advantages and disadvantages of the combined PET/MRI

Advantages
• Superior soft tissue contrast resolution of the MRI component provide precise anatomical details. • Other functional and molecular MRI sequences, such as arterial spin labeling (ASL), diffusion tensor imaging (DTI), and MRI spectroscopy, increase the diagnostic potentials of the hybrid scan. • Simultaneous acquisition of the PET and MRI data eliminates the need for two different scans, allowing better workflow and decreasing the patient's stress and the need for repeated general anesthesia administration in claustrophobic patients or young children. • Simultaneous acquisition of the MRI and PET data in space and time allows real-time data analysis and minimizes the chance of misregistration. • Reduces exposure to the ionizing radiation compared to the PET/CT which is more important in patients with repeated scans and in pediatric population.
Disadvantages
• Higher cost: the higher price of the PET/MRI machine is one of the major factors holding its availability. The price of the PET/MRI system is 3–4 times higher than that of PET/CT system [18]. • Longer scanning time: although some MRI-based attenuation correction methods, such as Dixon and HASTE (only 1 s to acquire), allow shorter scanning time, including extra diagnostic sequences eventually prolongs it [3]. • Lack of consensus: PET/MRI is a relatively new technology with limited spead, and this imposes a problem regarding finding standardized protocols and agreements among centers [19].

Key Points

Some of the main advantages and disadvantages of the combined PET/MRI are:

Advantages

- Superior soft tissue contrast resolution of the MRI component provides precise anatomical details.
- Simultaneous acquisition of the PET and MRI data eliminates the need for two different scans, allowing better work ow and decreasing the patient's stress and the need for repeated general anesthesia administration in claustrophobic patients or young children.
- Reduces exposure to the ionizing radiation compared to the PET/CT which is more important in patients with repeated scans and in pediatric population.

Disadvantages

- Higher cost: the higher price of the PET/MRI machine is one of the major factors holding its availability. The price of the PET/MRI system is 3–4 times higher than that of PET/CT system.

- Longer scanning time: although some MRI-based attenuation correction methods, such as Dixon and HASTE, allow shorter scanning time, including extra diagnostic sequences eventually prolongs it.
- Lack of consensus: PET/MRI is a relatively new technology with limited spread, and this imposes a problem regarding standardized protocols and agreements among centers.

References

1. Fraioli F, Punwani S. Clinical and research applications of simultaneous positron emission tomography and MRI. Br J Radiol. 2014;87(1033):20130464.
2. Kalemis A, Delattre BMA, Heinzer S. Sequential whole-body PET/MR scanner: concept, clinical use, and optimisation after two years in the clinic. The manufacturer's perspective. Magn Reson Mater Phys Biol Med. 2013;26(1):5–23.
3. Tudisca C, Nasoodi A, Fraioli F. PET-MRI. Nucl Med Commun. 2015;36(7):666–78.
4. Schwenzer NF, et al. Simultaneous PET/MR imaging in a human brain PET/MR system in 50 patients—current state of image quality. Eur J Radiol. 2012;81(11):3472–8.
5. Hirata Y, et al. Voxel-based morphometry to discriminate early Alzheimer's disease from controls. Neurosci Lett. 2005;382(3):269–74.
6. Guo X, et al. Voxel-based assessment of gray and white matter volumes in Alzheimer's disease. Neurosci Lett. 2010;468(2):146–50.
7. Goubran M, et al. Assessment of PET & ASL metabolism in the hippocampal subfields of MCI and AD using simultaneous PET-MR. EJNMMI Phys. 2015;2(Suppl 1):A73.
8. Oishi K, Mielke MM, Albert M, Lyketsos CG, Mori S. DTI analyses and clinical applications in Alzheimer's disease. J Alzheimers Dis. 2011;26(Suppl 3):287–96.
9. Prasad G, Nir TM, Toga AW, Thompson PM. Tractography density and network measures in Alzheimer's disease. In: 2013 IEEE 10th International Symposium on Biomedical Imaging, vol. 2013; 2013. p. 692–5.
10. Heiss W-D, Raab P, Lanfermann H. Multimodality assessment of brain tumors and tumor recurrence. J Nucl Med. 2011;52(10):1585–600.
11. Rees JH. Diagnosis and treatment in neuro-oncology: an oncological perspective. Br J Radiol. 2011;84(Spec Iss 2):S82–9.
12. Knopp EA, et al. Glial neoplasms: dynamic contrast-enhanced T2*-weighted MR imaging. Radiology. 1999;211(3):791–8.
13. Scott JN, Brasher PMA, Sevick RJ, Rewcastle NB, Forsyth PA. How often are nonenhancing supratentorial gliomas malignant? A population study. Neurology. 2002;59(6):947–9.
14. Bisdas S, et al. Metabolic mapping of gliomas using hybrid MR-PET imaging. Investig Radiol. 2013;48(5):295–301.
15. Bisdas S, lá Fougere C, Ernemann U. Hybrid MR-PET in neuroimaging. Clin Neuroradiol. 2015;25:275–81.
16. Halac G, et al. Compatibility of MRI and FDG-PET findings with histopathological results in patients with focal cortical dysplasia. Seizure. 2017;45:80–6.
17. Shin HW, et al. Initial experience in hybrid PET-MRI for evaluation of refractory focal onset epilepsy. Seizure. 2015;31:1–4.
18. Ward BP. Arab Health: is PET/MRI really worth the extra cost? AuntMinnie Europe; 2013. p. 28–29.
19. Bailey DL, et al. Combined PET/MR: the real work has just started. Summary Report of the Third International Workshop on PET/MR Imaging; February 17–21, 2014, Tübingen, Germany. Mol Imaging Biol. 2015;17(3):297–312.

Clinical Atlas of Brain PET/CT

14

Khulood Al Riyami and Francesco Fraioli

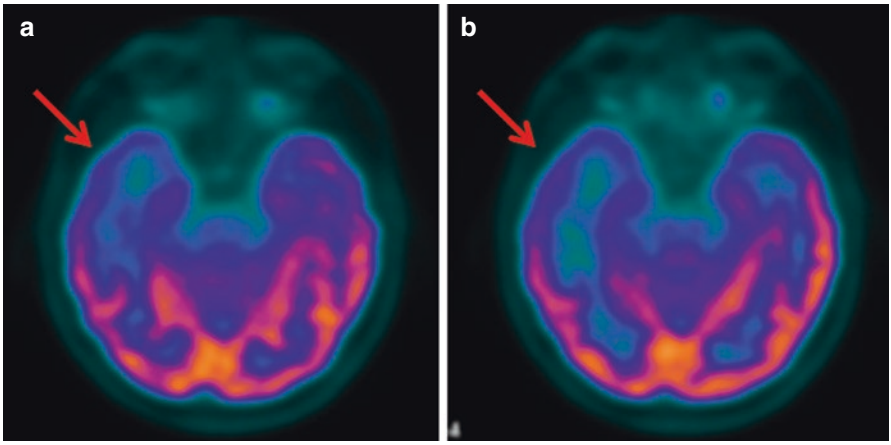

Fig. 14.1 (**a**–**d**) A 30-year-old patient with non-lesional right frontotemporal lobe epilepsy. Axial ^{18}F FDG PET (**a**, **b**) and fused ^{18}F FDG PET/MR (**c**, **d**) show perfect agreement between the two techniques with area of hypometabolism in the right temporal lobe (**a**–**d**, *arrows*) representing an epileptogenic focus.
Teaching point: Alteration in FDG metabolism can help determine epileptogenic foci in patients with non-lesional epilepsy

K. Al Riyami (✉)
Institute of Nuclear Medicine, University College of London Hospital, London, UK
e-mail: khulood.alriyami@nhs.net

F. Fraioli
Institute of Nuclear Medicine, University College London, London, UK

F. Fraioli (ed.), *PET/CT in Brain Disorders*, Clinicians' Guides to Radionuclide Hybrid Imaging, https://doi.org/10.1007/978-3-030-01523-7_14

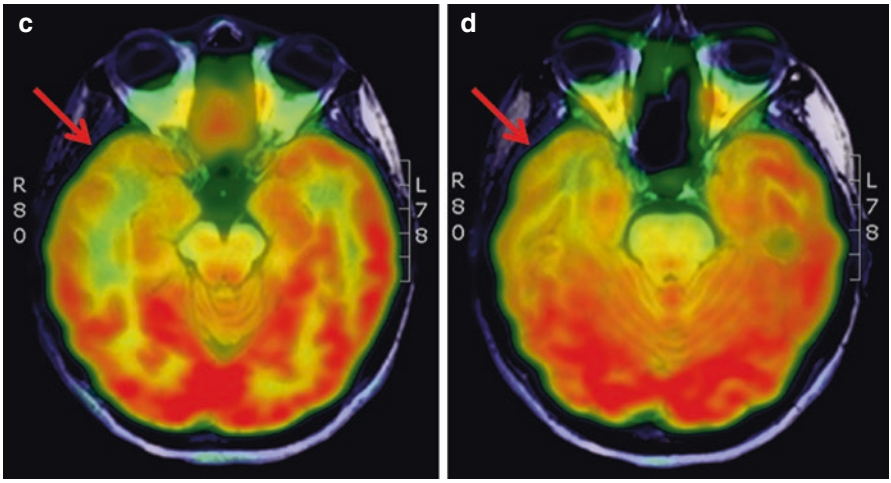

Fig. 14.1 (continued)

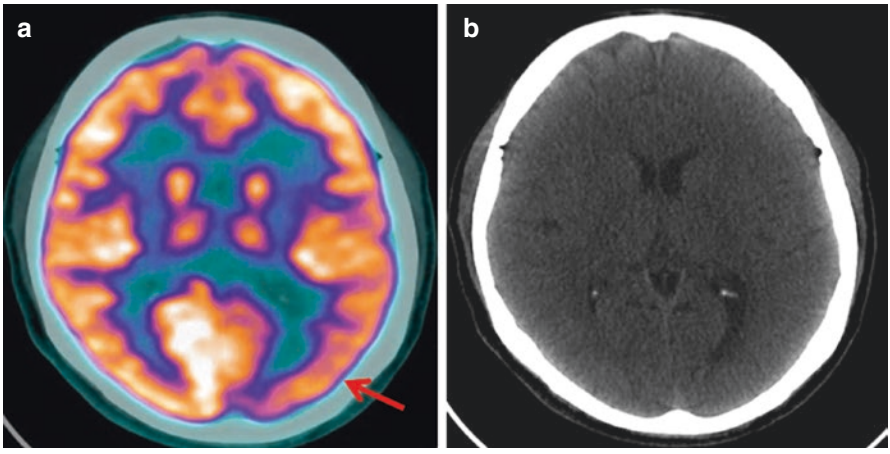

Fig. 14.2 (**a**–**d**) A 31-year-old patient with left hemisphere epilepsy. Axial fused ^{18}F FDG PET/CT (**a**), axial CT (**b**), fused ^{18}F FDG PET/MR (**c**) and T2 FLAIR (**d**) at the level of the thalami show area of hypometabolism in the left occipitotemporal region (**a**, **c** *arrows*) with corresponding high signal intensity in the periventricular region of the posterior horn of the left lateral ventricle (**d**, *arrow*) raising the suspicion of previous encephalitis.
Teaching point: Combined FDG PET/MR can assist in diagnosing location of epileptogenic focus and correlative morphological changes to determine possible underlying cause

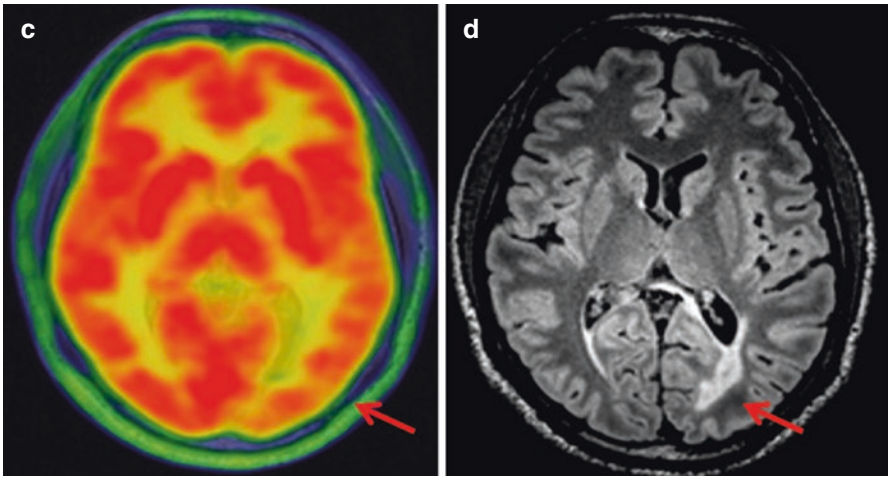

Fig. 14.2 (continued)

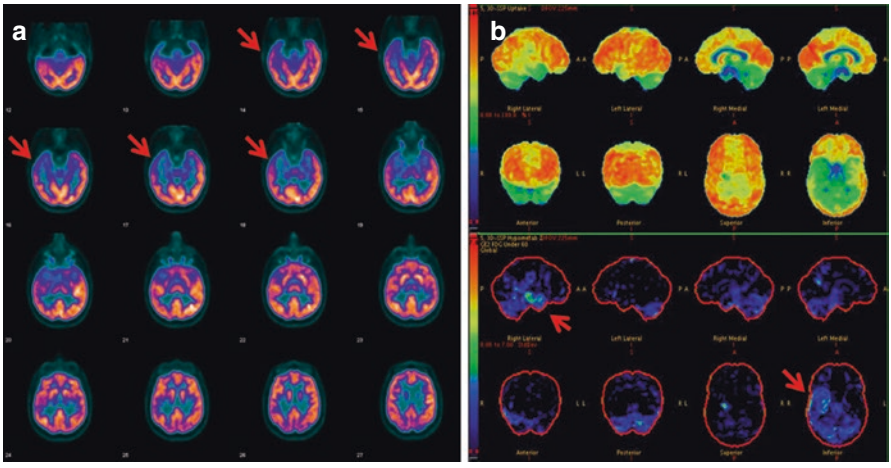

Fig. 14.3 (**a**, **b**) Patient evaluated for right hemispheric epilepsy. Axial FDG PET images (**a**) and *Z*-score maps (**b**) show right temporal lobe hypometabolism (**a**, *arrows*) which is confirmed on quantification assessment (**b**, *arrows*), in keeping with an epileptogenic focus.
Teaching point: The use of quantification maps can help in giving a more confident diagnosis when determining the most likely epileptogenic focus in patients with epilepsy

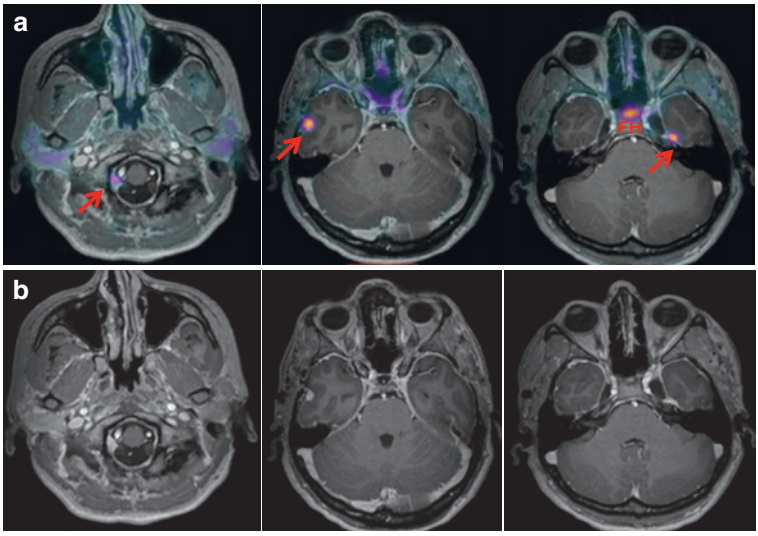

Fig. 14.4 (**a**, **b**) Fused 68Ga DOTATATE PET/MR (**a**) and axial post-contrast T1WI (**b**) show tracer-avid extra-axial lesions in the right side of the foramen magnum, right temporal lobe laterally and left temporal lobe medially (**a**, *arrows*). The focal hyper intensity adjacent to the clivus bone is the normal tracer uptake in the pituitary gland (**a**, FH). These correspond to small enhancing meningeal lesions (**b**), in keeping with multiple meningiomas.
Teaching point: Meningiomas may be considerably small-sized, and osseous structures (e.g. skull base) may hamper the diagnosis. ^{68}Ga DOTATATE is a tracer selective for the evaluation of somatostatin receptors which are rich in different tumours, such as neuroendocrine, meningioma and paraganglioma

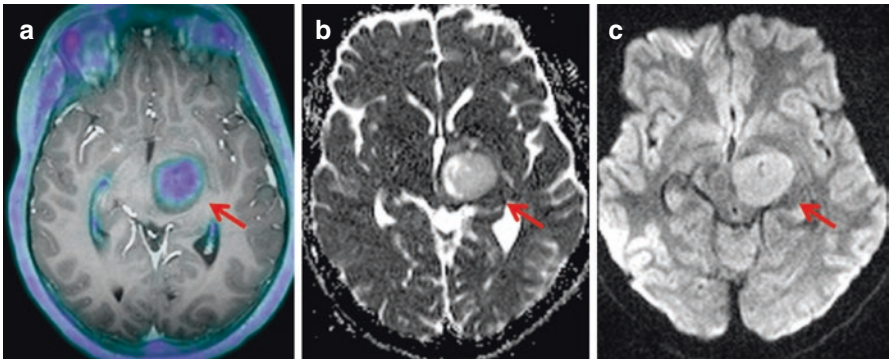

Fig. 14.5 (**a**–**c**) Axial fused ^{18}FCholine PET/MR (**a**), ADC map (**b**) and DWI (**c**) show an ^{18}FCholine avid lesion in the left thalamus (**a**, *arrow*), with corresponding restricted diffusion on the diffusion-weighted images (**b**, **c** *arrows*).
Teaching point: The use of multiparametric evaluation can help identify different components of the tumour including metabolism and cellularity

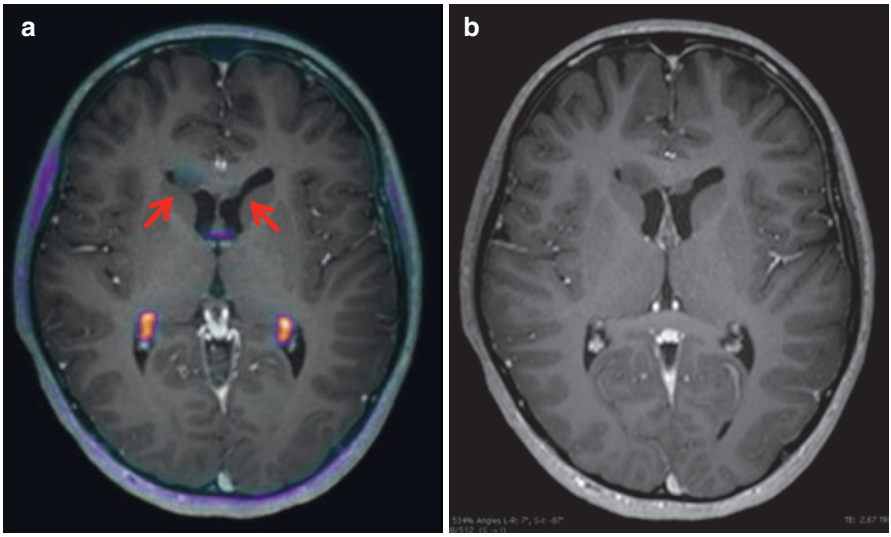

Fig. 14.6 (**a**, **b**) Axial fused ^{18}FCholine PET/MR (**a**) and axial post-contrast T1WI (**b**) show mildly avid subependymal lesions with partial intraventricular extension in the anterior horn of the lateral ventricle bilaterally (**a**, *arrows*) which correspond to non-enhancing small hypointense lesions (**b**).
Teaching point: Non-enhancing lesions can still present with uptake on ^{18}FCholine imaging and might be useful for treatment evaluation

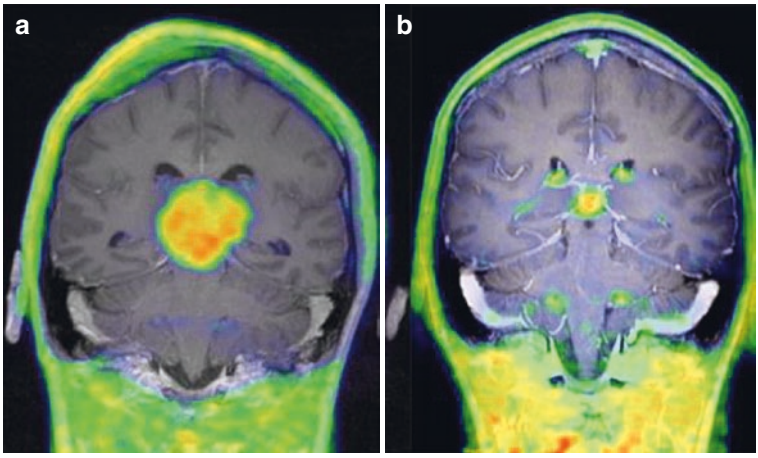

Fig. 14.7 (**a**, **b**) Coronal fused ^{18}FCholine PET/MR (**a**, **b**) show a large ^{18}FCholine avid non-germinomatous germ cell pineal body tumour prior to treatment (**a**) which shows interval reduction in size and tracer uptake post-treatment (**b**), in keeping with partial metabolic response.
Teaching point: The importance of having appropriate metabolic imaging prior to treatment as a baseline can help with better post-treatment assessment

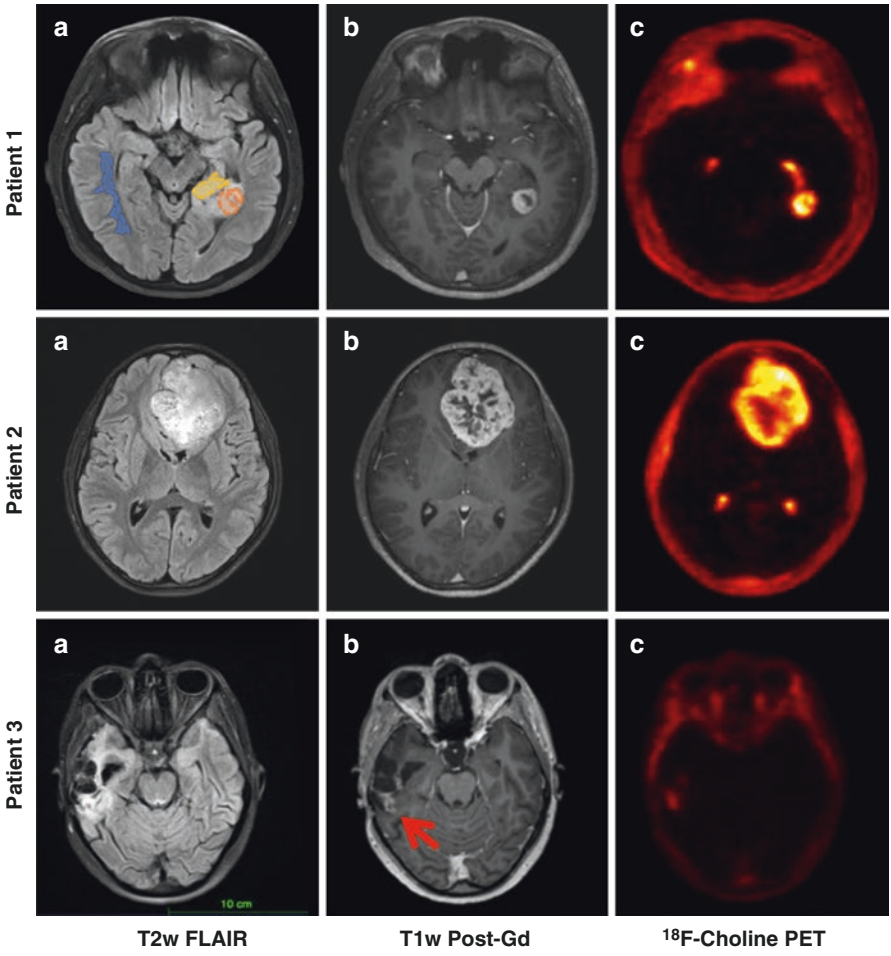

Fig. 14.8 Axial T2W FLAIR (**a**), axial post-contrast T1WI (**b**) and axial ^{18}FCholine PET (**c**) in Patients 1–3
Patient 1: A 17-year-old patient with grade I pilocytic astrocytoma demonstrates normal appearing 'white matter' ROI (blue), 'non-enhancing' tumour ROI (yellow) and 'enhancing' tumour ROI (pink) (**a**), enhancing tumour (**b**) with increased ^{18}FCholine uptake in the enhancing component (**c**)
Patient 2: An 18-year-old patient with grade I schwannoma demonstrates a high-intensity left frontal lobe mass (**a**), which shows peripheral enhancement with central non-enhancing area (**b**) which corresponds to increased ^{18}FCholine uptake in the enhancing component (**c**)
*Patient 3***:** A 21-year-old patient with grade IV glioblastoma (GBM) demonstrates high signal in the right temporal lobe with areas of susceptibility artefacts (**a**), which shows minimal enhancement at its posterior-lateral component (**b**, *arrow*) that corresponds to mildly increased ^{18}FCholine uptake.
Teaching point: The use of multiparametric evaluation can help identify different components of the tumour and possible sites for treatment targeting

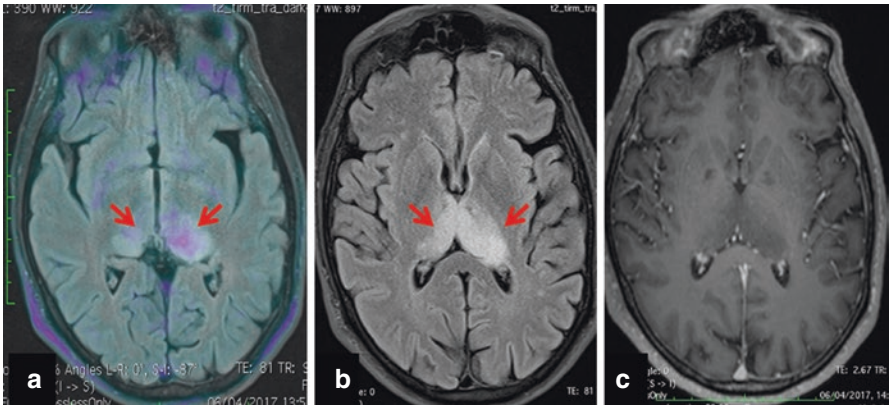

Fig. 14.9 (**a**–**c**) Axial fused ^{18}F DOPA PET/MR (**a**), axial T2W FLAIR (**b**) and axial post-contrast T1WI (**c**) show bilateral increased ^{18}F DOPA tracer uptake in the thalami (left > right) (**a**, *arrows*) with corresponding high-signal changes (**b**, *arrows*) and no significant enhancement on the post-contrast image (**c**). The left thalamic lesion was proven upon biopsy to be a low-grade tumour with transformation into high-grade glioma.
Teaching point: ^{18}F DOPA tracer uptake can detect early transformation of gliomas and impact treatment decision

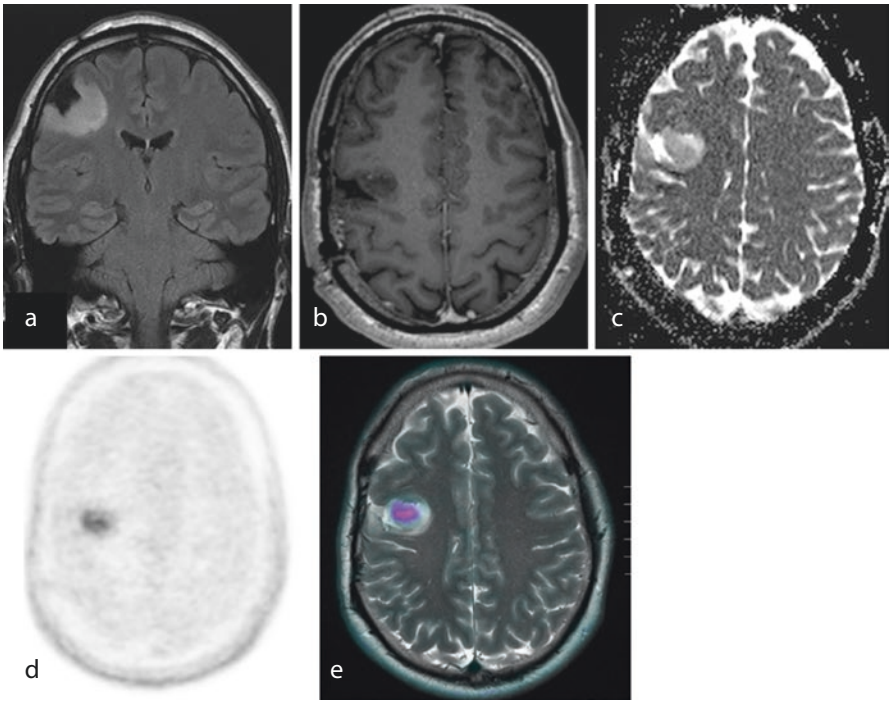

Fig. 14.10 (**a**–**d**) Coronal T2W FLAIR (**a**), axial post-contrast T1WI (**b**), axial ADC map (**c**), axial ^{18}F DOPA PET (**d**) and axial fused ^{18}F DOPA PET/MR (**e**) demonstrate a high-signal, non-enhancing area in the right frontal lobe (**a**, **b**) with diffusion restriction (**c**) in a patient previously operated for a high-grade glioma tumour in the right frontal lobe with similar stable postoperative MR appearances compared to prior postoperative imaging over the last 4 years. However, further imaging with ^{18}F DOPA shows increased tracer uptake in the right frontal lobe tumour (**d**, **e**), consistent with active residual disease. The patient had further treatment 2 weeks later which demonstrated active tumour which was completely removed.
Teaching point: Functional imaging can detect residual disease in otherwise morphologically stable changes in postoperative brain tumours

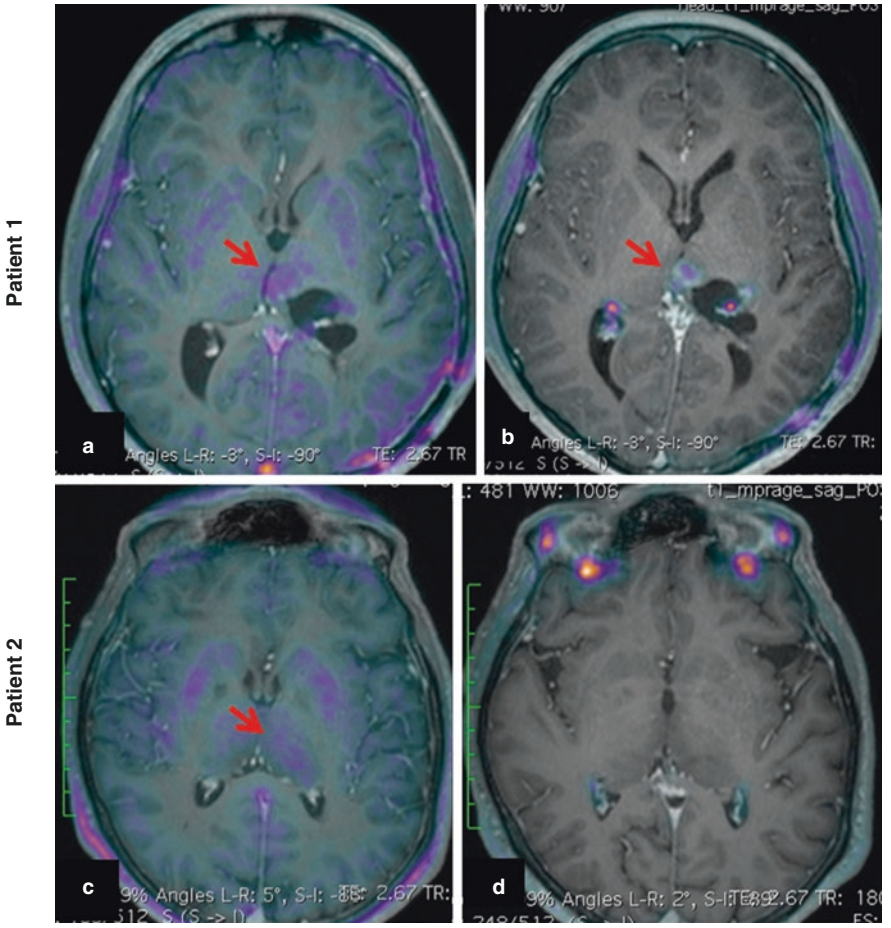

Fig. 14.11 (**a**–**d**) Axial fused ^{18}F DOPA PET/MR (**a**, **c**) and axial fused ^{18}FCholine PET/MR (**b**, **d**) in Patients 1 and 2. *Patient 1:* Biopsy-proven WHO grade IV left thalamic GBM demonstrates increased ^{18}F DOPA and ^{18}FCholine tracer uptake in the left thalamic lesion (**a**, **b**, arrows). *Patient 2:* Biopsy-proven WHO grade II left thalamic glioma with feature of transformation to grade III shows increased ^{18}F DOPA tracer uptake in the left thalamus (**c**, *arrow*) but no corresponding ^{18}FCholine tracer uptake (**d**).

Teaching point: The evaluation of brain lesions with different tracers can give an insight of various components within the tumour which help in assessing tumour grade and further impact management decision

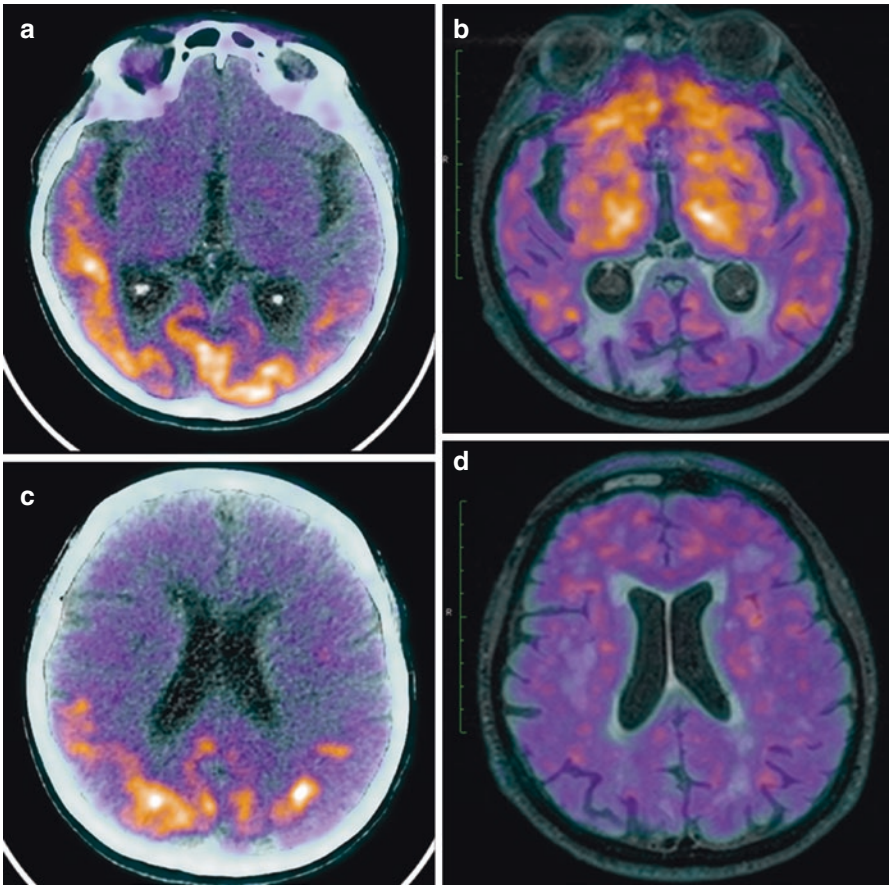

Fig. 14.12 (**a**–**d**) Axial fused Tau tracer PET/CT (**a**, **c**) and axial fused amyloid PET/MR (**c**, **d**) in the same patient imaged 2 weeks apart demonstrated increased Tau tracer uptake in the posterior parietal and occipital regions of the brain cortex (**a**, **c**) with amyloid PET showing completely different regions of amyloid deposition in the frontal lobes (**d**).
Teaching point: Tau and amyloid tracers can show different patterns of tracer distribution in the same patient. This may aid in the understanding of the different mechanisms in the degenerative changes occurring in patients presenting with dementia-like features

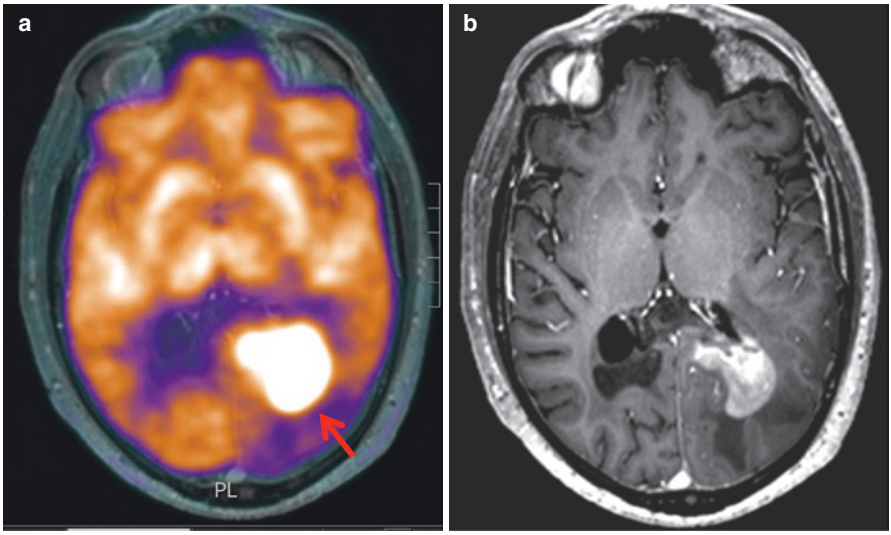

Fig. 14.13 (**a**, **b**) Axial fused ^{18}F-FDG PET/MR (**a**) and post-contrast T1WI (**b**) demonstrate intense increased FDG uptake in the periventricular region of the posterior horn of the left lateral ventricle (**a**, *arrow*) which corresponds to an enhancing lesion on the post-contrast MR (**b**), in a patient with CNS lymphoma.
Teaching point: Intense uptake on FDG can differentiate between CNS lymphoma and primary brain tumours like GBM which usually show less FDG uptake

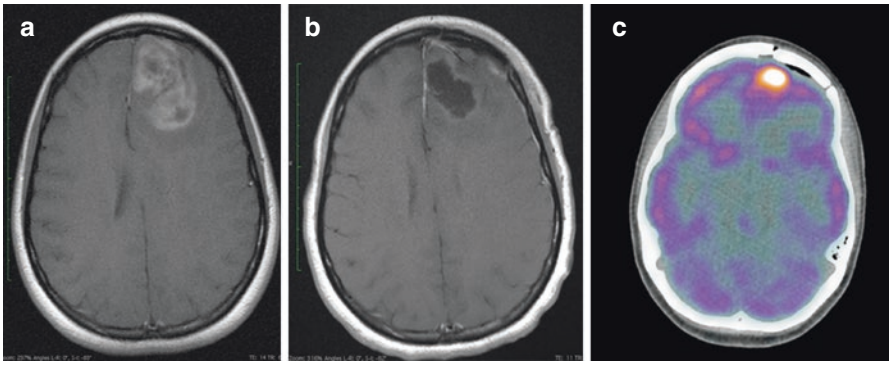

Fig. 14.14 (**a**–**c**) Axial post-contrast T1WI (**a**, **b**) and axial fused ^{18}F-FDG PET/CT (**c**) demonstrated an enhancing left frontal lobe mass in a patient diagnosed with GBM (**a**). Follow-up postoperative MR imaging shows postoperative changes in the left frontal lobe with no convincing enhancement of residual tumour (**b**). Additional functional imaging with ^{18}F-FDG PET/CT shows an avid focus in the left frontal lobe (**c**) which is consistent with active residual disease.
Teaching point: Functional imaging can determine the presence of residual disease in postoperative patients with unremarkable postoperative morphological imaging

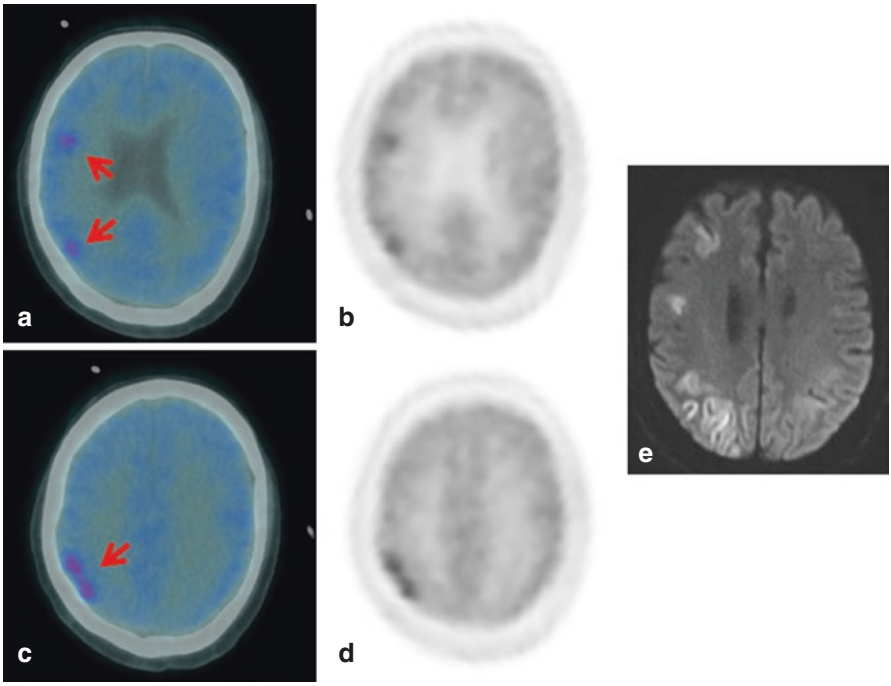

Fig. 14.15 (**a**–**e**) A 64-year-old patient with background AL amyloidosis treated with chemotherapy, presenting with widespread myoclonus, confusion, seizures and reduced consciousness. Axial fused ^{18}F FDG PET/CT (**a**, **c**), axial PET (**b**, **d**) and DWI image (**e**) show focal increased cortical uptake in right frontal and right parietal lobes (**a**–**d**, *arrows*), which correspond to areas of restricted diffusion on MRI (**e**), raising possible vasculitis secondary to cerebral amyloid angiopathy.
Teaching point: Visualization of vascular wall uptake in small vessel vasculitis is beyond the resolution of PET, however indirect signs can be demonstrated by the presence of abnormal cortical tracer uptake in the corresponding vascular territory. Furthermore, multiparametric imaging is required in assessing these challenging cases

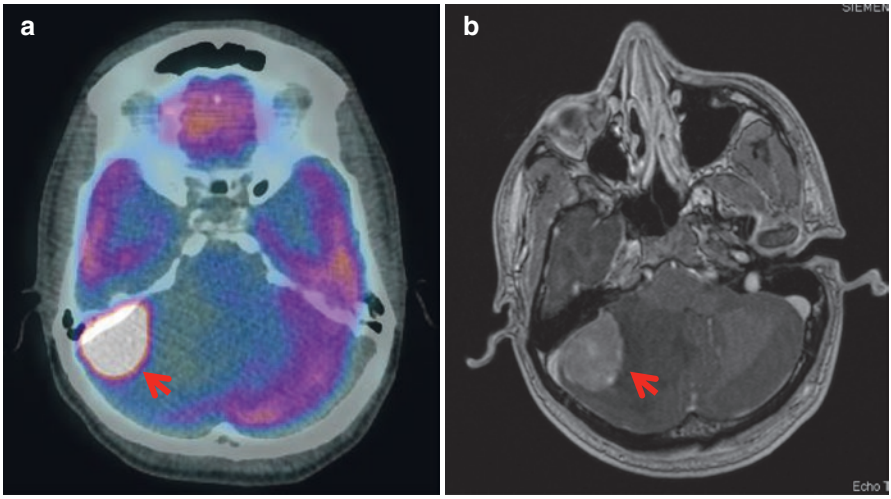

Fig. 14.16 (**a**, **b**) Patient with previous lymphoma completed chemotherapy 2 months ago and presented with cerebellar signs, and MRI showed a right cerebellar mass. Axial fused ^{18}F FDG PET/CT (**a**) and post-contrast T1WI (**b**) show intensely avid right cerebellar lesion (**a**, *arrow*) corresponding to the enhancing lesion (**b**, *arrow*), in keeping with relapsed CNS lymphoma.
Teaching point: Given the usual intense ^{18}F FDG uptake in lymphoma, evaluation of areas with usually high metabolic activity like the brain is possible, and evaluation with FDG PET/CT is particularly useful in assessing disease relapse in patients with prior history of lymphoma

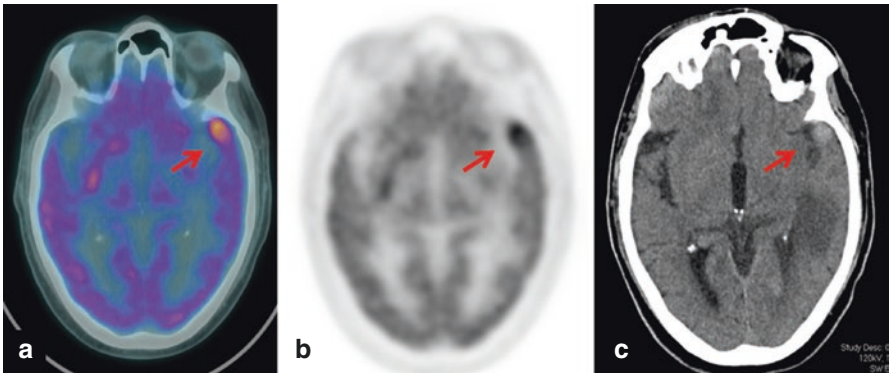

Fig. 14.17 (**a**–**c**) Axial fused ^{18}F FDG PET/CT (**a**), axial ^{18}F FDG PET (**b**) and noncontrast CT (**c**) show a FDG-avid lesion in the left temporal lobe (**a**, **b** *arrows*) which corresponds to a hyperdense lesion on subsequent CT (**c**, *arrow*) in a patient who underwent PET/CT for lung cancer staging, in keeping with brain metastasis.
Teaching point: Including the brain in the whole-body PET/CT imaging can sometimes detect metastatic brain lesions and is advised to be routinely done in cases with suspected malignancies that have or are likely to have brain metastasis

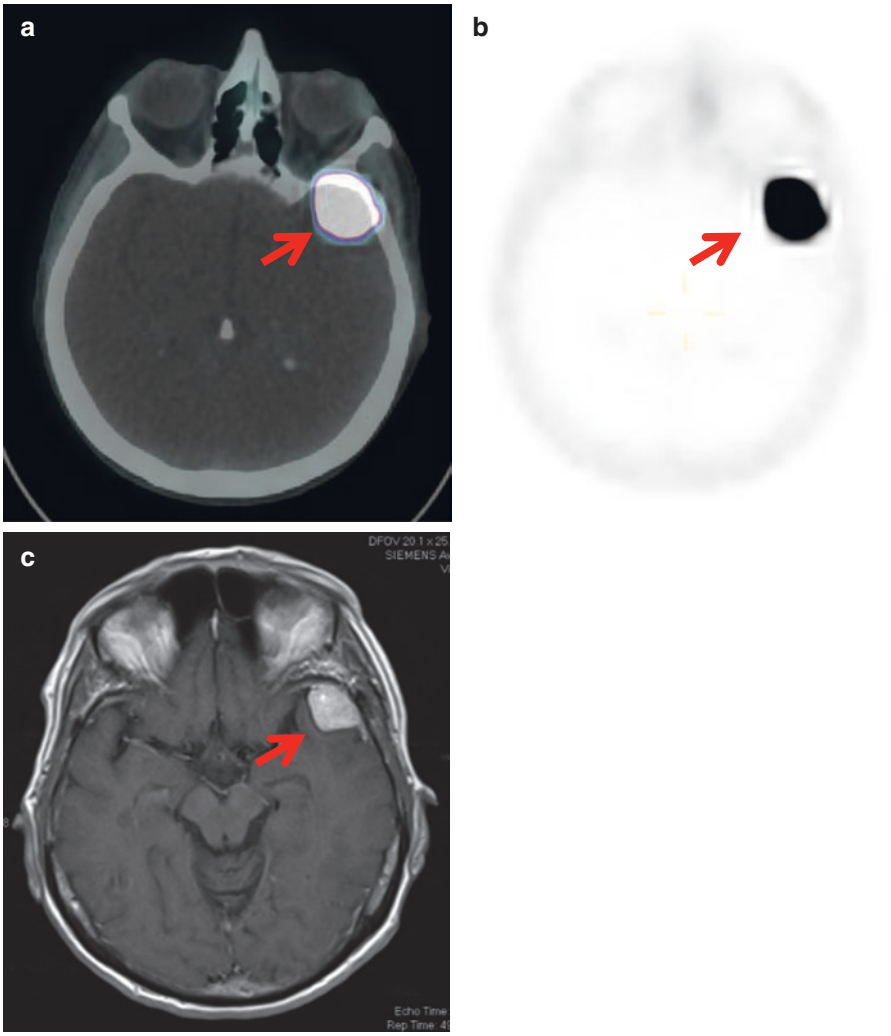

Fig. 14.18 (**a**–**c**) Axial fused ^{68}Ga DOTATATE PET/CT(**a**), axial ^{68}Ga DOTATATE PET (**b**) and contrast-enhanced T1WI MRI (**c**) show ^{68}Ga DOTATATE intensely avid left temporal fossa lesion (**a**, **b** arrows) corresponding to an enhancing left temporal extra-axial lesion on MRI (**c**, arrow) in which the differential included dural-based metastasis and meningioma. The reminder of the^{68}Ga DOTATATE PET/CT did not show uptake elsewhere, and findings were keeping with a meningioma.

Teaching point: Imaging with ^{68}Ga DOTATATE PET can help narrow down the differential diagnosis due to the positive uptake in lesions with somatostatin receptors, e.g. meningiomas or other neuroendocrine tumours

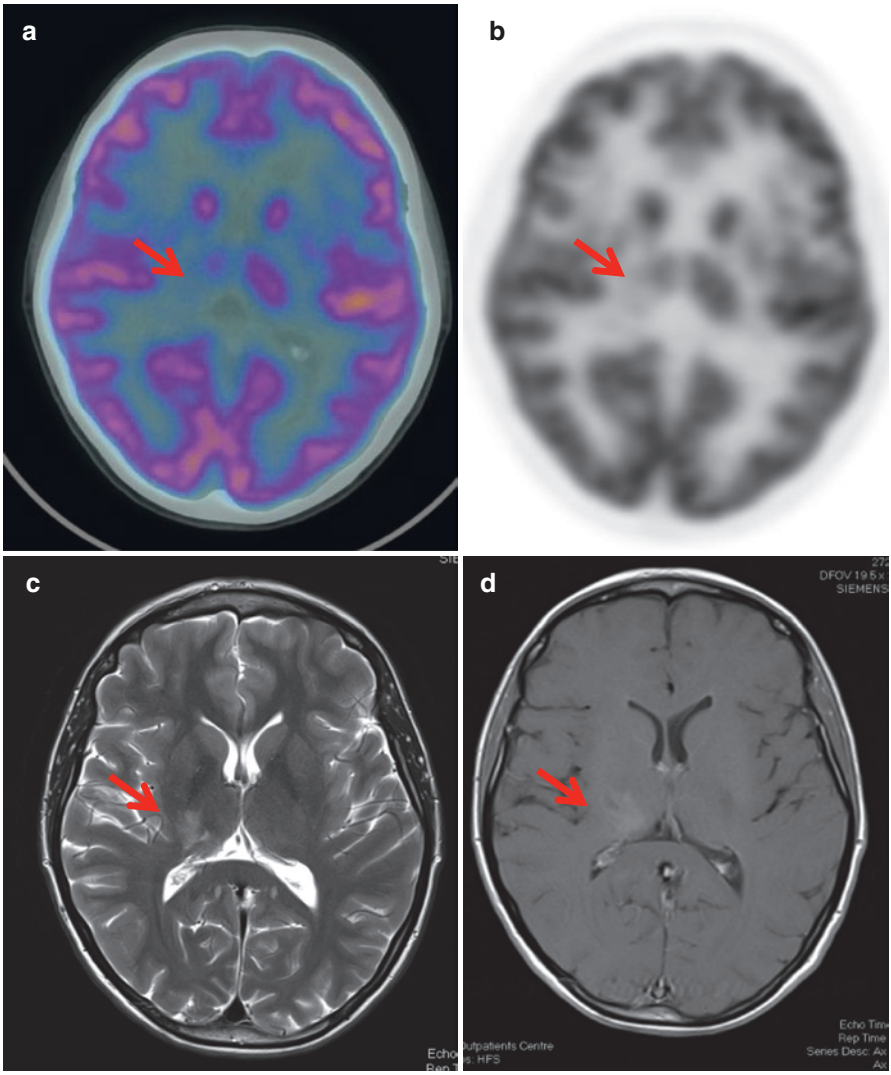

Fig. 14.19 (**a**–**d**) Axial fused ^{18}F FDG PET/CT (**a**), axial ^{18}F FDG PET (**b**), axial T2WI (**c**) and post-contrast T1WI (**d**) show area of focal reduction of tracer uptake in the right thalamus (**a**, **b**, *arrows*) which correspond to an area of high T2 signal and mild enhancement on MRI (**c**, **d** *arrows*) in a patient with multiple sclerosis.
Teaching point: Brain lesions can present as areas of reduced tracer uptake which may be missed, and comparison between both hemispheres is key

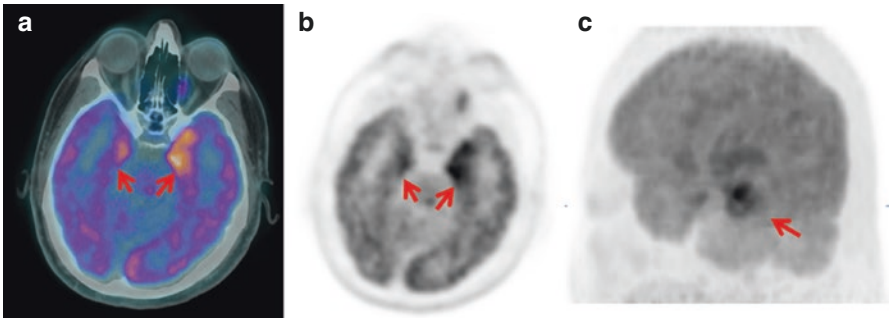

Fig. 14.20 (**a**–**c**) Axial fused ^{18}F FDG PET/CT (**a**), axial ^{18}F FDG PET (**b**) and 3D MIP (**c**) in a patient with worsening left arm, leg weakness and ataxia show increased tracer uptake in the medial temporal lobes, much more marked on the left side (**a**–**c**, *arrows*). These appearances can be seen in limbic encephalitis.
Teaching point: Recognizing uptake patterns in certain conditions can help aid in the diagnosis

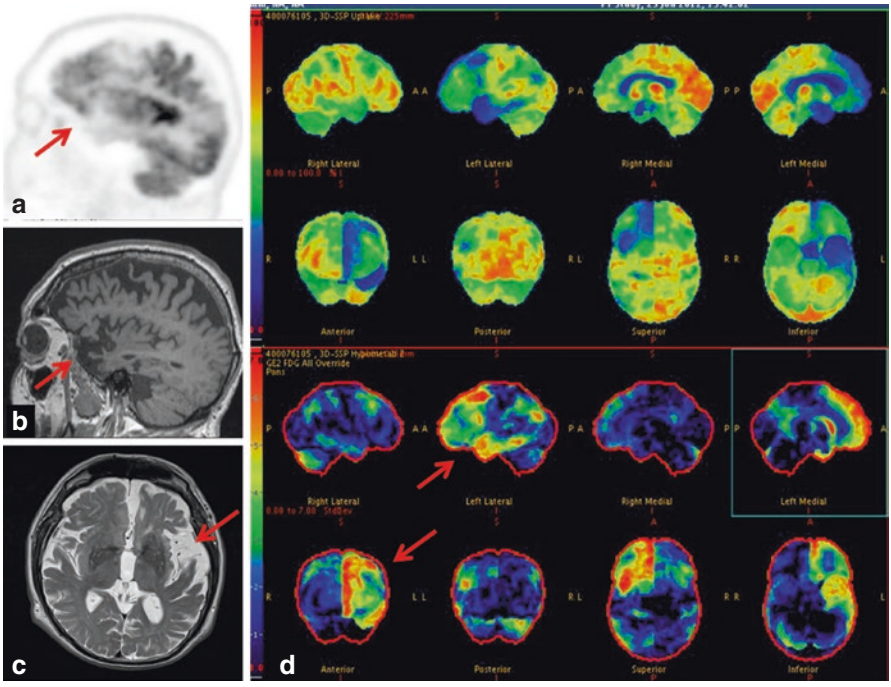

Fig. 14.21 (**a**–**d**) Sagittal ^{18}F FDG PET (**a**), sagittal T1WI (**b**), axial T2WI (**c**) and *Z*-score maps (**d**) show reduced FDG uptake in the left frontotemporal lobe (**a**, *arrow*) corresponding to cerebral atrophy on MRI (**b**, **c** *arrows*) and confirmed on quantification assessment (**d**, *arrows*), in keeping with frontotemporal dementia.
Teaching point: Multimodality imaging can help recognize different patterns of dementia

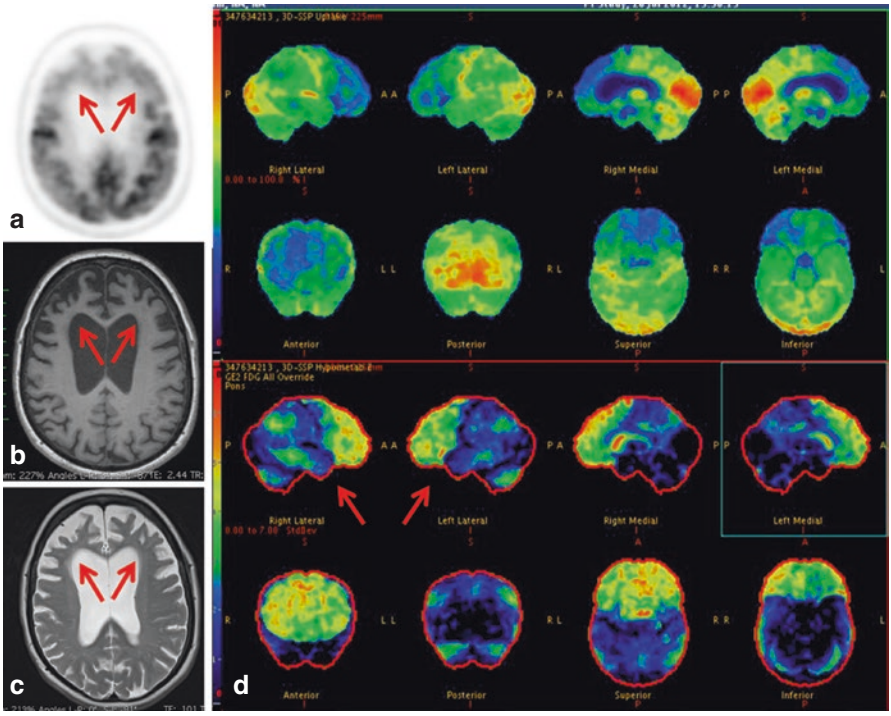

Fig. 14.22 (**a**–**d**) Axial ^{18}F FDG PET (**a**), axial T1WI (**b**), axial T2WI (**c**) and *Z*-score maps (**d**) show reduced FDG uptake in the frontotemporal lobes bilaterally more pronounced in the frontal lobes (**a**, *arrows*) corresponding to cerebral atrophy on MRI (**b**, **c** *arrows*) and confirmed on quantification assessment (**d**, *arrows*), in keeping with frontotemporal dementia.
Teaching point: Multimodality imaging can help recognize different patterns of dementia

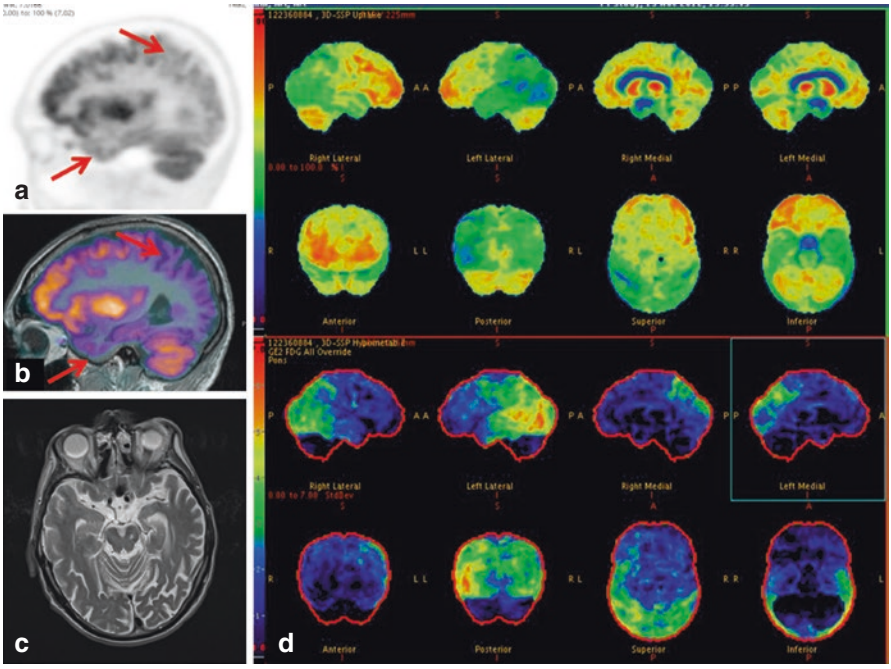

Fig. 14.23 (**a**–**d**) Sagittal ^{18}F FDG PET (**a**), sagittal fused ^{18}F FDG PET/MR (**b**), axial T2WI (**c**) and *Z*-score maps (**d**) show reduced FDG uptake in the temporoparietal lobes bilaterally (**a**, **b** *arrows*) corresponding to cerebral atrophy on MRI (**c**) and confirmed on quantification assessment (**d**), in keeping with Alzheimer's dementia.
Teaching point: Multimodality imaging can help recognize different patterns of dementia

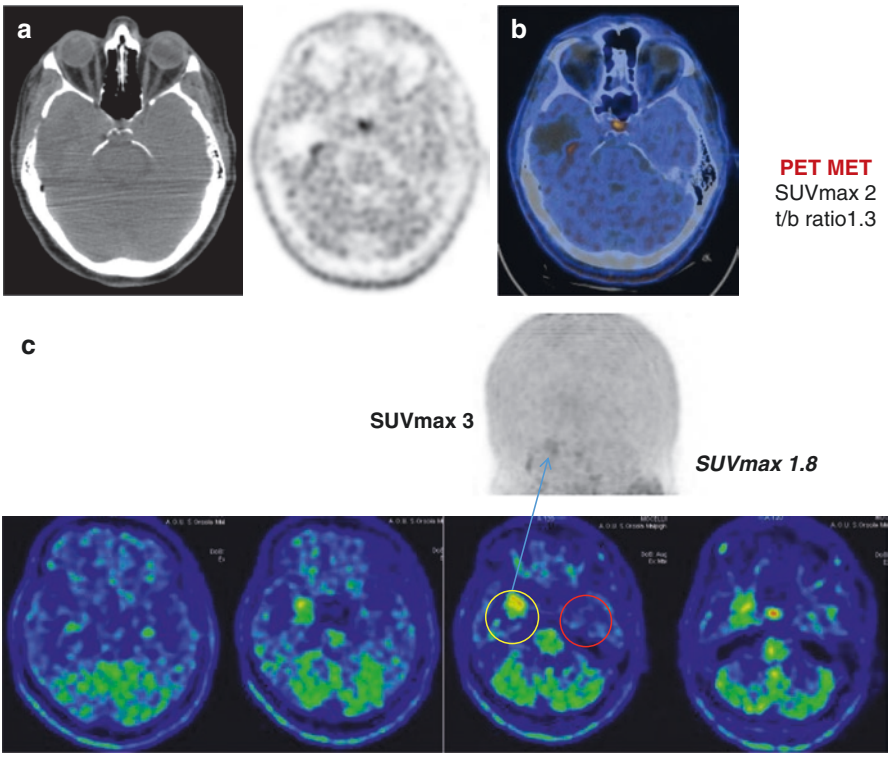

Fig. 14.24 (**a**–**c**) Axial CT (**a**), MET/PET (**b**) and axial fused PET/CT (**c**) show increased uptake in the residual tumour in the right temporal lobe. Bottom images show the differences in uptake in the tumour region and in the contralateral normal lobe.
Teaching point: MET/PET has a significant impact in assessing tumour recurrence. *Case courtesy of Dr. Castellucci, University St. Orsola Malpighi, Bologna, Italy*

Index

F. Fraioli (ed.), *PET/CT in Brain Disorders*, Clinicians' Guides to Radionuclide Hybrid Imaging, https://doi.org/10.1007/978-3-030-01523-7